# Imperial College London

# Measuring and Modelling Fire Behaviour in Timber Compartments Using Artificial Intelligence

A thesis submitted in partial fulfilment of the

requirements for the degree of

**Doctor of Philosophy**

in

Mechanical Engineering

by

**Rikesh Amin**

2024

Supervised by Prof. Guillermo Rein

# Declaration of Originality

I declare that this thesis and the work described within have been completed solely by myself under the supervision of Prof. Guillermo Rein. Where others have contributed or other sources are quoted, full references are given.

*Rikesh Amin*

2024

# Copyright Declaration

The copyright of this thesis rests with the author. Unless otherwise indicated, its contents are licensed under a Creative Commons Attribution-Non Commercial-No Derivatives 4.0 International Licence (CC BY-NC-ND). Under this licence, you may copy and redistribute the material in any medium or format on the condition that; you credit the author, do not use it for commercial purposes and do not distribute modified versions of the work. When reusing or sharing this work, ensure you make the licence terms clear to others by naming the licence and linking to the licence text. Please seek permission from the copyright holder for uses of this work that are not included in this licence or permitted under UK Copyright Law.

*To my Parents, Brother & in loving memory of my late Grandmother*

# ABSTRACT

## Measuring and Modelling Fire Behaviour in Timber Compartments Using Artificial Intelligence

by

**Rikesh Amin**

**Doctor of Philosophy in Mechanical Engineering**

**Imperial College London, 2024**

**Supervised by Prof. Guillermo Rein**

The building construction industry contributes 40% of global carbon emissions, emphasising the need for sustainable materials like mass timber over steel and concrete. Mass timber offers a higher strength-to-weight ratio, aesthetic appeal, lower cost, and greater sustainability. However, timber's inherent flammability poses fire hazards that require different fire protection measures. Current methods to understand fire behaviour to inform fire engineering are expensive and time-consuming. With an increase in high-rise mass timber buildings, there is a widening research gap in understanding compartment fires in such structures. This thesis addresses this, offering a historical review of how artificial intelligence (AI) is used alongside traditional and advanced computational tools to support engineering design. The thesis introduces the *CodeRed* compartment fire experiment series covering a 352 $m^2$ floor area, with timber ceilings and columns. The research develops data-driven models to predict timber charring rates, outperforming Eurocode-5. External flaming is also examined, where limited research exists on flame shape and size. A novel AI diagnostic tool was developed to instantly measure flames under crosswind conditions in both outdoor and laboratory environments. Results showed that timber impacts fire dynamics. The fully exposed cross-laminated timber (CLT) ceiling produced an average external flame height of 2.7 m compared to 1.4 m for the half-encapsulated ceiling. Ventilation also critically influences the duration and height of external flaming. Measurements from the diagnostic tool were used to calculate heat release rates (HRR) of external flames in *CodeRed*. Fully exposed CLT reached a peak of 43 MW with an

average of 10 MW, contributing 36% to the compartment's total HRR. By integrating AI with fire science, this thesis advances understanding of timber as a construction material and its fire behaviour and demonstrates AI's role in fire safety. Ultimately, the findings contribute to fire engineering and a more sustainable built environment.

# ACKNOWLEDGEMENTS

As I write this, memories of the past few years rush back to me, many I love to remember and many I had chosen to forget. I'll be honest, there was a point where I thought to myself, I wouldn't be around to even finish writing this section. It has been a difficult but invaluable and unforgettable journey.

Firstly, I would like to thank Dr. Chris Tighe, and Dr. Alex Ioannides, whose advice let me to starting this academic journey. I have been blessed to travel post-pandemic, creating fond memories that I will treasure forever. To Fabrizio, Ignacio, Jakub, Marcos, Maria, Imogen and Claudio. Thank you for the unforgettable experiences from Valparaiso to Gran Canaria.

I would like to thank my colleagues at Imperial, particularly the Thermofluids group; Tianyi, Khaled, Mustafa and Catarina also my brilliant co-author Yaxin. The wonderful members of Hazelab; Matt, Dwi, Wuquan, Afi, Alex, Ben, Eirik. Especially to Nick, for the impromptu beers at the union. Carlos, for the sauna sessions and many laughs. Francesca, for her support and always being up for a chat. Harry, for being the timber dream-team, through the pandemic, isolation and during CodeRed.

I extend my thanks to EPSRC, ARUP for funding my research, including the CodeRed team; Panos, Adam, Judith, Mohammed, Fabienne, Catherine and Egle. I specifically want to thank Imperial College London, for creating an environment for growth and success. Specifically extending my thanks to Sebastian, for the counselling sessions over the years. They were more helpful than I can explain.

Thank you to my friends who brought laughter and joy; Waris, Adeel, Kane, Marcello, Justin, Sarah, Abdullah, Shivani, Mannan, Ben, Andrew, Adrian, Kazi and Zeli. I would like to specifically thank the close friends in my life. Sriram, for the joys since school and Arsenal football matches. We will win it all one day I know. Elmeri, since the swim team, for the many gym sessions and for being a wonderful flatmate and friend. Ashraf, for the countless laughs and driving you to your wedding, I'll never forget. Leticia, for being there for me when others were not and supporting without hesitation. Jon, for starting this PhD journey together. For the many calls and venting sessions. Thank you for your unbiased advice and friendship. RM, I would like to thank you for coming into my life when things were so dark and being the shining light at the end of the tunnel. Thank you for bringing me peace and happiness with your love, kindness and patience. I look forward to the future. Justinas, I would like to thank you for being my friend, for not judging me for any part of my life or anything I say and for the many laughs we had over the years.

A heartfelt thank you to my supervisor, Prof. Guillermo Rein. I am extremely lucky to have him to guide me and always pushing me to strive for the best. He who kept believing in me even when I stop believing in myself. For supporting me through my academic doubts and giving me a chance to embark on this journey in his wonderful research group. Thank you.

Finally, and most importantly I would like to thank my family; my parents, my brother and foi's. To my brother, I am very proud of you, to the person you have become and look forward to visiting you in New Zealand. To my parents, I don't have the words. For raising me into the person I am today, always being there for me even during your times of hardship. For always providing me with everything to succeed, for support, love, motivation for my dreams and most importantly for encouraging me to do things that make me happy. I will keep the values you have taught me for life and hope to one day pass these onto my children.

*Rikesh Amin*
London, UK
September 2024

# TABLE OF CONTENTS


Declaration of Originality . . . . . ii

Copyright Declaration . . . . . iii

Dedication . . . . . v

Abstract of the Thesis . . . . . vi

Acknowledgements . . . . . viii

Table of Contents . . . . . x

List of Figures . . . . . xii

List of Tables . . . . . xx

Preface . . . . . xxi

1 Introduction to fire in mass timber buildings . . . . . 1
- 1.1 Background of mass timber buildings and fire safety . . . . . 1
- 1.2 Research motivation . . . . . 3
- 1.3 Thesis outline . . . . . 5

2 Literature review of artificial intelligence in fire science . . . . . 7
- 2.1 Introduction . . . . . 8
- 2.2 A meta review of AI in fire science . . . . . 11
- 2.3 Applications of AI: fundamentals of flaming combustion . . . . 15
- 2.4 Applications of AI: built environment . . . . . 24
- 2.5 Applications of AI: natural environment . . . . . 36
- 2.6 Conclusions . . . . . 43

3 Charring rates using statistics and artificial intelligence . . . . . 46
- 3.1 Introduction . . . . . 47
- 3.2 VAQT: database of charring rates of timber products . . . . . 49
- 3.3 Data-driven models . . . . . 51
- 3.4 Results and discussion . . . . . 57
- 3.5 Overall model comparison . . . . . 62
- 3.6 Conclusion . . . . . 65

4 CodeRed Experiment Series: Instrumentation for external flaming and human dimensions . . . 67
4.1 Introduction . . . 68
4.2 Introduction to *CodeRed* experiment series . . . 69
4.3 External instrumentation: setup and thermal protection . . . 74
4.4 Human dimensions to a large compartment fire experiment . . . 77
4.5 Visual analysis of *CodeRed* . . . 79
4.6 Conclusion . . . 82

5 Computer vision for external flames . . . 85
5.1 Introduction . . . 87
5.2 Review of external flaming in compartment fires . . . 88
5.3 Review of flames in image processing . . . 89
5.4 CodeRed experiment series . . . 92
5.5 Computer vision methodology . . . 92
5.6 Computer vision results . . . 97
5.7 Conclusions . . . 106

6 External heat release rate from a fire compartment . . . 110
6.1 Introduction . . . 111
6.2 Literature review . . . 113
6.3 Inverse modelling and optimisation . . . 118
6.4 CodeRed#03 . . . 119
6.5 External heat release rate: *CodeRed* . . . 123
6.6 Conclusions . . . 131

7 Conclusions . . . 133

A Chapter 5 - Appendix . . . 170

# LIST OF FIGURES


Figure 1.1: A total of 84 mass timber high-rise buildings, where timber construction had a boom in 2012 and stagnated in 2020 [2]. . . . . 3

Figure 1.2: (a) Image of Mjøstårnet high-rise timber building in Norway (b) Concept image of Google headquarters building in Kings Cross,London , opening in 2025. [6, 7] . . . . . 4

Figure 1.3: (a) Image of *CodeRed* compartment with external flaming from all openings (b) Inside the compartment with the crib fuel load and CLT ceiling, before ignition. . . . . 4

Figure 2.1: A triangle diagram representing the temporal and physical scale of fires starting from the fundamentals from flames to the built environment then natural environment. . . . . 9

Figure 2.2: Flowchart illustrating the categories and subset of artificial intelligence algorithms that are commonly used in fire science. . . . . 11

Figure 2.3: Key word search for fire topic, in specific fire journals only, coupled with its AI method. . . . . 14

Figure 2.4: Timeline of publications in fire journals on the applications of artificial intelligence. 2022 being the year with the most published work whilst, 1989-1994 being the pioneering years (which focused on using grey and histogram thresholding from image processing to interpret the evolution of pre-mixed flames) and exponential growth from 2020. . . 15

Figure 2.5: (a) Illustrates the fire journals with the most publications, with *Fire Technology* at 66 and *Fire Safety Journal* at 40. (b) Illustrates the artificial intelligence (AI) methods most commonly used - deep learning and supervising machine learning being the most common. (c) represents the fire topics where AI has been applied, where B + N, represent the sum of the built and natural environment. . . . . 16

Figure 2.6: Characterisation of small diffusion flame parameters using image processing, to determine the smoke point by Gomez et al [65]. . . . . 19

Figure 2.7: Represents the architecture of an artificial neural network with 3 hidden layers, illustrated by Duan et al [87]. . . . . 21

Figure 2.8: Jet flame, its shape and probability being outlined using image processing [92]. . . . . 22

Figure 2.9: A comparison between transient heat release rate prediction (AI), compared to calculation based on instrumentation measurements by Wang et al [95]. . . . . 24
Figure 2.10: (a) shows the building fire before flashover (b) shows the room in flashover attempting to be controlled by firefighters with flames protruding from opening, given by Li et al [104]. . . . . 26
Figure 2.11: YOLOv5 deep neural network architecture for detection of fire in different scenes, which can distinguish between smoke and a fire by Dou et al [140]. . . . . 29
Figure 2.12: Training and validation curve of Zhang et al showing that the model could potentially overfit, which can be prevented by early stopping, dropout layers and adding more data [148]. . . . . 31
Figure 2.13: Evacuation spatial layout of the experiment by Wang et al, showing the entrance and different exits in different scenarios [150]. . . . . 32
Figure 2.14: Optical flow (movement) tracking of the smoke by Chunyu et al [153]. 33
Figure 2.15: Xu et al shows the comparison of failure mode of tubular t-joint in a FEM model and experiment before training the neural network [167]. 35
Figure 2.16: Xu et al shows the comparison of failure mode of a steel planar tubular truss in an experiment and the FEM equivalent before neural network training [176]. . . . . 36
Figure 2.17: A Venn diagram representing drivers of personnel use that are observed during time of ignition by Cullen et al [202]. . . . . 39
Figure 2.18: A representation of the different stages of the detection. (a) represents the base image. (b) represents grey-scale of the flame in the scene. (c) represents binary image of the flame in the scene by Toulouse et al [205]. 40
Figure 2.19: Represents the grid split of the image with the red blocks indicating the smoke and blue with no smoke by Gubbi et al [214]. . . . . 43

Figure 3.1: The process of charring occurs when wood is exposed to intense heat, breaking down the timber into char and volatiles and reducing the load bearing capacity [224], . . . . . 47
Figure 3.2: VAQT fire resistance tests of mass timber elements from literature and test house reports [235–252] whilst [*] refers to the confidential reports. This figure illustrates the distribution from the sources with the two images representing example cut outs of the specimen. . . . . 49

Figure 3.3: Box and whisker plot for the most important numerical variables in VAQT. The red curve outlines the distribution of the data for each variable. . . . . 51
Figure 3.4: Bar plot for the most important categorical variables in VAQT. . . . 52
Figure 3.5: Measured average charring rates in VAQT compared to the value in EC5. Note that EC5 is close to the median, so it underpredicts the average charring rate for about 50% of the samples and it overpredicts it for the other 50%. . . . . 53
Figure 3.6: A feature correlation matrix that examines the relationships between the numerical variables in VAQT and the target variable, charring rate. Positive and negative values indicate varying degrees of correlation, while values close to zero suggest little to no correlation. . . . . 54
Figure 3.7: Comparison of average error using Eqn 3.2 in VAQT for the statistical models, where all models show a similar prediction whilst ridge regression ($\lambda = 0.001$) is the best and ridge ($\lambda = 1$) is the worst. . . . 57
Figure 3.8: Comparison of measured vs predicted for the best regression model – ridge regression ($\lambda = 0.001$). Data points falling above the regression line represent cases where the model is not conservative for design. . 58
Figure 3.9: Iteration feasibility study represents the plateau of MSE $\frac{\text{mm}}{\text{min}}$ values using Eqn 3.6 over 1000 iterations where 250 is the optimal point where results become independent of further iterations. . . . . 59
Figure 3.10: Comparison of measured vs predicted for a single-layer neural network. The data points above the regression line indicate cases where the model is not conservative for design, as these instances suggest it has a higher charring rate than what is desirable, where as in reality, a lower charring rate is preferred for fire safety and performance. However, due to the inherent variability in specimen attributes and other extrinsic conditions, the outcome will not always be the case. Ideally, predictions should lie on the regression line, indicating a minimal error and accurate estimation of the charring rate. . . . . 60
Figure 3.11: Learning curve of the single-layer neural network using Eqn 3.6. The two curves should converge during training, but in this case they do not and therefore the hyperparameters need optimising. . . . . 61

Figure 3.12: Learning curve for a multi-layer neural network using Eqn 3.6 which shows there is no overfitting as the two lines converge to show training is complete. . . . . 62
Figure 3.13: A model comparison using Eqn 3.2 with a fixed seed between the models implemented in this study whilst indicating the multi-layered neural network giving the most accurate predictions. . . . . 63
Figure 3.14: Distribution in stochastic results of the models chosen in this study and their $\varepsilon_{\mathrm{VAQT}}$ values using Eqn 3.2 for predicting the charring rate of timber in VAQT. The statistical models show the best reproducibility, while the multi-layer NN achieves the lowest error by a small margin. However, the higher expected error of both NNs indicates variability in their predictions due to the stochastic nature of NNs. . . . . 64
Figure 3.15: A sensitivity analysis was performed using Eqn 3.7 on VAQT through permutation importance which indicates that the insulation and its thickness has the largest effect on the models. The +– indicate the positive or negative change of the charring rate of timber. . . . . 66

Figure 4.1: (a) Schematic layout and cross-sectional dimensions of the door and window openings, highlighting the placement of façade screens equipped with plate thermometers for heat flux measurement and thermocouples for temperature readings. (b) Side view schematic of the *CodeRed* compartment, showing the overall dimensions of the openings and compartment structure. . . . . 69
Figure 4.2: Aerial view of the *CodeRed* compartment featuring a CLT ceiling, with façade screens positioned above two windows and one door for monitoring external flame behaviour. . . . . 71
Figure 4.3: External flaming observed in the three *CodeRed* experiments, with *CodeRed#02* featuring 50% reduced ventilation and *CodeRed#04* utilising 50% encapsulated CLT. . . . . 72
Figure 4.4: (a) The *CodeRed* team onsite, illustrating the human dimensions involved in conducting a large-scale compartment fire experiment. (b) Interior of the compartment during fuel bed preparation. (c) Post-experiment view of the compartment interior after the fire has burned out. . . . . 73
Figure 4.5: (a) no external flaming from the compartment. (b) external flaming from all openings. . . . . 74

Figure 4.6: During *CodeRed#03*, inside the compartment with nozzle 1 and 2 activation. Localised flaming in corner of the compartment/crib. . . . . 75
Figure 4.7: (a) External camera without extra thermal protection. (b) with thermal protection. . . . . 76
Figure 4.8: (c) External camera placement outside the compartment (d) Three external camera placement outside the compartment, with outline for in-filled and open window in *CodeRed#02*. . . . . 77
Figure 4.9: External camera placement map for all *CodeRed* compartment fire experiments. The strategic position of camera ensured comprehensive coverage of the external fire dynamics (and internal for *CodeRed#03* capturing critical data. This arrangement(s) was essential for conducting detailed post-experiment analysis and understanding the fire behaviour in different experimental conditions. . . . . 78
Figure 4.10: Camera placement, positioned tangentially to the compartment wall, capturing the side profile of the external flame during the experiment. This setup can potentially quantify flame thickness and the observation of firebrands, aligning with the study conducted by Mitchell et al [17] 79
Figure 4.11: External camera setup in-front of the compartment wall, capturing the external flaming from the openings with the facade screen above the door. The camera lens melting in the bottom right image distorting visual data capture. . . . . 80
Figure 4.12: An image of the stages of the cameras used in *CodeRed*, and the result of the experiment on the melting of the case and total data loss. . . . 81
Figure 4.13: Imperial Hazelab Scientists - *CodeRed#01* compartment fire experiment, before experiment. . . . . 81
Figure 4.14: CERIB Team and Imperial Hazelab - Setup of wood crib (1). . . . . 82
Figure 4.15: CERIB Team and Imperial Hazelab - Setup of wood crib (2). . . . . 83
Figure 4.16: Illustration for flame presence probability process. . . . . 84

Figure 5.1: (a) Diagram of external flaming through an opening in a compartment with an exposed mass timber ceiling and wooden crib. (b) The contour/edge of the external flame includes the difference flame parameters such as height, length, angle, and projected area from the compartment opening. The flame origin is the centre point of the opening. 87

Figure 5.2: The *CodeRed* compartment wall and external screen(s) above two windows and a door. *CodeRed#02* had reduced ventilation with openings 2, 4, 7, 10, 12 and 14, whereas *CodeRed#01* and *CodeRed#04* (50% encapsulation) have full ventilation [20]. . . . . 93
Figure 5.3: Validating manual visual analysis against computer vision shows a 3.3% error analysing the screen area. . . . . 95
Figure 5.4: (a) Diagram outlying the measurement domains for the external flaming of opening 7 *CodeRed#02*. (b) The computer vision domain captures the full flame height for the inclined flames in the presence of cross-winds that are observed to extend beyond the screen whilst the thermocouples can only measure temperature on the screen. . . . . 96
Figure 5.5: Ternary plot for opening 7 in *CodeRed#02*, indicating a parametric study of change in HSV (hue, saturation, value) thresholding to observe an effect in measured flame heights. The optimal value of HSV with computer vision gave a flame height of 4.3 m approximately 14 min after crib ignition. . . . . 97
Figure 5.6: Diagram of flame probability of *CodeRed#01* from openings 1 to 9. Flame merging is observed between openings 4 and 5. . . . . 98
Figure 5.7: Diagram of flame probability of *CodeRed#01* for openings 6 to 15. . 98
Figure 5.8: (a). External flame heights observed from opening 7 across all 3 *CodeRed* experiments. *CodeRed#02* has the largest heights and greatest duration of external flaming. (b) Bench marking thermocouple data against computer vision in full view with 53% difference. TC data cannot capture beyond the flame screen whilst CV can see the inclined flame due to cross-winds. . . . . 101
Figure 5.9: External flame heights across the compartment wall of *CodeRed#01*. Data loss occurs 17 to 30 m around 12.5 min after crib ignition. Dots mark the location of the openings with the rest interpolated. . . . . 102
Figure 5.10: Flame characteristic for flame height, length, angle and surface area from Opening 7 due to best data of *CodeRed#02* showing the frequency of occurrence from crib ignition to burnout. . . . . 103
Figure 5.11: Flame Height occurrence for all *CodeRed* experiments from crib ignition to burnout for Openings 7, 10 and 14 which were chosen as the best data available for selection. . . . . 104

Figure 5.12: (a). The flame length of opening 7 in all 3 *CodeRed* experiments. *CodeRed#02* measures the largest flame length whilst *CodeRed#01* and *CodeRed#04* measure similar lengths across the duration of the experiment. (b). Flame angle of opening 7 in all 3 *CodeRed* experiments. *CodeRed#02* shows the least amount of flame inclination and *CodeRed#01* the largest. . . . . 105
Figure 5.13: Flame length contour plot of *CodeRed#01* compartment. Data loss occurs from openings 1-5 from around 10 min after crib ignition however, the longest flames are exhibited at openings 4 and 10. The longest flames congregate around the openings with screens due to flame impingement and change in fire dynamics. Dots mark the location of openings the rest is interpolation. . . . . 106
Figure 5.14: Diagram of flame probability of *CodeRed#01* openings 4 and 5 which depicts the crossing of intermittency lines showing flame merging. . 107
Figure 5.15: Diagram shows the projected surface area of external flames from all compartment openings in *CodeRed#01*. Significant larger external flames are exhibited 20-25m away from the ignition end of the compartment. . . . . 108

Figure 6.1: External flaming from *CodeRed#04* fire compartment. . . . . 113
Figure 6.2: *Codered#03* experiment, showing the fire inside the compartment with sprinkler activation, and the wood crib prior to ignition. . . . . 120
Figure 6.3: (a) shows the characteristic measurements of the pool fire diameter and flame height. (b) shows the calculation of the internal heat release rate of the compartment using Thomas and Heskestad correlations. . . . . 121
Figure 6.4: (a) Hestetad and Thomas present an ensemble of solutions where the calculated heat release rate (kW) lies between the two curves. (b) Heptane pan NIST experiment. . . . . 122
Figure 6.5: Illustrates the percentage error of the two correlations as a function of time, where by the positive was 33% and the negative was 25% on average. . . . . 123
Figure 6.6: (a) The heat release rate calculations using existing correlations for *CodeRed#01*, opening , where Lee et al, has the highest prediction and Lu et al the lowest (b) shows the ensemble of solutions with the calculated heat release rate within the ensemble region. An average of 0.38 MW and maximum of 0.7 MW. . . . . 125

Figure 6.7: (a) The heat release rate calculations using existing correlations for *CodeRed#02*, opening , where Sun et al, has the highest prediction and Lu et al the lowest (b) shows the ensemble of solutions with the calculated heat release rate within the ensemble region. An average of 1.11 MW and maximum of 2.81 MW. . . . . 125
Figure 6.8: (a) The heat release rate calculations using existing correlations for *CodeRed#04*, opening , where Lee et al, has the highest prediction and Lu et al the lowest (b) shows the ensemble of solutions with the calculated heat release rate within the ensemble region. An average of 0.43 MW and maximum of 0.75 MW. . . . . 126
Figure 6.9: External heat release rate calculation correlating to wind velocity and resulting angle of inclination for *CodeRed#01*. . . . . 128
Figure 6.10: External heat release rate calculation correlating to wind velocity and resulting angle of inclination for *CodeRed#02*. . . . . 129
Figure 6.11: External heat release rate calculation correlating to wind velocity and resulting angle of inclination for *CodeRed#04*. . . . . 130
Figure 6.12: A contour plot for the external heat release rate from each individual opening of the *CodeRed#01* compartment where data loss incurred from openings 1-5 around 11-12 minutes after ignition. . . . . 131
Figure 6.13: Total heat release rate of the *CodeRed#01* compartment where 36% of this was attributed to the external flames outside the compartment. 132

Figure 7.1: Chart to outline the physical scale of the hazards covered in the thesis and the modelling complexity required to solve them. . . . . 136

Figure A.1: Matrix of external flame angle from all openings in *CodeRed#01* . . 171
Figure A.2: Matrix of projected surface area of external flame from all openings in *CodeRed#01* . . . . . 172
Figure A.3: Matrix of external flame height from all openings in *CodeRed#01* . . 173
Figure A.4: Matrix of external flame length from all openings in *CodeRed#01* . . 174
Figure A.5: Matrix of all external flame measurements from opening 7 in *CodeRed#02* 174
Figure A.6: Matrix of external flame angle from all openings in *CodeRed#04* . . 175
Figure A.7: Matrix of projected surface area of external flame from all openings in *CodeRed#04* . . . . . 176
Figure A.8: Matrix of external flame height from all openings in *CodeRed#04* . . 177
Figure A.9: Matrix of external flame length from all openings in *CodeRed#04* . . 178

# LIST OF TABLES

Table 5.1: A comparison of various methods used for flame shape analysis in published literature, with a specific emphasis on the advantages and disadvantages of computer vision. . . . . 109

Table 6.1: Results for Internal HRR measurements for *CodeRed#03*. . . . . 121
Table 6.2: Calculation for validation HRR with a comparison of maximum and average HRR. . . . . 123
Table 6.3: External heat release rates for opening 7 of the *CodeRed* experiment. 126
Table 6.4: External heat release rate calculation for conditions under side-ward perpendicular wind of opening 7 of all *CodeRed* experiments. . . . . 127
Table 6.5: Total and external heat release rates of *CodeRed#01*. . . . . 130

Table A.1: HSV calibration values for CodeRed Experiments . . . . . 171

# Preface

This thesis has an introduction chapter presenting the background and motivation for this research. All subsequent chapters are integrated documents suitable for journal publication. The material is presented as follows:

**Chapter 2** is based on:

> **R. Amin**, G. Rein. (2024) *A Historical Review of Artificial Intelligence Applications in Fire Science for the Built and Natural Environment*, **Submitted to journal for peer-review**

**Chapter 3** is based on:

> **R. Amin**, Y. Mo, F. Richter, C. Kurzer, N. Werther, G. Rein (2024) *Predicting the Average Charring Rate of Mass Timber Using Data-Driven Methods for Structural Calculations*, **Fire Technology, Published**

**Chapter 4** presents the instrumentation of the mass timber compartment *CodeRed*, alongside the human dimensions and camera setup.

**Chapter 5** is based on:

> **R. Amin**, H. Mitchell, G. Rein, A. Glew, P. Kotsovinos, N. Kalogeropoulous, M. Heidari, D. Barber, J. Schulz (2024), *AI Flame Diagnostics: Using Computer Vision to Quantify External Flame Behaviour in Large-Scale Compartment Fires*, **Submitted to journal for peer-review** (Corrections)

**Chapter 6** is based on:

> **R. Amin**, H. Mitchell, G. Rein (2024) *Measuring the External Heat Release Rate from a Fire Compartment using Computer vision*, **Submitted to journal for peer-review**

## Other Publications

The following scholarly journal outputs have also been produced as a result of this research:

> ◦ P. Kotsovinos, E. Rackauskaite, E. Christensen, A. Glew, E. O'Loughlin, H. Mitchell, **R. Amin**, F. Robert, M. Heidari, D. Barber, G. Rein, J. Schulz (2021), *Fire dynamics inside a large and open-plan compartment with exposed timber ceiling*

*and columns: CodeRed* #01, **Fire and Materials**, 47(4), 542-568.

◦ P. Kotsovinos, E. Christensen, E. Rackauskaite, A. Glew, E. O'Loughlin, H. Mitchell, **R. Amin**, F. Robert, M. Heidari, D. Barber, G. Rein, J. Schulz (2021), of ventilation on the fire dynamics of an open-plan compartment with exposed timber ceiling and columns: CodeRed #02, **Fire and Materials**, 47(4), 411-626.

◦ P. Kotsovinos, E. Christensen, A. Glew, E. O'Loughlin, H. Mitchell, **R.Amin**, F. Robert, M. Heidari, D. Barber, G. Rein, J. Schulz (2022), *Impact of partial encapsulation on the fire dynamics of an open-plan compartment with exposed timber ceiling and columns: CodeRed* #04, **Fire and Materials**, 47(4), 411-626.

◦ H. Mitchell, **R. Amin**, M. Heidari, P. Kotsovinos, G. Rein,(2023), *Structural hazards of smouldering fires in timber buildings*, **Fire Safety Journal**, 140;103861

◦ P. Kotsovinos, E. G. Christensen, J. Gale, H. Mitchell, **R. Amin**, F. Robert, M. Heidari, D. Barber, G. Rein, J. Schulz (2023), *The Effectiveness of a Water Mist System in Open-plan Compartment with an Exposed Timber Ceiling: CodeRed#03*, **SFPE Magazine**

# Chapter 1

# Introduction to fire in mass timber buildings

## 1.1 Background of mass timber buildings and fire safety

The construction industry is currently responsible for nearly 40% of global carbon emissions, where the operational energy is 30% and embodied carbon associated with the sourcing of materials and construction process is 10% [1]. This negative environmental impact necessitates the use of sustainable construction materials such as timber. Mass timber or engineered timber sequesters carbon during its growth and when sustainably sourced, can result in buildings with 18% less embodied carbon compared to those constructed with conventional materials such as steel and concrete [1]. Mass timber is an engineered wood product made by combining smaller timber panels to create larger, structural components. These components are used in construction for a range of applications, including ceiling panels, columns, and walls. Common examples of mass timber products include cross-laminated timber (CLT) and glued-laminated timber (glulam), both of which offer strength, versatility, and sustainability in contemporary buildings. As a result, timber is gaining prominence in the built environment as a construction material, driven by the global need for a greener and more sustainable future.

The use of timber in buildings is increasing worldwide; some structures are built entirely from it, whilst others incorporate timber as part of hybrid buildings. As of

February 2023, there are a global total of 84 high-rise timber buildings, 38 (45%) of which are built exclusively made of timber, as in Fig 1.1 [2]. However, the number of sole timber structures has been significantly increasing since 2017 [3]. As a result, the demand for mass timber, such as CLT, in the construction of tall buildings is rising. This overall rise is driven by its advantages over steel and concrete, which include: aesthetic appeal, sustainability as discussed above, and a low environmental impact, whilst also providing a higher strength-to-weight ratio [1, 4, 5].

Additional benefits include quick transportation, rapid construction and quick-easy assembly facilitated by its low density. An example of a tall timber building is Mjøstårnet in Norway, which stands at 85m tall, and the new Google headquarters in Kings Cross, London, UK, as shown in Fig 1.2 [6, 7]. However, such projects present challenges to the construction industry particularly regarding fire safety concerns due to the flammability of timber [8]. Historically, timber has been used in construction for millennia. The revitalisation of timber in construction is a cause for concern amongst fire engineers due to the number of recent high-rise timber building projects and the unfamiliarity with the material in the context of high-rise buildings, especially when human lives are at greater risk [3, 9]. Despite the many advantages of timber, there remains considerable reluctance to adopt it on a broader scale. This hesitation stems from a lack of large-scale research, particularly in areas such as open-plan compartments that mirror expansive floor plans. Currently, the research on timber in fire is insufficient, and a deeper understanding of its potential in large-scale applications is still needed [10–13].

Timber structures have an impact on fire dynamics, and the reduction of structural integrity caused by charring which can potentially lead to further catastrophic damage to the structure. The introduction of exposed timber introduces a new fuel source leading to a more intense and faster fire development. When timber pyrolyzes, some of these pyrolyzates will burn outside the compartment. This may lead to vertical fire spread in the building containing the point of fire origin or to a neighbouring building [14]. The development of taller buildings using mass timber necessitates addressing the flammable nature of the material whilst ensuring fire safety requirements are met. Additional challenges, such as vibration, acoustics, and evacuation, also need to be overcome [15, 16].

Therefore, understanding the performance of timber in tall buildings from a fire safety perspective is crucial, yet it has not been extensively studied [13, 17], particularly using

new conventional tools such as artificial intelligence (AI) algorithms. To enable the widespread use of timber in various building types, heights, and risk profiles, robust design methods to mitigate these fire hazards are essential.

As a result, research in this field has increased to understand timber fire behaviour. For example, this includes the series of experiments conducted in France, named *CodeRed*, to test the intensity of a fire on a large-open plan compartment with an exposed CLT ceiling [8, 18–20], which is part of this PhD thesis as shown in Fig 1.3. By using new technologies to examine the safe use of structural timber in building design, this research contributes to the carbon reduction of the construction industry and improving public health by creating a built environment which promotes greater well-being.

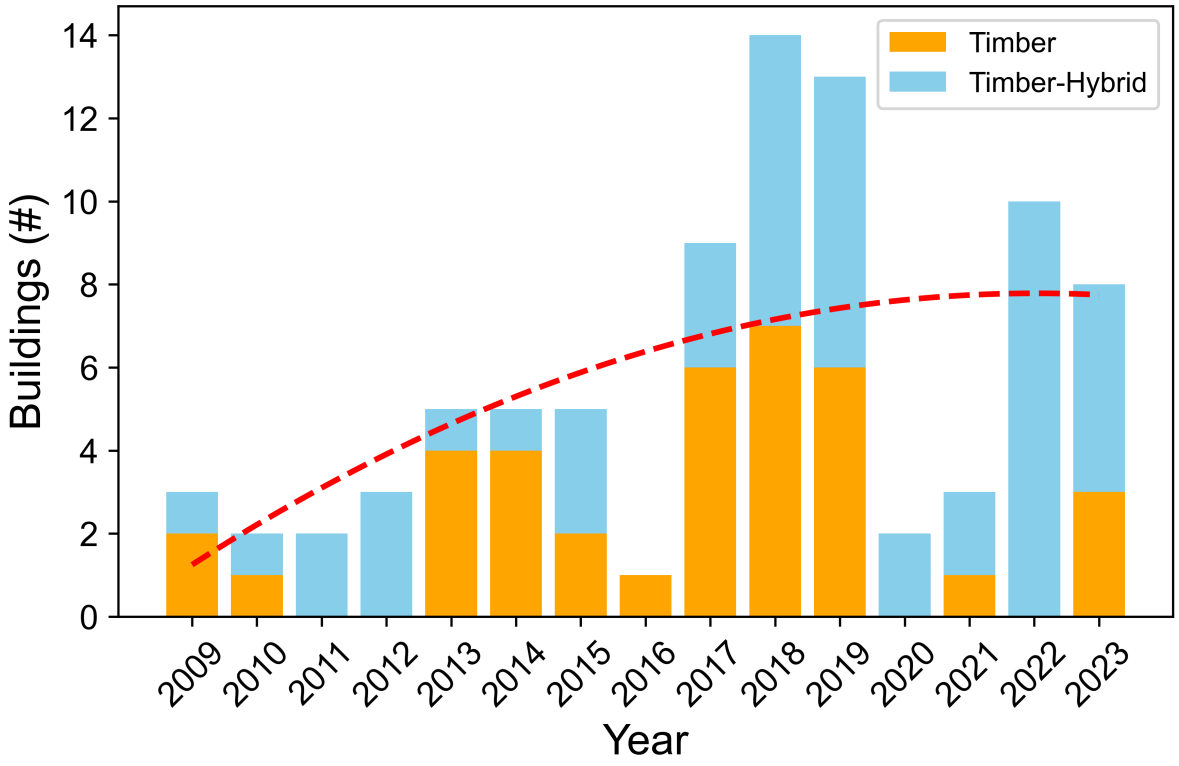



**Figure 1.1** – A total of 84 mass timber high-rise buildings, where timber construction had a boom in 2012 and stagnated in 2020 [2].

## 1.2 Research motivation

This research aims to highlight the importance of adopting new methods in the field of fire engineering, such as artificial intelligence (AI), which is currently heavily underutilised as outlined in Chapter 2. This thesis bridges the gap in identifying the key research gaps



**Figure 1.2** – (a) Image of Mjøstårnet high-rise timber building in Norway (b) Concept image of Google headquarters building in Kings Cross,London , opening in 2025. [6, 7]



**Figure 1.3** – (a) Image of *CodeRed* compartment with external flaming from all openings (b) Inside the compartment with the crib fuel load and CLT ceiling, before ignition.

in the application of AI to fire by presenting a historic review of the published literature. It also presents an understanding of how to predict the average charring rate whilst also addressing the understudied topic of external flaming and its measured heat release rate in large compartment fires. In this thesis, I computationally study how to predict the average charring rate of mass timber products using statistics and AI (Chapter 4), experimentally study external flaming (Chapter 5) and external heat release rate (Chapter 6), with the latter two in the context of large open-plan mass timber compartments. This thesis primarily focuses on three *CodeRed* experiments (1, 2, 4). All experiments described have unique conditions which are changed as to such vary compartment ventilation and CLT exposure.

The core methods of analysis for the subsequent chapters of this thesis focus on using data-driven approaches and AI algorithms, specifically to study charring rates of mass timber products and the external fire dynamics of the *CodeRed* experiments. The *CodeRed* experiments are studied using visual imaging from a total of 25 cameras inside and outside the compartment and specifically using AI diagnostics built using computer vision to look into external flaming and heat release rates. Other forms of instrumentation were used such as thermocouples, plate thermometers and a weather station to measure the temperature distributions, heat-flux and wind speed/direction, all of which are important in this thesis which assists in understanding the fire performance of large open-plan mass timber compartment fires. Computer vision (CV) is a novel-framework, built using different AI algorithms to derive information from visual data [21]. It is introduced and further elaborated in this thesis, and it facilitates the simultaneous and instantaneous quantification of the size and shape of multiple external flame parameters in the presence of cross-winds. These parameters include: flame probability, height, length, angle, surface area and merging which are then used to inverse model from existing correlations in literature, the external heat release rate in the *CodeRed* experiment series.

CV leverages automation, speed, and precision in line with current design codes and apparatus setups, offering a more efficient and time-saving solution. This diagnostic tool shows great potential through the measurements it delivers by solving an inverse problem to calculate the external heat release rate of large-scale compartment fires. As proposed in this thesis, it also facilitates future fire experiments, aiding in a deeper understanding of fire dynamics.

## 1.3 Thesis outline

In the body of this thesis, I present the subsequent chapters:

**Chapter 2:** I present a historic review of the literature for the use of AI in fire, specifically fundamentals of combustion and in the built and natural environments. I examine how the technology has advanced and been used in the field since the pioneers, in chronological order, the different AI algorithms, and how they are used to tackle fire engineering problems. This chapter specifically highlights the motivation for the following

chapters in this thesis by identifying the current gaps in research.

**Chapter 3:** I introduce the problem of accurately measuring the charring rate of mass timber in fire for structural calculations. I use different statistical and AI algorithms to create models that compare to current industry standards such as Eurocode-5 by creating a novel database of 231 furnace tests of timber charring experiments, called VAQT.

**Chapter 4:** I introduce the experimental and instrumentation design of the mass timber compartment fire experiment, *CodeRed*. I summarise the building design, the human dimensions aspect of the largest mass timber compartment to date amidst the Covid-19 pandemic, instrumentation setup to study external fire dynamics and the use of computer vision analysis in Chapters 5 & 6.

**Chapter 5:** I investigate external flaming, a hazard present in compartment fires which is currently understudied in the field. I use the *CodeRed* experiment series to quantify the size and shape of external flames using computer vision. I measure flame probability, height, length, surface area, and merging.

**Chapter 6:** I use inverse modelling to calculate the heat release rate of external flames from the *CodeRed* fire compartment series, utilising visual data measured with computer vision. This approach involves comparing the results from solving the inverse problem with established correlations found in the literature. The visual data quantifies various flame shape parameters, including flame height, length, angle of inclination, and wind speed.

# Chapter 2

# Literature review of artificial intelligence in fire science

## Summary [1]

Current methods for understanding fire behaviour to inform fire engineering are both expensive and time-consuming. This chapter presents a historical review exploring the application of artificial intelligence (AI) to understand fire dynamics, address fire safety engineering challenges, and model fire behaviour across both the built and natural environments. The review found a wide range of AI techniques used in fire, from simple supervised machine learning algorithms like regression, support vector machine and random forest, to more complex models such as neural networks in different deep learning frameworks. A chronological overview of key developments is presented, tracing the evolution of AI fire research from its pioneering work in 1989 to the exponential growth started in 2010. It encompasses a total of 213 publications in peer-reviewed journals specifically related to fire science. The AI literature covers a variety of phenomena, including smoke and fire detection, flame spread, flame shape, and heat release rate. We highlight the strengths and limitations of AI in solving fire-related problems, particularly in comparison to other methods such as empirical correlations and numerical modelling approaches. Finally, the review identifies current research gaps, such as the overfitting of

1. This chapter is based on "R. Amin, G. Rein. (2024) *A Historical Review of Artificial Intelligence Applications in Fire Science for the Built and Natural Environments*, **Submitted to journal for peer-review**

AI models, need for large centralised databases, need for conducting sensitivity analysis, which algorithms are used and which are underutilised depending on the use case. It concludes by providing future directions, emphasising the potential of AI to assist fire engineers and scientists in adopting new tools and to improve fire safety.

## 2.1 Introduction

Fires hold significant importance due to their profound impact on safety, particularly in the built environment where human lives are at risk, such as in residential buildings or high-rise structures. In addition, wildfires pose a significant threat to safety in natural environments. Therefore, it is essential to understand both the physical and temporal scales of these fires. Fig 2.1 illustrates this relationship through a triangle plot, where the scale of a fire correlates with its potential for damage. This potential is also closely linked to the availability of fuel. For instance, in wildfires, the presence of large quantities of dry vegetation significantly increases the risk of ignition and rapid fire spread compared to areas with little or no vegetation, or where vegetation has high moisture content [22]. Similarly, in building fires, such as those involving timber structures, exposed timber can contribute to additional fuel load, while a lack of ventilation can increase fire severity, as demonstrated in various studies [8, 18–20].

In response to the persistent challenge posed by fires, the Institute of Fire Engineers (IFE) was established in the UK in 1918, followed by the founding of the Society of Fire Protection Engineers (SFPE) in 1950 [23]. Since then, fire engineering has emerged as a distinct discipline within the broader field of engineering. However, it remains relatively understudied, largely due to the complexity of modelling flaming combustion and its behaviour. Current methods, such as the Fire Dynamics Simulator (FDS), though widely used, are computationally expensive and time-consuming, creating the need for alternative approaches.

One promising avenue is the application of emerging technologies, particularly artificial intelligence (AI), which has seen significant growth in recent years. This chapter will present a historical review of AI applications in fire science, exploring how AI can be employed as a tool alongside regulations, prescriptive building codes, and performance-based design to enhance fire safety engineering.

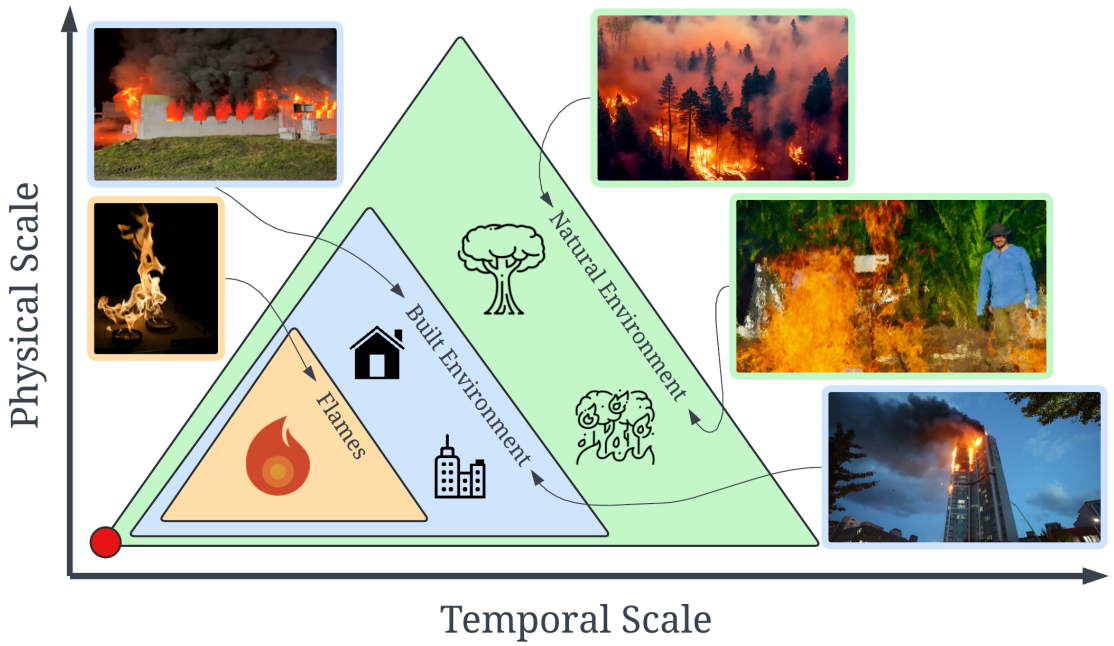



**Figure 2.1** – A triangle diagram representing the temporal and physical scale of fires starting from the fundamentals from flames to the built environment then natural environment.

### 2.1.1 Overview of artificial intelligence algorithms

Artificial intelligence (AI), is a branch of computer science, being numerical, logical, or interpretive in nature [21]. At its core, AI trains machines to make predictions through an ensemble of algorithms applied to extensive datasets. Although the concept of AI was first introduced in the 1940s, its application to fire science and engineering only began in the late 1980s. Since the 2010s, the exponential growth of AI has been driven by advancements in computational power and a reduction in associated costs, leading to significant advancements in AI techniques. This progress presents an opportunity to modernise fire science and engineering, using AI to provide more data-driven, performance-based solutions.

AI is an umbrella term that encompasses two primary subsets: machine learning (ML) and Vision. Each of these categories contains a range of algorithms, with ML and Vision having distinct methods and applications. The specific algorithms relevant to covered in this review and are relevant to fire science and engineering, illustrated in Fig 2.2.

There exists a vast array of AI algorithms, however, only a select few are particularly relevant. ML, a key subset of AI, can be divided into three main categories: deep learning,

unsupervised learning, and supervised learning. Among these, deep learning is the most widely applied and has driven AI's proliferation across nearly all engineering disciplines, largely due to the development and implementation of neural networks (NN), which is a system that mimics the neural structures of the human brain, similarly allowing machines to predict and solve problems through pattern recognition [24, 25]. It has become one of the most prominent AI algorithms due to the increasing availability of computational power, large datasets, and resulting storage capacity [26]. There are several types of neural networks, each with specific applications. The most used include convolutional neural networks (CNNs), recurrent neural networks (RNNs), physics-informed neural networks (PINNs), Bayesian neural networks (BNNs), and generative adversarial networks (GANs) [27]. Each of these networks serves unique purposes and will be explored further in this chapter where relevant.

Unsupervised learning is another important subset of AI, focused on unlabelled datasets, where patterns are identified without human supervision. This branch of AI is more computationally complex than its supervised counterpart and tends to produce less accurate predictions, as it relies on methods such as probability, association, and clustering [28, 29]. Popular algorithms within unsupervised learning include principal component analysis (PCA) and k-means clustering. In contrast, supervised learning is commonly used due to its simpler setup and clearer mathematical foundations. It generally produces higher accuracy and reliability since data is labelled during preprocessing, enabling the machine to make predictions based on these labelled examples [30]. This preprocessing significantly aids the algorithm in learning and making more precise predictions [25]. Supervised learning's structured approach makes it a favoured choice in many AI applications, including fire science and engineering. Popular supervised learning algorithms include statistical methods such as regression modelling, support vector machine, decision trees and random forests [31].

The other major subset of AI is Vision as shown in Fig 2.2, which can be divided into two categories: CV and image processing (IP) [32, 33]. Image processing involves relatively simple mathematical transformations, such as segmentation, which is used to divide objects within a scene; thresholding, binarising an image; filtering, which alters the range of pixel values; and transformation, which modifies the image [34]. These algorithms often work together for a specific use case—such as detecting a fire or flame

within a scene, as will be discussed in this study. CV, on the other hand, operates more intuitively and runs both spatially and temporally in time. It consists of a combination of algorithms used for tasks such as object detection, image classification, and pattern recognition instantaneously and simultaneously. CV provides a more sophisticated approach by interpreting and understanding images or videos at a higher level, which makes it particularly valuable for applications requiring advanced visual analysis such as fire and smoke detection in smart firefighting application [35].

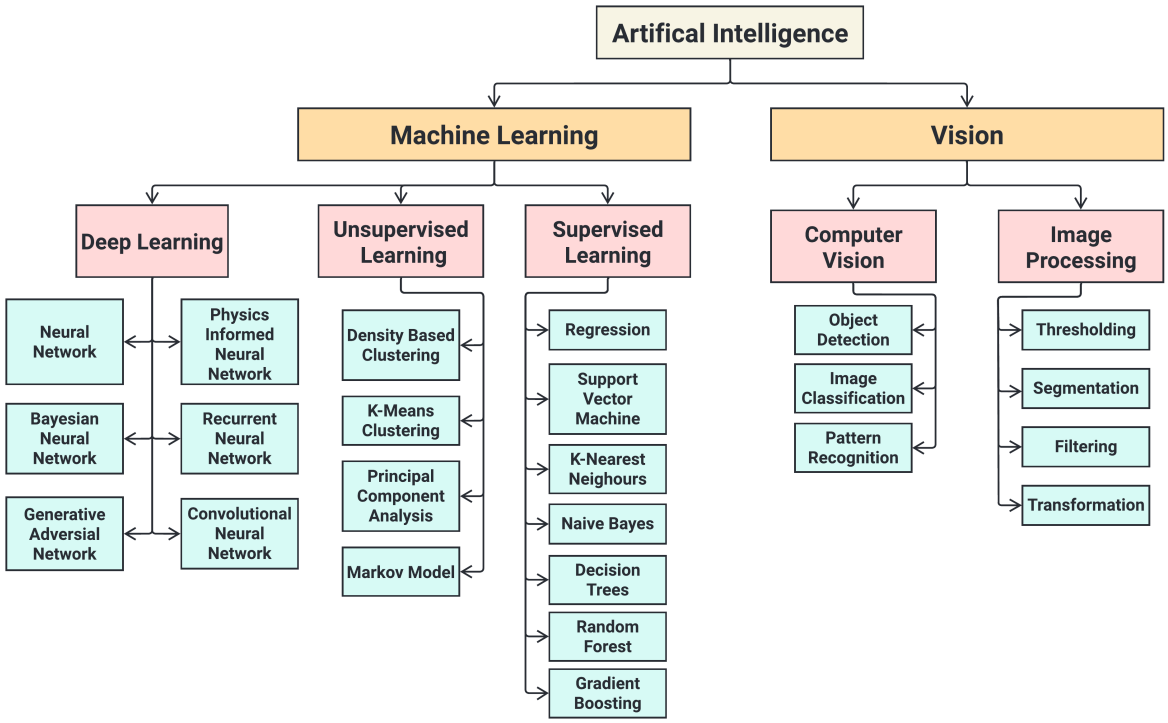



**Figure 2.2** – Flowchart illustrating the categories and subset of artificial intelligence algorithms that are commonly used in fire science.

## 2.2 A meta review of AI in fire science

Currently, there are 7 literature review papers that have sought to bridge the gap between artificial intelligence (AI) and its applications to fire-related challenges, particularly in the context of buildings with fire and smoke monitoring.

The earliest review was conducted by Gaur et al, in early 2020, which examined current algorithms for flame and smoke detection using visible and infrared cameras [36]. The methods discussed ranged from colour detection in image processing to the use of convolutional neural networks (CNNs) in deep learning.

Subsequently, Geetha et al. conducted a review also in 2020, providing a survey of fire detection using machine vision [37]. This review covered earlier studies focus for colour and object detection, but its primary emphasis was on the application of CNNs. Geetha et al, spanning from 1996 to 2020, concluded that CNNs exhibit high performance in detecting smoke and fire in images.

In the same year, Adib et al, presented a review focusing on wildfire detection and prediction using various ML algorithms. This review concluded that NN's and logistic regression are the most widely used approaches, which can be integrated into fire monitoring [38].

In 2021, Naser et al, covered the broader applicability of various ML algorithms to fire [39]. This review provided detailed explanations of how each ML algorithm—including deep learning, decision trees, and support vector machines—function at a fundamental level and explored their potential benefits in fire safety engineering (FSE). The review concluded by suggesting that future work in FSE should facilitate the use of AI by developing key data-based assemblies and dedicated algorithms. Unlike previous reviews, this work focused more on the algorithms themselves and their potential applications to FSE problems.

More recently, in 2022, Huu-Tai, provided an overview of state-of-the-art ML methods for structural engineering with one section focused on fire [40]. It described in detail seven different ML algorithms used in fire safety engineering, aiming to establish a foundational knowledge base for practitioners to apply these algorithms to structural engineering problems. The review also highlighted future research directions and discussed existing limitations, however with minimal focus on fire problems.

In the same year, Huang et al. focused on the historical application of CFD in FSE and demonstrated how AI holds great promise, particularly in the areas of fire detection and forecasting, potentially offering time effective solutions [35]. The most recent review was by Bakas et al, in 2023, that examined the contributions of AI to fire safety engineering with a specific emphasis on designing more sustainable buildings [41].

Given the current research gaps in existing literature reviews, which often cover only a limited range of topics without addressing their limitations, this chapter focuses exclusively on fire-related journals. It provides a literature review that examines the application of AI techniques in FSE, encompassing both fundamental aspects and applications in built

and natural environments. This specialised resource aims to assist fire engineers and scientists by addressing research gaps, particularly in smart detection systems using CV, enhancing currently employed CFD models, such as FDS, data importance and optimization. However, research published in AI-focused journals is excluded, as these often emphasize broader methods, including transformers and large language models, which leads away from the problem of fires reducing its significance but more onto the problem of the method. The review includes all relevant published works from 1989 to 2024.

### 2.2.1 Literature search

Building on the previous review papers, a comprehensive literature search was conducted to encompass all aspects of fire-related research. This search employed broad umbrella terms such as "machine learning," which included specific algorithms like random forests and neural networks, as mentioned earlier. However, the scope of the search was confined to peer-reviewed fire journals only. There are various approaches for reviewing scientific literature, ranging from critical reviews to umbrella reviews. This chapter, however, presents a historical review, emphasising the breadth and scope of the available literature. The primary objective is to identify, integrate, and highlight trends as well as research gaps within the existing body of work. The search terms utilised for this review are compiled and displayed in Fig 2.3 and were chosen based on the different fire topics, the fire journals available and the core AI methods. To identify relevant literature on the application of AI methods to fire science, online databases such as Google Scholar, ScienceDirect, and Scopus were employed, with a focus on three specific fire-related topics; fundamentals of combustion, the built environment and the natural environment.

General AI terminology was used as search terms, as these often suffice to capture the relevant literature. Nevertheless, this chapter delves into the application of specific AI techniques. For fire-related topics, more precise search terms were necessary to ensure a comprehensive and thorough review of the available literature. This approach ensures that the review captures the full extent of current research and publications in this field as given in Fig 2.3.

A total of 219 papers were found, since 1989, as illustrated in Fig 2.4. The highest number of publications occurred in 2022, with the pioneering work in this field initiated by *Goix et al.* in 1989, *Okayama et al.* in 1991, and *Smallwood et al.* in 1994 [42–44]. The

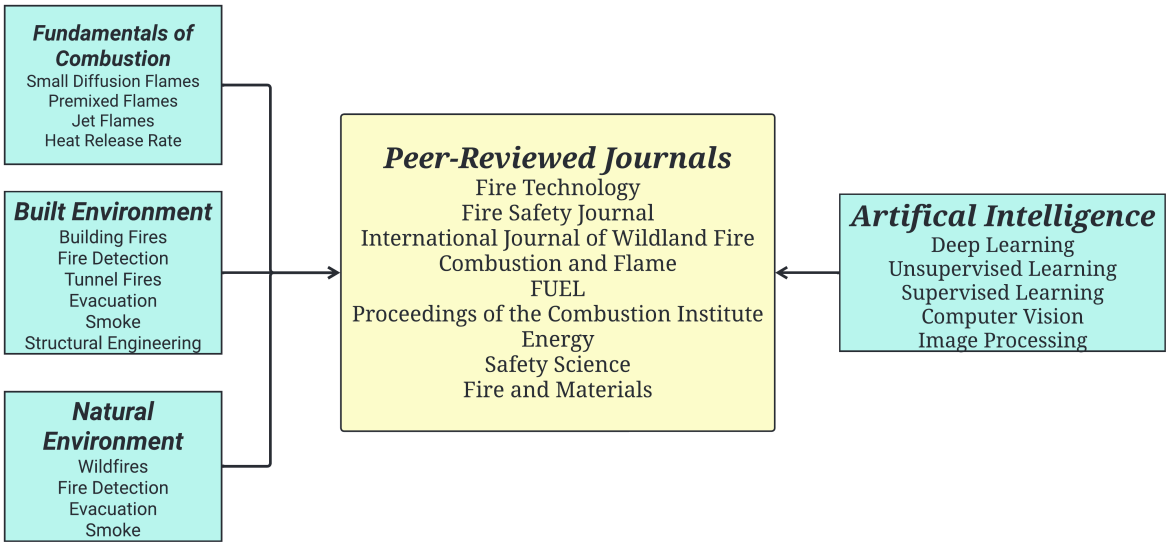



**Figure 2.3** – Key word search for fire topic, in specific fire journals only, coupled with its AI method.

application of AI to fire science and engineering started gaining momentum in 2010 and has shown consistent growth since. Highlighting the journals with the highest number of publications on applying AI, is represented in Fig 2.5 (a). The top three most-cited papers were all published in the *Fire Safety Journal*: *Celik et al.* in 2009 with 423 citations, *Marbach et al.* in 2006 with 239, and *Yuan et al.* in 2011 with 196, all of whom focused on fire and smoke detection [45–47], with research gaps in the built environment specifically buildings and structural engineering problems as given in Fig 2.5 (c). Fig 2.5 (b) highlights the most used AI applications within the field of fire science. Deep learning emerged as the most frequently applied method, with 76 publications focusing on neural networks (NN) and 32 on convolutional neural networks (CNN). Supervised learning followed, with 29 publications on support vector machines (SVM) and 18 on random forests. These findings emphasise the prominence of deep learning in fire science, while other supervised learning techniques also make notable contributions to the field. Vision-based approaches were also significant, with 70 publications focusing on image processing techniques but lack of using computer vision. These methods, particularly colour and grey-level thresholding, were commonly employed for fire and smoke detection, a topic that will be explored in further detail later in this chapter.

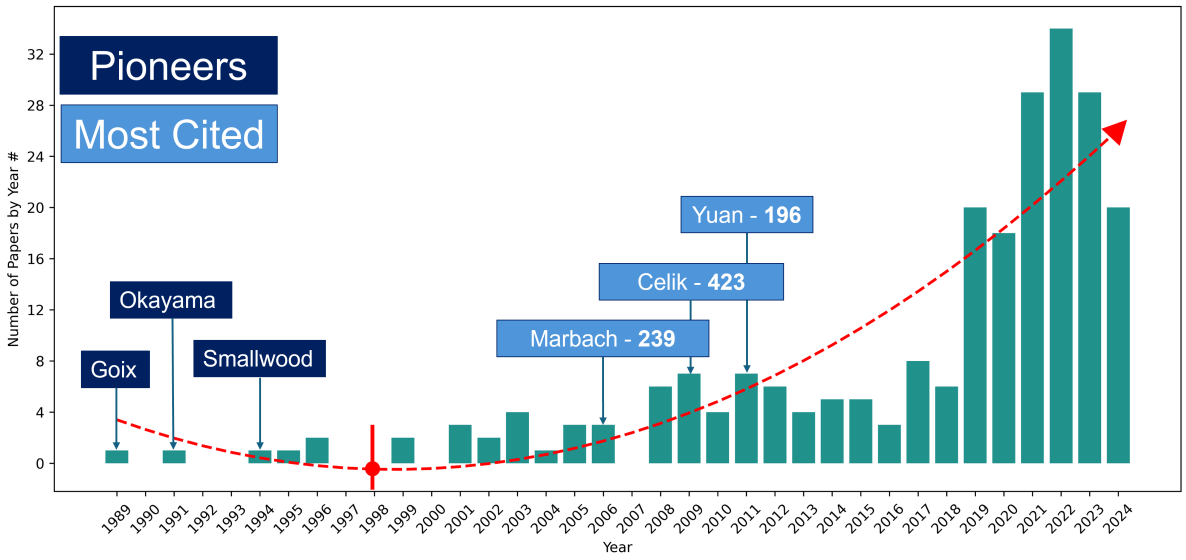



**Figure 2.4** – Timeline of publications in fire journals on the applications of artificial intelligence. 2022 being the year with the most published work whilst, 1989-1994 being the pioneering years (which focused on using grey and histogram thresholding from image processing to interpret the evolution of pre-mixed flames) and exponential growth from 2020.

## 2.3 Applications of AI: fundamentals of flaming combustion

### 2.3.1 Small diffusion flames

Diffusion flames occur when the fuel and oxidiser are not premixed but instead combine through the process of diffusion before combustion takes place. In such flames, the rate of burning is governed by the transport of these reactants rather than by chemical kinetics, as there is no spontaneous combustion [48]. The foundational study on small diffusion flames, conducted by Audouin et al. in 1995, employed image thresholding—an image processing technique—to estimate the average centre line temperature of small pool fires. The results were validated through comparison with flames generated from gas burners of various geometries. While this method successfully approximated flame probability and height, the study underlines the need of further laboratory experiments under more realistic fire conditions [49].

In 2005, Kempf et al. advanced this research by simulating piloted diffusion flames using large eddy simulations (LES) in conjunction with a neural network (NN), to quantify characteristics, including length, dissipation, orientation, mass fractions, density, and

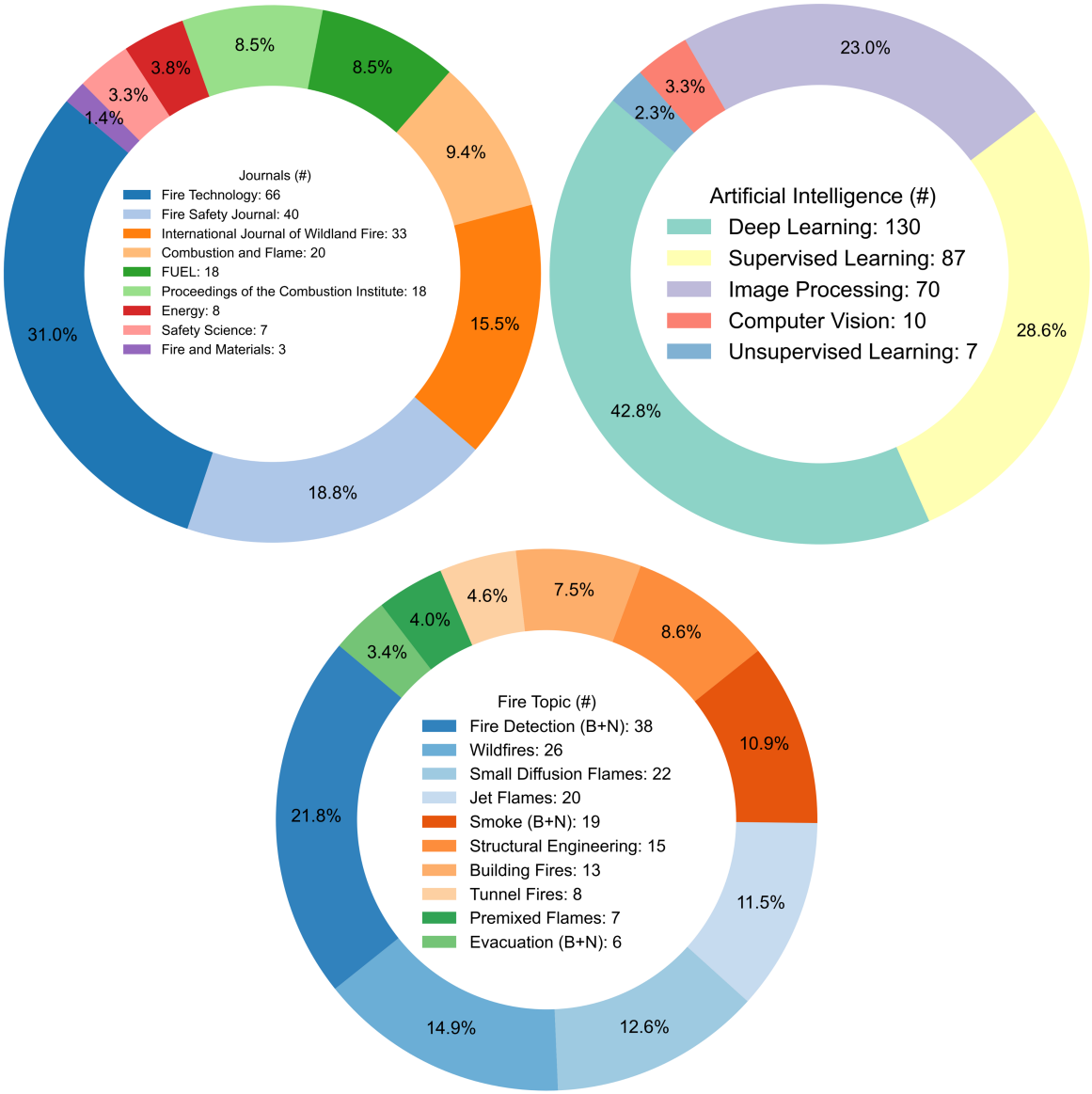



**Figure 2.5** – (a) Illustrates the fire journals with the most publications, with *Fire Technology* at 66 and *Fire Safety Journal* at 40. (b) Illustrates the artificial intelligence (AI) methods most commonly used - deep learning and supervising machine learning being the most common. (c) represents the fire topics where AI has been applied, where B + N, represent the sum of the built and natural environment.

viscosity. Validation against experimental data revealed strong agreement between the simulations and observed results [50]. Building upon Kempf's work, Sen et al. applied a NN in two studies focusing on the chemical kinetics of turbulent and non-premixed flames. Their findings highlighted that, while artificial intelligence (AI) accelerates computational processes, it remains challenged by complex empirical equations [51, 52]. Several other studies also employed NN's and convolutional neural networks (CNN) to model chemical kinetics and demonstrated faster computational performance compared to traditional

solvers while effectively predicting flame shape [53–55].

In 2008, Hernandez et al. used image processing to quantify flame geometry from an industrial burner. A NN was then trained on these measurements to predict the combustion stage of the flame, offering a less computationally intensive alternative to numerical simulations [56]. Similarly, Ji et al. used the same method, to measure flame length and determine the point at which flames merge between two pool fires in tunnels. Their study introduced a correlation for estimating the heat release rate (HRR) [57]. Other studies also employed image processing to examine the geometric properties of turbulent buoyant diffusion flames, some under the influence of wind. These findings demonstrated that turbulence significantly affects flame geometry, which impacts the flame's surface area and volume as it fluctuates over time [58–62].

Image processing is widely applied to various aspects of small-diffusion flame analysis beyond flame geometry. In 2011, Huang et al. investigated the effects of acoustic excitation on flame oscillation frequency, using colour thresholding in both RGB and HSV colour spaces [63]. In 2018, Pino et al. utilised Eulerian video magnification to extract flame features, specifically identifying the flame tip. This data was then used to train a support vector machine (SVM) for classifying the soot propensity of the flame [64]. That same year, Gomez et al. applied computer vision (CV) and image processing techniques to determine the smoke point of diesel fuel blends, as shown in Fig 2.6 [65]. To extend beyond traditional Vision techniques, Goligiyaz et al. used a NN to predict flue gas temperature and emissions based on flame images. Features were extracted using image processing like those employed by Pino et al. The trained network was validated and showed that flue gas temperature can be accurately estimated from images [66].

AI has also been applied to various diffusion flame-related predictions. In 2021, Wan et al. used a CNN to predict the composition of turbulent non-premixed flames [67]. That same year, Lehn et al. trained a NN to predict the laminar flame speed of hydrocarbons and oxygenated hydrocarbons. Their model, which incorporated temperature, pressure, and equivalence ratio data, outperformed other methods such as multivariate linear regression [68]. In another study, Yao et al. predicted the dissipation rate of turbulent spray flames by training a NN on data extracted from numerical simulations. With an error margin of less than 15%, their results demonstrated the viability of AI for this application. Notably, their study was the first to conduct a sensitivity analysis to identify

the model parameters that had the greatest impact on predictions of diffusion flames [69]. In 2022, Preiler et al. used a combination of SVM and a NN to predict the same physical conditions. The SVM classified non-flame and flaming regions, which improved the NNs accuracy and overall performance [70]. However, increased complexity in AI models does not always guarantee success. Wang et al. used image processing based on fuzzy pattern recognition to assess the stability of gas-fired combustion flames. When compared to both a NN and a SVM, the image processing technique outperformed both, achieving an average accuracy of 90% [71].

In conclusion, AI has proven to be a valuable tool in the study of small diffusion flames, with image processing being the most widely used technique due to its simplicity of implementation and lower computational cost compared to more complex methods such as a NN. However, image processing is limited in its ability to capture time-averaged measurements, highlighting a potential area for further research. CV, particularly in time-series analysis, offers a solution for addressing these temporal challenges. Several studies have successfully coupled tools such as image processing with CNN or SVM. Overall, AI is predominantly used to quantify flame geometry, rather than applied to chemical kinetics or combustion phenomena. Nonetheless, it shows significant potential as a tool for tackling fundamental combustion problems and could be applicable even to larger-physical scale systems, which will be explored further in this chapter.

### 2.3.2 Premixed flames

Premixed flames occur when the fuel and oxidiser are combined prior to combustion. In such cases, the flame propagates through the mixture, as seen in applications like spark-ignition engines or pilot flames, and as the reactants are already mixed, combustion happens more uniformly and rapidly [48]. Two pioneers in the application of AI to flame studies were Goix et al. (1989) and Smallwood et al. (1994), as previously mentioned [42, 43]. Goix et al. employed image processing to study V-shaped $H_2$ – Air, focusing on interpreting their turbulent flame evolution. They used grey-level thresholding to identify the flame front and applied a median filter to remove noise, such as light scattering. Smallwood et al. used similar methods to study turbulent pre-mixed methane-air flames and defined their probability distributions. However, they used histogram thresholding instead. Subsequent studies utilised image processing to investigate

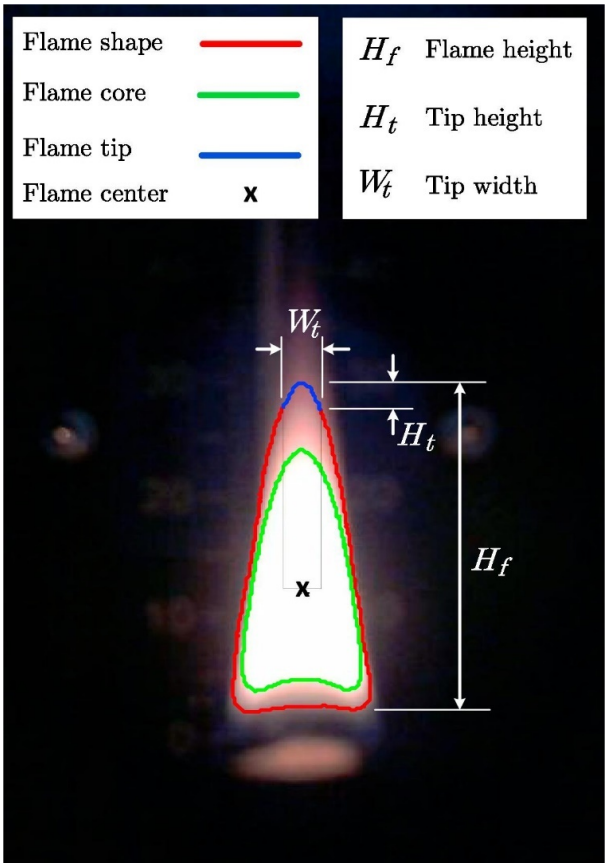



**Figure 2.6** – Characterisation of small diffusion flame parameters using image processing, to determine the smoke point by Gomez et al [65].

the stability of premixed flames, employed the RGB colour scale to detect flame dynamics. These studies successfully obtained dynamic flame characteristics and established relationships between flame behaviour and image colour [71–77].

In 2003, Inal et al. advanced applications by using a neural network (NN) to investigate soot formation in premixed hydrocarbon flames, with predictions showing good agreement with experimental data [78]. Similarly, Liu et al. reconstructed soot fields in laminar flames using physics-informed machine learning (ML) and a DeepONet auto-encoder to map soot distribution in flames, which outperformed simpler AI techniques [79].

In 2009, Ihme et al. applied an NN to model the chemistry of a swirl-stabilised flame using large eddy simulations (LES), with results that closely matched experimental data [80]. Building on this, Sen et al. applied the same method to study chemical kinetics in turbulent premixed flames using LES, demonstrating better performance to traditional methods, such as solving ordinary differential equations [81]. Similar studies also employed LES for premixed turbulent flames but used a convolutional neural network (CNN) [82, 83].

In 2021, Yu et al. introduced a data-driven kinematic model to predict oscillations in gas turbine premixed flames. Image processing techniques, including edge and ridge detection using a Sobel filter, were used to extract features, with results showing strong alignment with experimental data [84]. That same year, Ding et al. combined LES with an NN to simulate flamelets, 1D premixed flames, and hydrocarbon piloted flames, yielding good agreement with traditional integration methods [85].

In 2022, Yadav et al. employed a physics-informed recurrent neural network (PRNN) to predict the linear and non-linear responses of premixed laminar flames, as well as their velocities. Their model, trained on simulations which required fewer training samples due to the specificity of the RNN, accurately predicting the heat release rate (HRR) [86]. In 2023, Duan et al. used an ensemble of ML methods, including an SVM and NN, to predict the propagation and combustion processes in lean premixed flames, where the general NN architecture is given in Fig 2.7. The SVM was found to be the most effective model with lower setup complexity and faster processing times [87].

In conclusion, from the early pioneers to modern-day applications of AI in premixed flames, it is evident that future research should focus on expanding current frameworks to cover different flame types, varying dimensional configurations, and broader applications. Additionally, many studies do not fully optimise their models, such as through hyper-parameter tuning. Optimising models can reduce over-fitting and improve generalisation, while adding more data in training can further mitigate these issues. Overall, research highlights that AI provides time-efficient solutions for complex combustion problems and is particularly well-suited to premixed flame applications. Image processing and computer vision can be used in the same method as used for small diffusion flames to study flame geometries in premixed flames.

### 2.3.3 Jet flames

Jet flames, while typically smaller than pool fires, can surpass them in size depending on the fuel exit flow rate. These fires pose significant danger due to their potential to cause a domino effect, where the scale of destruction is greatly amplified [88]. Jet flames are generally defined as inverted cylindrical cones, with their shape characterised by the edge and area of the flame surface, whether in a laminar or turbulent state. Accurately quantifying the shape and size of jet flames is essential for correlating these characteristics

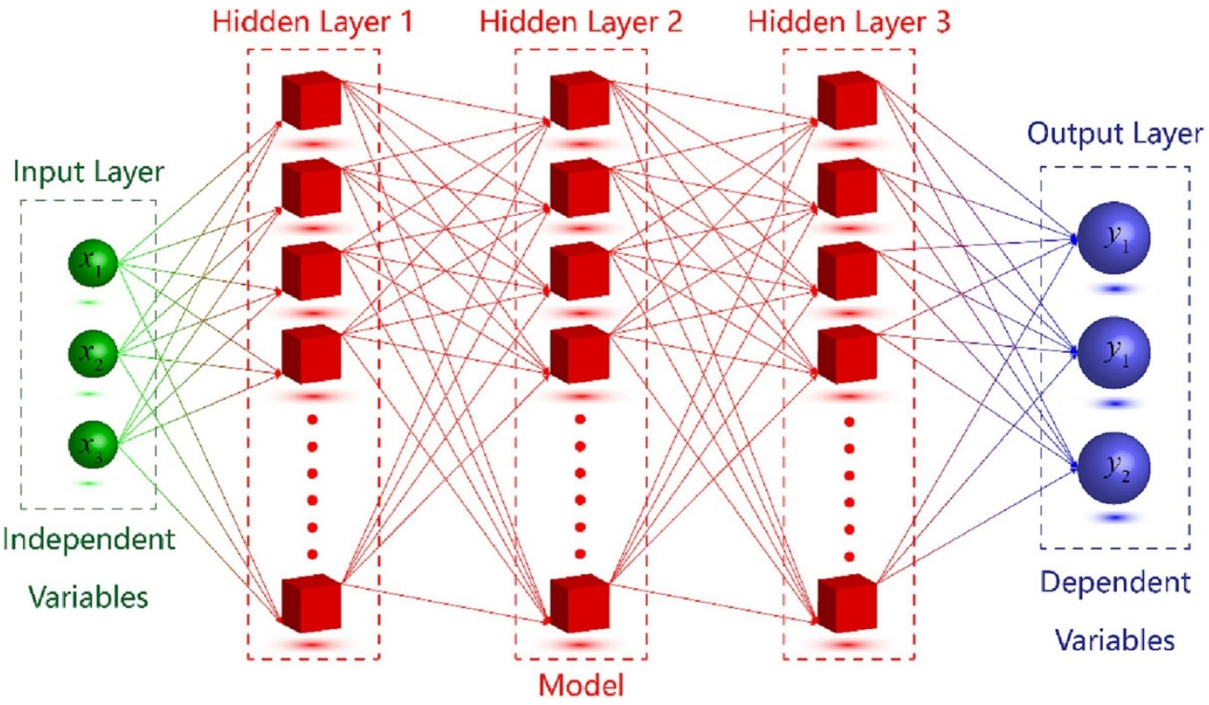



**Figure 2.7** – Represents the architecture of an artificial neural network with 3 hidden layers, illustrated by Duan et al [87].

with the potential damage they may cause [88–91].

The first use of artificial intelligence (AI) in jet flame modelling was pioneered by Christo et al. in 1996 [91]. They utilised neural networks (NN) to simulate turbulent jet diffusional flames, showing good similarities with experimental data and other modelling approaches. However, NN's only excelled in complex cases but under performed for simpler flames.

In 2011, Palacios et al. used image processing to study the flame shape of a vertical jet flame, measuring its length and width using infrared images. Their work addressed research gap by being able to predict the shape and proposing an empirical correlation based on their experimental findings [88].

In 2024, Kong et al. used Otsu binary thresholding, an automatic technique to create a binary image, to study the length of a hydrocarbon-blended natural gas jet flame from experiments. They utilised inverse modelling to optimise their multi-point source model, iteratively thresholding each image over the entire dataset. The method had an 10% improvement in measurements compared to previous studies and quantified the probabilistic profile of the jet flame, as shown in Fig 2.8 [92]. In the same year, Kildare et al. applied a pre-built deep learning framework called U-Net to predict temperature fields in jet flames. The network was trained on data from Rayleigh scattering measurements

comprising 17,000 images, resulting in an error margin of 7-10% compared to actual measurements [93].

AI techniques, particularly those involving image processing and neural networks (NNs), have been successfully applied to jet flames, specifically for characterising flame shapes. Complex NNs, such as convolutional neural networks (CNNs), have proven effective in predicting key characteristics like fuel type, flame location, and temperature distribution. However, these networks have faced challenges in accurately simulating the flow dynamics of even simple jet flames. This suggests that while NNs can excel in certain predictive tasks, traditional methods like computational fluid dynamics (CFD) may still outperform them in simulating fluid flow, highlighting that NNs are not always the optimal solution for all aspects of jet flame modelling.




**Figure 2.8** – Jet flame, its shape and probability being outlined using image processing [92].

### 2.3.4 Heat release rate

Heat transfer mechanisms are critical metrics in fire growth, typically quantified by the heat release rate (HRR). HRR is a function of the mass loss rate or burning rate and is often expressed as a quadratic function of time [94]. This metric is challenging to quantify in complex scenarios, such as compartment fires, due to the numerous factors that must be considered, including the fuel load within the compartment and the available ventilation. Currently, HRR measurement methods are largely empirical and based on assumptions [95]. However, advancements have been made using AI methods to improve accuracy and reliability in estimations.

In 2018, Li et al. employed image processing coupled with inverse modelling to estimate key parameters of pool fires along with estimating the HRR, where non-flame elements were filtered out. However, this method had limitations due to the uncertainties introduced by the inverse solution, with specific uncertainties in the empirical

equations. Additionally, image processing struggles to handle multiple fires simultaneously [96]. Bonner et al. encountered similar challenges with their computer vision (CV) algorithm, Visual Fire Power, which resulted in a 30% uncertainty in HRR estimations during validation. They suggested that this uncertainty could be reduced by expanding the range of measured data in experiments, which would inherently enhance the fundamental understanding of fire dynamics [97].

In 2022, Chi et al. used physics-informed neural networks (PINNs) to predict the HRR of premixed flames, specifically $NH_3 - H_2 - Air$ mixtures. The training data for the PINN was generated through numerical simulations across various equivalence ratios [98]. In the same year, Zhou et al. trained and tested different machine learning (ML) algorithms, including a support vector machine (SVM), multiple linear regression, and NN's. Their findings indicated that the regression model was the most effective for predicting HRR, offering a good balance between computational complexity and accuracy [99].

In 2023, Wang et al. published two studies focused on estimating the HRR of fires using deep learning methods, specifically convolutional neural networks (CNNs). The first study utilised the NIST dataset of fire calorimetry, which included approximately 70,000 images labelled with their respective transient HRR, covering both lab and real-life scenarios, where the predictions of the model are shown in Fig 2.9 [100]. The second study employed a pre-existing deep learning framework, YOLOv5, trained on the same dataset. Both models performed with an error range of 15-20%, contributing significantly to the field of smart firefighting [95].

The most recent study, conducted by Rivera et al. in late 2023, tested an ensemble of ML algorithms—including linear regression, SVM, KNN, decision trees, random forests, gradient boosting, and NN's—to predict the critical heat flux of solid fuel ignition, a key metric for quantifying flammability. The decision tree, gradient boosting, and KNN algorithms performed best when predicting values compared to the literature, while the NN excelled in predicting outcomes for scenarios the model had not previously encountered [101].

Current research in combustion fundamentals often overlooks optimising deep learning models, particularly when it comes to tuning hyper-parameters, which is crucial for minimising generalisation errors. To address this issue, training these models on larger and more diverse datasets could significantly improve accuracy and reduce overfitting.

However, a major challenge is the limited availability of such data in the public domain. This highlights the need for large, centralised datasets, like those provided by NIST, to support the development and refinement of deep learning models in the field.

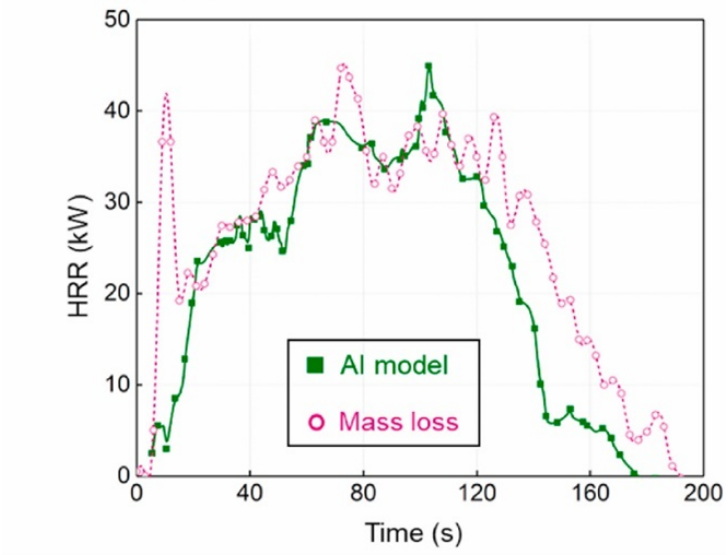



**Figure 2.9** – A comparison between transient heat release rate prediction (AI), compared to calculation based on instrumentation measurements by Wang et al [95].

## 2.4 Applications of AI: built environment

### 2.4.1 Building fires

Building fires are critically important due to their relevance across the built environment, from residential buildings to high-rise structures with large open-plan office spaces. The first pioneering study in this area was published in 2002 by Hansen et al., who developed a model to predict the time to flashover in a room corner during an ISO 9705 test [102]. Flashover refers to the transition of a growing fire into a fully developed stage, where all fuel within a compartment is burning. Hansen et al. utilised statistical methods to identify key relationships between factors such as heat release rate, time to ignition, and smoke concentration, all of which are critical in predicting flashover. Similarly, Dexters et al. also applied statistical modelling, including regression techniques, successfully, with both studies serving as proof-of-concept demonstrating that AI can be effectively applied using simple approaches [103]. Building on these foundations, Li et al. increased the complexity by integrating image processing with a generative adversarial

network (GAN) to predict flashover in compartment fires, with an example in Fig 2.10. Their approach transformed standard images into infrared images to predict temperature localisation [104]. Other studies followed, incorporating methods such as convolutional neural networks (CNN) trained on various fire parameters within compartments, support vector machines (SVM) trained on temperature data, and explainable ML algorithms for creating classification maps of fire behaviour inside compartments. These models all achieved 90% accuracy on unseen data [105–108].

In 2003, Lee et al. became the first to apply NN to predict the thermal interface location in compartment fires, an approach further developed by Yuen et al. in 2006. Both studies addressed the challenge of noisy data and achieved accuracy comparable to computationally expensive methods like Computational Fluid Dynamics (CFD) [109, 110]. Hodges et al., in 2019, advanced this research by employing CNNs trained on larger datasets, achieving a higher accuracy compared to earlier studies. However, they emphasised the need for further research to incorporate physical parameters into the model [111].

In 2020, Lattimer et al. used a CNN to simulate fires by integrating physical principles, creating a high-fidelity model that addressed the research gap mentioned by Hodges et al. Their model was validated against CFD, showing that the CNN provided comprehensive predictions at significantly faster speeds [112].

In 2021, Yang et al. employed a GAN to enhance fire segmentation in warehouse buildings. They tested their model against state-of-the-art deep learning frameworks like U-Net and demonstrated superior performance [113].

In 2022, Buffington et al. developed their own deep neural network called Brain-STORM, a surrogate model for their CFD-based Fire-STORM system. Brain-STORM successfully simulated transient fires in high-rise buildings, delivering results 100 times faster than Fire-STORM while accurately quantifying the heat release rate [114].

The most recent study, conducted by Chen et al. in 2023, utilised a Bayesian probabilistic NN to assess fire risk in historical buildings. Their model was trained using expert knowledge, historical data, logical relationships, and empirical equations, alongside fire protection and design codes from China. The results indicated that the model performed most accurately for buildings with wooden structures and brick-wood combinations, with accuracy varying based on the building's use [115].

AI has demonstrated that when trained on large, diverse datasets, it can not only outperform conventional methods but also do so more efficiently, offering faster and more cost-effective solutions. Future research could build on this approach by applying it to a wider range of scenarios, such as various building configurations and fire dynamics, further enhancing the potential of AI in complex simulations and applications in the built environment.



**Figure 2.10** – (a) shows the building fire before flashover (b) shows the room in flashover attempting to be controlled by firefighters with flames protruding from opening, given by Li et al [104].

### 2.4.2 Fire detection

Fire detection and monitoring is typical through sensors, such as thermal, smoke, or gas sensors. These are essential for notifying building occupants and alerting emergency services or first responders. In many cases, these sensors also activate fire suppression systems. However, a common issue is the occurrence of false detection's and delayed response. To minimise these problems, the integration of advanced technologies, such as AI, is increasingly being introduced. AI can enhance detection accuracy by analysing sensor data more effectively, reducing false alarms, and improving the overall reliability of fire detection systems. The same applies in the natural environment and smoke detection.

The pioneering work on early fire detection began in 1991 with Okayama, who used a neural network (NN). This was the first study to apply deep learning in fire detection, though serving as a proof-of-concept, approximating fire characteristics rather than providing precise measurements [44]. Subsequent studies expanded on this concept, integrating NN's with sensor data for enhanced detection [116–118].

In 1996, McVoy et al. applied principal component analysis (PCA) in combination with sensor signals to detect flaming, smouldering, and nuisance sources. This approach demonstrated greater accuracy than conventional fire alarms, though it was limited by false alarms [119]. Further research by Milke in 1999 and 2003 explored fire signature monitoring using the same PCA method. Milke's studies tested fire detection in naval ships, conducting 137 different experiments on the same sources as McVoy. The results showed improvements in fire monitoring and detection time compared to the work in 1996, enhancing the field of fire detection [120, 121].

In 2003, Rohse-Pehrsson et al. introduced a probabilistic NN for early fire warning systems, using an array of sensors. This method was a direct advancement over Milke's 2003 work. However, challenges arose, particularly with detecting smouldering fires. Many studies expanded on this by using convolutional neural networks (CNNs), which are specialised NN's trained on image data. These studies typically trained their models on large datasets—as many as 12,000 images. The detection accuracy ranged from 97% to 99%, though it dropped to 86% in extreme fire scenarios, highlighting the need for varied and extensive training data to ensure high accuracy in all conditions [122–125].

In 2006, Marbach et al. used image processing, specifically YUV colour thresholding, to detect fires by analysing flame characteristics [16]. Similar studies employed image processing using colour spaces like RGB and YCbCr to segment fires and detect motion and flickering between frames, as image processing analyses frames sequentially. While these methods are computationally simpler and less complex than NN's, they remain effective for simple fire scenes [126–129].

In 2008, Ko et al. developed a fire detection system using a support vector machine (SVM) classification algorithm coupled with a vision sensor, which successfully detected smoke and fire. This same method was later applied by Baek et al. [130–132]. Ko et al. expanded their study by implementing a Bayesian NN to address the irregular patterns observed in their earlier work, resulting in a 6-23% improvement in accuracy [133].

In 2015, Kong et al. employed logistic regression with temporal smoothing to enhance fire detection in surveillance videos, aiming to reduce the high false positive rates common with traditional detection methods. Their model was trained on features such as size, motion, and colour [134]. Meanwhile, Mondal et al. developed a computer vision-based system for automatic fire detection, achieving a true accuracy rate of 92% and a false

positive rate of 8%. They demonstrated an improvement over other studies, validating their model through small lab-scale experiments [135].

In 2020, Liu et al. transfer learning for fire detection in community buildings, achieving an 89% detection accuracy, surpassing other models such as FastText and ULMFiT. Their model required only half the training data compared to other methods, highlighting the strength of transfer learning and its application to smart fire safety systems [136].

By 2022, fire detection methods had advanced further. Jana et al. used an ensemble of ML algorithms with multi-modal sensor data, including logistic regression, SVM, decision trees, and a naïve Bayes classifier. They trained their models on the NIST fire scene database, demonstrating improved accuracy over previous studies [137].

In 2023, Wu et al. became the first to implement the state-of-the-art pre-trained deep learning neural network YOLOv5 for real-time video fire detection and monitoring. They incorporated feature extraction techniques, significantly outperforming previous models with a detection accuracy of 98% and faster processing times [138]. Similar studies that utilised YOLO achieved comparable results [139]. In 2024, Dou et al. further improved fire detection by employing YOLO architecture alongside object detection algorithms such as MobileNetV3, ShuffleNetV2, and GhostNet. Their study demonstrated more robust fire detection capabilities, even in cases of irregular smoke and flame colour variations as given in, Fig 2.11 [140].

In conclusion, while many fire detection algorithms have been developed, often coupled with sensors for the built environment, false detection's remain a significant issue. To address this, models should be trained on a variety of fire scenes, including smoke and other irregularities coupled with an array of sensors. Image processing remains a common method due to its simplicity and quick setup but lacks automation compared to other methods such as CV and pre-trained deep NN frameworks like YOLO which are the best performing for detection and monitoring as it can be applied real-time. Future work should explore integrating image processing with YOLO or CNNs to improve fire detection accuracy and robustness.

### 2.4.3 Tunnel fires

In 2005, Ono et al. were the first to employ artificial intelligence (AI) for detecting car fires in tunnels using neural networks (NN). They implemented colour thresholding via




**Figure 2.11** – YOLOv5 deep neural network architecture for detection of fire in different scenes, which can distinguish between smoke and a fire by Dou et al [140].

image processing to identify fires and extracted features to train the NN, demonstrating successful detection capabilities. While this study served as a proof-of-concept, it highlighted the need for further development to improve detection range and the ability to detect smaller fires in tunnels [141].

In 2009, Han et al. also utilised image processing to support a real-time detection system for flames and smoke in tunnel fires. Their approach involved segmenting algorithms to detect flames based on colour range and motion detection. Validation against experimental results showed good agreement, contributing to real-time tunnel fire monitoring [142].

In 2020, a study by Wu et al, employed a long short-term memory (LSTM) framework to create a smart detection system for tunnel fires. This model was trained on temperature data from sensors, with a prediction accuracy of 90%. The system could quantify the fire power and the location [143].

In 2022, Sun et al. published two studies focused on predicting ceiling temperatures in tunnel fires using NN. Their models were applied to large-scale experiments and compared to China's tunnel fire experiment platform, successfully predicting ceiling temperatures

and offering an alternative to traditional ceiling temperature measurement methods [144, 145]. In the same year, Hong et al. used various machine learning models to predict smoke movement in tunnel fires. They trained models, including random forest (RF), support vector machine (SVM), and a NN, on 1,000 unique cases with varying thermal and geometric conditions. Air velocity identified as the most crucial factor influencing smoke movement in the tunnel with the SVM and RF being the best models [146].

The most recent studies in this field include one by Guo et al. in 2024, which utilised a transformer-based deep learning model to predict the full-field temperature distribution in tunnel fires, trained on ceiling flow temperature data. The model demonstrated a prediction range of up to 750 meters, representing a 19% improvement over a previous LSTM model [147]. Also in 2024, Zhang et al. employed computer vision to assess real-time risk in tunnel fires and evaluate potential evacuation safety parameters by monitoring tunnel exit and entry flow. Vehicles were identified as a key parameter due to their potential as fuel loads and contributors to heat release rates in the event of a fire, with the model training and validation plot given in Fig 2.12. The study used YOLOv7, a pre-trained deep learning framework, for vehicle detection and classification, with potential applications in existing and future tunnels, as well as in train stations, car parks, and industrial facilities [148].

### 2.4.4 Evacuation

The first significant study on evacuation modelling during fire scenarios was conducted by Lo et al. in 2008. They utilised a neural network (NN) to predict human responses during domestic building fires. Modelling human behaviour in such situations is inherently difficult due to its unpredictability, driven by randomness and uncertainty. Understanding human reactions during fire evacuations is crucial for designing effective fire safety strategies and improving building design. Evacuation modelling is often referred to as a "black box" because human behaviour cannot be easily validated or predicted with certainty [149].

In 2019, Wang et al. expanded on this work by predicting pedestrian movement dynamics during emergency evacuations, including fires. They employed an ensemble of machine learning (ML) models, with the neural network performing best in complex scenarios. However, given the unpredictability of human behaviour, this remains compu-

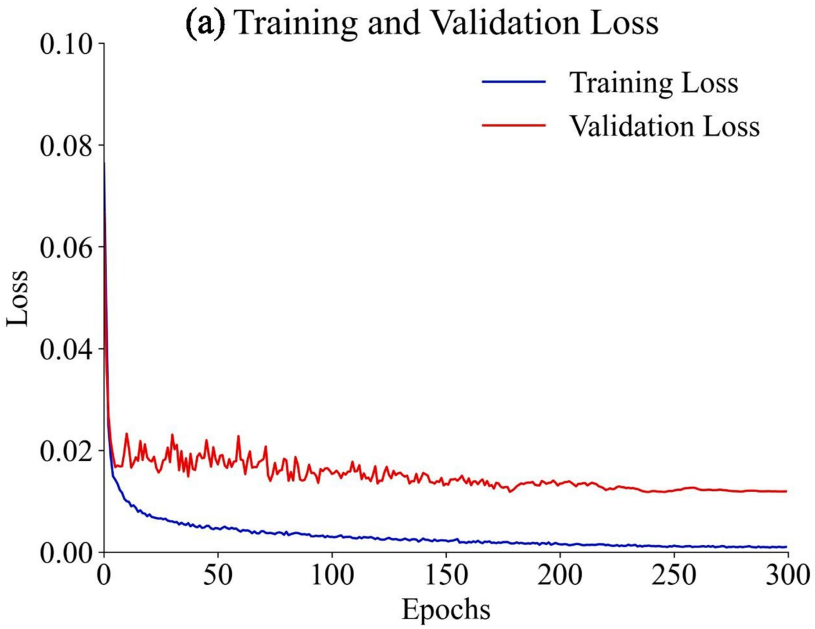



**Figure 2.12** – Training and validation curve of Zhang et al showing that the model could potentially overfit, which can be prevented by early stopping, dropout layers and adding more data [148].

tationally challenging, and different models may be better suited to different evacuation scenarios. Wang et al. identified key parameters influencing human behaviour, such as the distance to exits and the actions of other individuals, with an example of their evacuation study given in Fig 2.13 [150]. In the same year, Sanctis et al. adopted a Bayesian approach for data collection to inform future model training. They noted a significant limitation in fire evacuation research: the scarcity of publicly available fire data, which leads to overfitting and poor generalisation in many models [151].

The most recent study, conducted by Balboa et al. in 2024, used an ensemble of ML algorithms trained on data from 1,807 participants, like Wang et al in 2019. Their findings indicated that a simpler model, specifically regression, achieved the highest accuracy at 83%. This again highlights that more complex models are not always necessary or optimal [152].

Evacuation modelling presents significant challenges, primarily due to the complexity of human decision-making. Human reactions are inherently difficult to quantify, making it challenging to create reliable datasets where predicted outcomes align with real-world behaviour. Despite these difficulties, studies in this area are crucial for improving future building designs and enhancing evacuation strategies in fire scenarios.

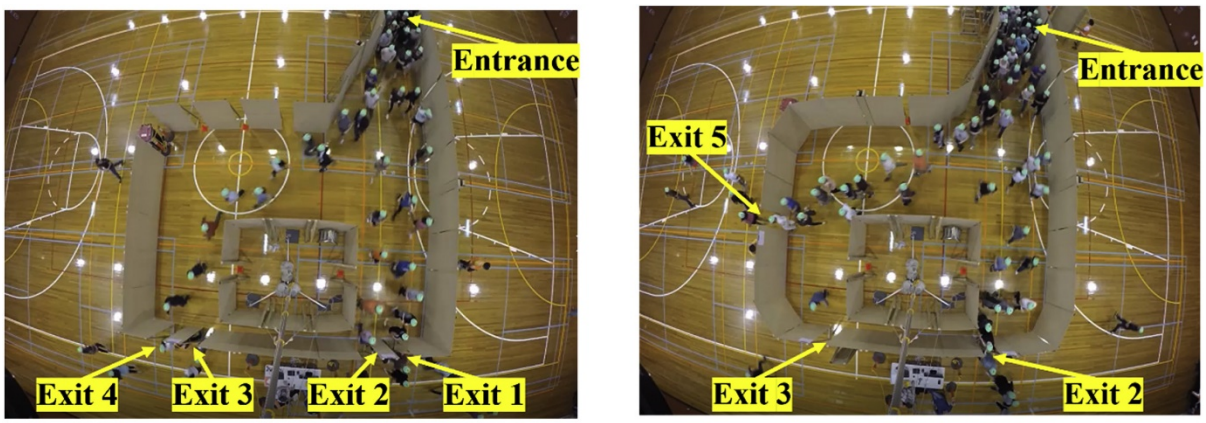



**Figure 2.13** – Evacuation spatial layout of the experiment by Wang et al, showing the entrance and different exits in different scenarios [150].

### 2.4.5 Smoke

The first application of AI in the built environment for smoke detection was pioneered by Chunyu et al. in 2009, who utilised image processing to segment smoke and train a neural network (NN) for classification. Their model successfully distinguished between smoke and non-smoke scenarios, representing a significant advancement over previous methods and demonstrating the feasibility of AI in smoke detection, Fig 2.14, showing the optical tracking of the smoke [153].

Building on this, Yuan et al., in 2011, improved smoke detection by employing histogram sequencing in video data to train a NN, which performed well across various scenes, including those with variable illumination and video rotation. Their model was validated experimentally and demonstrated robust performance [47]. Similarly, Ye et al. used a different machine learning (ML) approach, combining a hidden Markov tree with a support vector machine (SVM) for smoke classification in videos. Their model achieved high precision and suggested that combining multiple models, such as NN, Bayesian methods, and Adaboost, could further improve detection accuracy, validating previous work [154]. In the same year, Kim et al. developed a real-time smoke detection model using a Bayesian classifier for firefighting robots in buildings. This system processed thermal images and utilised 76,000 data points, achieving an error rate of 6.8% [155].

In 2018, Alamgir advanced this research by integrating RGB image processing with a fuzzy c-means algorithm to train an SVM. His method demonstrated 92% accuracy across diverse environments with varying illumination conditions, outperforming other

techniques tested on the same dataset [156] . Further progress was made in 2020 by Li et al., who introduced a convolutional neural network (CNN) for real-time smoke detection in live video. Their model tackled challenges like colour brightness and background noise using dark channel dehazing and Gaussian mixtures, outperforming earlier methods in accuracy [157].

In 2021, Huang et al. utilised a generative adversarial network (GAN) for smoke removal in images, a novel approach compared to previous smoke detection models. Their GAN-based method generated training images and excelled at smoke segmentation, surpassing state-of-the-art techniques such as CNN's [158].

The trend of using CNNs continued in 2022 with Huo et al., who developed a real-time object detection model based on both static and dynamic features, achieving 99% accuracy on unseen data [159]. Cheng et al. (2023) built upon this with a hybrid model combining a CNN and an enhanced vision transformer for smoke recognition. Their model was validated with experimental data and achieved similar accuracy reinforcing the effectiveness of advanced NN's in smoke detection [160].

Over time, advancements in AI have shifted from basic image processing techniques to more sophisticated deep learning methods for smoke detection in the built environment. Modern approaches focus on training a NN directly, reducing the need for preprocessing with image processing. Although real-time smoke detection has become increasingly viable, one limitation remains—the significant data storage required for these applications, particularly in both fire and smoke detection contexts.



**Figure 2.14** – Optical flow (movement) tracking of the smoke by Chunyu et al [153].

### 2.4.6 Structural engineering

The first study to address structural engineering problems using AI was conducted by Al-Khaleefi et al. in 2001. This research utilised neural networks (NN) to predict the fire resistance of concrete-filled tubular steel columns. The NN was trained on experimental data from fire resistance tests and achieved predictions with an average error of 8.5%. This pioneering approach provided structural engineers with a cost-effective solution for fire resistance predictions [161]. Following this, several other studies employed NN's for fire resistance testing, with some integrating ensemble methods such as support vector machines (SVM) and regression models. These were applied to various use cases, including predicting the charring rate of timber, composite shallow floor systems, gypsum plasterboard walls, intumescent flame-retardant coatings, and the behaviour of exposed reinforced concrete columns. Each of these studies contributed to improving fire safety strategies by enabling more accurate structural calculations alongside design codes and prescriptive design [10, 162–166].

Xu et al., in 2012 and 2013, published two papers where they applied similar NN's to different structural fire engineering problems. In the first study, they predicted the load-bearing capacity of tubular T-joints in fire, while the second study focused on forecasting the temperature of tubular trusses in fire. Both NN's were trained on simulated data from ABAQUS and demonstrated accurate predictions with examples of their FEM model with respective to the experiment given in Fig(s) 2.15 and 2.16 [167, 168].

In 2019, Abbas et al. employed NN's to predict the residual strength of high-strength concrete (HSC) when exposed to elevated temperatures. Unlike earlier studies that relied solely on raw experimental data, this work trained the network on relationships between key parameters. The results indicated that a single-hidden-layer NN was the most accurate, suggesting that more complex, multi-layer networks are not always necessary [169]. Other studies on residual strength have utilised different algorithms, including recurrent neural networks (RNN), long short-term memory (LSTM), SVM, random forest (RF), and regression models, highlighting the versatility of approaches available for this problem and structural engineering [170–172].

In 2022, Karaki et al. adopted probabilistic regression models to predict the temperature properties of construction materials in fire tests. They compared to models from other literature including an ANN, showing good agreement, validating their re-

search. Probabilistic regression are less complex than NN's and thus showing that NN's are not required where regression can perform the same task with similar accuracy [173]. In contrast, Kim et al. (2023) employed an LSTM model to predict spatio-temporal temperature data in piloti structures. The model was validated against Computational Fluid Dynamics (CFD) methods, demonstrating the efficacy of advanced AI techniques for structural fire analysis [174].

The most recent advancement, in 2024, came from Sun et al., who explored a novel approach for forecasting the behaviour of industrial cables in fire. They employed a pre-trained deep learning framework based on the YOLOv8 architecture to segment fire scenes, improving upon previous studies that used YOLOv5, whereby this method can also be used for flame detection [175].

The structural engineering literature offers a wide range of AI methods for addressing fire-related challenges, primarily focused on traditional construction materials like concrete. However, there is a notable lack of research on sustainable materials, such as mass timber, particularly as the construction of high-rise mass timber and hybrid buildings is on the rise. This gap in the research is addressed in this thesis, with a focus on the behaviour of mass timber in fire conditions. Additionally, the complexity of structural engineering problems is far greater compared to areas like fire detection or tunnel safety, due to the many interconnected components within the built environment. This complexity allows for the application of a broader array of AI techniques in structural engineering, whereas fields like detection are more limited, with vision-based methods being the most effective.

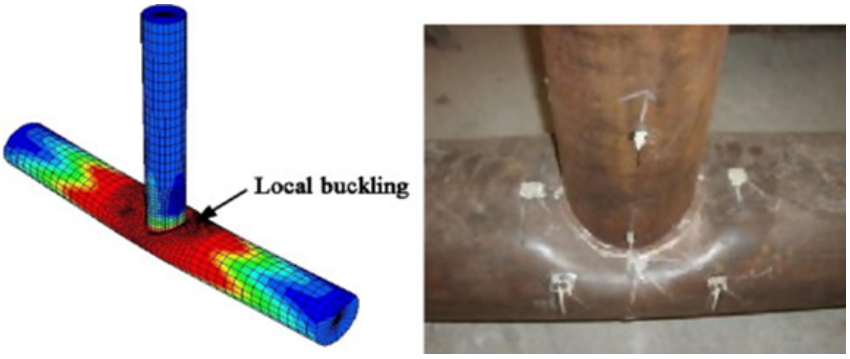



**Figure 2.15** – Xu et al shows the comparison of failure mode of tubular t-joint in a FEM model and experiment before training the neural network [167].

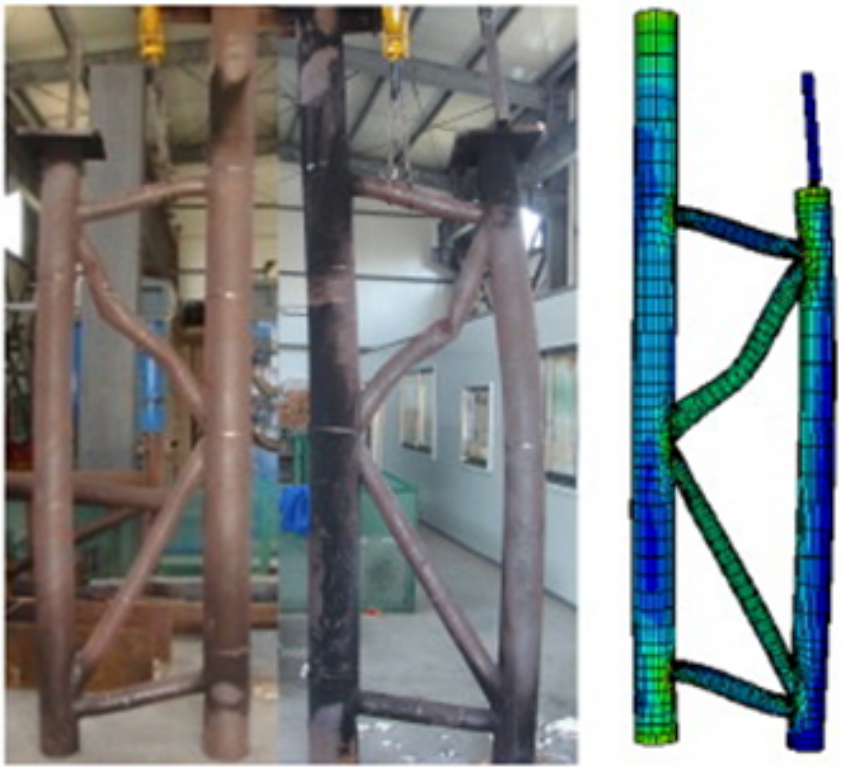


**Figure 2.16** – Xu et al shows the comparison of failure mode of a steel planar tubular truss in an experiment and the FEM equivalent before neural network training [176].

## 2.5 Applications of AI: natural environment

### 2.5.1 Wildfire dynamics

Pioneering work in wildfires began in 2006 with Dios et al., who employed image processing techniques to assess spreading fire fronts using visual cameras. They extracted wildfire parameters such as shape, spatial position, and inclination angle, from which the rate of spread was validated in a laboratory setting using pine needles, demonstrating potential for field applications [177]. Similar studies have also modelled the rate of spread using more advanced methods, including neural networks (NN), convolutional neural networks (CNN), long short-term memory (LSTM) networks, support vector machines (SVM), and naïve Bayes [178–182].

The next significant contribution came in 2009 from Catry et al., who used logistic regression to predict the likelihood of ignition occurrences and created an ignition map for mainland Portugal. The model incorporated factors such as population density, human accessibility, land cover, and elevation, showing potential applications for wildfire management [183]. Similar studies have applied this approach to different locations, in-

cluding southern California, Central America, Brazil, and India, using models such as random forests, SVM, k-nearest neighbours (KNN), and NN [22, 184–188].

In 2012, Bisquert applied NNs coupled with logistic regression to predict wildfire danger to communities in Galicia, Spain. The model was trained on the MODIS dataset, with inputs such as land surface temperature and vegetation index, aiming to enhance wildfire prevention and suppression [189]. Another study conducted in Spain used data from 1991 to 2005 with logistic regression and regression trees to identify correlations between predictions and various factors, including climate, topography, and vegetation, similar to the work by Bisquert et al [190].

In 2019, Botequim et al. used classification and regression trees (CART) to study wildfire behaviour based on canopy fuel characteristics [191]. Similarly, Bergardo et al. in 2020 employed a more complex method, AllConvNet, a type of CNN, to analyse wildfire data over a seven-day period in Australia. Bergardo's model outperformed other methods such as regression and SegNet, achieving greater predictive accuracy [192]. Future work should focus on data that includes spot ignition in different locations.

In 2020, Coffield et al. used decision trees and random forests to predict the final size of wildfires at the time of ignition. They successfully predicted 40% of ignitions that led to large-scale wildfires and 75% of the total burned area, offering a strong proof-of-concept for insights into wildfire movement [193].

In 2021, Capps et al. used random forests to model fuel moisture content across California, training the model on high-resolution weather data and comparing it with field observations, which demonstrated good validity [194]. Similar studies expanded on this work by employing more complex methods, such as temporal NNs and CNNs, to predict and automatically classify fuel types like grasses, shrubs, and timber, as well as their moisture content, in some cases over a three-month period [195, 196].

In the same year, Phelps et al. used an ensemble of machine learning algorithms, including NN, CART, random forest, logistic regression, and logistic generalised additive models (GAMS), to predict wildfire occurrences in Alberta, Canada, using historical data from 1996 to 2016. The GAMS model was found to be the most interpretable [197]. This research was further developed in 2023 by Quan et al., who used a random forest model to predict the probability and effects of unburned fuels, specifically trained on data from Yunnan province, China, from 2001 to 2020 [198, 199].

In 2023, Trucchia et al. employed random forest modelling, trained on 10 years of wildfire data from the eastern Mediterranean landscape, to create wildfire hazard maps. This approach effectively classified fire intensity and hazards based on environmental factors and successfully distinguished between different climates and vegetation types across various landscapes [200].

In the same year, Wang et al. coupled large eddy simulations (LES) with deep learning for physical simulation of large-scale wildfires, focusing on combustion representation. Their results, which estimated spread rate and burned area, showed good agreement with experimental data [201].

The most recent study, conducted by Cullen et al. in 2024, utilised simple regression techniques, including logistic and linear regression, to characterise ignition in collaboration with wildland fire personnel. The model identified key factors such as fire location, weather conditions, canopy cover, wildland-urban interface (WUI), fuel characteristics, and human movement, with Fig 2.17 representing the framework of the main drivers [202].

In conclusion, wildfire modelling has progressed with AI techniques, primarily using random forest and CNNs. Future research should focus on improving these methods by incorporating physical models, as wildfires are complex phenomena influenced by various factors, including diverse climates and the varying complexities of vegetation. Integrating physics-based approaches with AI could enhance the accuracy and robustness of wildfire prediction across different environmental conditions.

### 2.5.2 Wildfire detection

Wildfire detection using artificial intelligent (AI) techniques began in 2008 with Celik et al., who utilised image processing, specifically the YCbCr colour space, to detect natural fires in videos. This method achieved a 99% detection rate, demonstrating strong potential for real-time detection [45]. Gunnay et al. expanded on this work by incorporating least mean squares and a Markov model to detect flame motion and boundaries [203].

The application of AI in this field was further advanced by Fernandez-Berni et al. in 2012, who used computer vision (CV) for early wildfire detection. They validated their method across different wildfire scenarios, achieving a low false alarm rate [204]. A similar study also employed CV and recommended that a centralised wildfire detection database be developed and expanded over time through ongoing research, with Fig 2.18

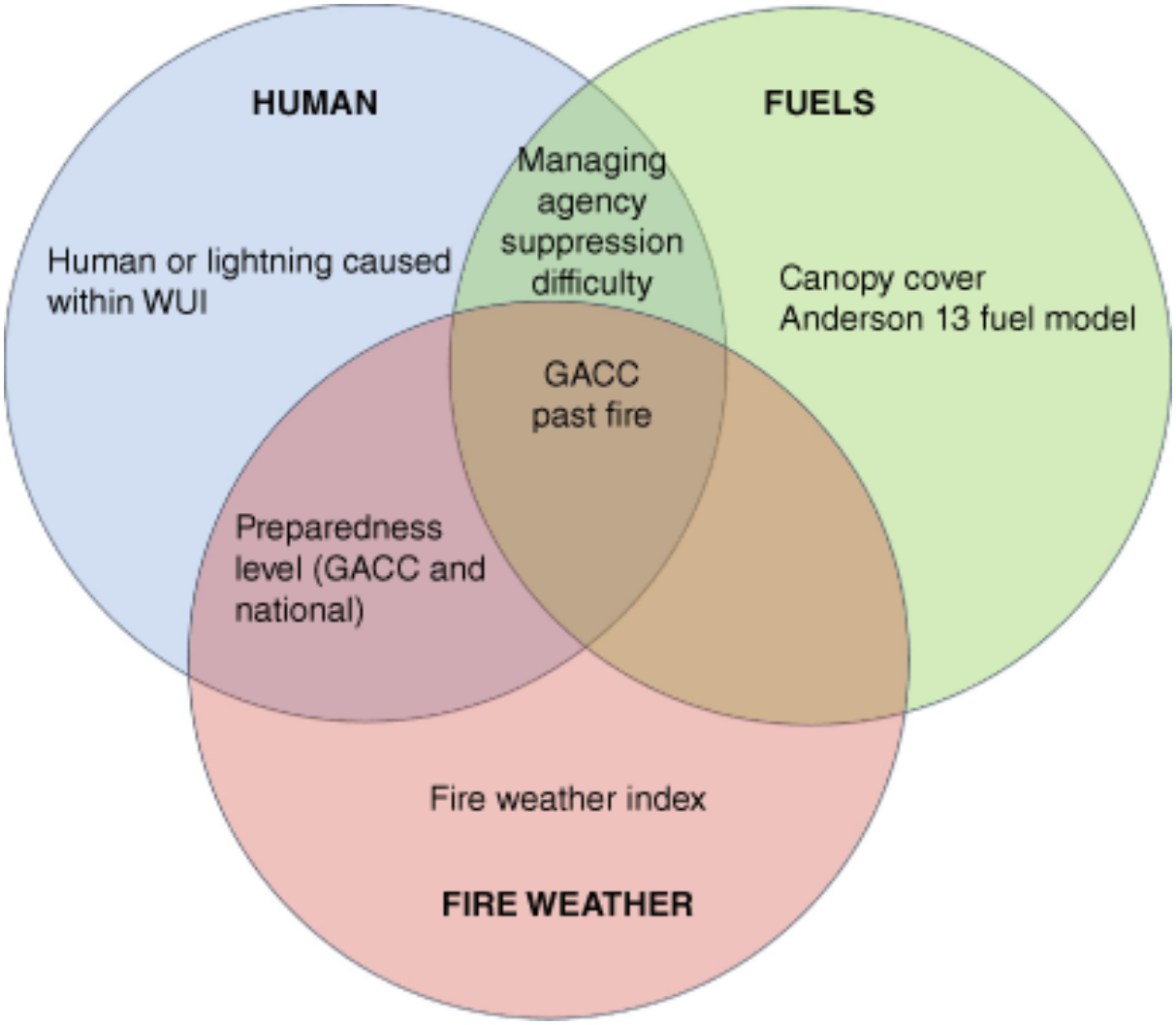



**Figure 2.17** – A Venn diagram representing drivers of personnel use that are observed during time of ignition by Cullen et al [202].

showing the different stages of the detection and segmentation [205].

In 2016, Prema et al. used image processing combined with feature analysis, a computer vision algorithm, for early wildfire detection, employing the YUV colour map to segment the spatial and temporal features of smoke from wildfires. They used a support vector machine (SVM) to classify different regions [206]. This study was further expanded in 2017, when they implemented an extreme learning machine (ELM) instead of an SVM, resulting in an improved detection rate of 96%. This method demonstrated the ability to classify wildfires across different scenarios [207]. That same year, Qui et al. employed a hybrid algorithm combining image processing and temporal smoothing to enhance detection rates. While this method proved effective for early wildfire detection, it also had high computational costs, highlighting the need for future research to focus

on an integrated wildfire detection approach [208].

In 2020, Khalil expanded upon previous work by employing a multi-colour space approach using RGB and L*a*b* colour spaces along with a motion detection algorithm. They also calculated the rate of wildfire growth to assist in motion detection validation, achieving an average detection rate of 97%, significantly higher than previous studies [209].

In 2023, the field saw significant advancements with the implementation of state-of-the-art, pre-trained deep learning frameworks. Zhou et al. used YOLOv5, for detecting multi-scale wildfires, trained on ground and UAV data to enhance model variability and reduce generalisation. This model achieved an accuracy of 94% [210]. Similar studies in 2024 further YOLOv5 for wildfire detection by integrating different pooling methods such as ASPP, SPP, and CBAM, or combining it with other architectures like MobileNetV3, achieving detection rates of around 93% [211, 212].

In conclusion, advancements in wildfire detection have transitioned from traditional image processing techniques to more sophisticated AI-based methods, particularly with the use of deep learning frameworks like YOLO. However, the pioneering work remains foundational for any future developments, as it demonstrated the highest detection rates for natural fires. Future research should prioritise enhancing model robustness and scalability, especially by integrating multiple architectures and utilising larger, more diverse datasets in natural environments however available datasets are a known issue in the field. This will improve the effectiveness of wildfire detection systems and their applicability in real-time monitoring.



$(a)$ $(b)$ $(c)$

**Figure 2.18** – A representation of the different stages of the detection. (a) represents the base image. (b) represents grey-scale of the flame in the scene. (c) represents binary image of the flame in the scene by Toulouse et al [205].

### 2.5.3 Wildfire evacuation

Evacuation is the most critical aspect of any wildfire event due to the inherent risk to human life. In natural environments, evacuation strategies become even more crucial, as they can greatly influence how quickly people reach safety. Unlike wildfire modelling, evacuation requires a different approach due to the complexity of predicting human behaviour, as previously discussed in this study on evacuations in the built environment.

While evacuation models exist, they are often computationally time-consuming to run. One of the earliest AI tools for evacuation modelling was introduced by Katzileris et al. in 2022, where they used random forest and logistic regression models to analyse human evacuation behaviour during wildfires. The data was gathered through field surveys from individuals who had experienced wildfire events, with significant factors such as age, length of residence, and the presence of minors or elderly individuals influencing decision-making. In this study, the random forest model outperformed others due to its capability to manage binary inputs effectively [213].

In 2023, Xu et al. utilised an ensemble of machine learning models, including support vector machines (SVM) and neural networks (NN), to predict wildfire evacuation behaviour. The classification and regression tree emerged as the best-performing model, with the study identifying the perception of fire safety as the most influential factor in decision-making [168].

Future research in evacuation modelling should prioritise the development of larger datasets to improve model training, given the complexity of human behaviour and the issue of multicollinearity, where many variables are interrelated. Alternatively, AI can be leveraged to accelerate existing simulation methods, allowing for more efficient modelling of evacuation scenarios.

### 2.5.4 Wildfire smoke

The first significant study of smoke detection in the natural environment, specifically for wildfires, was carried out by Gubbi et al. in 2009. They used a support vector machine (SVM) to test various wildfire scenarios, demonstrating high accuracy with a 90% validity rate, with Fig 2.19 indicating the smoke movement detection in the scene through a grid [214]. Similar studies have also utilised SVM for smoke detection, particularly in

open and large areas for smoke alarm systems, achieving strong performance [215].

In 2017, Pundir et al. employed a deep belief neural network (NN) for smoke detection in wildfires, training on 10,000 images. The network identified smoke based on its colour, motion, and texture, achieving a classification accuracy of 97% [216]. They later expanded this study by coupling the NN with an SVM and training it on 20,000 images, which improved the accuracy to 99% [217].

In 2019, Gao et al. developed a smoke diffusion model to detect wildfire smoke using computer vision algorithms. They applied background extraction to identify stable smoke points in consecutive images and compared them with original images with only 10% false positives [218]. In the same year, Lin et al. used a convolutional neural network (CNN) for smoke detection. They trained the network on various wildfire scenes to introduce variability, resulting in a 95% detection rate, particularly excelling at smoke localisation and recognition. However, they noted the need for additional training data to prevent overfitting—a common challenge in AI applications—and reduce false positives in smoke detection [219]. Other studies have also reported this [220].

In 2022, Huo et al. introduced a multi-scale object detection algorithm called CSP-Darknet53, a pre-trained CNN architecture used for wildfire smoke detection. When compared to other state-of-the-art architectures, such as YOLO, CSPDarknet53 had a low false positive rate of 1.7%, outperforming other networks [221]. That same year, Cheng et al. also utilised a CNN to identify wildfire smoke at the pixel level, achieving a detection rate of 98% [222], Prema et al., however, took a simpler approach, using image processing techniques and an extreme learning machine for wildfire smoke classification and detection. They used the YUV colour space to segment smoke, reaching an overall classification accuracy of 95% [223]. Their study demonstrated that simpler methods could achieve accuracy levels comparable to more complex AI architectures.

In conclusion, the most effective method for wildfire smoke detection is the use of pre-trained, state-of-the-art NNs. However, when training standalone CNNs, it is crucial to apply large datasets with considerable variability, as smoke is a complex phenomenon. AI is generally more suited for smoke detection rather other modelling approaches due to the complexity of defining the physical parameters in a black-box approach. Nonetheless, AI can be employed to accelerate current methods and smoke models, reducing computational time and cost.

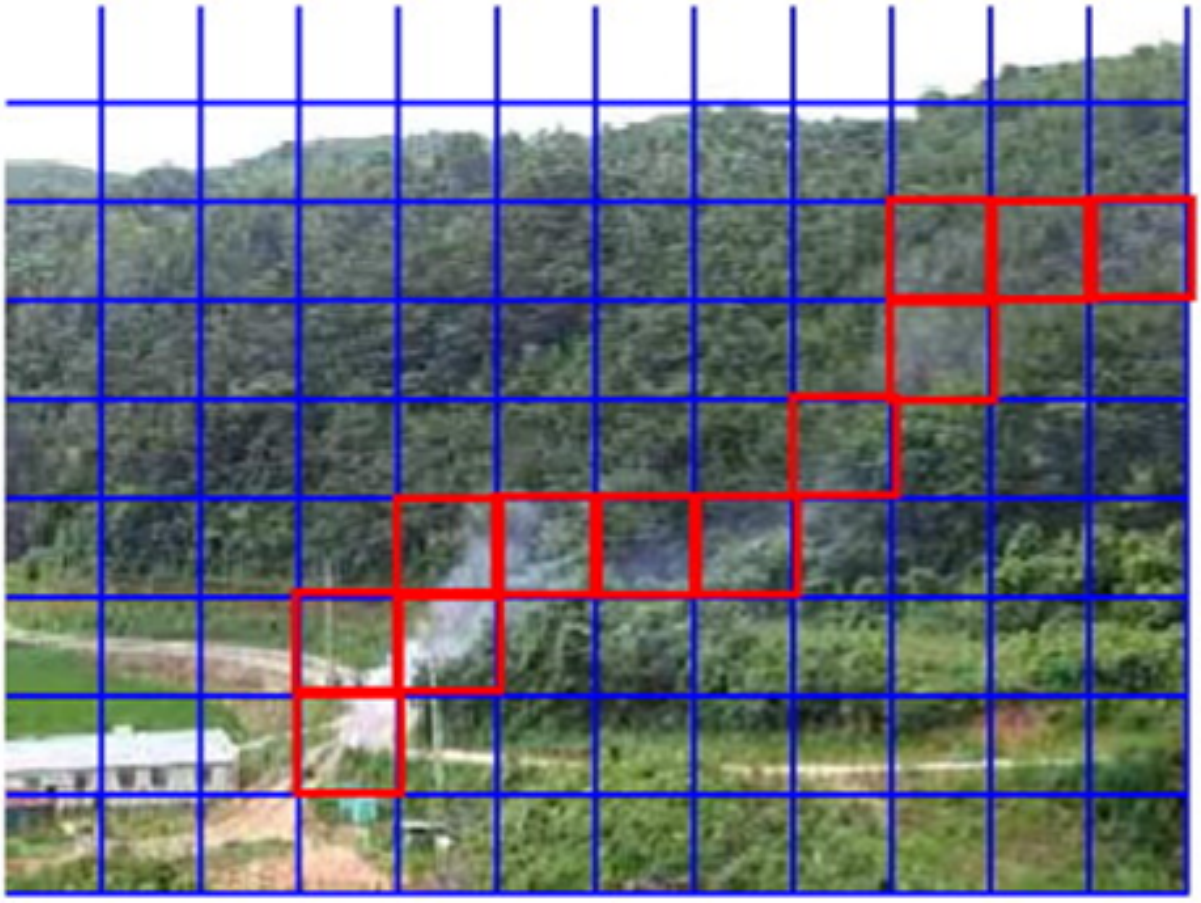


**Figure 2.19** – Represents the grid split of the image with the red blocks indicating the smoke and blue with no smoke by Gubbi et al [214].

## 2.6 Conclusions

This chapter provides a historical review of the application of artificial intelligence (AI) algorithms to fire science and engineering with a focus on peer-reviewed fire journals, covering research from pioneering studies in 1989 through to the latest advancements in 2024. In terms of research gaps in fire science, most AI applications have focused on detection and wildfire modelling, with limited research in areas such as evacuation, buildings, and structural engineering—particularly for structures made from sustainable materials like mass timber and its behaviour in fire, which is addressed in the rest of the thesis. Although significant work has been done on traditional materials like concrete and steel columns or beams, there is a clear need for further investigation into sustainable alternatives. Different AI techniques are particularly well-suited to addressing specific fire-related challenges. For instance, deep learning techniques, such as convolutional neural networks (CNNs), are highly effective for fire and smoke detection. When combined with sensors,

these methods enhance fire and smoke monitoring capabilities for smart firefighting. However, deep learning is computationally intensive and time-consuming, and may not always be necessary when simpler, more efficient methods can achieve comparable results. For example, computer vision, which is tailored for image-based problems, often provides comparable accuracy with significantly lower computational complexity and without requiring extensive training which is utilized Chapter 5. Additionally, other algorithms, such as support vector machines and random forests, can yield similar outcomes to deep learning methods with less computational overhead specifically for classification tasks such as detection. A key issue identified in the reviewed studies is the tendency of many researchers to jump directly into utilizing complex tools, particularly deep learning architectures, without exploring intermediary methods. Future research should place greater emphasis on starting with traditional statistical techniques and gradually progressing to decision trees or ensemble methods, particularly in the context of computer vision and image processing. The increasing complexity of algorithms does not necessarily equate to improved predictions, as will be further discussed in Chapter 3 [163]. Additionally, many studies overlook the importance of model optimization, often training their models on datasets without conducting iterative tuning to mitigate overfitting and enhance generalization. These issues, and their potential solutions, will also be addressed in Chapter 3.

Overfitting is a prevalent problem in the application AI, not just in fire science but across various fields. Several optimisation methods exist, such as Bayesian optimisation and grid search, which are computationally simple and can improve model performance. However, many papers provide insufficient explanations regarding hyper-parameter tuning, even though this is a crucial aspect of using AI effectively. Another gap is the lack of interpretability of results, which can be enhanced by performing sensitivity and parametric studies. They provide insights into the degree to which different parameters impact the model's predictions, allowing for comparisons with physical understanding. If certain parameters disproportionately affect the model, it is essential to assess whether this aligns with experimental evidence and the underlying physics of the fire problem to ensure logical consistency.

A critical challenge in applying AI to fire science is the limited availability of data and the need for combining with domain-specific knowledge. Fire science is a highly

sensitive field, and the large, diverse datasets required to effectively train AI models are not yet readily accessible. Without addressing this data gap, the full potential of AI for fire applications to support smart firefighting or real-time monitoring remains limited. The above research gaps and questions are technically addressed in the rest of the thesis including the inference and explainability of these methods.

In conclusion, while AI has been successfully applied to a variety of fire-related challenges, particularly in flame and smoke detection within both built and natural environments. Despite the accuracy and reliability of these models, there are concerns surrounding the "black box" nature of AI, which raises questions about its transparency and justification, particularly when human lives are at stake. A deeper understanding of AI's role in fire safety is crucial to ensuring its responsible and effective deployment in life-critical situations.

# Chapter 3

# Charring rates using statistics and artificial intelligence

## Summary [1]

Engineered timber is increasingly in demand for tall buildings due to its positive impact on building sustainability. However, quick adoption raises fire engineering questions regarding flammability and structural performance. Understanding the behaviour of timber in fire is crucial, particularly for structural calculations of tall buildings. The charring rate of timber plays a significant role in its structural performance because the loss of cross section reduces the load bearing capacity of the element. Eurocode-5 (EC5) provides a simple method to calculate the charring rate where it is the most widely adopted for design in many countries while more complex physics-based models exist but are rarely used for design. This chapter compares different data-driven methods, including statistical and artificial intelligence (AI) algorithms, for predicting the average charring rate of timber in fire. A new database of charring rates, VAQT, was created comprised of 231 furnace tests of timber products found in the scientific and technical literature. Statistical methods such as ridge regression ($\lambda = 0.001$) predict the charring rate with a minimum 11% error whilst EC5 predicts with 27% error. A trained neural network predicts the charring rate with minimum 9% error. This chapter presents a novel database

1. This chapter is based on "R. Amin, Y. Mo, F. Richter, C. Kurzer, N. Werther, G. Rein (2024), *Predicting the Average Charring Rate of Mass Timber Using Data-Driven Methods for Structural Calculations*, **Fire Technology**, Published."

of timber charring experiments and provides a set of data-driven predictive models, all of which calculate the average charring rate with a significantly higher accuracy than EC5 for a wide range of mass timber products.

## 3.1 Introduction

Mass timber can play a crucial role in enhancing the sustainability of the building construction industry. The increasing adoption of mass timber stems from the advantages it offers over conventional construction materials such as concrete and steel are previously mentioned [1,4,5]. Unfortunately, there has been insufficient research conducted in the fire safety of tall mass timber structures and the problems that arise from its flammability, fuel load and structural strength which need to be studied further [10–13]. When exposed to increased temperatures, timber undergoes several processes; preheating, drying, charring and oxidation, as illustrated in Fig 3.1. Charring is a process also known as pyrolysis that causes thermal degradation by breaking down the polymer chains into solid char and flammable volatiles [224,225]. The boundary between the charred and uncharred layers of wood is referred to as the char-line, typically located around the 300°C isotherm [226,227]. Understanding the charring process and its rate is a crucial factor when calculating the fire resistance of timber structures, as it enables the determination of the residual cross-section and load bearing capacity of structural timber members. However, the current methods of predicting the charring process remain limited [224].

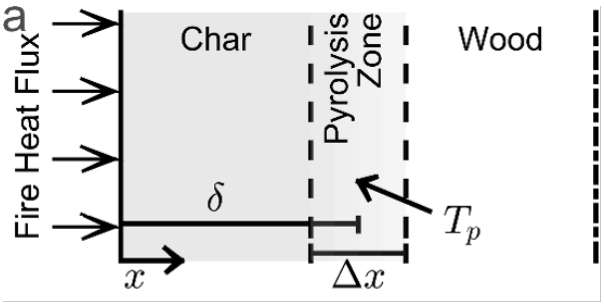



**Figure 3.1** – The process of charring occurs when wood is exposed to intense heat, breaking down the timber into char and volatiles and reducing the load bearing capacity [224],

Industry standards such as Eurocode 5 (EC5) adopt a simplistic approach for structural calculations, quantifying char depth linearly over time, as represented in Eqn 3.1 [228].

$$\delta = \beta t \tag{3.1}$$

Equation 3.1 relies on a linear correlation between the final char depth, $\delta$, and the duration of fire exposure, t, with the gradient representing the average charring rate, $\beta$ [224, 228–230]. In reality, charring rate is not often constant over time but can be approximated as such when using simple models for calculations [231]. Studies show the influence of various factors on the charring rate such as wood species, moisture content, density, permeability and heat flux [230, 232, 233]. As such, there is a need to develop sophisticated tools to accurately calculate charring rate of timber in fire. EC5 assumes a constant charring rate depending on the wood type and density; for instance, softwood is assigned a charring rate of 0.65 $\frac{\text{mm}}{\text{min}}$, whilst hardwood (with exception of beach) is allocated 0.5 $\frac{\text{mm}}{\text{min}}$ [10, 228]. More advanced models predict charring rates across various design fires using a multi-scale approach in Gpyro with an error range of 5-22% [227]. This study employs the EC5 standard to benchmark as a comparative tool for the development of the data-driven models discussed in this chapter [232].

Alternative methods to EC5 and multi-scale include the utilisation of data-driven tools such as machine learning (ML). Naser (2019) conducted a study on temperature-dependent models for charring rate using artificial intelligence (AI). Naser's study applied a neural network (NN) to predict a uniform charring rate equivalent to Eqn 3.1 which demonstrates the potential of AI as a substitute for empirical models, highlighting the need for additional investigation. His study served as a proof-of-concept for employing AI in addressing fire engineering challenges [10, 39, 234]. One of the challenges faced when employing ML in fire engineering is the requirement for large datasets to train the models [103, 232, 233],which may not always be readily available. Although some fire limited datasets are available, ML algorithms offer substantial advantages, as they can learn and predict what cannot be explained yet by simple physical models. As more data becomes available in the field of fire engineering, the accuracy of predictive models will improve over time.

This chapter presents a novel database comprising of timber charring experiments and tests, subsequently employing statistical methods and AI algorithms to predict the average charring rate of timber in fire for structural calculations.

## 3.2 VAQT: database of charring rates of timber products

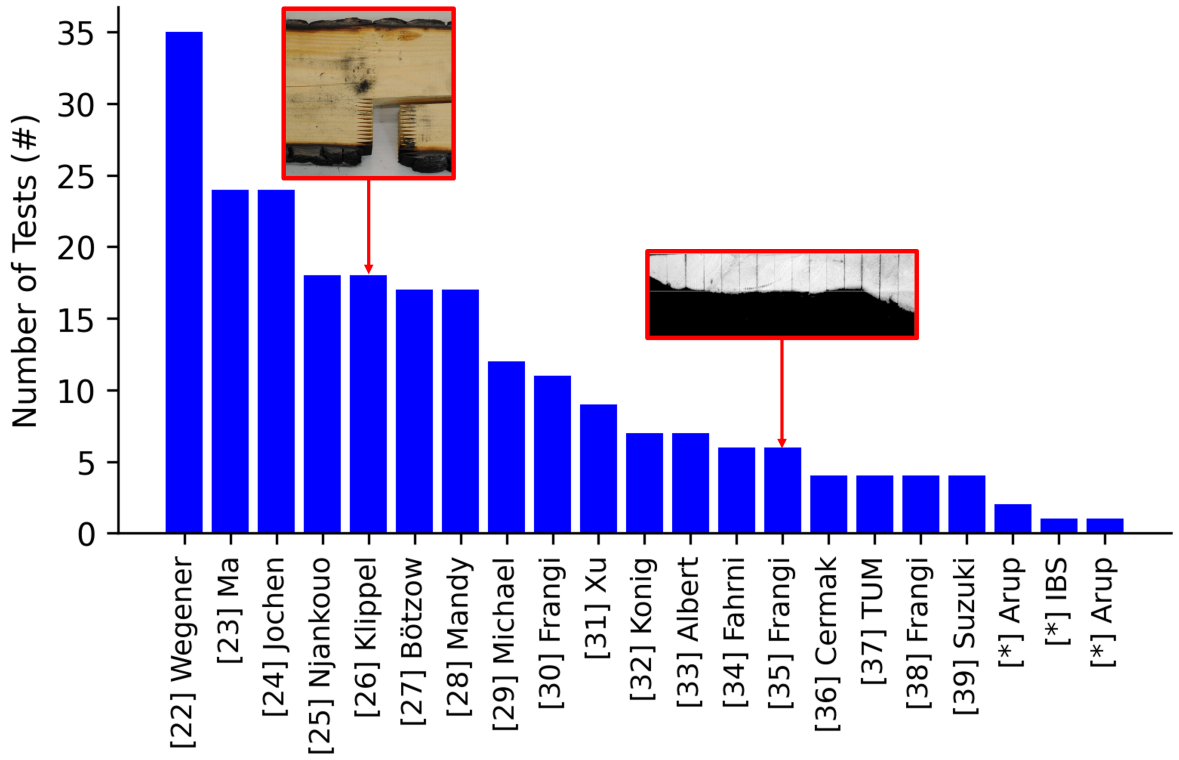



**Figure 3.2** – VAQT fire resistance tests of mass timber elements from literature and test house reports [235–252] whilst [*] refers to the confidential reports. This figure illustrates the distribution from the sources with the two images representing example cut outs of the specimen.

Machine learning (ML) relies on the quantity and quality of data to train and create an accurate model. The initial step in this study involved creating a comprehensive database of average charring rates obtained from fire resistance tests following the ISO 834 standard. Collaborations with testing houses, ARUP and IBS, facilitated access to confidential data. Additionally, a thorough search of the available literature was conducted. By consolidating data from 21 different sources, the VAQT database was established, totalling 231 individual furnace tests, significantly larger (177%) than previous datasets [10, 103]. Fig 3.2 illustrates the distribution of data sources within VAQT, with 94% originating from literature. VAQT encompasses both softwood and hardwood, including species such as beech, spruce, fir and oak. The dataset incorporates input variables, such as density, moisture content, and thickness, while others were categorized such as insulation which refers to material applied to the top, bottom, and side faces of the sample in the fire tests, namely; calcium silicate and gypsum. The average charring rate is derived through a lin-

ear fit using Eqn 3.1 through the origin, from which the gradient is computed. Numerical variables are retained in their original numerical format, while categorical variables are encoded, for instance, categories such as (A, B, C) are represented as (1, 0, 0), (0, 1, 0), and (0, 0, 1), respectively [30]. VAQT was structured to incorporate essential features pertinent to timber charring experiments, as in Fig(s) 3.3, 3.4 and the correlation matrix of Fig 3.6, where some features exhibit skewness addressed later in this study. VAQT also comprises information, including specimen composition, material type, size, moisture content, details about the test environment (furnace specifications, temperature), and measurements taken during the experiments (char depth, mass loss). To address missing values, for example moisture content, which serves as an input parameter for the models, a normalisation process was implemented, where missing values were replaced by the mean value of the entire dataset [10, 253]. Comparing this with the study conducted by Liu et al., focusing on the review of charring rates among various timber species, specifically, shows the distribution of density against average charring rates reported an $R^2$ of 0.4 whilst VAQT yields 0.3 [12]. This indicates that both studies show a weak correlation between density and charring rates but are not negligible showing that other variables are also important. However, it also shows the need for future experiments to encompass a broader range of densities.

Eurocode-5 standard was compared against VAQT using Eqn 3.2 calculating an average $\varepsilon_{\mathrm{VAQT}}$ of 27%. This considers both soft wood and hardwood. P represents the total number of samples, i denotes the $i_{\mathrm{th}}$ sample and $y_{\mathrm{m,i}}$ and $y_{\mathrm{p,i}}$ represent the measured and predicted charring rates respectively.

$$\varepsilon_{\mathrm{VAQT}}(\%) = \frac{1}{\mathrm{P}} \sum_{\mathrm{i}=1}^{\mathrm{P}} \left| \frac{y_{\mathrm{m,i}} - y_{\mathrm{p,i}}}{y_{\mathrm{p,i}}} \right| \tag{3.2}$$

Despite a low $\varepsilon_{\mathrm{VAQT}}$ , there was a noticeable difference when comparing it to the distribution of measured charring rates from VAQT as represented in Fig 3.5. EC5 underpredicts the charring rate for about 50% of the samples, sometimes by a large margin, which is unsafe. In contrast, it overpredicts it for the other 50%, which is cautious, sometimes overly so. We want to know when EC5 underpredicts or overpredicts and by how much. The uncertainties specific to the measurement of charring rates are poorly documented in the scientific literature and a quantification of these falls beyond

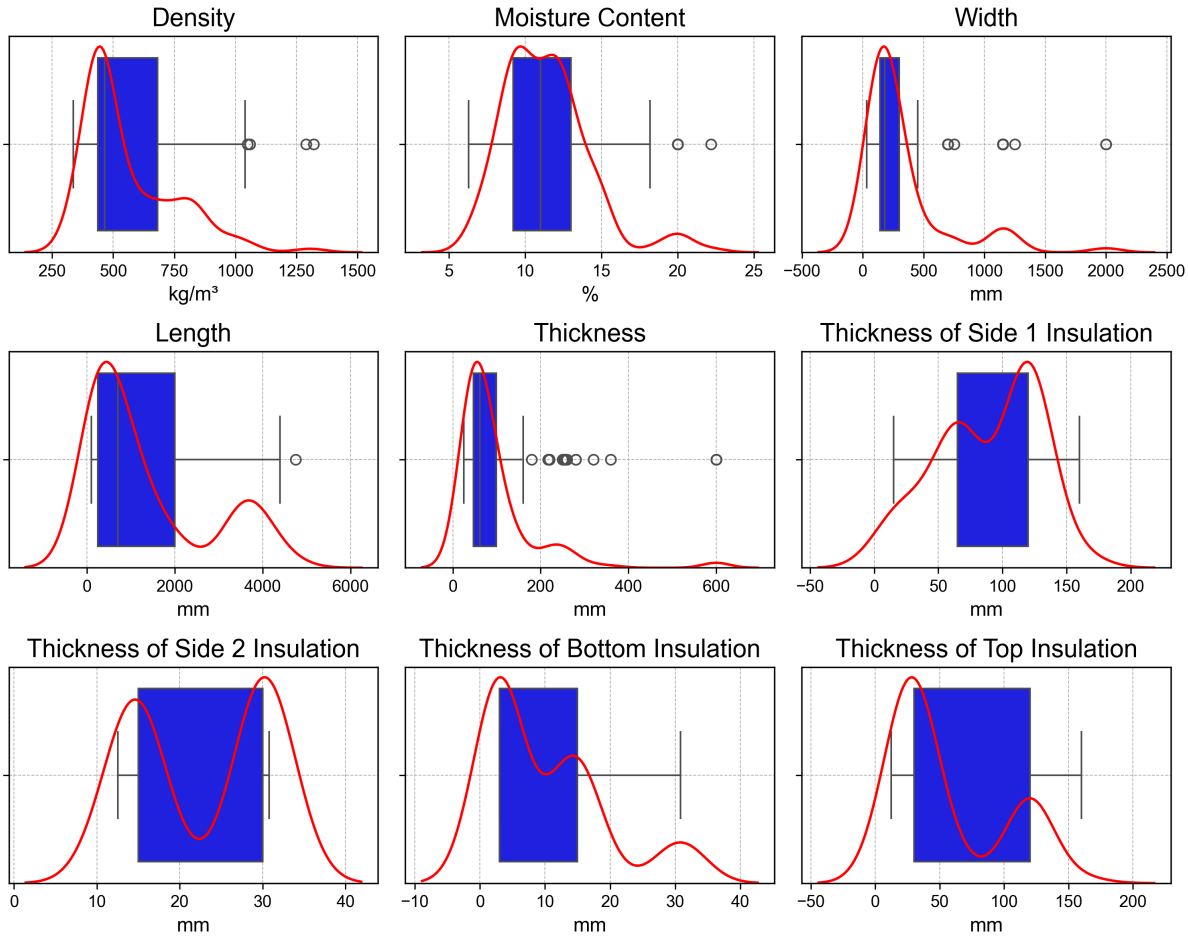



**Figure 3.3** – Box and whisker plot for the most important numerical variables in VAQT. The red curve outlines the distribution of the data for each variable.

the remit of the chapter and thesis.

## 3.3 Data-driven models

In ML, a dataset the size of VAQT is generally considered small for tackling complex problems, and as a result it poses an increased risk of model overfitting and or less accurate predictions [25]. Overfitting occurs when a model fits well to the training data but fails to generalise effectively to unseen data, a phenomenon commonly caused by complex models, skewed data distributions and size. It is noteworthy to mention that skewed data distributions do not imply a scarcity of data within specific ranges; consequently, predictions made in these regions may exhibit higher probabilities of inaccuracy [254]. Furthermore, ML models tend to perform optimally when interpolating data; hence, they may encounter challenges in learning the underlying function in regions with limited

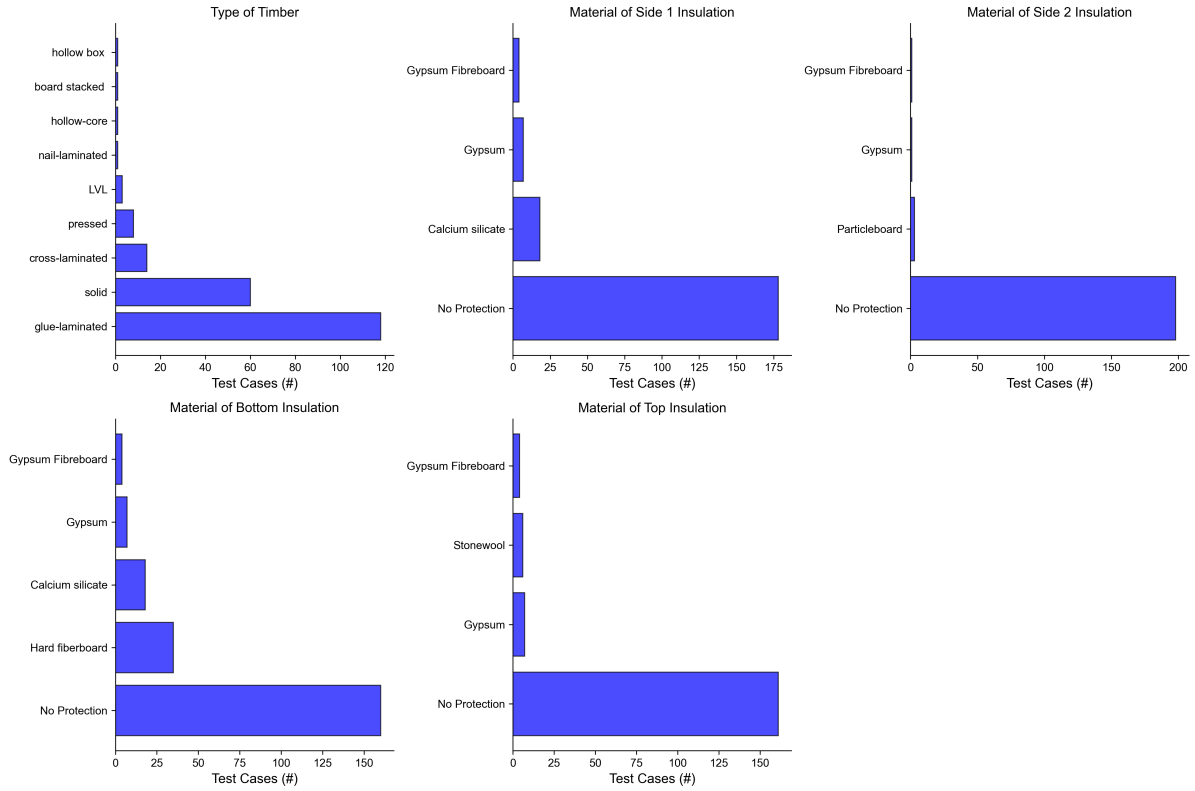



**Figure 3.4** – Bar plot for the most important categorical variables in VAQT.

data. Addressing this issue involves including more data in VAQT, but, due to the limited availability of data in the field, this approach may not be feasible.

To minimise the risk of overfitting, VAQT was randomly divided into training (80%) and testing sets (20%) following the standard practice in most ML frameworks to facilitate validation and reduce bias [255]. Moreover, the training set was further subdivided to include a validation set, accounting for 20% of the training data. The inclusion of a validation set is vital in ML training, as it facilitates evaluating the model's performance during the training process and early detection of overfitting before introducing the testing set to make predictions [254]. Specifically for a neural network, the need for a validation set is equally crucial due to the possibility of random fluctuations or noise in the data, which can adversely affect the model's overall performance. The validation set also becomes instrumental in tuning hyperparameters to optimise a NN's performance. NN's have parameters that need to be specified before training the model and these are called hyperparameters. These hyperparameters, include the learning rate, number of layers, number of neurons, activation and error functions [31, 256]. To enhance hyperparameter tuning, this study utilises Bayesian optimisation.

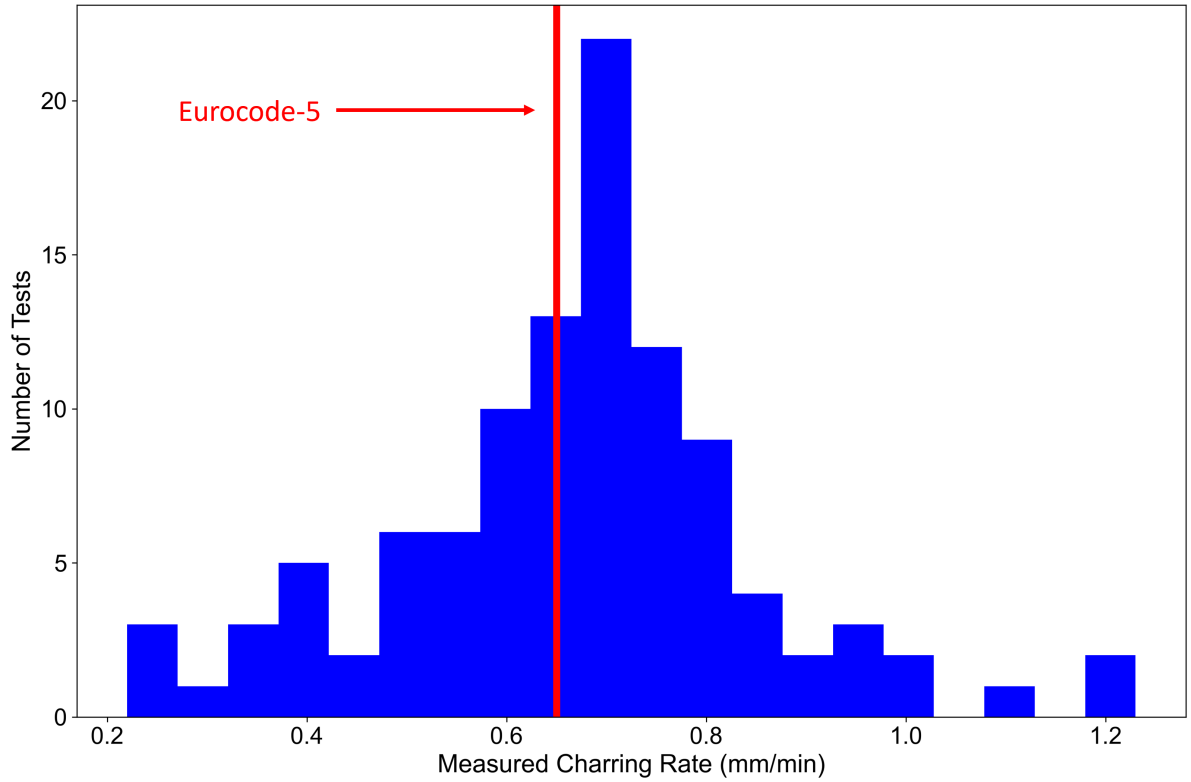



**Figure 3.5** – Measured average charring rates in VAQT compared to the value in EC5. Note that EC5 is close to the median, so it underpredicts the average charring rate for about 50% of the samples and it overpredicts it for the other 50%.

To further mitigate the risk of overfitting and to determine the best model for VAQT, a k-fold cross-validation approach was applied before implementing training [254]. This technique involves dividing the training set into random k-equal subsets, folds, where cross-validation iteratively designates one subset as the validation set while using the rest for training, repeating k times as represented by Eqn 3.3 with E as the final evaluation score and k as the number of folds [254].

$$E = \frac{1}{k}\sum_{k}^{i=1} E_i \tag{3.3}$$

Utilising ML to address the specific problem, it is crucial to address some fundamental questions of importance. Understanding the type of problem at hand is essential; in our context, identifying it as a regression problem is significant, as it influences the choice of appropriate algorithms and techniques needed for analysis. Additionally, determining the factors that contribute to the success of the ML model is critical. This involves assessing various evaluation metrics, ensuring that the model's performance aligns with

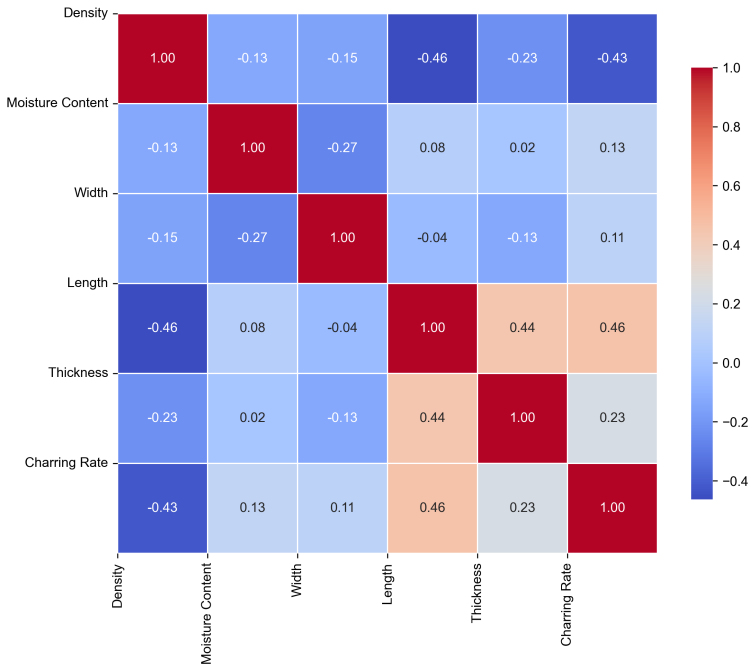



**Figure 3.6** – A feature correlation matrix that examines the relationships between the numerical variables in VAQT and the target variable, charring rate. Positive and negative values indicate varying degrees of correlation, while values close to zero suggest little to no correlation.

the intended objectives and requirements. To ensure reproducibility in the results the seed for the data splitting was fixed, which determines the distribution of the dataset split allowing a consistent comparison of the different models. However, it is important to note that the fixed seed was randomised to demonstrate the robustness of the trained models later in this study. In summary, addressing these crucial questions creates a foundation for a successful application of ML.

### 3.3.1 Statistical methods: regression

Regression models, specifically, ridge and lasso, were chosen for their ease of implementation and foundational understanding, aiming also to provide a proof of concept for ML as they also allow the quantification of an algebraic expression for the models. These models are regularised versions of the fundamental linear regression equation, represented as objective functions given in Eqn(s) 3.4 and 3.5 where regularisation is used to minimise overfitting [27, 254, 257, 258].

$$\mathrm{SSE}_{\mathrm{L}_2} = \sum_{\mathrm{i}=1}^{\mathrm{P}} \left( \mathrm{a_o} + \sum_{\mathrm{n}=1}^{\mathrm{P}} \mathrm{a_{n,i} x_{n,i}} - \widehat{\mathrm{y}}_\mathrm{i} \right)^2 + \lambda \sum_{\mathrm{j}=1}^{\mathrm{N}} \mathrm{a_j^2} \tag{3.4}$$

$$\mathrm{SSE}_{\mathrm{L}_1} = \sum_{\mathrm{i}=1}^{\mathrm{P}} \left( \mathrm{a_o} + \sum_{\mathrm{n}=1}^{\mathrm{P}} \mathrm{a_{n,i} x_{n,i}} - \widehat{\mathrm{y}}_\mathrm{i} \right)^2 + \lambda \sum_{\mathrm{j}=1}^{\mathrm{N}} |\mathrm{a}| \tag{3.5}$$

In context, $\mathrm{x_n}$ denotes the predictor variable (e.g., density, moisture content), and $\mathrm{y_i}$ represents the target variable (charring rate), and a represents the weight of regularisation applied. The degree of regularisation applied is determined by the value of $\lambda$, typically set between 0 and 1 and is determined by comparing the respective models mean squared errors (MSE) as indicated in Eqn 3.6. The MSE is used to measure how well the model fits the data in Euclidean space using $\mathrm{L}_2$ normalisation distance.

$$\mathrm{MSE} = \frac{\sum_{\mathrm{i}=1}^{\mathrm{P}} \left( \mathrm{y_i} - \hat{\mathrm{y}}_\mathrm{i} \right)^2}{\mathrm{P}} = \frac{\mathrm{SSE}}{\mathrm{P}} \tag{3.6}$$

Another regression model, Bayesian ridge, which uses a Gaussian distribution and adapts to the data given, was used [259]. The approach is probabilistic, contrasting with the deterministic approach employed in the previous regression models. This probabilistic framework is deemed appropriate as it offers rapid inference and efficiency aligning well with the scale of VAQT.

### 3.3.2 Supervised machine learning: support vector machine

Supervised learning encompasses a variety of algorithms in machine learning (ML), with support vector machine (SVM) standing out as an influential and widely used tool [260]. Although this study considered the inclusion of alternative models like Random Forest, they were ultimately not used here but could be part of future studies. SVM, known for error-based learning, has been used in many different fields and more specifically in fire engineering [255]. Panev et.al (2021) used SVM to assist in the prediction of fire resistance of composite shallow floor systems and concluded that this method rapidly assesses the feasibility of different details at the early stages of the design process [166, 261]. In this study, we utilise the support vector regressor (SVR), a variant of SVM, as predicting the charring rate is a regression task. SVM uses a kernel trick, a

technique that allows SVM to perform non-linear learning through convex optimisation in infinite-dimensional space [262]. The kernel used is a Gaussian Radial Basis kernel which helps control the convergence of the algorithm by finding non-linear relationships [262]. Due to its ability to generalise well with small datasets meaning having accurate predictions, SVM is viable choice for this study. SVM and a neural network (NN) share similarities as parametric models. However, SVM distinguishes itself by utilising kernels. SVM serves as a bridge between statistical methods like regression, which may not generalise well on specific datasets to more complex models such as a NN which were developed and are now widely adopted, providing a solution that is also implemented in this study.

### 3.3.3 Deep Learning: neural networks

To introduce more advanced predictive methods, a neural network (NN) was developed for this study which captures hidden patterns through adaptive learning [10]. The architecture of the network is sequential, with no loops connecting different parts of the network. Our NN consists of three layers; an input layer with 17 nodes due to the 17 predictor variables of VAQT, a single dense-hidden layer with 19 nodes, and a single output layer which is represented through 1 node to predict the charring rate. The general rule of thumb suggests that increasing the depth of the network is more effective than infinitely increasing its width which creates a network with multiple hidden layers called a multilayer perceptron (MLP) [255]. The model is defined using the rectified linear unit (ReLu) activation function in the hidden layer and a Linear function in the output layer since the output represents continuous data. ReLu is a common choice for most NN architectures due to its efficiency and speed, making it suitable for regression problems and thus specifically this study. The mean squared error (MSE) as represented previously in Eqn 3.6 was selected for both the error function and evaluation metric to allow a direct comparison with the statistical models. Using MSE as the error function is a standard practice when dealing with regression problems [262]. The Adam optimiser, a variant of stochastic gradient descent, was chosen with a learning rate of 0.0001. Furthermore, the weights and biases of the network are randomly initialised where the same value was chosen for the $L_2$ regularisation applied on the network layers. The role of the optimiser is to minimise the error, pushing the model towards a global minimum whilst avoiding the local minima; therefore, selecting an appropriate learning rate is crucial for optimal

performance.

## 3.4 Results and discussion

Amongst the statistical models, the ridge regression model ($\lambda = 0.001$), performed the best, which predicted the charring rate of timber with a minimum $\varepsilon_{\mathrm{VAQT}}$ of 11%, performing better than EC5. The performance of all the models is represented in Fig 3.7 with the corresponding ridge regression model being depicted in Fig 3.8. To re-iterate the seed is fixed for these results and is later removed to show reproducibility. Initial results from these regression models are encouraging, suggesting that further pursuing this approach could lead to more accurate charring rate predictions. However, the goal is to have the predicted charring rate close to the measured one, as visually demonstrated by the charring values being closer to the regression line in Fig 3.8.

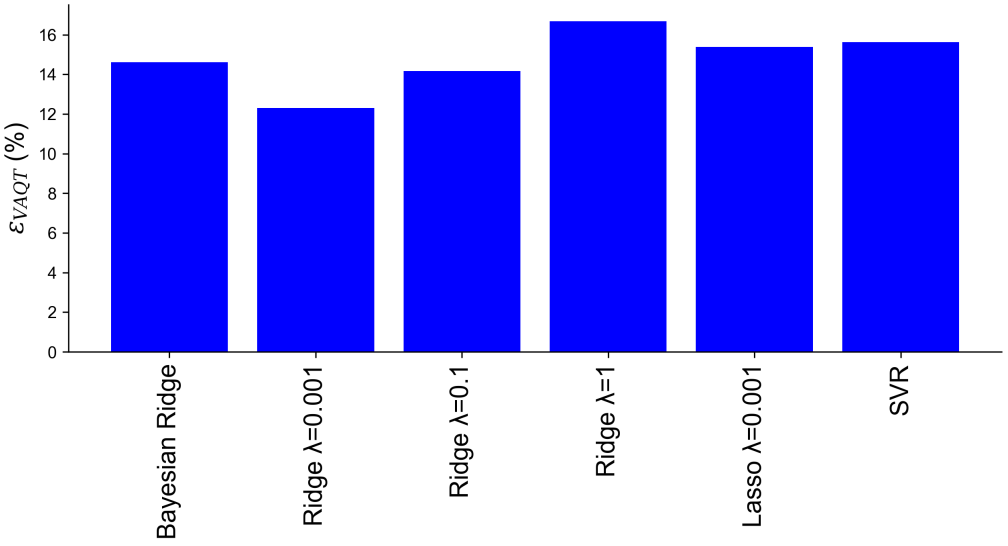



**Figure 3.7** – Comparison of average error using Eqn 3.2 in VAQT for the statistical models, where all models show a similar prediction whilst ridge regression ($\lambda = 0.001$) is the best and ridge ($\lambda = 1$) is the worst.

These results could potentially be improved further using a more advanced model such as a NN, as both linear and non-linear relationships are considered. The current statistical models namely ridge regression ($\lambda = 0.001$) used for predicting charring rate

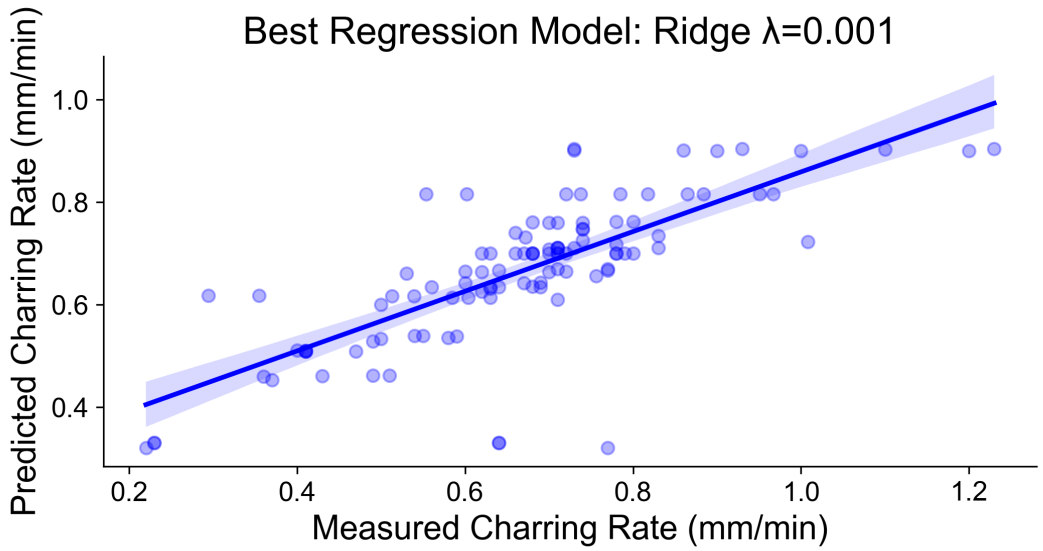



**Figure 3.8** – Comparison of measured vs predicted for the best regression model – ridge regression ($\lambda = 0.001$). Data points falling above the regression line represent cases where the model is not conservative for design.

relying on linear relationships, except for Bayesian ridge regression and SVM both of which indicate good predictive performance. However, it's important to note that this is not always guaranteed, and there may be only a marginal increase in accuracy with disproportional increased computational cost.

### 3.4.1 Iteration feasibility study

The nature of training a NN is stochastic, meaning that it can follow a different learning path even with a fixed data split this is due to the random initialisation of weights and biases at the start of training. Weights are included in each neuron in the layers of a network and a bias is a constant term added which results in the output from the neuron. To address this issue and ensure reliable results, an iteration feasibility study was conducted to show reproducibility [263]. The iteration feasibility study revealed that when the total number of iterations exceeded 200, the results became independent and further iterations are not needed. This finding is illustrated in Fig 3.9, where the validation error (MSE) values reach a plateau after approximately 200 iterations. Consequently 250 unique training iterations were selected for each NN model. It's essential to distinguish between "iterations" and "epochs" in this study, as epochs will be mentioned in the next section of this chapter. Iterations refer to the number of times the model will uniquely

train meaning a new model with new weights and biases, while epochs determine the number of times the model repeats over the entire training dataset during the training process. This feasibility study aims to obtain a single output that potentially provides the lowest validation error from the 250 unique training iterations.

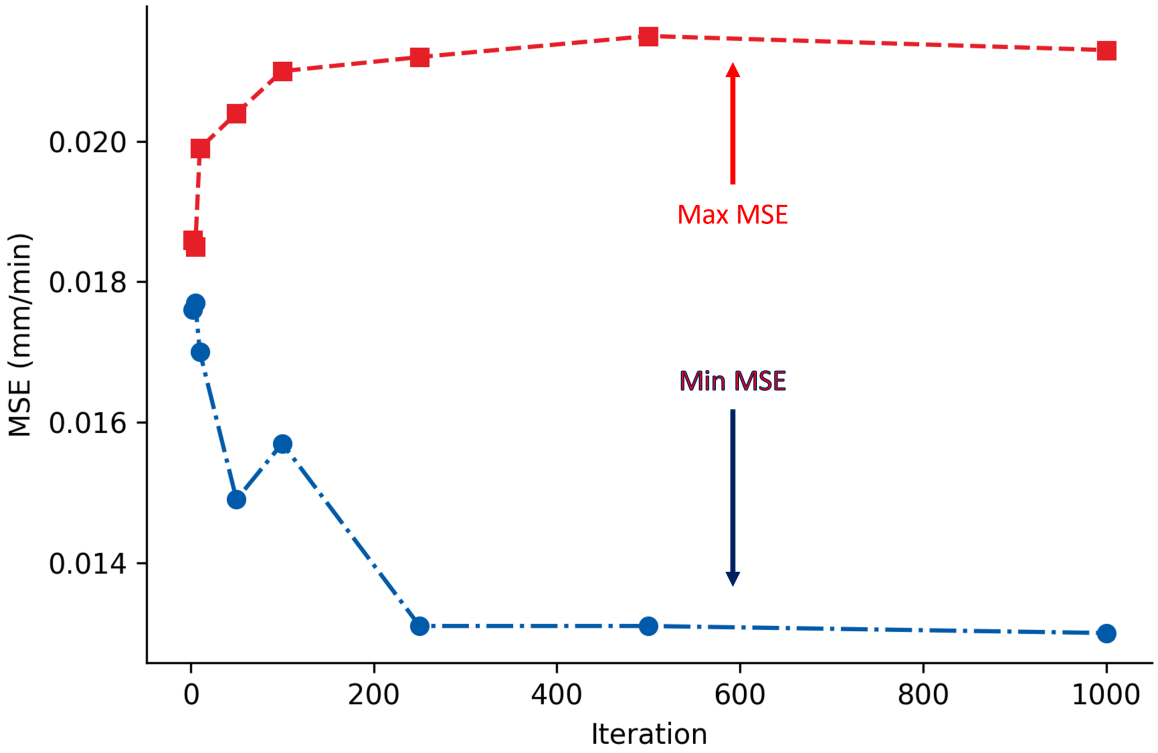



**Figure 3.9** – Iteration feasibility study represents the plateau of MSE $\frac{\text{mm}}{\text{min}}$ values using Eqn 3.6 over 1000 iterations where 250 is the optimal point where results become independent of further iterations.

The first NN trained uses a simple network architecture with a single dense-hidden layer comprising of 19 neurons. The model predicted the charring rate of timber with a minimum $\varepsilon_{\text{VAQT}}$ of 10% over the 250 iterations, demonstrating an improvement over Eurocode-5 (EC5) and ridge regression ($\lambda$=0.001). This initial model represents the simplest form of a general NN architecture. However, to explore the potential for further increased performance, other hyperparameters were tuned to which the number of layers and neurons in each layer were altered while keeping other hyperparameters constant, this is known as a heuristic training approach [264]. The first trained model had the best performance, indicating that increasing model complexity through the network architecture does not always lead to better performance. Fig 3.10 depicts the result of this NN. However, it is evident that this model suffers from slight overfitting as shown in Fig

3.11 through the training validation loss curve. The two curves meet but the validation curve starts to ascend indicating the model is starting to overfit where the predictions fit closely to the training set rather than the testing set. Ideally the two curves should converge and plateau during the training process. The other trained models also exhibit similar trends, suggesting that other hyperparameters, such as learning rate or layer regularisation, should be optimised to find a balance with a low validation error whilst mitigating overfitting. Stopping training or reducing the number of epochs might lead to the convergence of the training and validation lines, indicating a more optimal model.

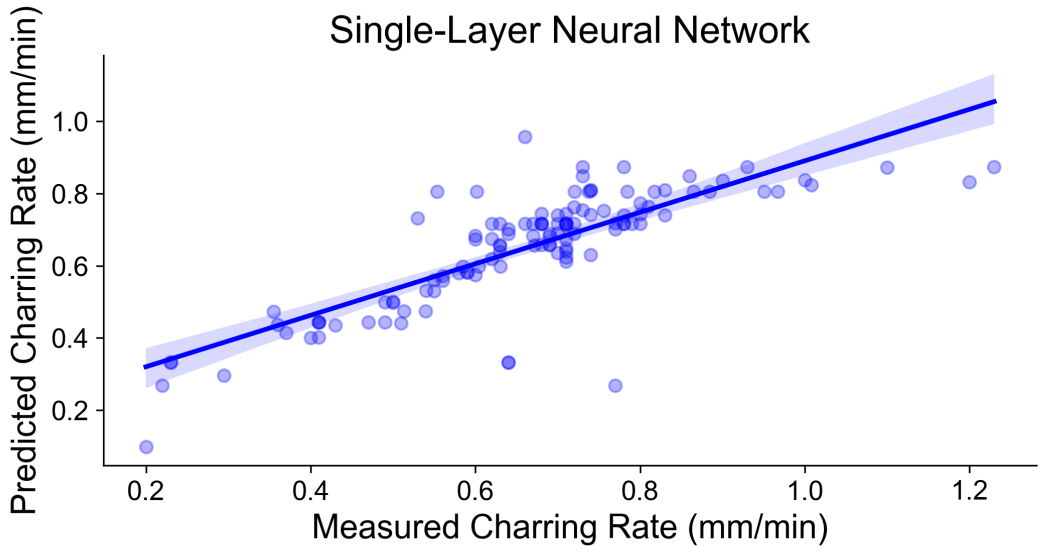



**Figure 3.10** – Comparison of measured vs predicted for a single-layer neural network. The data points above the regression line indicate cases where the model is not conservative for design, as these instances suggest it has a higher charring rate than what is desirable, where as in reality, a lower charring rate is preferred for fire safety and performance. However, due to the inherent variability in specimen attributes and other extrinsic conditions, the outcome will not always be the case. Ideally, predictions should lie on the regression line, indicating a minimal error and accurate estimation of the charring rate.

### 3.4.2 Neural network hyper-parameter optimisation

Tuning hyperparameters for a neural network (NN) is a stochastic process, where the parameters are modified arbitrarily to optimise the model's performance by minimising the error function until a satisfactory criterion is met. The set of hyperparameters includes choices such as the number of neurons, layers and learning rate. Tuning hyperparameters using a stochastic approach can be computationally expensive and time-consuming

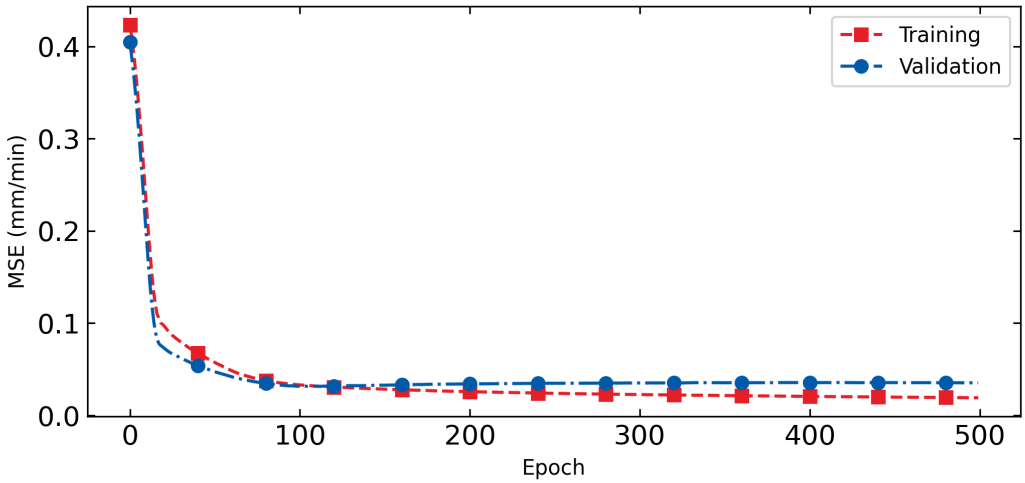



**Figure 3.11** – Learning curve of the single-layer neural network using Eqn 3.6. The two curves should converge during training, but in this case they do not and therefore the hyperparameters need optimising.

due to the numerous possible combinations of choices. There are simple algorithms such as Grid/RandomizedSearchCV [262, 265] and more sophisticated ones, namely Random Forests [266]. However, these algorithms are still performed manually and iteratively, lacking a systematic way to build upon previous results. Bayesian optimisation (BO) is the preferred method for this study as it considers previous results of hyperparameter choices to guide the search for better solutions in the next iteration. BO takes a probabilistic approach by mapping a distribution over an objective function to the region of interest using a Gaussian process through a surrogate model. Although BO is computationally expensive, it is well-suited for optimising models with many hyperparameters as it covers a wider range of possibilities through probabilistic distribution. Through the application of BO, a multi-layered NN was trained, and this predicted a charring rate with a minimum $\varepsilon_{\mathrm{VAQT}}$ of 9% with its corresponding loss graph in Fig 3.12. The graph demonstrates that overfitting has been negated as the two curves converge and meet as the training process is complete. This outcome highlights the critical importance of striking a good balance between minimising the validation error whilst controlling overfitting in the NN training process which in our case the Bayesian optimisation approach proved to be effective in achieving this balance.

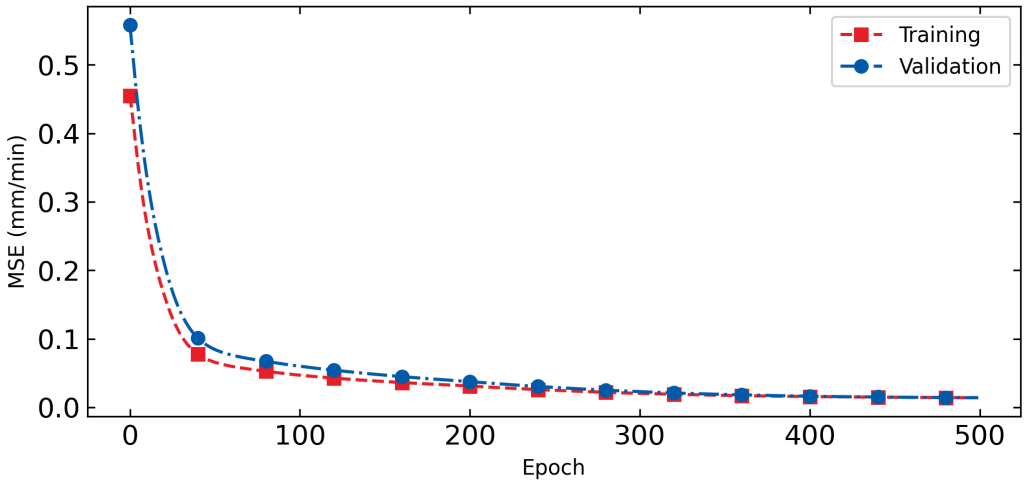



**Figure 3.12** – Learning curve for a multi-layer neural network using Eqn 3.6 which shows there is no overfitting as the two lines converge to show training is complete.

## 3.5 Overall model comparison

A model comparison shows a multi-layered NN trained through Bayesian hyperparameter optimisation exhibited the best performance compared to the initial single hidden layer NN and Eurocode-5 (EC5). It also demonstrates the best balance between overfitting and validation error, making it the top performing model in this study. The comparison is illustrated in Fig 3.13 where the seed remains fixed for all models. Nevertheless, this leads us to question whether the computational cost associated with training a multi-layered NN in addition to probabilistically optimised hyperparameters outweighs the simplicity, efficiency of simpler statistical models, especially when there is a minimal difference in predictions. Despite this consideration, both the statistical models and the NN's outperformed EC5 in predicting the charring rate of timber based on VAQT, achieving higher accuracy in their predictions. This indicates the viability of using data-driven models to predict the average charring rate of timber for structural engineering calculations equivalent to existing data-driven models that exist in the literature given by empirical correlations to predict the fire resistance of timber beams and columns [267].

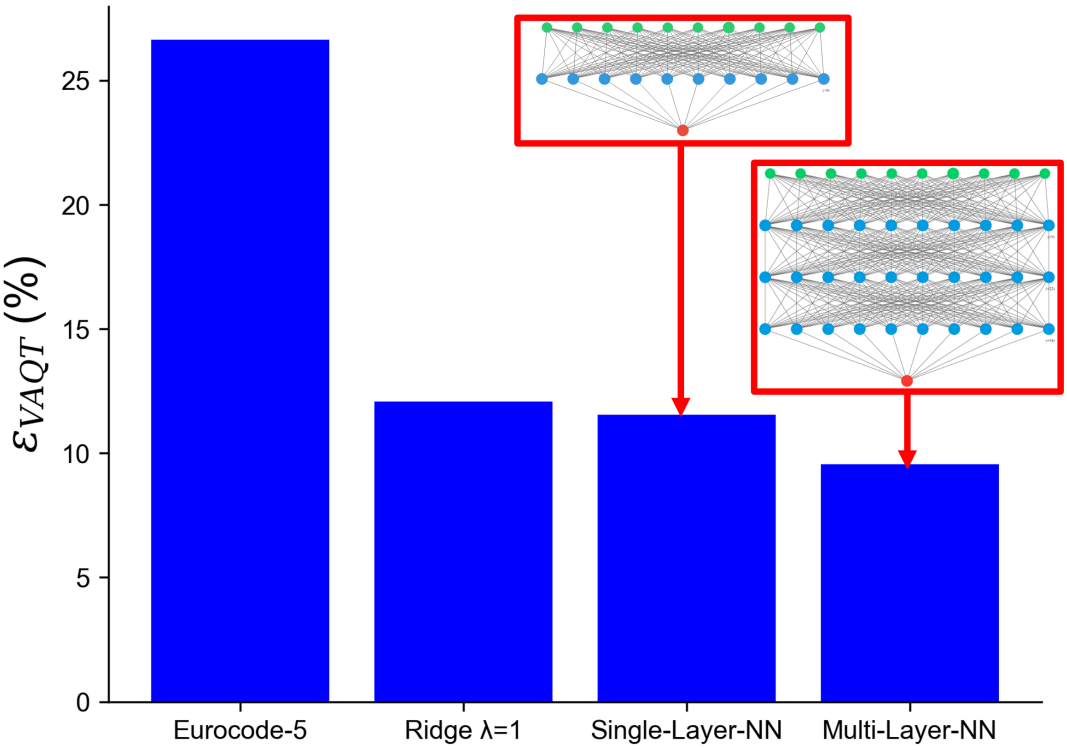



**Figure 3.13** – A model comparison using Eqn 3.2 with a fixed seed between the models implemented in this study whilst indicating the multi-layered neural network giving the most accurate predictions.

### 3.5.1 Problem of reproducibility and overfitting

Reproducibility poses a significant challenge in the field of machine learning (ML), as it strives to attain consistent and reliable results with minimal variability [268]. Reproducibility is achieved when the trained algorithm repeatedly produces similar or equal results during each run. The stochastic nature of ML models contributes to this challenge, with various factors introducing randomness, such as dataset splitting prior to training. To mitigate this, it is common to select an even distribution for each variable when splitting the data. However, in this study, due to the large number of data points from different experiments, such an approach would be counterproductive. Instead, we opt for random splitting and k-fold cross-validation following standard practices to achieve reproducibility. Additional sources of randomness in ML models include the random initialisation of weights and biases before training a neural network (NN). Each model is trained uniquely 250 times as determined by the preliminary iteration feasibility study.

The charring rate predictions from these iterations are presented in Figure 3.14. The results exhibit stochastic behaviour, as evidenced by the distribution of percentage error for each model. Less complex models, such as ridge regression with strong regularisation applied, and the Bayesian regression model, show the most reproducible results due to the smaller range in results and less outliers. On the other hand, the more complex models, the NNs, exhibit higher stochasticity with $\varepsilon_{\mathrm{VAQT}}$ values but they have more accurate predictions. To address the variability in predictions, using a larger dataset would help in achieving more consistent results.

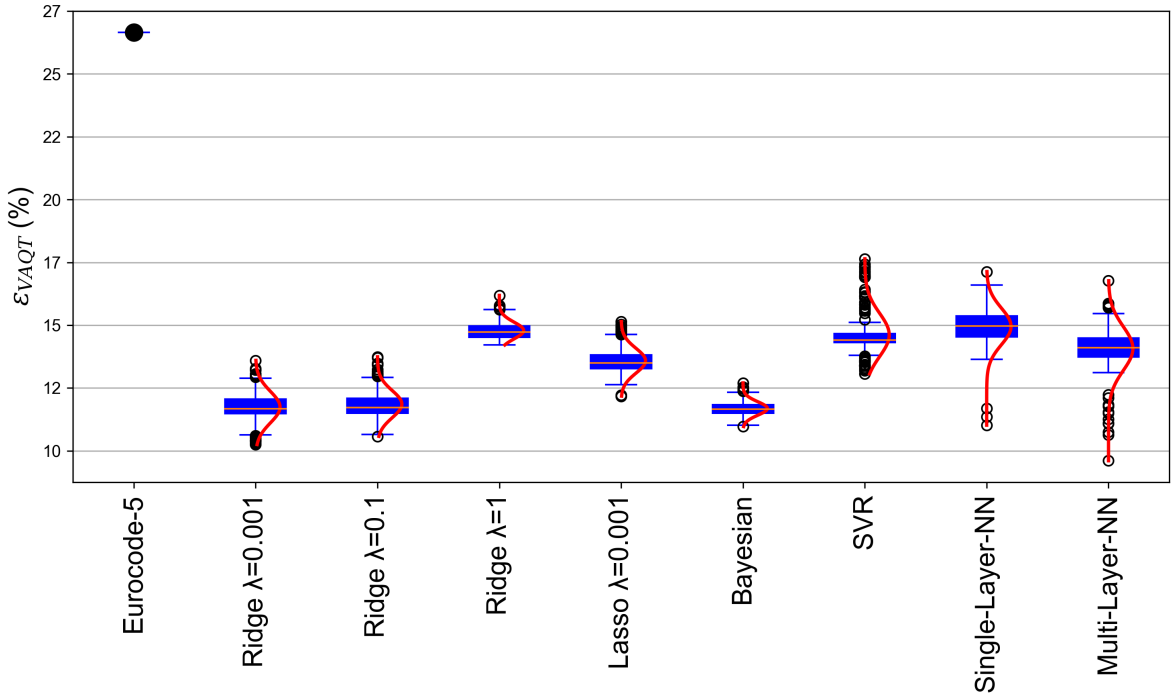



**Figure 3.14** – Distribution in stochastic results of the models chosen in this study and their $\varepsilon_{\mathrm{VAQT}}$ values using Eqn 3.2 for predicting the charring rate of timber in VAQT. The statistical models show the best reproducibility, while the multi-layer NN achieves the lowest error by a small margin. However, the higher expected error of both NNs indicates variability in their predictions due to the stochastic nature of NNs.

### 3.5.2 A sensitivity study

A sensitivity study using permutation importance was conducted on the fully trained model to identify the most important features in VAQT that influence charring rate [269]. The sensitivity was measured by observing the resulting change in the model's mean squared error (MSE), the method is governed by Eqn 3.7 where the importance of each

feature is measured by $i_j$, where k is the number of repetitions in set K and s is the score of the model [269].

$$i_j = s - \frac{1}{k}\sum_{k=1}^{k} s_{k,j} \tag{3.7}$$

Fig 3.15 illustrates the outcome of this analysis, where insulation being the most important factor, which in term indicates as a crucial determinant in the model's predictions. This is commonly known from previous studies which also conclude that insulation significantly reduces the charring rate [11, 243].

In addition, variables such as moisture content, density and type of timber have a similar effect on the model, which is supported in a study by Bartlett et al., reporting that the aforementioned variables have a strong effect on the charring rate of timber [11]. Studies by Richter et al., demonstrated through sensitivity analysis that timber charring is highly sensitive to extrinsic parameters of the test such as heat flux, oxygen concentration and convective heat transfer [13]. nother concern is multicollinearity as it directly effects sensitivity studies. It occurs when one or more features are correlated with each other, making it challenging to estimate the model accuracy. In this study, regularisation techniques were employed in the models to minimise multicollinearity [257, 258]. Overall, the sensitivity study conducted in this research is based on predictivity of the model and not on VAQT data directly which would relate to factors based on physics.

## 3.6 Conclusion

Industry standards, such as Eurocode-5, are a simple and a quick approach to quantifying an average charring rate of timber in fire for structural calculations yielding an $\varepsilon_{VAQT}$ of 27%. However, the tests and experiments in VAQT prove that there is no singular value representative of the charring rate of timber as many different factors play a role including the type of timber product, insulation, thickness and density. Insulation was found to be the most important factor. The best statistical model was ridge regression (k = 0.001) which predicted the charring rate with a minimum $\varepsilon_{VAQT}$ of 11%. A complex method, a multi–layer neural network, was employed and predicted the charring rate with a minimum $\varepsilon_{VAQT}$ of 9%. These errors can be further reduced by adding additional data into VAQT, which would reduce the skewness and increase data

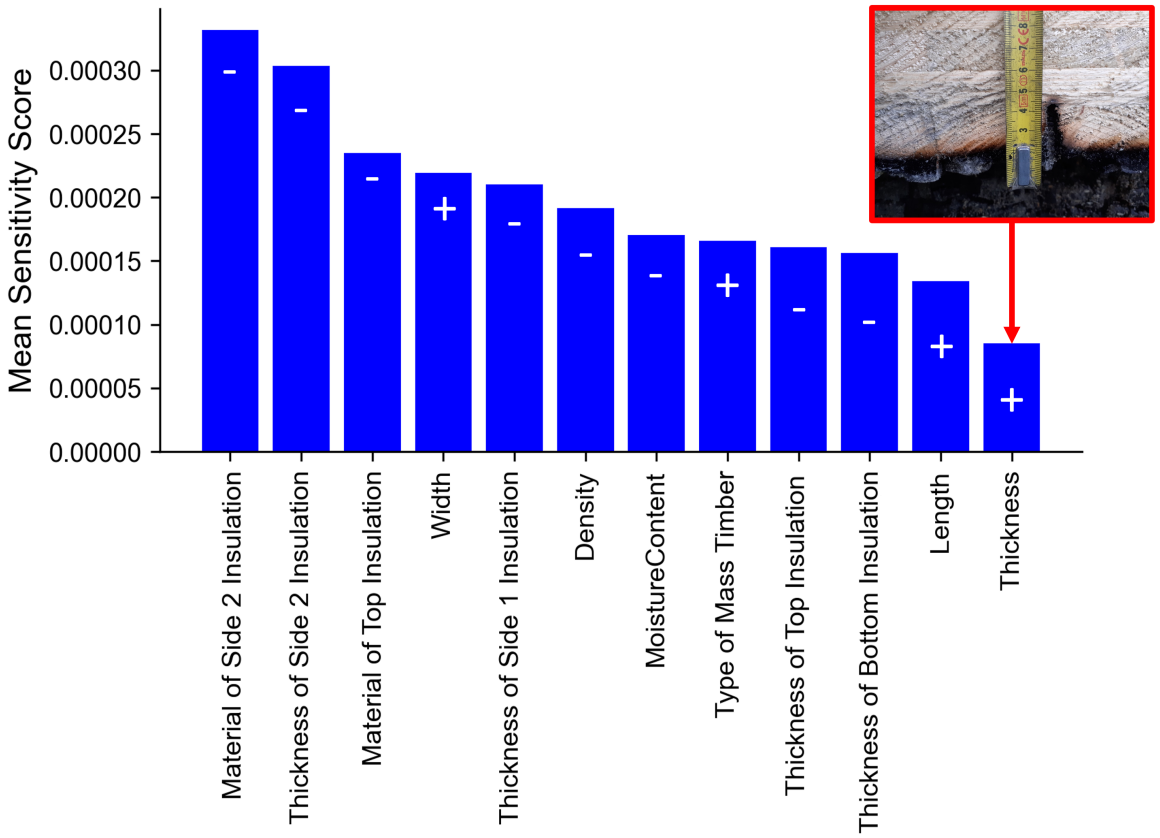



**Figure 3.15** – A sensitivity analysis was performed using Eqn 3.7 on VAQT through permutation importance which indicates that the insulation and its thickness has the largest effect on the models. The $\pm$ indicate the positive or negative change of the charring rate of timber.

variability. For this study there is a small added benefit of increasing model complexity by using a neural network when the charring rate of timber is predicted within a small range for all models. However, all models outperformed Eurocode-5. Prediction reproducibility is important when utilising data-driven methods, as they are stochastic. Thus it is important to improve models, so there is minimal change in the predicted average charring rate. This study shows that statistical models produced the most repeatable results, and artificial intelligence is the most accurate but by a small margin. This study presents a novel database of timber charring experiments in VAQT, and provides a set of data-driven predictive models, all of which calculate the average charring rate with a significantly higher accuracy than Eurocode-5 for a wide range of mass timber products.

# Chapter 4

# CodeRed Experiment Series: Instrumentation for external flaming and human dimensions

This chapter presents a series of compartment fire experiments, known as *CodeRed*, which form a core part of this PhD thesis for chapters 5 and 6. Chapters 1 and 2 outline the research gaps within the built environment, particularly in relation to mass timber buildings, with a focus on high-rise structures. The *CodeRed* experiments address these gaps by conducting large-scale experiments, in contrast to previous studies that relied on small scale lab experiments (less than 100 $m^2$). *CodeRed* covers a much larger area of 352 $m^2$, featuring a cross-laminated timber (CLT) ceiling and glulam columns. The experimental setup designed to be a large, open-plan floor space exposed to fire, with a wooden crib fuel load, along the length of the compartment. This thesis studies external flaming from the compartment fire in chapter 5 and 6. In this chapter, the experiment is introduced along with a detailed explanation of the instrumentation setup used to collect visual data, the thermal protection measures implemented for the instrumentation, and the human considerations involved in conducting such a large-scale experiment. The *CodeRed#03* experiment will be introduced where a waste-mist system was tested to assess the performance in suppressing the internal fire spread and prevent ignition to the CLT ceiling. While this chapter provides an overview of all four *CodeRed* experiments, the remainder of the thesis will delve into each in greater detail specifically measuring

external flaming and external heat release rate from the experiments.

## 4.1 Introduction

High-rise buildings often feature large open-plan spaces, particularly in offices, retail or industrial sites, where fires pose a significant hazard to both the structure and its occupants. These compartments typically range in size from 900-4000 $m^2$ [15–17] and contain complex fuel loads, such as chairs, books, and other flammable materials. In the event of a fire, flames can spread across the floor of the compartment, eventually venting through openings and creating external flames. External flames occur due to the burning of pyrolysis gases outside the compartment, when there is an imbalance of excess fuel load and lack of oxygen inside the compartment. As a result, these external flames can extend vertically along the façade, potentially igniting upper floors or buildings in proximity. This process is a critical phenomenon in fire safety due to its ability to extend the fire beyond the initial compartment [8, 18–20].

As discussed in Chapter 1, the construction industry is increasingly adopting mass timber to enhance sustainability and reduce embodied carbon in the built environment [4]. However, mass timber is inherently flammable if left exposed, introducing a challenge regarding its safe use in high-rise structures. There is a global push towards achieving a net-zero carbon future to combat climate change, which has driven the built environment to explore more sustainable materials. Notable examples of high-rise structures incorporating mass timber, including Mjøstårnet (4700 $m^2$) in Norway and Google's headquarters (80,000 $m^2$) in Kings Cross, London, UK [6, 7].

This growing use of sustainable materials presents a key knowledge gap, as it necessitates the development of fire safety designs and strategies that account for their combustibility. According to previous research, such as that by Mitchell et al [13, 17], large-scale compartment fire experiments are urgently needed, as small-scale tests cannot reliably predict fire behaviour in larger, open-plan buildings especially with mass timber as it is a complex fuel. Previous studies investigating external flames have primarily been conducted using small-scale experiments [270]. These are elaborated upon in Chapter(s) 5 and 6 of this thesis. However, until the *CodeRed* experiments, no large-scale experiments (greater than 82 $m^2$) had been conducted at the same magnitude [13, 17].

This chapter presents a series of four large open-plan compartment fire experiments featuring a mass timber ceiling, conducted in Epernon, France, in collaboration with ARUP and CERIB during the peak of Covid-19. The goal of these experiments was to understand the internal and external fire dynamics within a compartment, focusing on the impact of exposed timber on fire behaviour. Understanding these dynamics is crucial for ensuring the safe design of high-rise buildings that incorporate exposed mass timber.

## 4.2 Introduction to *CodeRed* experiment series

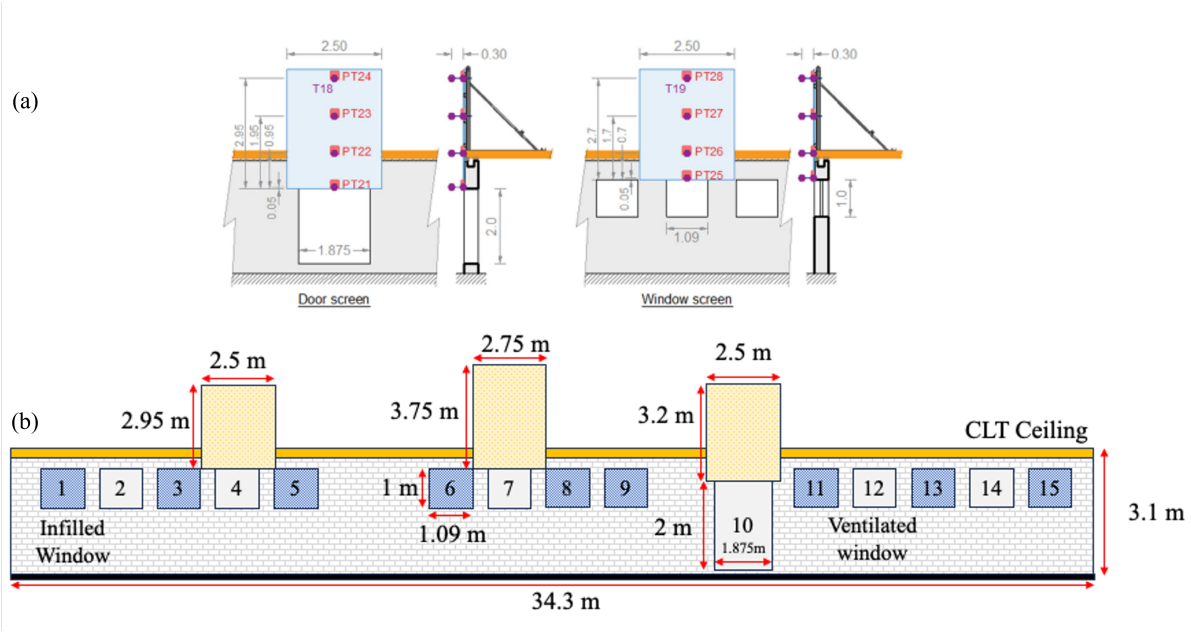



**Figure 4.1** – (a) Schematic layout and cross-sectional dimensions of the door and window openings, highlighting the placement of façade screens equipped with plate thermometers for heat flux measurement and thermocouples for temperature readings. (b) Side view schematic of the *CodeRed* compartment, showing the overall dimensions of the openings and compartment structure.

Three *CodeRed* experiments were conducted in 2021, each with variations in ventilation and exposure of the cross-laminated timber ceiling (CLT) with detailed specifications of these experiments found in the following publications [8, 18, 20, 271]. The compartment, constructed with concrete walls and base, had dimensions of 3.1 m in height, 34.3 m in length, and 10.3 m in width, resulting in a total floor area of 352 $m^2$. Ventilation conditions varied between the experiments, with door and window openings providing airflow from all sides of the compartment. In *CodeRed#02*, ventilation was reduced by 50%, achieving an opening factor of 0.039 with a total opening area of 28 $m^2$. In con-

trast, *CodeRed#01* and *CodeRed#04* did not have such reductions. The opening factor, was derived from the formula $\frac{A_w\sqrt{h}}{A_{total}}$, which describes the amount of ventilation within the compartment and is also applicable to the specific openings [8, 18, 20]. Most of the openings in the experiments were windows (1 m x 1.09 m), symmetrically positioned on opposite sides of the compartment, with one side featuring a door opening (2 m x 1.875 m), as shown in Fig 4.1.

There were three door openings—two at the ignition end and one at the opposite end of the compartment—and fifteen window openings on each long side. The ceiling was constructed of cross-laminated timber (CLT), consisting of 14 individual panels with hinge connections at the walls, supported by a central concrete beam. This specific CLT configuration was previously tested in an ISO 834 fire test for delamination. The focus of this study is to examine the effects of varying levels of exposed timber on fire dynamics, as illustrated in Fig 4.2, outlining the encapsulated region of CLT. For instance, *CodeRed#04* had 50% of its CLT encapsulated, reducing the potential fuel load in the fire. Fig 4.3 highlights the differences in external flaming observed across the three *CodeRed* experiments, with detailed analysis presented in Chapters 5 and 6 of this thesis.

The fuel load for these experiments consisted of a wood crib composed of 1 $m^2$ sections arranged in a cross-sectional pattern similar to that used in the x-ONE and x-TWO experiments [272, 273]. The wood density ranged from 392 to 526 $\frac{kg}{m^3}$, with a heat of combustion of 19.05 $\frac{MJ}{kg}$ [8, 17–20]. The wood crib was ignited using spark ignition, with 500 mL of methanol distributed in fuel pans and ignited simultaneously. Each experiment had different ignition times, and the experiments were conducted over a 12-month period, covering various seasons, which influenced the ambient conditions on the day of the experiment. *CodeRed#01* was conducted in February, *CodeRed#02* in June, and *CodeRed#04* in December, with the ambient temperature affecting the moisture content of both the CLT ceiling and the wood crib. Wind conditions also varied from quiescent to relatively low speeds, with averaged respective measurements; 0.2 m/s, 0.04 m/s and 0.4 m/s, which were also qualitatively observed from the movement of the smoke plume from the compartment. These wind measurements were used to calculate the external heat release rate, in Chapter 6.

The initial observations from these experiments provide valuable insights into the dynamics and behaviour of external flaming. In *CodeRed#01*, the CLT ceiling ignited

approximately 3 min after ignition, compared to 4 min in *CodeRed#02* and 24 min in *CodeRed#04*. This variation suggests that ventilation conditions and the extent of CLT encapsulation significantly influence fire behaviour. In *CodeRed#01*, the fire spread to the opposite end of the compartment 5 min after ignition, whereas in *CodeRed#02* this spread was delayed by 2 min, and in *CodeRed#04*, it took 26 min [8, 18, 20].

The first external flames were observed 4 min after ignition in *CodeRed#01*, intensifying as the fire progressed along the wood crib inside the compartment. Taller external flames were observed in *CodeRed#02*, likely due to reduced ventilation, which caused pyrolysis gases to ignite outside the compartment due to insufficient oxygen inside. In contrast, *CodeRed#04* exhibited small external flames similar to *CodeRed#01*, attributed to the encapsulation of the CLT ceiling, which limited the additional fuel load contributing to the fire.

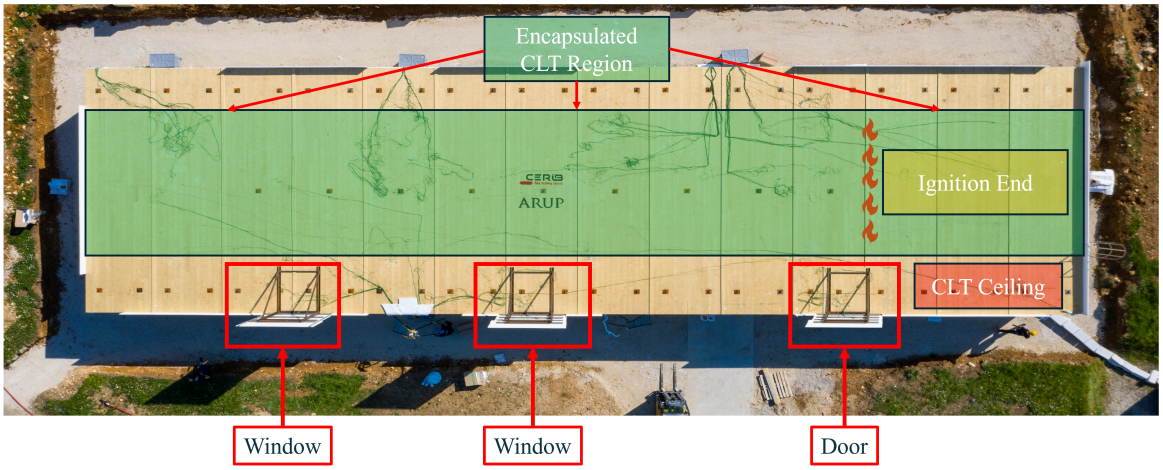



**Figure 4.2** – Aerial view of the *CodeRed* compartment featuring a CLT ceiling, with façade screens positioned above two windows and one door for monitoring external flame behaviour.

### 4.2.1 *CodeRed#03*: water mist suppression system

*CodeRed#03* was specifically designed to investigate the impact of a water-mist suppression system in an open-plan compartment fire with an exposed timber ceiling, with the aim of limiting fire growth and preventing ignition of the CLT ceiling, as illustrated in Fig 4.6. The experimental setup was similar to other *CodeRed* experiments, with some windows left open to maintain ventilation during the early fire stages. The fuel load consisted of a wood crib with a fuel load density of 57 $\frac{\text{MJ}}{\text{m}^2}$, covering 50 $\text{m}^2$ of the floor,

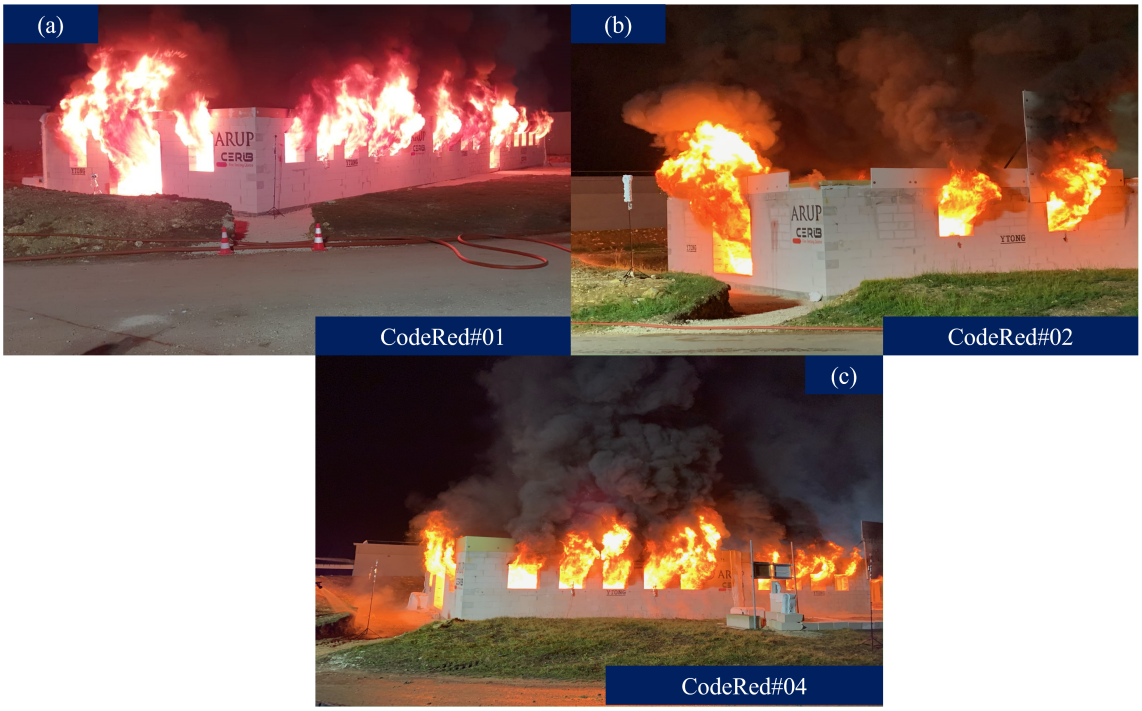



**Figure 4.3** – External flaming observed in the three *CodeRed* experiments, with *CodeRed#02* featuring 50% reduced ventilation and *CodeRed#04* utilising 50% encapsulated CLT.

which is smaller compared to *CodeRed#01*, *CodeRed#02*, and *CodeRed#04* as illustrated in Fig 4.9. The suppression system was automatic, a common feature in modern fire detection and suppression setups however prone to false alarms, as discussed in Chapter 2. In mass timber buildings, suppression systems are typically used in conjunction with other fire mitigation strategies, such as CLT encapsulation, as seen in *CodeRed#04*, as well as advanced fire monitoring and firefighting techniques.

The water-mist system used in this experiment followed criteria set by FM Global, adhering to standard codes of practice for buildings with low-hazard occupancy's, which are common in the UK [19]. The system was specifically configured for the *CodeRed* compartment, with an activation temperature of approximately 68°C and a mist pressure of around 6 bar. The nozzle layout and spacing followed the design specifications provided by the manufacturer, with a total of five nozzles activated during the experiment [19].

Initial observations showed that the fire grew uniformly at the localised ignition point, where a methanol pan was placed, similar to the configuration in other *CodeRed* experiments, as shown in Fig 4.9. The first nozzle activated approximately 1 min and 30 s after ignition, when the flame height reached 2 m from the floor. This stagnated further




**Figure 4.4** – (a) The *CodeRed* team onsite, illustrating the human dimensions involved in conducting a large-scale compartment fire experiment. (b) Interior of the compartment during fuel bed preparation. (c) Post-experiment view of the compartment interior after the fire has burned out.

fire growth, creating a steady flame. The second nozzle activated at 1 min and 50 s after ignition, with a maximum flame height of 2.8 m measured above the floor, where the compartment height was 3.1 m. The third and fourth nozzles activated around 3 min after ignition, reducing the flame height, and the final nozzle activated at 5 min and 30 s, effectively decreasing the fire size. This demonstrated the effectiveness of the water-mist system in suppressing the fire, with near-extinction achieved around 20 min after ignition. Only 4% of the total wood crib was fully or partially ignited, further indicating that the system successfully controlled fire growth [19].

This study is elaborated in Chapter 6, where the effects of the water-mist system on flame height and the internal heat release rate of the compartment were calculated.




**Figure 4.5** – (a) no external flaming from the compartment. (b) external flaming from all openings.

## 4.3 External instrumentation: setup and thermal protection

As discussed earlier, the protrusion of flames from openings in a compartment presents a significant hazard and requires thorough study. During the *CodeRed* experiments, as shown in Fig 4.5, flames were observed emerging from the compartment openings—these are known as external flames. External flames are crucial to characterise, as they pose a serious risk of igniting floors above in multi-story buildings and potentially impacting adjacent structures or the surrounding environment.

A design specification for camera placements to capture external flaming was initially established in *CodeRed#01* and was iteratively refined in *CodeRed#02* and *CodeRed#04*. Fig(s) 4.7 and 4.8 provides an overview of these camera configurations, position outside the compartment, illustrating the setup used to monitor external flames.

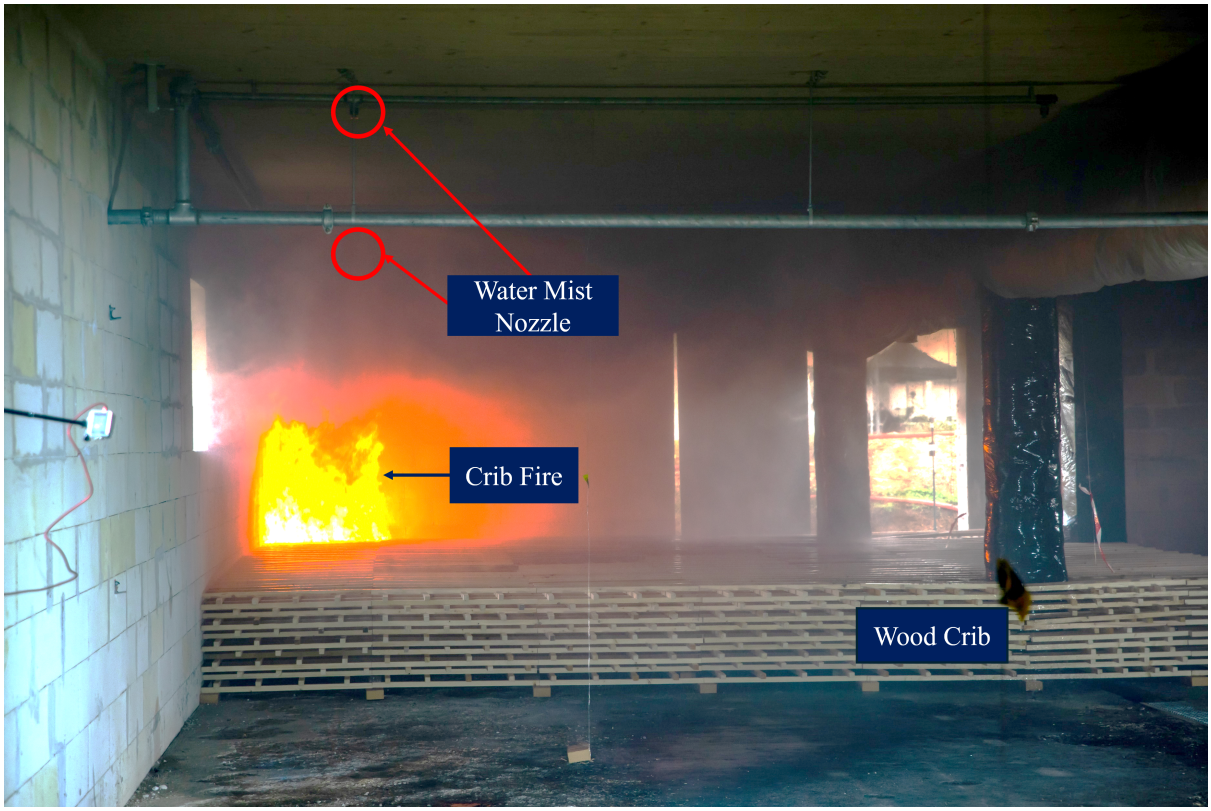



**Figure 4.6** – During *CodeRed#03*, inside the compartment with nozzle 1 and 2 activation. Localised flaming in corner of the compartment/crib.

The first iteration of the external flaming setup was implemented in *CodeRed#01*, where cameras were mounted on tripods (Fig 4.7 (a) and encased in mineral thermal protection (Fig 4.8 (b)). These cameras were positioned outside the compartment prior to ignition. Fig 4.9 presents a schematic illustrating the camera placements for all four experiments. In *CodeRed#02*, due to half of the windows being sealed, fewer cameras were needed, and the number of direct window cameras was strategically reduced. Cameras were positioned to capture side profiles of the external flames, as shown in Fig 4.10, which depict the external flaming at various stages of the experiment. The primary objective of the camera setup was to visually record the flames emerging from beneath the façade and the entire opening, as illustrated in Fig 4.11. Thermocouple measurements were also taken to record temperature data, enabling the interpolation of flame height based on the 540°C isotherm [8, 18, 20, 274, 275].

The cameras positioned within the compartment windows followed the specifications and schematics with collaboration with Mitchell et al. [17]. During the experiments, the external cameras were exposed to significant radiative heat from the fire, leading to partial or complete camera and data loss, as external flame temperatures can reach up to

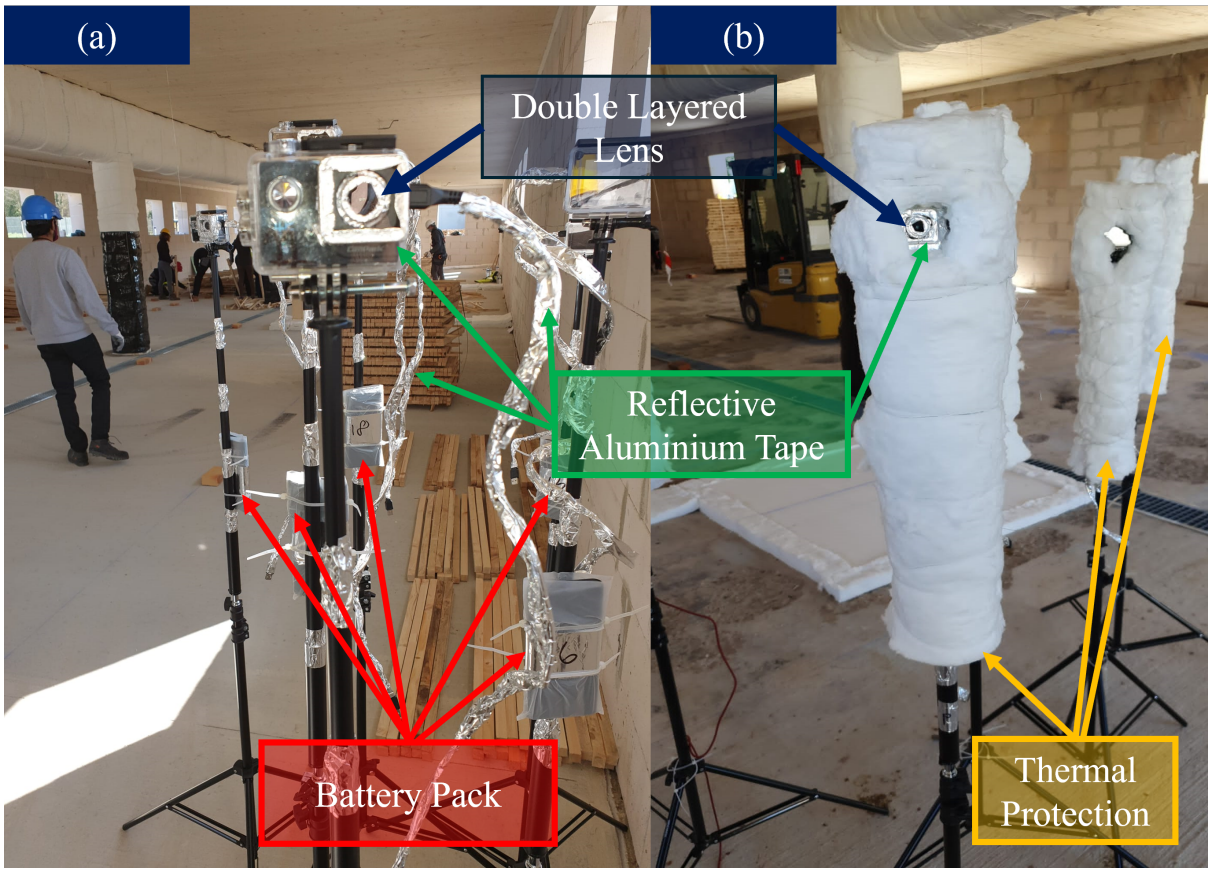



**Figure 4.7** – (a) External camera without extra thermal protection. (b) with thermal protection.

1100°C. In *CodeRed#01*, multiple cameras were destroyed by the fire, resulting in the loss of half the data for opening 4. In *CodeRed#02*, only one camera remained functional, successfully capturing data from opening 7. The use of low-cost cameras minimised financial losses in the event of failure, but the thermal protection measures enabled the cameras to operate beyond their typical temperature limits, effectively shielding them from the intense radiative heat.

Each external flaming camera was equipped with a memory card, but after a memory card failure during the *CodeRed#01* experiment, subsequent memory cards were housed in protective enclosures and connected to a 1-meter-long memory card extender. In cases of total camera failure, the results would mirror those shown in Fig 4.12. To further protect the cameras during all experiments, a double-layered glass lens was added to the front of each camera's lens casing, providing additional heat resistance. The cameras were also wrapped in aluminium adhesive tape to reflect radiative heat, thereby enhancing their durability under extreme temperatures. Internal cameras were also critical to the

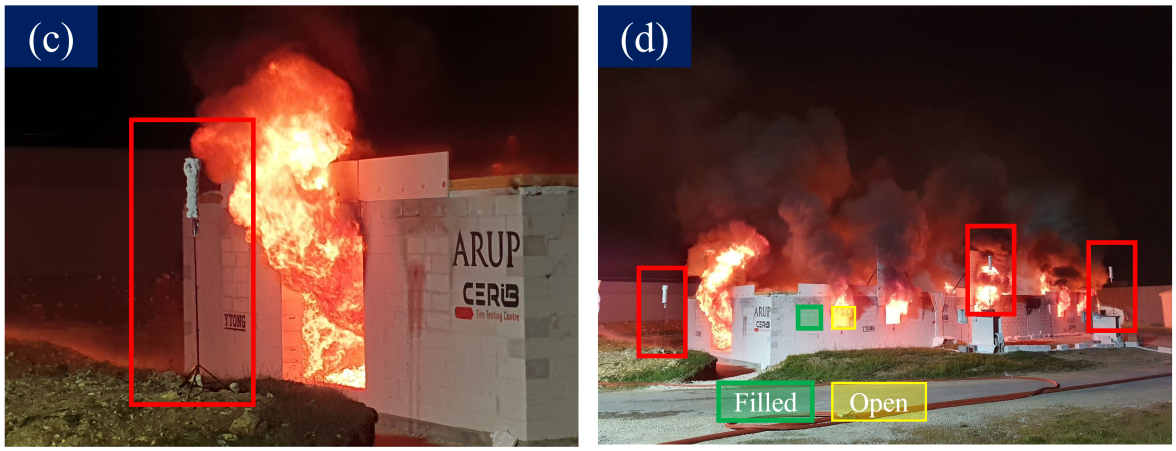



**Figure 4.8** – (c) External camera placement outside the compartment (d) Three external camera placement outside the compartment, with outline for in-filled and open window in *CodeRed#02*.

*CodeRed* experiment series, which were similarly protected and setup in the following literature [17].

## 4.4 Human dimensions to a large compartment fire experiment

The human aspect of conducting these experiments is equally important, as none of the aforementioned and consequent chapters would have been possible without the dedication and effort of the research team, particularly during the challenges posed by the COVID-19 pandemic. The complexities and difficulties of conducting large-scale experiments like *CodeRed* need to be emphasised, as they mirror the challenges faced in similar works, such as those by Mitchell et al. [17,272,273]. Numerous logistical hurdles were overcome, including travel restrictions, quarantine, isolation, and the transportation of large-scale instrumentation required for the setup prior to conducting the *CodeRed* experiments over the course of two years. Furthermore, executing the experiment on time, followed by data collection, post-processing, and analysis for relevant journal publications within specific deadlines, added to the complexity [8,17–20]. Significant preparatory efforts were required before the experiments, such as protecting and strategically placing cameras to collect the best possible data, creating a detailed map for camera placement, and conducting numerous iterations of the experiment to minimise errors and continuously improve the

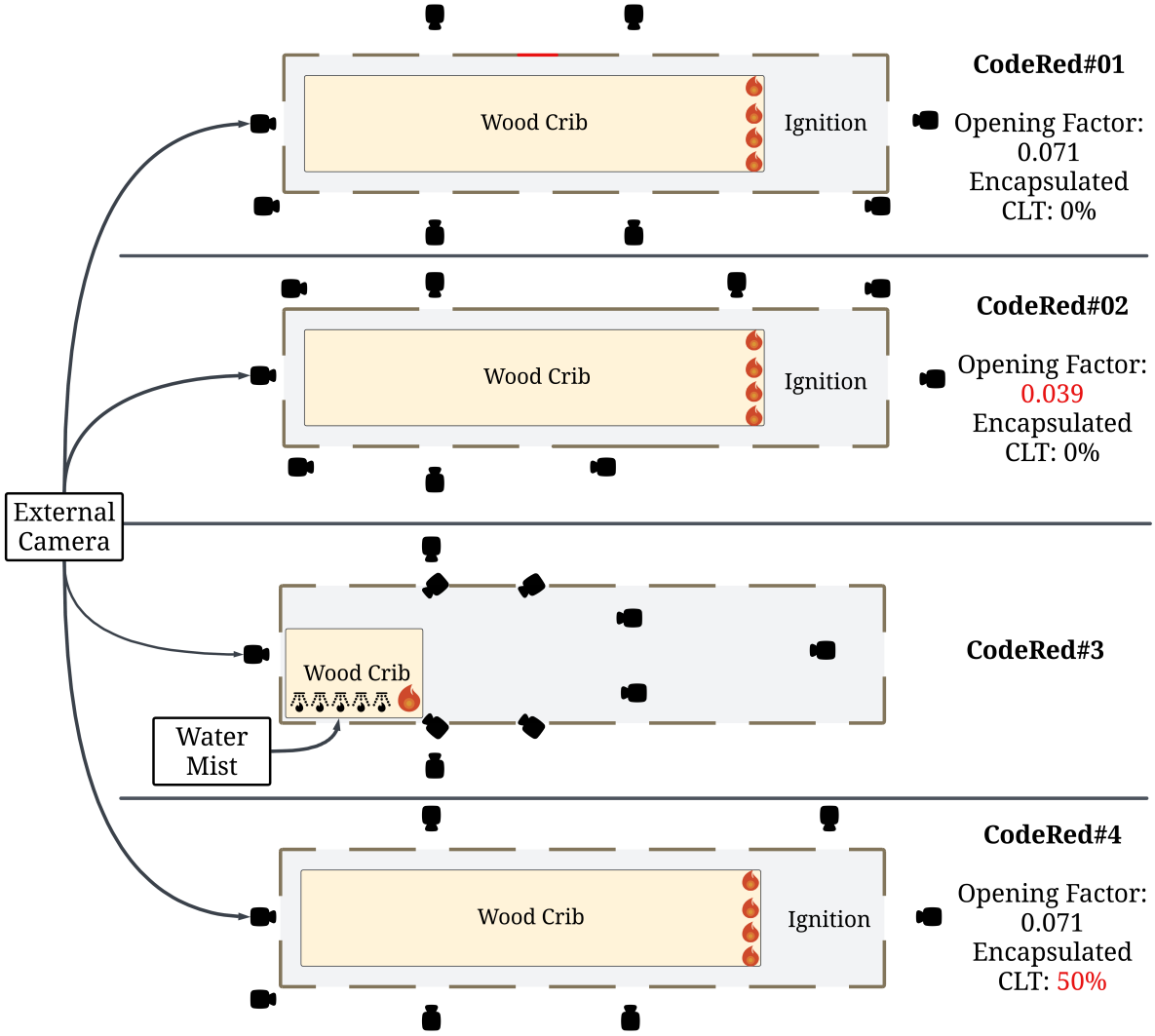



**Figure 4.9** – External camera placement map for all *CodeRed* compartment fire experiments. The strategic position of camera ensured comprehensive coverage of the external fire dynamics (and internal for *CodeRed#03* capturing critical data. This arrangement(s) was essential for conducting detailed post-experiment analysis and understanding the fire behaviour in different experimental conditions.

setup.

The human factors involved in such experiments are crucial. Collaborators from Imperial College London (Hazelab), ARUP (London and Australia), CERIB, and the Paris Fire Brigade played a critical role in making the experiments successful. It is easy for researchers to overlook the importance of these connections, relationships, and bonds that underpin the success of any experiment and the resulting publications. It is difficult to fully reflect on the countless hours of work leading up to the *CodeRed* experiments, which themselves lasted less than an hour but yielded critical results and observations

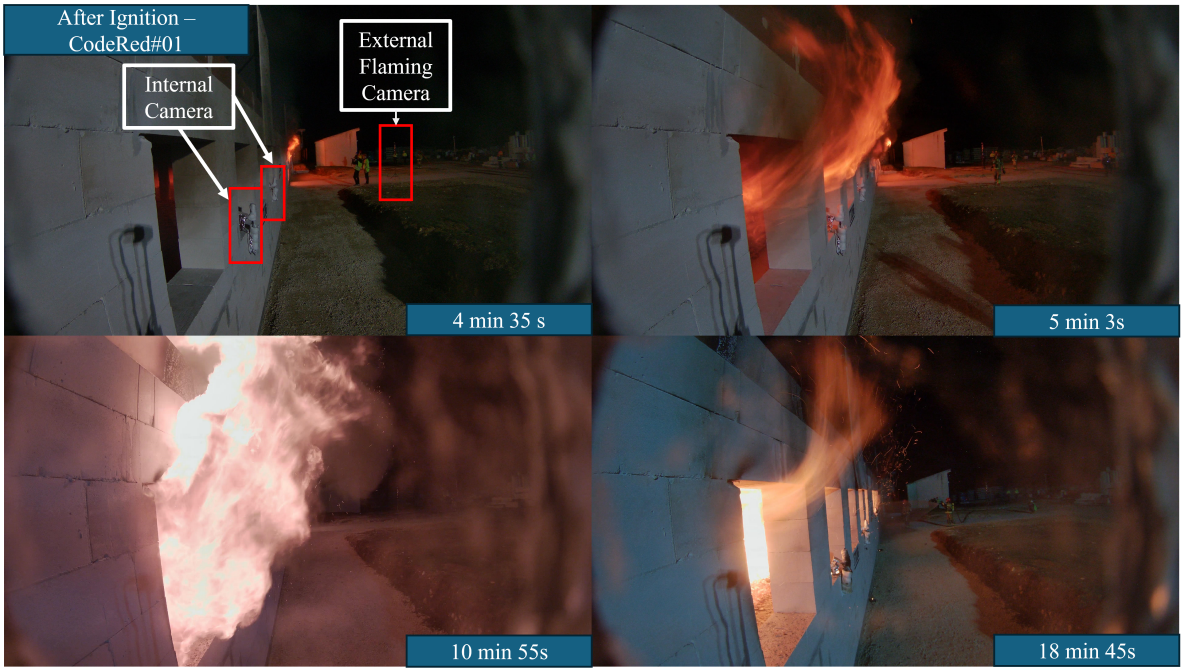



**Figure 4.10** – Camera placement, positioned tangentially to the compartment wall, capturing the side profile of the external flame during the experiment. This setup can potentially quantify flame thickness and the observation of firebrands, aligning with the study conducted by Mitchell et al [17]

for the improvement of the built environment, sustainability and fire safety. But it is key to mention in every publication, piece of research and thesis, human dimensions play a significant scientific role.

Fig(s) 4.4, 4.13, 4.14 and 4.15 illustrate the scale of the *CodeRed* experiment, and the extensive effort involved in setting up the wood crib inside the compartment, highlighting the level of coordination and preparation needed for a successful experiment during the pandemic.

## 4.5 Visual analysis of *CodeRed*

All visual data gathered during the *CodeRed* experiments underwent pre- and post-processing, as well as detailed analysis, which are key components of the work covered in Chapters 5 and 6. Data processing is critical to ensure accuracy and reliability before analysis.

The visual diagnostics of external flaming begin with the identification of flames within the fire scene (individual images), which is achieved using thresholding techniques. Vari-

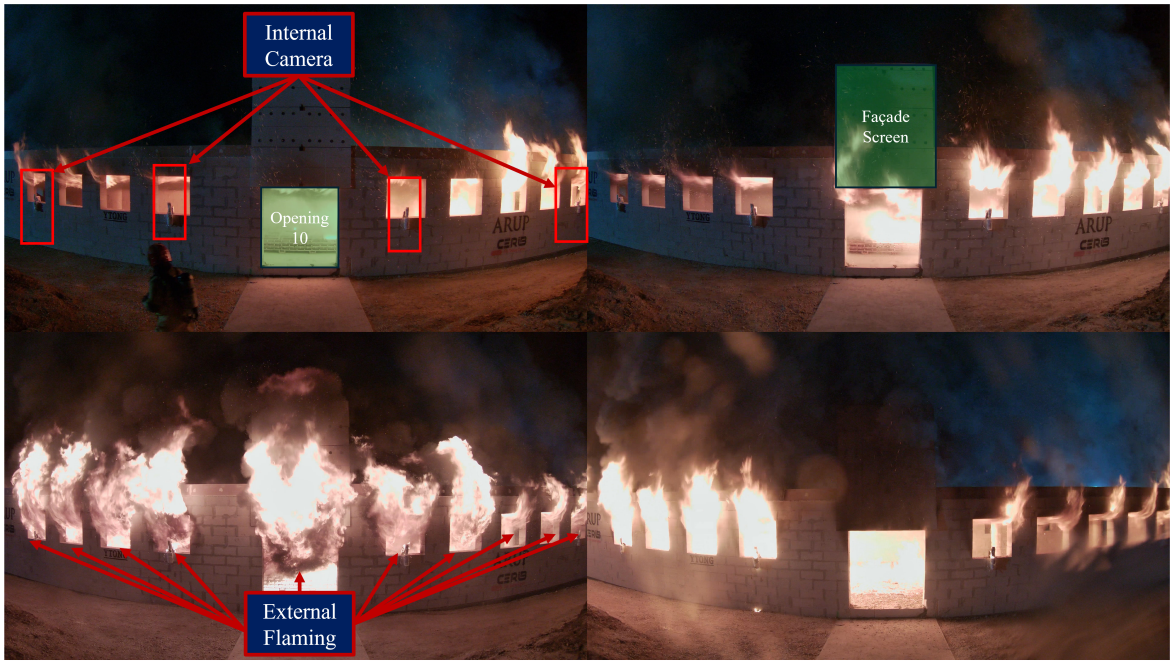



**Figure 4.11** – External camera setup in-front of the compartment wall, capturing the external flaming from the openings with the facade screen above the door. The camera lens melting in the bottom right image distorting visual data capture.

ous thresholding methods exist, such as Otsu's method which is an automatic histogram-based method that iterate over the entire set of images [276]. Otsu's method calculates an optimal threshold value, denoted as t, by minimising the weighted within-class variance, assuming the image has a bimodal distribution. This is represented in Eqn 4.1. Otsu's method identifies the optimal threshold value that lies between the two peaks of the histogram, minimising the variances of both classes. However, while Otsu's method provides an automatic solution, it is important to acknowledge that certain unique features may not be accurately detected, resulting in potential inaccuracies. This method was applied and tested in the analysis of the *CodeRed* experiments, and thresholding is discussed in further detail in Chapter 5 during the evaluation of external flames.

In addition to thresholding, the presence of flames at any given time during an experiment, referred to as flame probability, is crucial in experiments of design fires. Flame probability provides a quantitative measure of the likelihood of flame occurrence and characterises fires into three distinct regions: persistent, intermittent, and buoyant flame regions [277, 278]. The intermittent region, defined as having a 50% probability, is of particular importance as it represents the point of maximum combustion intensity [49]. Mathematically, flame probability is expressed as a function of time, represented by Eqn

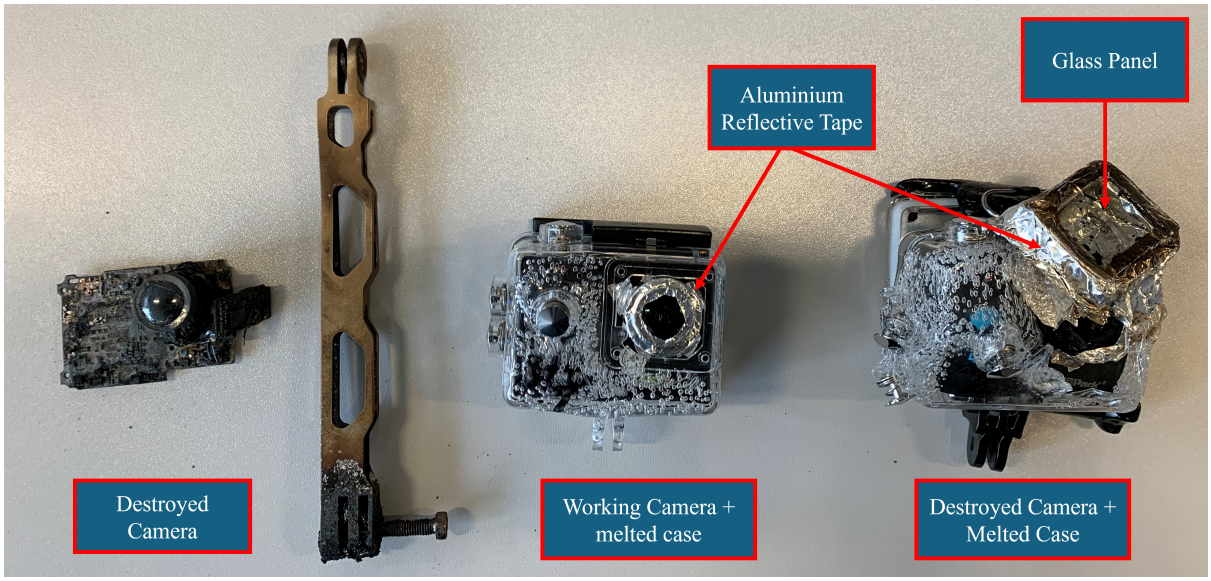



**Figure 4.12** – An image of the stages of the cameras used in *CodeRed*, and the result of the experiment on the melting of the case and total data loss.



**Figure 4.13** – Imperial Hazelab Scientists - *CodeRed#01* compartment fire experiment, before experiment.

4.2, where N denotes the total number of frames in the experiment, n represents the frame number, and Z represents the $N_{th}$ matrix. The variable t signifies the specific point in time during the experiment between ignition and extinction.

This process is illustrated in Fig 4.16, where each image is binarized and converted into a numerical matrix, with values corresponding to the binary state of pixels. These values are then summed to create an array of $N_{th}$ matrices. To visualise this, the average is taken across the entire experiment, and a contour plot is generated. The results of this




**Figure 4.14** – CERIB Team and Imperial Hazelab - Setup of wood crib (1).

analysis are further explored in Chapter 5.

$$\sigma_w^2(t) = w_0(t)\sigma_0^2(t) + w_1(t)\sigma_1^2(t) \tag{4.1}$$

$$\text{Flame Presence} = \frac{\sum_{i=1}^{n} z_i}{N} \tag{4.2}$$

## 4.6 Conclusion

The *CodeRed* experiments highlight the importance of studying external flaming, a critical yet understudied phenomenon, particularly in large-scale compartment fires involving exposed mass timber. Understanding external flame behaviour is essential for ensuring the safety of high-rise buildings and their occupants. The *CodeRed* series addresses a significant research gap by conducting experiments with varying ventilation conditions and different levels of CLT exposure to analyse. Visual analysis plays a cru-




**Figure 4.15** – CERIB Team and Imperial Hazelab - Setup of wood crib (2).

cial role in measuring the size and shape of external flames in *CodeRed*, as well as in calculating the heat release rate outside the compartment. This study can help in the development of future external flaming models and design fires, as tall flames have the potential to ignite floors above or adjacent openings and buildings. This chapter reviews the four *CodeRed* experiments, discusses the challenges of conducting these experiments during the COVID-19 pandemic, details the instrumentation setup for external cameras, and provides an introduction to visual diagnostics presented in this thesis.

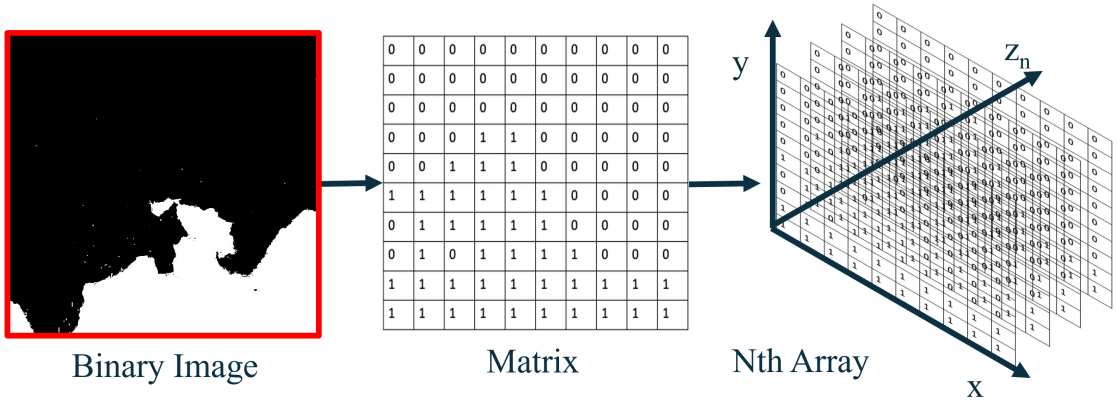



**Figure 4.16** – Illustration for flame presence probability process.

# Chapter 5

# Computer vision for external flames

## Summary [1]

External flames from openings in compartment fires pose a significant hazard, especially in buildings constructed with combustible materials like mass timber. These materials can generate larger external flames compared to non-combustible ones like steel or concrete, increasing the risk of fire spreading to adjacent floors and buildings. This study introduces computer vision (CV) as an innovative diagnostic tool for analysing external flames in timber compartment fire experiments. CV, powered by artificial intelligence, can assess flame characteristics such as flame probability, height, length, angle of inclination, merging behaviour, and projected area using only images, making it highly effective both in controlled environments and real-world situations. After initial calibration on a small set of images, CV provides instantaneous and automatic results, regardless of the number of flames or video length, streamlining fire analysis significantly. The study applies CV to the largest fire-compartment experiments ever conducted, known as *CodeRed*, performed outdoors with unavoidable crosswinds. In such conditions, traditional methods are limited, but CV's image-based approach excels. The method was able to capture variations in external flame behaviour across multiple openings and in three separate experiments, which studied different ventilation levels and timber exposure. For example, when the timber ceiling was fully exposed, the average flame height reached $1.5 \pm 0.6\,\mathrm{m}$.

1. This chapter is based on "R. Amin, H. Mitchell, G. Rein, A. Glew, P. Kotsovinos, N. Kalogeropoulos, M. Heidari, D. Barber, J. Schulz (2024), *AI Flame Diagnostics: Using Computer Vision to Quantify External Flame Behaviour in a Large-Scale Compartment Fire*, **Submitted to journal for peer-review**, Revisions."

Reducing the ventilation by 50% caused a significant increase, with an average flame height of $2.8 \pm 1.3\,\mathrm{m}$. Encapsulating 50% of the timber lowered the average flame height to $1.4 \pm 0.5\,\mathrm{m}$. Compared to conventional methods like thermocouple trees and Manual Vision, CV proved to be a superior technique, enabling faster, more accurate, and simultaneous observation of multiple flames at higher time resolutions. This advancement in flame diagnostics could greatly improve our ability to understand and mitigate the risks associated with external flames in buildings, and other flame phenomena for different applications.

## 5.1 Introduction

As previously mentioned in this thesis, exposing large areas of timber introduces additional fuel load to a compartment. If there is excess fuel and a lack of ventilation, the volatile gases from wood pyrolysis may exit the compartment openings and contribute to external flaming, illustrated in Fig 5.1 (a) [14]. This may lead to vertical fire spread along the façade or to a neighbouring building, through direct flame contact or incident heat flux [279]. It is critical to understand the impact of timber on external flaming in compartment fires. External flame behaviour was first studied by Law & O'Brien (L&O) in the 1970's to allow the assessment of external structural elements [275]. L&O assumes uniform temperature distribution across width and thickness of the external flame, locating the flame tip where temperature reaches 540°C, and idealising flame shape when protruding from openings. L&O was developed for non-combustible compartments and as a result its use in timber compartments needs further study.

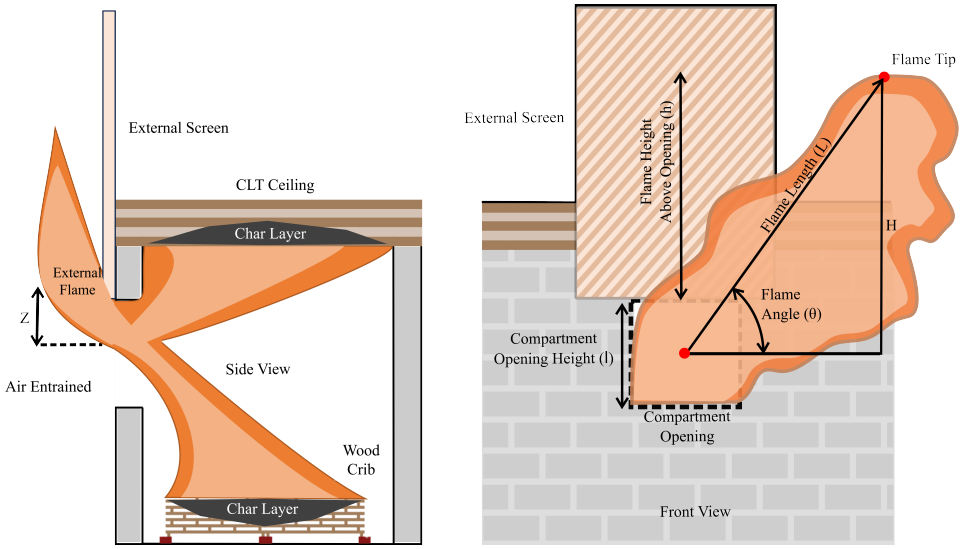



**Figure 5.1** – (a) Diagram of external flaming through an opening in a compartment with an exposed mass timber ceiling and wooden crib. (b) The contour/edge of the external flame includes the difference flame parameters such as height, length, angle, and projected area from the compartment opening. The flame origin is the centre point of the opening.

This chapter investigates a new method to study external flames as an alternative to the complex instrumentation and raw data processing such as those used in L&O. Computer vision (CV) simultaneously can enhance accuracy and provide instantaneous measurements by applying various artificial intelligence (AI) algorithms to construct models that analyse unprocessed visual data [34]. Despite the extensive use and exploration of

CV in various fields, its potential in fire research has remained unexplored [35]. Previous studies have been conducted on measuring a single fire parameter such as flame height using simple image processing methods by observing distinct flame regions [49,277,279,280]. These methods involve manual computational transformations, such as contrast adjustment and colour saturation. In contrast, CV operates automatically and instantaneously, offering a more efficient approach to manual image processing. Accurately identifying the flames' shape necessitates the implementation of appropriate algorithms. To bridge this research gap, this study leverages the core principles of using CV algorithms by validating a model against manual visual analysis and L&O thermocouple measurements to contribute to the state-of-the-art by simultaneously measuring multiple flame characteristics including flame probability, height, merging, length, angle of inclination and projected area, thereby offering an instantaneous fire diagnostic tool.

## 5.2 Review of external flaming in compartment fires

A previous review [13], outlines the research gaps in current fire experiments in mass timber compartments. Limited research has been completed on external flaming, whilst some researchers made simple observations such as measuring the flame height during the experiments [13].

At the small-scale, Gorska et al. observed increasing external flame size with increased area of exposed cross-laminated timber (CLT) when conducting a series of 24 small (0.25 $m^2$ floor area) compartment experiments with a single opening. Gorska et al. stated that the excess of pyrolysis gases from exposed timber panels, along with induced horizontal velocities at the openings, can increase and change the shape of the external flame compared to non-combustible compartments [278].

At the medium scale, increased flame sizes and higher external temperatures were reported for the CLT compartments [281], where the Épernon programme comprised a series of six (24 $m^2$ floor area) compartment experiments. Engel et al. conducted three medium-scale (20 $m^2$ floor area) and two large-scale (40.5 $m^2$ floor area) experiments where the external flame was similar in all experiments, but the very high moveable fuel load may have decreased the impact of the exposed CLT [282].

At the larger-scale, Su et al. conducted six large-scale (42 $m^2$ floor area) experiments

with fully and partially encapsulated mass timber. Higher heat fluxes to the external screen above the opening were recorded in the experiments, with the largest compartment opening exhibiting the largest external flaming [283]. Bøe et al. conducted two large-scale (95 $m^2$ floor area) experiments with fully exposed CLT ceilings and large window openings, the largest external flame observed measured 3 m above the screen [283].

The majority of compartment experiments to-date best represent, residential-type buildings with smaller floor areas, whereas contemporary office buildings are often open-plan, and have floor areas that are substantially larger which leaves a gap in understanding for fire-safe mass timber design. An experimental series – *CodeRed* – with a mass timber ceiling was conducted to create new knowledge that is relevant to large open plan compartments [8, 18, 20]. *CodeRed#01* was a fully ventilated compartment with zero encapsulated CLT which observed external flaming with heights of 2.5-3 m where *CodeRed#02* with a 50% reduced ventilated compartment exhibited taller flames at around 3-3.5 m the severity of external flaming was determined by the control in ventilation. However, *CodeRed#04* exhibited 1.5 m smaller flame heights than those in *CodeRed#01* due to 50% CLT encapsulation. The data from the *CodeRed* experiments has been utilised in this study and expanded upon throughout the chapter.

## 5.3 Review of flames in image processing

This section is a chronological review of the literature of visual imaging to study flames size and shape which includes flame edge detection and colour thresholding. Previous research has employed various approaches to study flame shapes. Early methods involved analytical techniques, such as the correlation between temperature distributions from thermocouple readings and flame height by Law and O'Brien, which have limitations [274, 275]. For instance, thermocouple readings are unable to measure and interpolate flames outside their immediate region. Laboratory measurement of flame shape and sizes have increasingly shifted towards image processing methods [284–286].

In 1995, Audouin et al. [49], analysed 160 images using image processing with grey-level thresholding to determine the average centreline temperature of pool fires. They compared these results to thermocouple measurements along the centreline to measure flame probability and height. In 2004, Lu et al. [287], applied innovative digital image

processing algorithms based on brightness to monitor and characterise flames. They identified the ignition point by analysing gray-scale levels between pixels.

In 2006, Lu et al. [288], investigated the properties of pulverised coal flames using image processing techniques to remove background noise and study their oscillation frequency.

In 2008, Huang et al. [289], utilised image processing techniques to observe flames across different colour scales, including RGB and HSV. Their research demonstrated that conventional cameras could monitor various flame characteristics by employing different colour scales, thus enabling imaging across both visible and infrared spectra.

Palacios et al and Gomez-Mares et al, in 2009 and 2010 [88,290], respectively assessed the shape of jet flames including its length and width using infra-red images. Both studies used image processing to analyse each IR image manually where the former suggested there is lack of research in predicting the shape and proposed an expression whilst the latter studied the axial temperature distribution.

In 2012, Yadav et al. [291], used image processing techniques to identify gray-scale pixels near flames amidst smoke, aiming to optimise flame edge detection to allow for flame characteristic measurements such as flame height. Their study concluded that while previous research predominantly relied on colour scales, motion detection, and edge detection methodologies, their research uniquely focused on segmenting both RGB and gray-scale components. In the same year, Qiu et al. [292], introduced an algorithm to determine flame edges and validated it across various Bunsen flames. They suggested that future research could advance by quantifying flame parameters such as volume, surface area, and flame spread rate. The algorithm's versatility was highlighted when applied to more complex shapes, such as turbulent diffusion flames and pool fires. Numerous other studies also used various image processing techniques for flame characterisation, edge detection, and overall imaging [286, 293–296].

In 2015, Lu et al. [297], used image processing with grey-level thresholding from Otsu's method to study the merging behaviour of external venting flames from parallel windows of an under-ventilated compartment. Also in 2015, Tang et al. [298], used the same method to obtain the average flame contour across all images, studying flame tilt characteristics for pool-fires with cross-airflow interference.

In 2016, Zhang et al. [299], used gray-level thresholding from Otsu's method to define

the flame intermittency contour, measuring flame heights and horizontal flame lengths based on the flame presence probability of jet diffusion flames.

In 2019, Hu et al. [300], used Otsu's method of gray-level thresholding to obtain the flame intermittency for different wind speeds, measuring façade flame height and horizontal extending distance. In the same year, Ren et al. [301], employed the same method to obtain the flame intermittency distribution, measuring façade flame height evolution and studying the transitional behaviour of a fully developed under-ventilated compartment fire.

In 2021, Rackauskaite et al. [272], used image processing analysis to identify flame location by capturing fire size and flame spread rates using colour thresholding of the HSV, RGB, and HSI colour scales, depending on the different camera locations.

In conclusion, the novel method proposed in this paper, Computer Vision (CV) serves as a crucial bridge between traditional image processing techniques and advanced black-box models, such as convolutional neural networks (CNN). Previous methodologies have primarily focused on gray-level thresholding and manual imaging techniques employed by experimentalists to imaging of flames and measure flame height. Additional methods, including flame edge and colour detection, have also been explored. However, these manual approaches are often constrained to individual flame characteristics and lack the scalability and automation required for complex fire scenarios such as external flames of buildings. Tab 5.1 gives an overview of the different methods that are applicable to external flames as mentioned above, with their advantages and disadvantages and relevant use in literature. Recent advancements, particularly the integration of deep learning frameworks with computer vision, have shown promise in predicting heat release rates and other flame characteristics [95, 201]. Despite these developments, a significant gap remains in applying such techniques to external flames in large fire compartments while maintaining the necessary simplicity, speed, and accuracy [201]. This research addresses this limitation by presenting a robust diagnostic tool that automates and instantaneously quantifies the size and shape of external flames using CV, thereby enabling comprehensive flame analysis.

Moreover, the utility of this method is not confined to external flames in fire compartments. It extends to a broader range of applications, including small canonical flames, fire behaviour under oil reservoir conditions to larger flames such as wildfires and building

fires. While previous studies, have employed image processing to analyse the geometry of small diffusion flames [59,61], this work advances the field by demonstrating how CV can automate and enhance the extraction of flame geometries, offering a scalable and precise solution for diverse fire scenarios but also without the need for more complex method such as CNN's.

## 5.4 CodeRed experiment series

To recap from the previous chapter, a series of four compartment fire experiments of 352 $m^2$ were conducted. These experiments aimed to study the fire dynamics in large, open-plan compartments with a CLT (cross-laminated timber) ceiling, with varying ventilation and CLT exposure. *CodeRed#01* had a fully exposed CLT ceiling with all openings left open for a fully ventilated compartment. *CodeRed#02*, had 50% of the openings closed to investigate the impact on the severity of external flames with reduced ventilation. *CodeRed#04*, had full ventilation, but 50% of the CLT ceiling was encapsulated. Detailed descriptions on the specific configurations of these experiments can be found in the works of Kotsovinos et al [8, 18, 20]. The analysis presented in this study uses external camera instrumentation around the compartment to record the full extent of external flaming, however the external flaming has not been studied in-depth until now. Non-combustible screens were placed above openings 4, 7 and 10 as represented in Figure 5.2. The screens are fitted with thermocouples and plate thermometers to record temperature distribution and heat flux [8]. For the acquisition of visual data, external cameras were positioned perpendicular to each opening with the screen. To minimise heat damage from the flames, the cameras and the memory cards were enclosed within protective housing made of gypsum board [163, 271], adopting a similar approach of Rackuskaite et al [272].

## 5.5 Computer vision methodology

Computer vision (CV) is utilised in this study using visual data captured from four cameras across three experiments, two from *CodeRed#01*, and one each from *CodeRed#02* and *CodeRed#04*. Two remaining cameras were damaged from the fire where the record-

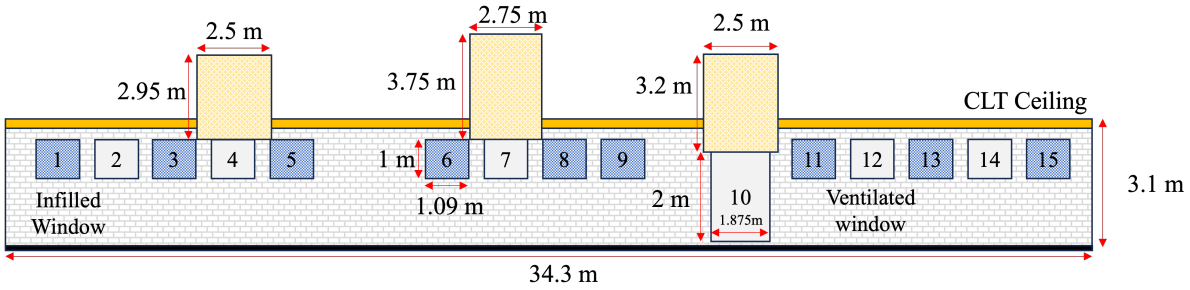



**Figure 5.2** – The *CodeRed* compartment wall and external screen(s) above two windows and a door. *CodeRed#02* had reduced ventilation with openings 2, 4, 7, 10, 12 and 14, whereas *CodeRed#01* and *CodeRed#04* (50% encapsulation) have full ventilation [20].

ing was completely lost. Firstly, the images are colour thresholded, an initial essential step to isolating fire pixels and mitigating noise. Thresholding is most commonly employed through automatic techniques such as Otsu-binary thresholding which calculates the optimal threshold value across the entire dataset [276]. While Otsu's method has been widely utilised in prior studies on flame detection and segmentation [299], its efficacy may be compromised when dealing with features, such as low-luminosity fires, potentially leading to inaccuracies.

Alternatively, researchers have employed more intricate approaches, utilising a pre-trained neural network, YOLOv5, to automatically segment fires in complex environments within the image containing objects such as smoke, weather, light sources, cars [95, 100, 284]. Given the noise in *CodeRed*, which primarily involves smoke, external light from floodlights, and firebrands, an approach using a HSV colour scale was deemed more suitable, and has already been effective in similar compartment fire studies [272]. This process demonstrated superior accuracy compared to Otsu's method whilst being a more time-effective solution than employing YOLOv5.

Subsequent to colour thresholding, a masking CV algorithm is used which is a convolution operation that identifies a kernel region in each image as a matrix. The kernel region is critical, as it encapsulates the anticipated flame observation area. To further reduce image noise and isolate more fire pixels, median blurring is applied, wherein individual pixels are substituted with the median value derived from neighbouring pixels within a specified square spatial region in the kernel area. The final CV algorithm uses contour mapping to detect flame edges and outline the outer flame region, contrary to prior methods using bounding boxes that identify a square region around the flame [95, 100]. These

contours are transverse curves connecting continuous points in 2-D space, forming a singular polygon, as illustrated in Fig 5.4 (b). The vertex of the polygon is defined as the tip of the flame, and the separation distance between the tip and the flame origin is the flame length which is quantified as the Euclidean distance. The angle of flame inclination is defined by the arc-tangent function in Eqn 5.1 and illustrated in Fig 5.4 (b).

$$\vartheta = \arctan\frac{\mathrm{H}}{\mathrm{L}} \tag{5.1}$$

In summary, CV begins by performing colour thresholding on all fire images in the *CodeRed* dataset using the HSV colour scale (after calibration). Following this, masking is applied to isolate the regions of the image containing fire. To reduce noise from sources such as floodlights and firebrands, median blurring is employed. Finally, contour mapping is utilised to delineate the flame, allowing for the measurement of its characteristics such as flame probability, height, length, angle of inclination, merging and surface area all of which are in this chapter.

To expand on the initial calibration process required by CV and clarify its importance, a parametric study was conducted to evaluate the effect of varying HSV (Hue, Saturation, Value) thresholding. We selected the flame height at opening 7 in *CodeRed#02* for the parametric study due to the higher data availability across the three experiments. Manual Vision yields time-averaged measurements, which was done similarly to the literature previously reviewed [300,305,306]. The maximum and minimum coordinates of the flame above the opening within a binary pixel region in 2D space are manually identified, yielding the maximum flame height at any given time during the fire. This approach aligns with previous research that measured flame height by identifying the coordinates of the highest binary pixel [277]. The height, initially measured in pixels, is interpolated into distance (m). An arbitrary time instance was chosen, approximately 14 min after ignition, where the optimal HSV thresholding is found when the flame height with CV agrees with Manual Vision at 3.3 m (shown in Fig 5.3). Each *CodeRed* experiment required calibration before CV was applied and a different optimal HSV thresholding value due to visual variations in the experimental setup and environment, which introduced different visual disturbances. One source of disturbance was identified as floodlights present around the compartment. For example, the flames in *CodeRed#02* were more luminous and exhibited different colour tones, possibly due to variations in ventilation. The parametric

study found that sub-optimal HSV values introduced measurement errors, as illustrated in Fig 5.5. The figure shows different contour lines representing the varying flame height measurements resulting from different HSV thresholding. The optimal HSV ranges for each *CodeRed* experiment are detailed in Table A.1, where obtaining the optimal HSV for *CodeRed#01* and *CodeRed#04* followed suit from *CodeRed#02*.

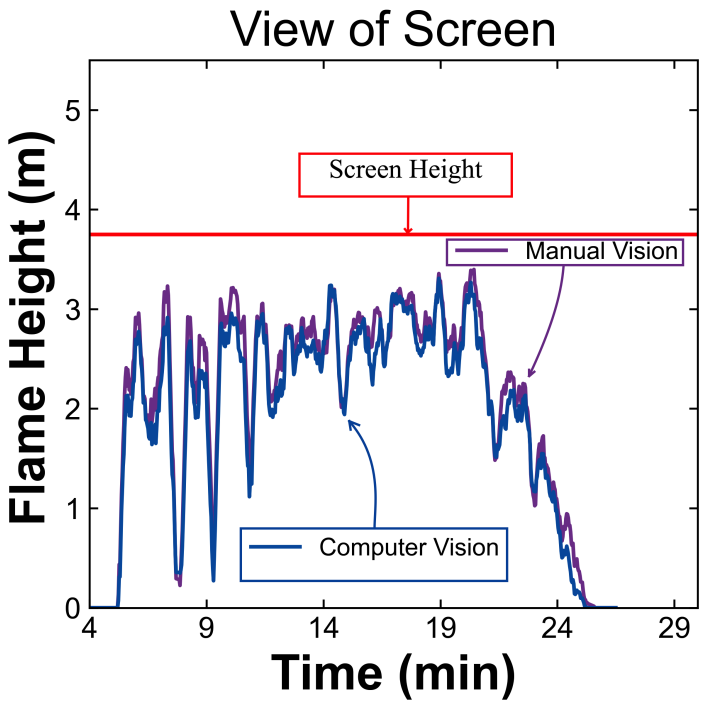



**Figure 5.3** – Validating manual visual analysis against computer vision shows a 3.3% error analysing the screen area.

After calibration with one arbitrary image, we used Manual Vision to validate CV. Manual Vision was applied to measure flame heights as a function of time for 1143 images. The data was batch-processed and a region of interest encompassing only the external screen (to align with thermocouple readings) was chosen as a measurement domain, shown in Fig 5.4 (a). Validating CV against the manual visual method results in an average error of 3.3% when analysing opening 7 of *CodeRed#02*. In Fig 5.3 the maximum flame height is 3.30 m and 3.39 m, respectively. Consistency and precision in flame height measurements in both methods indicate shared fundamental principles in visual analysis. It shows that CV is a reliable tool for flame imaging, with higher time resolution, at much faster rate, scalable for automation, and with the same accuracy.

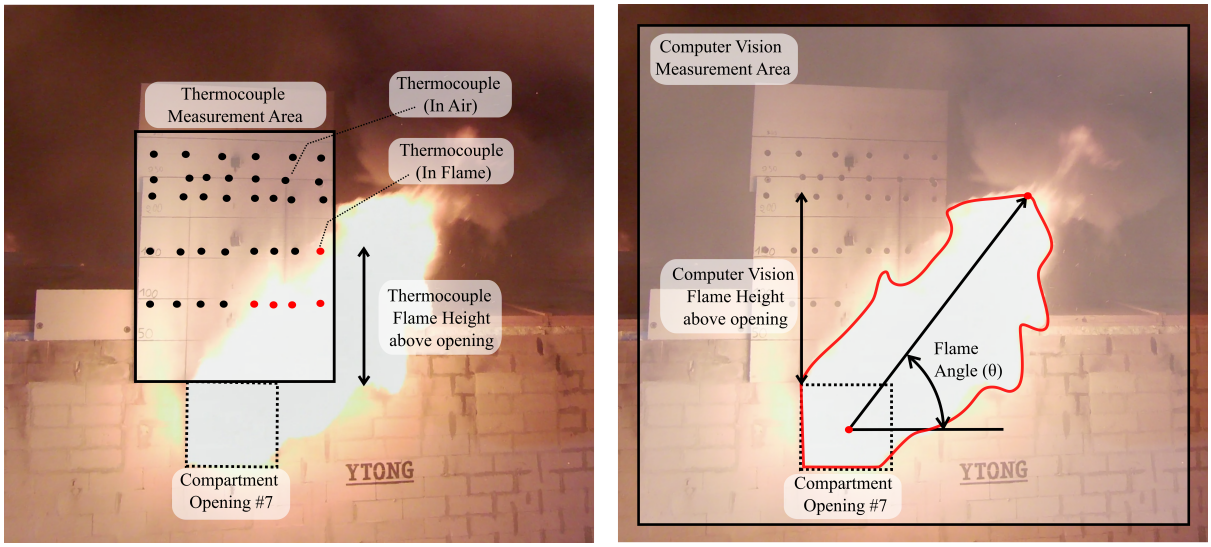



**Figure 5.4** – (a) Diagram outlying the measurement domains for the external flaming of opening 7 *CodeRed#02*. (b) The computer vision domain captures the full flame height for the inclined flames in the presence of cross-winds that are observed to extend beyond the screen whilst the thermocouples can only measure temperature on the screen.

### 5.5.1 Flame probability

The probability of flame presence over time is important in fire behaviour analysis. Flame probability (FP) quantifies the likelihood of flame presence within a spatial region and categorizes fires into persistent, intermittent, and buoyant flame zones, according to McCaffrey's three-region flame regime [277]. The intermittent region is particularly significant as it denotes the area where the flame intermittently reaches its maximum height with a 50% probability, correlating with the location of the most intense combustion [49, 277, 280, 300, 301, 305, 307]. In this study, each image is converted into a matrix, with individual pixels binarized using a threshold value of 127/255. This threshold was determined to be most suitable for the *CodeRed* dataset, based on the average pixel values across all images. In contrast, other studies have utilised a threshold of 110 [88, 288, 289]. In a real-world context, CV is an optimal tool as it mimics human vision and recognition, making it relatively straightforward to identify the ideal threshold [34]. However, in the context of *CodeRed*, the complexity increases with changes in the image scene whilst balancing automation and speed, introducing sensitivity issues. These challenges are addressed through the parametric study presented in this chapter. The resulting flame probability contour for *CodeRed#01*, examining all openings, is illustrated in Fig(s) 5.6 and 5.7 respectively, as this was the only experiment to capture data for all compartment

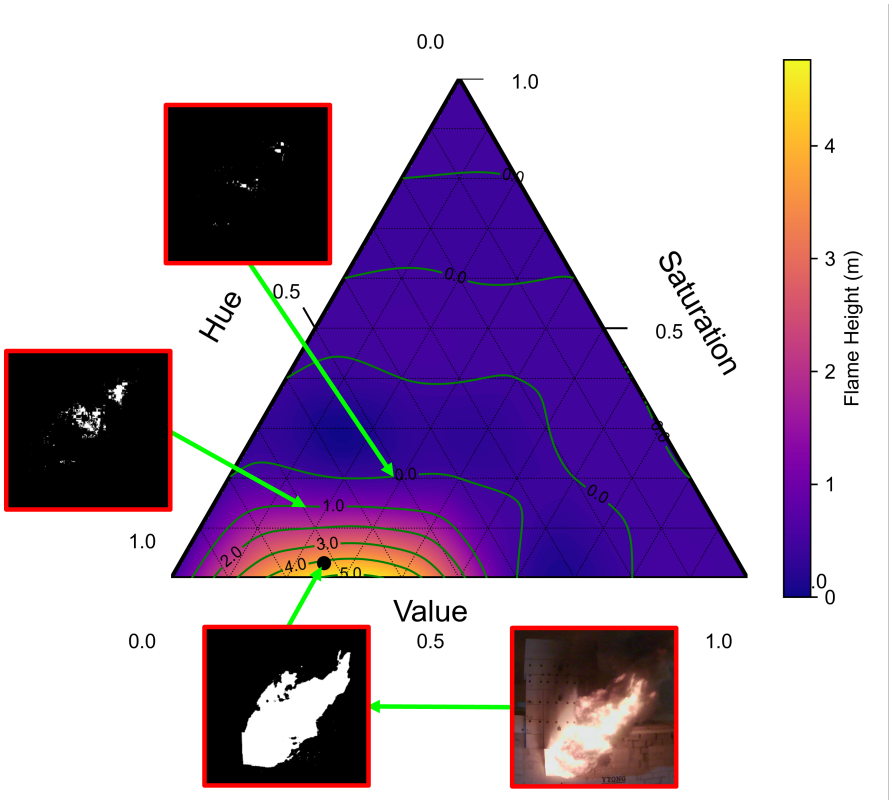



**Figure 5.5** – Ternary plot for opening 7 in *CodeRed#02*, indicating a parametric study of change in HSV (hue, saturation, value) thresholding to observe an effect in measured flame heights. The optimal value of HSV with computer vision gave a flame height of 4.3 m approximately 14 min after crib ignition.

openings where data was not lost.

## 5.6 Computer vision results

### 5.6.1 Flame height above opening

One of the critical characteristics of a flame, its height, is defined as the vertical location where excess unburned fuel is consumed through air entrainment within a flame which is also the distance from the opening to where the flame exhibits 50% intermittency [307]. It is important as it is a potential hazard for fire spread to the floor above. Flame height delineates the extent to which a flame can reach opening. Flame impingement is a severe condition, especially when combustible materials are present, as it can lead to upward flame spread and propagation to the surrounding environment [270, 279]. The data derived from computer vision (CV) was compared against the thermocouple data indicating disparities, particularly when estimated flame heights from thermocouple

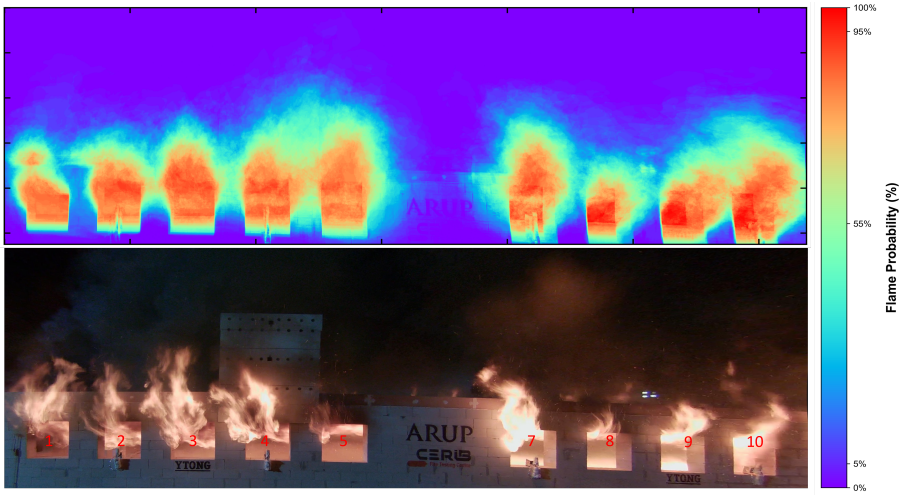



**Figure 5.6** – Diagram of flame probability of *CodeRed#01* from openings 1 to 9. Flame merging is observed between openings 4 and 5.

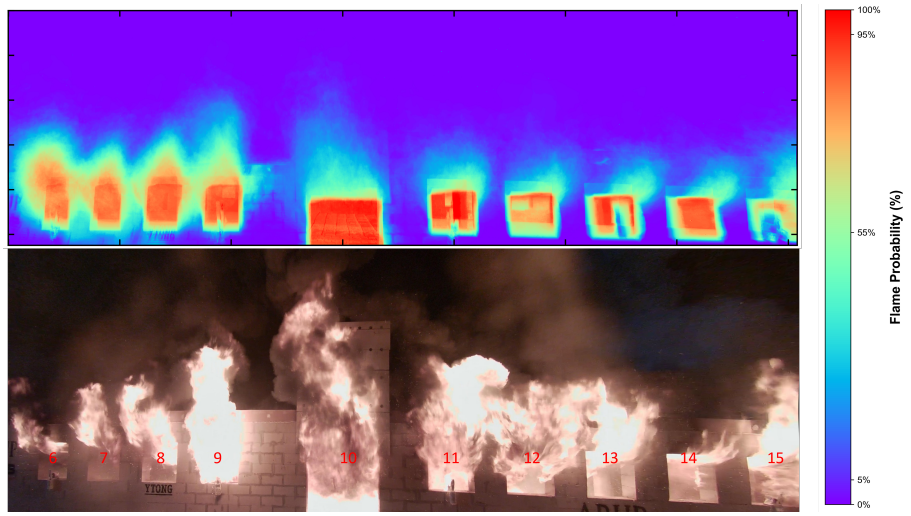



**Figure 5.7** – Diagram of flame probability of *CodeRed#01* for openings 6 to 15.

readings surpassed the 3.75 m screen height, measuring between 6-8 m. Flame heights were determined by estimating the flame tip height using the screen above the openings and the temperature data which was interpolated to estimate the height of the 540°C isotherm, as an approximation of flame height [8, 18, 20]. Thermocouples are limited to capturing axisymmetric flames in front of the screen, thus struggling to quantify the inclined flames present in *CodeRed* as illustrated by the measurement domains in Fig 5.4. In contrast, CV can observe above and around the screen, including inclined flames as shown in Fig (s) 5.1 (b) and 5.4 (b), presenting a more comprehensive spatial domain utilisation. Fig 5.8 (b) illustrates estimations capped at the screen height (red line) to account for overestimated thermocouple readings for flames exceeding this limit. The

advantage of employing CV lies in its ability to efficiently capture data above and around all thermocouples, contrasting with the limitations of thermocouples in capturing inclined flames. While both methods exhibit a consistent pattern in flame height analysis, thermocouples offer smoother data capture due to instrument sensitivity. In contrast, CV provides instantaneous frame by frame measurements. A 53% difference in flame height readings is observed with thermocouples compared to CV, primarily attributed to the inability of thermocouples to capture inclined flames due to crosswinds [308]. This emphasises the superiority of CV in measuring flame heights, further supported by its low analytical time, cost-effectiveness, and less complex apparatus setup.

Figure 5.10 shows the frequency plot from CV, which indicate that flame heights in opening 7 for *CodeRed#02* were predominantly around 4 m, with a peak at 6.4 m, in contrast to *CodeRed#01* and *CodeRed#04*, which displayed smaller peaks and shorter duration's of external flaming for the same openings, with most height readings concentrated between 1.5 and 2 m. This is also illustrated in Fig 5.8 (a), where it is critical to understand external flame behaviour due to change in experimental conditions.

In *CodeRed#01*, the CLT ceiling ignited approximately 2 min 57 s after ignition, leading to the rapid spread of the crib fire. External flames were first spotted at 4 min, and by 5 min 36 s, the entire crib had ignited. Around 6 min, external flames were visible from all openings, with the tallest external flaming occurring at 7 min. These flames persisted for roughly 13 min, ceasing around 18 min after ignition—coinciding with the cessation of CLT ceiling flaming, which also occurred at approximately 18 min. This correlation between CLT flaming and external flaming was consistent in *CodeRed#02*, despite a 50% reduction in ventilation, which resulted in taller flames due to the combustion of pyrolysis gases outside the compartment. In *CodeRed#02*, the CLT ceiling ignited at 4 min 11 s—slightly delayed compared to *CodeRed#01*—and external flames appeared around 5 min. The tallest external flame was observed from opening 7 at 20 min after ignition, with external flaming lasting a total of 21 min and ceasing around 26 min, coinciding with the end of CLT flaming.

In contrast, *CodeRed#04* featured a 50% encapsulated CLT ceiling, which significantly delayed the appearance of external flames. These flames were first observed 26 min after ignition, 22 and 23 min later than in *CodeRed#01* and *CodeRed#02*, due to the slower spread of crib flames and delayed CLT ignition, caused by the reduced fuel load from

encapsulation. The encapsulation was directly above the wood crib. The peak flame height was observed at opening 7 around 29 min 14 s. External flames were present for 10 min, ceasing 36 min after ignition—much shorter than in the other *CodeRed* experiments. Across all three experiments, rapid fire spread occurred once the CLT ceiling ignited, leading to the onset of external flames shortly after. However, different experimental conditions resulted in varying external flame behaviour. For example, in *CodeRed#02*, flames were generally taller due to reduced ventilation, as more pyrolysis gases ignited outside the compartment. In *CodeRed#04*, the encapsulated CLT ceiling limited the fuel load, resulting in shorter external flaming duration. When CLT was left exposed, as in *CodeRed#01* and *CodeRed#02*, external flaming ceased shortly after the end of CLT flaming. This was not the case in *CodeRed#04*, where the encapsulation played a significant role in flame behaviour and duration.

Only opening 7 had external flame measurements across all three experiments as other cameras from different windows were damaged, as given in Fig 5.8 (a), which was chosen for comparison. Fig 5.10 presents the frequency of flame height for all *CodeRed* experiments for openings 7, 10, and 14, as cameras from other openings were damaged as to keep a consistent comparison from the same openings. *CodeRed#01* and *CodeRed#04* commonly recorded flame heights between 1 and 2 m, whereas *CodeRed#02* recorded flame heights between 2 and 4 m. No frequency plots are available for openings 10 and 14 for *CodeRed#02* due to the loss of visual data from cameras melting during the experiment. The variation in flame height measurements suggests that differences in ventilation and CLT exposure significantly impact the severity and duration of external flaming, while the size of the compartment openings also affects flame behaviour as reported in other studies [270]. Specifically, opening 7 and 14 (windows) showed similar flame height measurements in comparison to opening 10 (door). Fig 5.11 represents the frequency plot of all the measured external flame parameters for Opening 7 across all *CodeRed* experiments. Additional information regarding all openings from 1 to 15 and all parameters including height, length, angle and surface area is provided in the appendix. Found in Appendix; A.1, A.2, A.3, A.4, A.5, A.6, A.7, A.8, A.9.

*CodeRed#01* was studied and the flame heights from all openings from one side of the compartment wall is shown in Fig 5.9. The contour shows the relationship of flame height across the compartment wall. Initially, small external flame heights are closer to

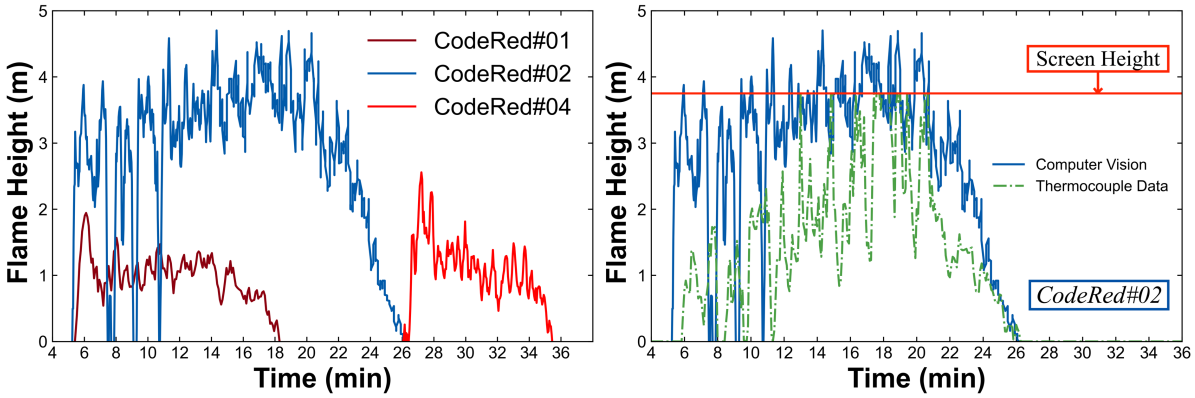



**Figure 5.8** – (a). External flame heights observed from opening 7 across all 3 *CodeRed* experiments. *CodeRed#02* has the largest heights and greatest duration of external flaming. (b) Bench marking thermocouple data against computer vision in full view with 53% difference. TC data cannot capture beyond the flame screen whilst CV can see the inclined flame due to cross-winds.

the crib ignition area of the compartment. However, once the CLT ceiling ignites, there is a substantial increase in external flame height, attributed to the contribution of pyrolysis gases from the CLT. The tallest flames are observed in front of the two screens at openings 4 and 10, with the former measuring a maximum flame height of 5.6 m. However, due to camera failure there is data loss observing openings 1-5 from 12.5 min as indicated in Fig 5.9. The last external flames are observed around 18 min in the middle of the compartment.

Observations include flame impingement from openings onto the screen, resulting in larger external flames, as the screen affects the flame dynamics. This occurs when the area of air entrainment is reduced due to the presence of a screen or wall [279].

### 5.6.2 Flame length and flame angle

Crucial parameters of an external flame include its length and the angle of inclination from the opening as it is significantly influenced by buoyancy and wind which relates to its fire power. Flame length is often expressed as a function of wind velocity due to its significant influence on flame geometry under crosswind conditions. In the absence of wind, air entrainment into the fire plume occurs uniformly from all directions, resulting in a vertically oriented flame with minimal inclination, resembling a freely burning flame in open space, which is observed in *CodeRed#02* [309, 310]. The tilt of the flame increases the likelihood of flame merging. The tilt is defined as the angle between the

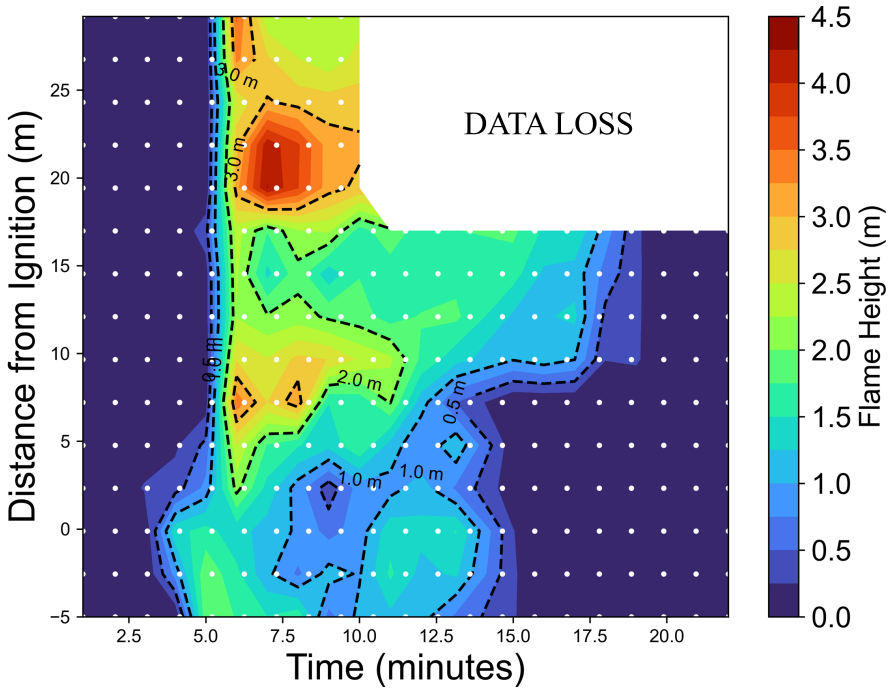



**Figure 5.9** – External flame heights across the compartment wall of *CodeRed#01*. Data loss occurs 17 to 30 m around 12.5 min after crib ignition. Dots mark the location of the openings with the rest interpolated.

flame's centerline (length) and its vertical projection (height), where a flame angle of 90° represents a vertical flame along its centreline [300,311]. The extent of flame inclination is dependent on the influence of wind velocity and the fire's heat release rate [231,309]. The *CodeRed* experiments were conducted at different months allowing for the assumption of varying wind velocities and their effects on flame length and angle. In the presence of crosswinds, some researchers suggest that air entrainment intensifies combustion within the flame, consequently reducing its length but this aspect remains inadequately understood [297,300]. Conflicting findings from other studies indicate that inclined flames exhibit increased length [312,313]. However, vertical flames generally have a longer length, as evident in the observed relationship between angle and length which is also observed in the *CodeRed* experiments.

Instantaneous measurements of flame length in all three *CodeRed* experiments are presented in Fig 5.12 (a). The longest flame, recorded at 6.6 m, was observed during *CodeRed#02*. Fig 5.13, provides a contour plot specifically for *CodeRed#01*, where all openings were examined. Openings 4 and 10 exhibited the longest flames, with the tallest flame heights also recorded in these openings. The flame angles across all three *CodeRed* experiments remained relatively consistent. *CodeRed#01* and *CodeRed#04* had average

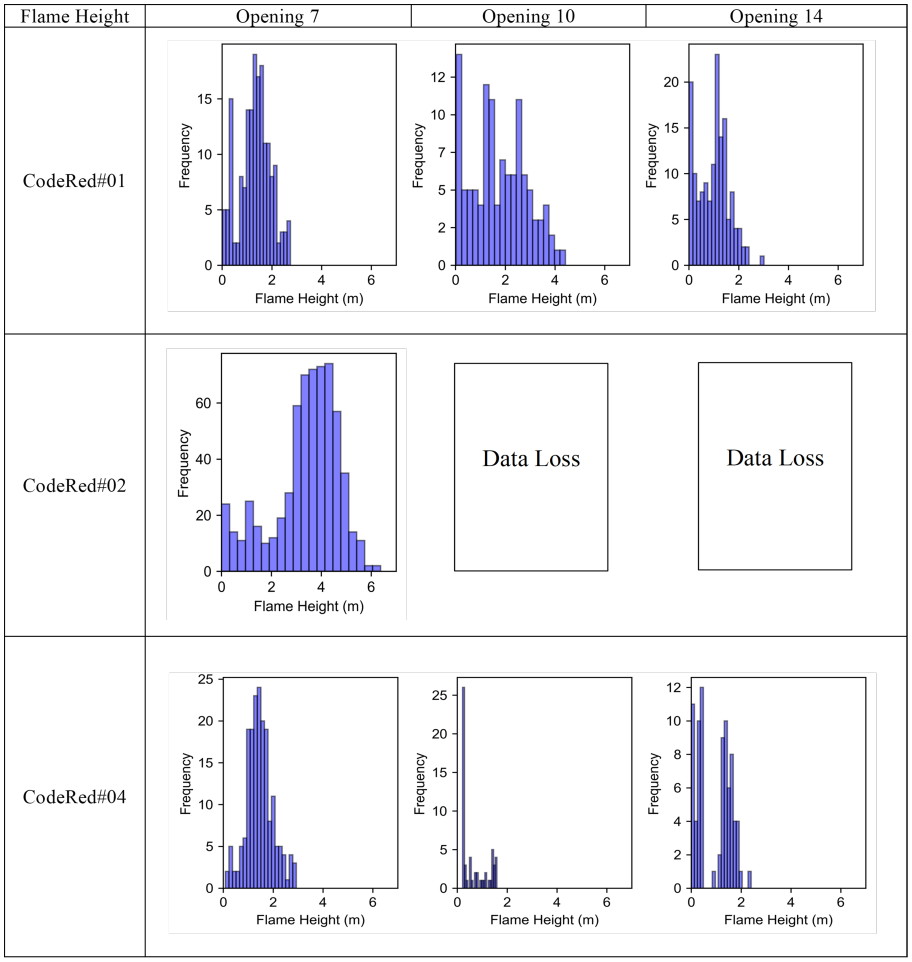



**Figure 5.10** – Flame characteristic for flame height, length, angle and surface area from Opening 7 due to best data of *CodeRed#02* showing the frequency of occurrence from crib ignition to burnout.

flame angles of 65° and 78°, respectively, whereas *CodeRed#02* had the smallest average deviation of 88°, indicating small crosswind influence during the experiment. Some studies suggest, higher crosswinds are associated with shorter flame lengths and increased flame angles [314].

Overall, wind conditions that are ambient play an important role in fire dynamics especially in building fires and wildfires as it dictates the airflow into the compartment or angle of flame as mentioned above . It was observed in *CodeRed#02* where incomplete combustion occurred due to reduced ventilation further influenced by low wind-speeds, where crosswinds hardly dictated the taller external flames in comparison to *CodeRed#01* and *CodeRed#04*. Currently there is lack-of research in compartment fire studies with side-ward perpendicular winds, which is a cause for the fire-safe design of buildings which

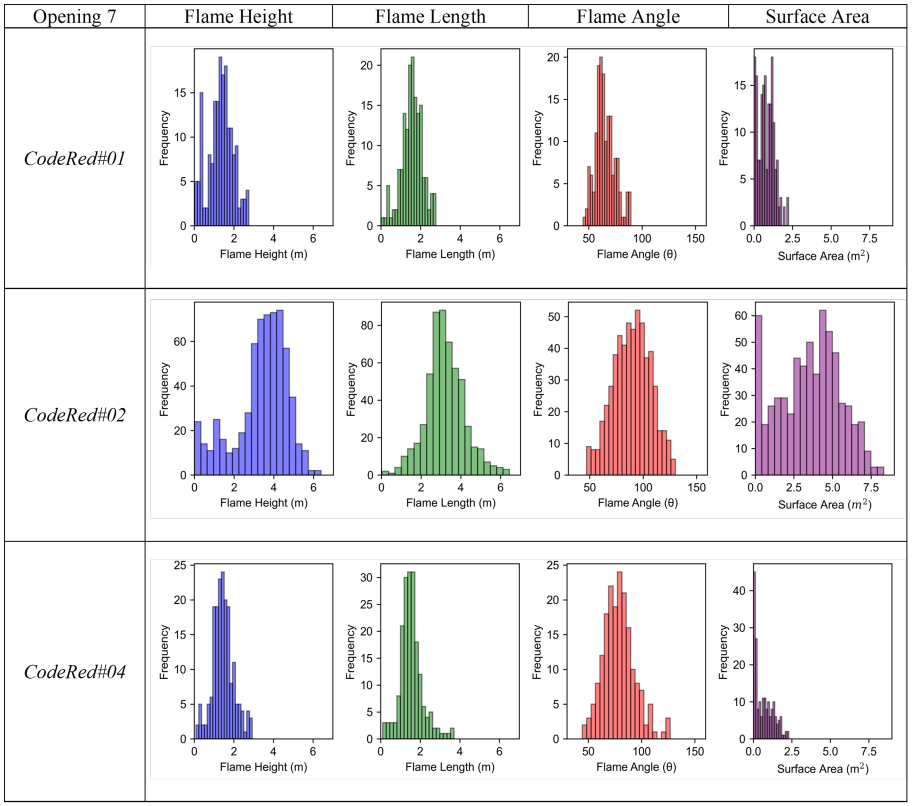



**Figure 5.11** – Flame Height occurrence for all *CodeRed* experiments from crib ignition to burnout for Openings 7, 10 and 14 which were chosen as the best data available for selection.

particularly influence the separation distance of openings and to adjacent buildings.

### 5.6.3 Flame Merging

A phenomenon known as flame merging is observed at openings 4 and 5 of *CodeRed#01*, where the contour plot, shown in Fig 5.14, demonstrates the connection of intermittent flame regions. The occurrence of flame merging presents a significant concern in building fires. Flame merging occurs when flames from neighbouring openings are in close proximity, restricting airflow entrainment between them. This condition causes the flames to elongate and tilt towards each other [297, 315, 316]. Observations from *CodeRed#01* indicated that openings exhibiting greater flame heights were more prone to merging. This aligns with previous research [315, 316]. Another critical factor increasing the probability of flame merging is the presence of inclined flames which is evident in the *CodeRed#01*, as mentioned earlier, as flames merge at openings 4 and 5. Lu et al. [297], reported that flames tend to merge more frequently with higher heat release rates. In

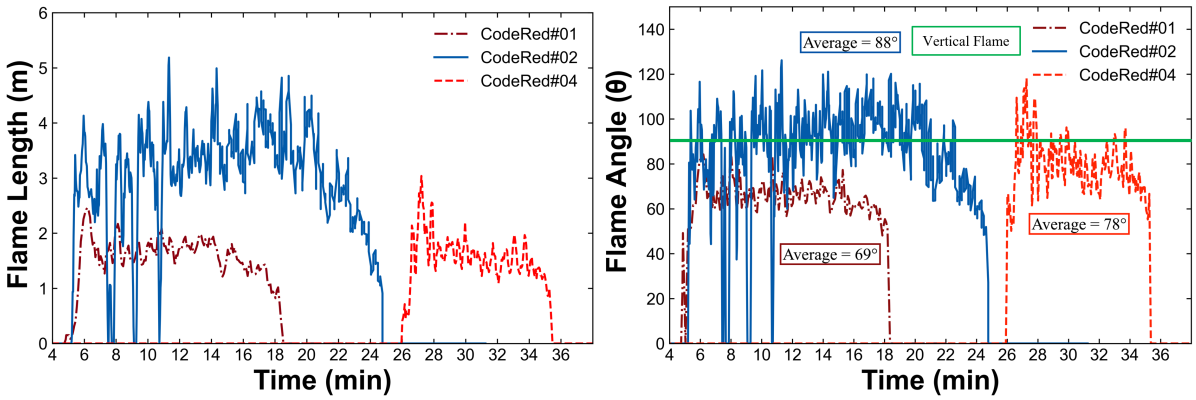



**Figure 5.12** – (a). The flame length of opening 7 in all 3 *CodeRed* experiments. *CodeRed#02* measures the largest flame length whilst *CodeRed#01* and *CodeRed#04* measure similar lengths across the duration of the experiment. (b). Flame angle of opening 7 in all 3 *CodeRed* experiments. *CodeRed#02* shows the least amount of flame inclination and *CodeRed#01* the largest.

contrast, *CodeRed#02* and *CodeRed#04* do not exhibit instances of flame merging. For *CodeRed#02*, the absence of flame merging is attributed to the substantial separation distance between neighbouring openings, resulting from a 50% reduction in compartment openings. In the case of *CodeRed#04*, the 50% encapsulation of the timber ceiling reduces the severity of external flames, leading to shorter flames. The dimensions of the opening are a key factor influencing flame merging, as they are directly informed by fire design guidance, such as the statutory guidance in Approved Document B. This guidance also considers other factors, including presence and size of fire doors and evacuation routes, to name a few [317].

### 5.6.4 Projected surface area

Qualitative analysis of projected surface area is measured by identifying the flame edge and measuring the area of its contour shape, which results in Fig 5.15. The visual data shows large areas of external flames are observed in *CodeRed#01*. This is observed where the screens are placed. This aligns with observations earlier in this chapter, as this is the same region where the largest flame heights occur. Projected surface area is a proxy for flame volume, which in turn has a direct correlation with heat release rate (HRR). According to Orloff and De Ris, flame volume is proportional to heat release rate, indicating that the highest HRR is observed where the largest surface area assuming constant thickness is observed, in this case the region where screens are present for

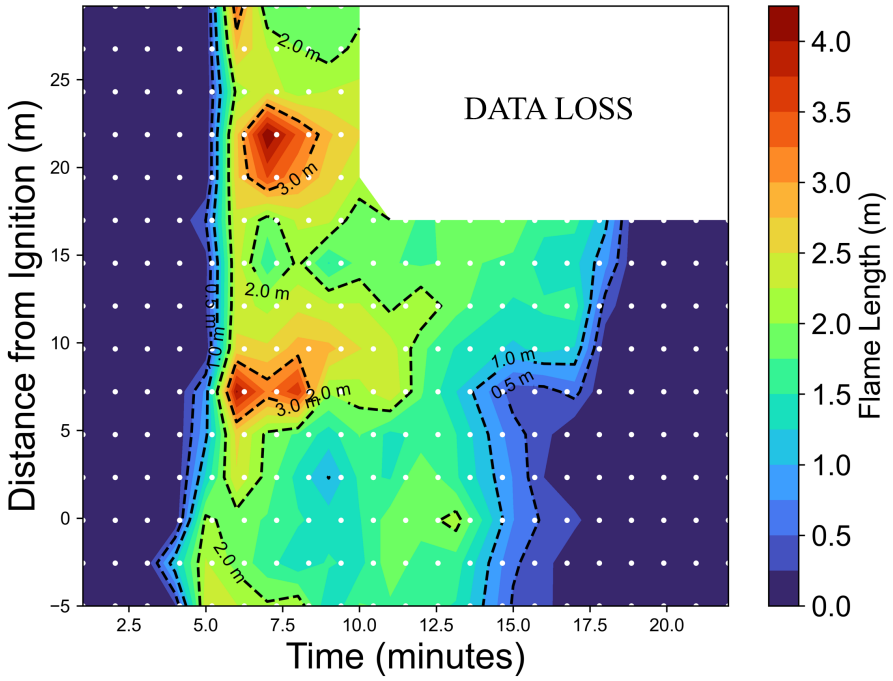



**Figure 5.13** – Flame length contour plot of *CodeRed#01* compartment. Data loss occurs from openings 1-5 from around 10 min after crib ignition however, the longest flames are exhibited at openings 4 and 10. The longest flames congregate around the openings with screens due to flame impingement and change in fire dynamics. Dots mark the location of openings the rest is interpolation.

*CodeRed#01* [97,318]. However, calculating flame volume requires an additional cameras viewing the side of the flame to measure thickness similar to a study conducted by [97].

## 5.7 Conclusions

This study demonstrates the successful application of computer vision (CV) as an innovative and effective diagnostic tool for analysing external flames in fire compartment experiments. By employing both quantitative and qualitative analyses, we highlight the significant influence of ventilation and timber encapsulation on external flame behaviour, with ventilation increasing flame severity and timber encapsulation delaying the onset and reducing intensity. Additionally, crosswinds were found to create inclined flames, challenging the traditional measurement method of thermocouple trees. However, CV's image-based approach effectively captures complex flame characteristics, including flame height, length, inclination, and merging behaviour, providing much more accurate results (53% error vs. 3% error). Compared to Manual Vision, CV offers the same accuracy but at a much faster rate, which is highly scalable for automatising. In fact, CV is built

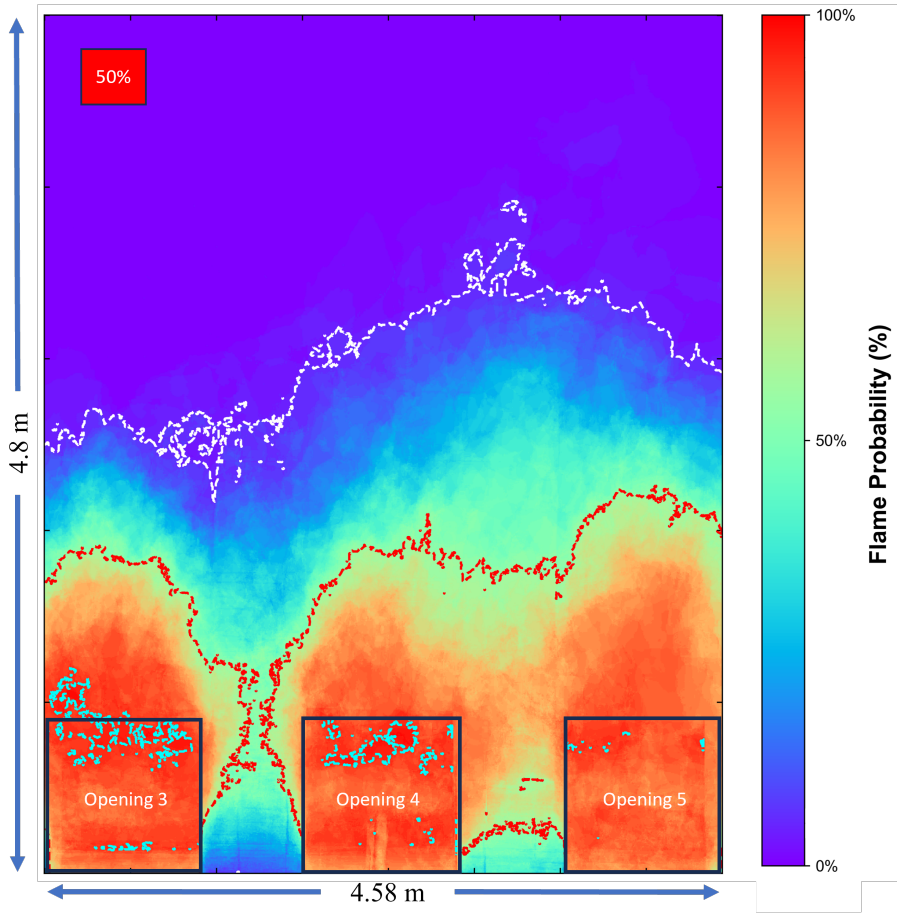



**Figure 5.14** – Diagram of flame probability of *CodeRed#01* openings 4 and 5 which depicts the crossing of intermittency lines showing flame merging.

upon Manual Vision, which is still required in a minimal set of images for calibration building robustness for CV. The ability of CV to quickly analyse flames across multiple openings in outdoor conditions, such as in the *CodeRed* experiments, highlights its versatility and time efficiency, especially in situations where conventional methods struggle. The chapter demonstrates that CV outperforms traditional measurement techniques and offers a low-cost, scalable, and highly accurate alternative for studying flame dynamics at high time resolutions. In conclusion, the framework presented in this study advances the state-of-the-art in fire diagnostics, enabling a deeper understanding of flame behaviour in experimental settings and actual fire accidents. The methodology can be used for diagnostics of other flame phenomena inside and outside the lab, well beyond compartment fires. For example, it could be extended to canonical flames, flame spread, jet flames and pool fires, to name a few that already use Manual Vision. This technology holds great promise for enhancing fire science and can play a role in future fire research whilst also

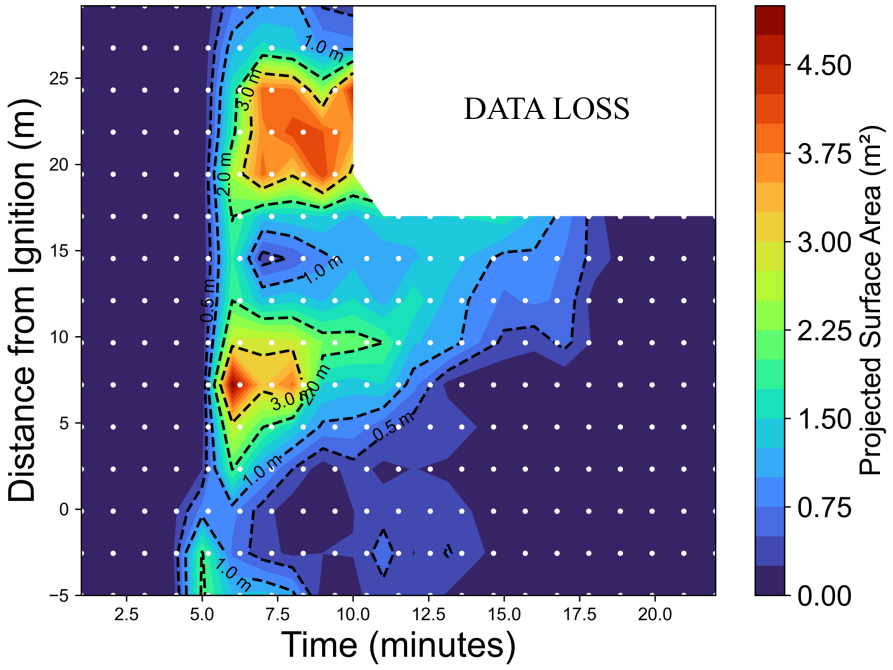



**Figure 5.15** – Diagram shows the projected surface area of external flames from all compartment openings in *CodeRed#01*. Significant larger external flames are exhibited 20-25m away from the ignition end of the compartment.

being compatible for smart-sensing systems in fire and smoke detection.

| Method | Advantage(s) | Disadvantage(s) | Literature |
|---|---|---|---|
| **Thermocouple** | • Robustness of measurements over external noise such as smoke, soot and general visibility<br>• Direct measurements<br>• Minimal post-processing<br>• Instrumentation durability<br>• Reliability | • No visual insight<br>• Requires interpolation<br>• Low resolution on measurements<br>• Limited to measurement domain<br>• Cannot measure flames under crosswinds<br>• Slow response time | [8, 18, 20, 281, 302–304] |
| **Image Processing** | • Simple implementation<br>• Small computational cost<br>• Applicable in controlled settings | • Limited scalability and applications<br>• Affected by environmental factors such as smoke, lighting<br>• Requires calibration<br>• Real-time capabilities<br>• Low-level insights | [49, 56–61, 86, 88, 280, 287–289, 292, 293] |
| **Computer Vision** | • Flame geometry extraction and detection is automated<br>• Applicable to different environments<br>• Instantaneous depending on computational power<br>• Higher accuracy than image processing<br>• Large data and application scalability<br>• Combines multiple features such as image matrix transformations and trained modules<br>• Real-time measurements | • Requires calibration<br>• Computational power<br>• Pre-processing of data<br>• Complex tasks require further trained modules | [37, 65, 97, 135] |
| **Convolutional Neural Network** | • Complex flame patterns in different fire scenes<br>• Instantaneous and automatic<br>• Large data and application scalability<br>• Real-time measurements<br>• Can measure heat release rate and other parameters if training data is provided<br>• Static and dynamic features | • Computationally expensive and time consuming<br>• Accuracy of model dependent on quality of data<br>• Cannot calibrate after training<br>• Interpretability of results (black-box)<br>• Models may overfit | [95, 138–140, 201] |

**Table 5.1** – A comparison of various methods used for flame shape analysis in published literature, with a specific emphasis on the advantages and disadvantages of computer vision.

# Chapter 6

# External heat release rate from a fire compartment

## Summary [1]

This study investigates a critical fire phenomenon of external flames for understanding compartment fires where images are fed into fundamental correlations to measure heat release rate (HRR). The methodology leverages computer vision and inverse modelling to calculate HRR when instrumentation is not available such as oxygen calorimetry, using the variables such as flame height, wind speed, and angle of inclination from existing correlations in the literature. These variables are measured using AI flame diagnostics, enabling simultaneous and real-time measurements of external flames from multiple openings in a compartment fire. I apply this to calculating the external HRR in the *CodeRed* compartment fire series, with a focus on the influence of exposed mass timber and varying ventilation conditions. In *CodeRed#01*, the total maximum HRR of the compartment was 120 MW, with external HRR accounting for 36% of this, at $43^{+14}_{-10}$ MW. I further analysed opening 7 across all *CodeRed* experiments. In *CodeRed#02*, where ventilation was reduced by 50% and the entire cross-laminated timber (CLT) ceiling was exposed, the external HRR reached a maximum of $2.81^{+0.93}_{-0.70}$ MW. In contrast, in *CodeRed#01*, where no ventilation reduction occurred, the maximum external HRR was $0.70^{+0.23}_{-0.18}$ MW.

1. This chapter is based on "R.Amin, H. Mitchell, G. Rein (2024) *Measuring the External Heat Release Rate from a Fire Compartment using Computer Vision*, **Submitted to journal for peer review**

In *CodeRed#04*, where 50% of the CLT ceiling was encapsulated, limiting the fuel load inside the compartment, the external HRR measured $0.75^{+0.25}_{-0.19}$ MW. This approach is a new way to measure external HRR without specific instrumentation. By concentrating on large-scale measurements, this chapter tackles a critical limitation in large-scale experiments where it cannot directly be measured. This research fills that gap by providing an innovative approach to measuring external fire behaviour to assist decisions in fire safety design of buildings and firefighting.

## 6.1 Introduction

Building fires increasingly poses significant threats to safety in the built environment, particularly due to the flames that emerge from compartment openings, known as external flames. These flames have the potential to ignite the floor above or adjacent structures, making them a critical area of research, especially as high-rise timber buildings become more common. Timber, being inherently flammable, heightens the fire risk, creating the need for fire-safe building designs and improving evacuation strategies [1, 2, 8].

External flames also present challenges in understanding fire dynamics, as they can occur in both under-ventilated and well-ventilated compartments, as demonstrated in Chapters 3 and 5 of this thesis through the *CodeRed* experimental series as given in Fig 6.1. Complete combustion is sometimes not achieved in compartment fires, particularly in timber buildings, making it a crucial study. Fires typically begin in small, enclosed spaces where conditions can quickly lead to rapid fire spread [23, 94]. In the early stages of a building fire, there is usually sufficient ventilation, as not all fuel sources are ignited. However, as the fire develops, a critical point is reached where the available oxygen within the compartment is insufficient to sustain the rate of fuel combustion. At this stage, pyrolysis gases ignite outside the compartment, resulting in external flames.

The characteristics of these external flames, such as flame height and resulting heat transfer, are key to determining the temperature profile and their impact on the building's façade, particularly through the heat release rate (HRR) [270]. HRR, a fundamental mechanism in fire growth, quantifies the energy released during combustion and is essential for characterising compartment fires and the dangers it poses. The general expression for HRR is given by Eqn 6.1, where $\dot{Q}$ represents the HRR, $\dot{m}$ is the mass loss rate, and

$\Delta h_c$ is the specific heat of combustion of the fuel, which can also be applied to flames burning outside the compartment. This expression allows for the calculation of the maximum HRR within a compartment fire [23]. The external HRR, in turn, can be derived by subtracting the HRR inside the compartment from the total HRR, as shown in Eqn 6.2 [305].

$$\dot{Q} = \Delta h_c \tag{6.1}$$

$$\dot{Q}_{total} = \dot{Q}_{ex} + \dot{Q}_{in} \tag{6.2}$$

Specifically, the HRR is also influenced by factors such as the aspect ratio of the opening and the internal HRR of the compartment. Yokoi was one of the first to study compartment fire characteristics, using a small-scale model (0.4 x 0.4 x 0.2 m) to measure the temperature distribution of external flames under different compartment openings [319]. Delichatsios later conducted a series of experiments focused on flame height in under-ventilated fires, proposing a physical model to quantify this [320]. There are various forms of these physical models for a range of conditions that can be found in the literature [270]. HRR measurements in fire experiments are traditionally conducted using oxygen calorimetry, where all combustion gases, including oxygen and carbon dioxide, are captured and analysed under a cone calorimeter. However, for large-scale fire experiments such as *CodeRed* as mentioned in Chapter 5 and outdoor fires, the use of such apparatus becomes impractical due to the requirement of an exhaust hood large enough to contain the combustion gases. This limitation creates a gap for alternative methods to measure external HRR in large-scale compartment fires. As a result, study explores innovative approaches by combining inverse modelling with computer vision. Specifically, it aims to calculate external HRR using established correlations from the literature, informed by measurements obtained through an AI diagnostic tool, as discussed in Chapter 5.




**Figure 6.1** – External flaming from *CodeRed#04* fire compartment.

## 6.2 Literature review

### 6.2.1 Correlations for external heat release rate

In the literature, correlations exist for behaviour for external flames in small compartment fires and their corresponding measured external heat release rates (HRR) under varying conditions. In 2000, Sugawa et al. conducted a compartment fire experiment to investigate the effects of external side wind on the flow behaviour of flames ejected from an opening. The study systematically varied external wind speeds while measuring flame temperature and velocity. Based on the findings, a correlation was proposed for flame inclination angle because of wind velocity coupled to external HRR, Froude number, and the aspect ratio of the compartment opening. The compartment used in the experiment measured 10 cm x 50 cm x 10 cm in size. The resulting correlation is presented in Eqn 6.3, where $\vartheta$ is flame inclination, g is the gravitational constant, T is ambient temperature, $C_p$ is specific heat capacity, and $\frac{D}{W}$ is the aspect ratio of the compartment opening [321], where this nomenclature will carry through in the rest of the chapter.

$$\sin\vartheta = \frac{U_{wind}}{\left(\frac{gQ_{ex}}{\rho C_p T_W}\right)^{1/3}\left(\frac{D}{W}\right)^{1/3}} \tag{6.3}$$

In 2007, Lee et al. derived a correlation for the HRR of a fire plume as a function of flame height outside the compartment. Their study involved small-scale experiments using enclosures with varying opening geometries, ranging from 7.5 cm x 20 cm to 30 cm x 10 cm, and different burner locations. The aim was to investigate flames emerging from openings that extend onto the façade of the compartment, potentially causing ignition in the floor above in multi-story buildings. By conducting small-scale experiments, the

HRR was accurately measured using oxygen calorimetry, a method that is difficult to implement in large-scale or outdoor experiments. The proposed correlation is presented in Eqn 6.4, where $\dot{Q}^*_{ex}$ represents the dimensionless external HRR, where the equivalent is also given Eqn 6.5 [305].

$$\frac{Z_f}{l_1} = \text{fcn}\left(\dot{Q}^*_{ex}\right) \tag{6.4}$$

$$\dot{Q}^*_{ex} = \frac{\dot{Q}_{ex}}{\rho_\infty C_p T_\infty \sqrt{g} D^{5/2}} \tag{6.5}$$

In 2012, Tang et al. studied buoyant window spill plumes in under-ventilated compartment fires, measuring flame heights and temperature profiles. The experiments were conducted in a compartment measuring 3 m x 5 m, with varying opening geometries like those used by Lee et al. A propane gas burner with a controlled fuel supply was used to regulate the burn rate. Tang et al. proposed a correlation, presented in Eqn 6.6, to model HRR rate outside the compartment and the height of the ejected flames for different geometries. In this correlation, Zn is the height of the window at the neutral plane, and l is the characteristic length scale determined by the opening geometries. The characteristic length, l is given by Eqn 6.7, where A is the area of the window and H is the height of opening [322].

$$\frac{Z_f - Z_n}{l} = 2\dot{Q}^{*0.44}_{ex} \tag{6.6}$$

$$l = A\sqrt{H}^{\frac{2}{5}} \tag{6.7}$$

In 2020, Lu et al. studied external flame behaviour from multiple compartment experiments with varying openings at different elevations. They found that flame heights varied depending on the elevation of the openings, where higher elevated windows had smaller flames resulting in less HRR outside the compartment. They proposed two correlations, in Eqn(s) 6.8 and 6.9 for small and large flames respectively and found smaller flames for openings next to side walls with axisymmetric flame behaviour. The results indicated that higher elevated openings reduced the critical heat release rate required for flame ejection to occur. [323].

$$\dot{Q}_{ex} = Z_f^{\frac{3}{2}} \tag{6.8}$$

$$\dot{Q}_{ex} = Z_f^{\frac{5}{2}} \tag{6.9}$$

Also in 2020, Sun et al. conducted experiments to investigate the pulsating behaviour of external venting flames from a compartment with a façade above its opening. The study involved 15 different opening geometries. Based on their findings, they proposed a correlation for the external HRR, relating it to flame height and characteristic length, as presented in Eqn 6.10. Their experiments were validated against numerical simulations, demonstrating the robustness of the proposed correlation [324].

$$\dot{Q}_{ex} = \frac{Z_f}{l_1}^{\frac{5}{2}} \tag{6.10}$$

These specific correlations were chosen because they represent compartment fire experiments conducted under varying conditions, allowing for a wide range of experimental and measurement possibilities to be captured. The primary aim is to understand how characteristics of an external flame correlate its HRR, by its flame height, the wind velocity and resulting flame angle. The correlations in this section use flame height, characteristic length as a proxy for HRR, each varying on experimental conditions such as elevation and size of opening. Another key distinction is the ambient conditions of the experiment such as wind velocity and its effect on the flame inclination, such that considering environmental factors and their effects. Overall, these correlations were selected to reflect quiescent conditions and sideward, perpendicular wind, both conditions similar to those found in the *CodeRed* experiments. Additionally, others were chosen to explore general expressions of flame height, a common factor in pool and crib fire measurements.

Moreover, while these previous studies were conducted as small-scale laboratory experiments, it is important to note that measuring the external HRR in large-scale outdoor fires, such as the *CodeRed* experiment present significant challenges. Common methods of measurement like oxygen calorimetry, while viable in small-scale lab experiments, are not possible in larger scenarios both indoors and outdoors. Additionally, while certain studies in the literature explore different opening shape, such as triangular or circular, these were excluded as *CodeRed* had openings which were rectangular [325, 326]. These

studies also showed that fire behaviour changes with shape. As a result, this chapter proposes a new method of calculating the external HRR from a compartment fire, where traditional measurement techniques are not viable.

This study accomplishes this by inverse modelling using an AI diagnostic tool. The inverse modelling uses observable characteristics, that are measured from *CodeRed* such as flame height, wind velocity and flame angle providing a robust alternative for large-scale outdoor experiments. This approach provides a more adaptable and scalable framework for future fire safety analysis in large structures and open environments.

### 6.2.2 Inverse modelling external heat release rate

This section is a critical review of the published works that exist for calculating the heat release rate (HRR) from direct and inverse modelling. The first study conducted was in 1996, by Richards et al. proposed a solution for an inverse heat transfer problem related to fire detection and localisation by utilising transient temperature data from a compartment fire. Their findings indicated that both model inaccuracies and measurement errors affected the estimated HRR. The model was subsequently validated against simulated data, with the results showing strong agreement, thereby demonstrating the viability of computer simulations as a reliable method for evaluating the solution to the inverse problem. The model successfully predicted the heat release rate in 95% of the simulated fires [327].

In 2011, Jahn et al. applied an inverse modelling approach to forecast fire growth in a compartment. Sensor temperature readings were integrated into the model to estimate key parameters, including spread rate (used to calculate HRR), entrainment coefficient, and smoke transport time. These parameters were optimized using tangent linear differentiation. The researchers concluded that the HRR was accurately forecast, demonstrating the effectiveness of the approach in fire growth prediction [328]. In the same year, Overholt et al. characterised the HRR using inverse modelling from measured temperature data, utilising the CFAST zone model as HRR was not directly measured. The inverse solution was compared to experimental measurements from compartment fire temperature data. However, the researchers noted that quantifying the error in the inverse solution remains challenging, nevertheless the inverse model closely matched the experimentally measured HRR [329].

In 2015, Price et al. applied inverse modelling to predict the HRR of a compartment fire using smoke layer data collected from temperature sensors. The compartment was based on a small-scale, steady, over ventilated fire experiment. A key limitation of this method is that the optimisation problem yields multiple possible solutions and a configuration using thermocouples with relatively few unknown variables [330].

In 2016, Chu et al. employed a probabilistic inferential algorithm to determine the HRR location using an inverse modelling approach. Their study demonstrated that the error between the measured and predicted temperatures was less than 5% for small fires and 10% for large-scale fires of HRR [331].

In 2018, Li et al. employed inverse modelling techniques, utilising visual data from image recognition to estimate key parameters of pool fires, such as, flame height, HRR, and fuel type. Their image processing method effectively filters non-flame elements. They used Fourier transformations to determine the pool diameter, a crucial factor in calculating the flame height. However, a notable limitation of the model lies in the significant uncertainty introduced by the inverse solution, which relies on empirical correlations such as those by Heskestad et al [89, 96].

In 2019, Kurazawski et al. applied Bayesian-based inversion techniques for fire scene reconstruction for forensics and the measurement of total HRR. This study builds upon the work of Overholt et al. (2011), which utilised CFAST and FDS as forward models within inverse modelling. The study concludes that the model successfully calculated the HRR below 1 MW [332].

In 2020, Buffington et al. employed deep learning emulators for transient compartment fire simulations to solve inverse problems and calculate the HRR. A neural network was trained to predict transient temperatures at various fire locations based on transient HRR inputs, with Gaussian processes used to generate training data for the neural network. The results demonstrated that the model could predict temperatures with a mean absolute error (MAE) of 2°C and for HRR predictions, the error was 11.3% to 28.6% [114].

In 2020, Bonner et al, created an algorithm called Visual Fire Power to measure the HRR of visible flames in a two-camera setup perpendicular to each other, validated with façade fire experiments. The method reports an average uncertainty of 30%. They measure the flame thickness to calculate the flame volume using the Orloff-DeRis constant

which linearly relates to HRR [97].

In 2023, Wang et al. published two studies focused on estimating the HRR of fires using deep learning methods, specifically convolutional neural networks (CNNs). The first study utilised the NIST dataset of fire calorimetry, which included approximately 70,000 images labelled with their respective transient HRR, covering both lab and real-life scenarios [100] The second study employed a pre-existing deep learning framework, YOLOv5. Both models performed with an error range of 15-20%, contributing significantly to the field of smart firefighting [95]

Previous studies, as discussed, have utilised various inverse modelling techniques to calculate the HRR, often relying on data from numerical simulations, specific camera configurations, and the use of artificial intelligence (AI). However, these approaches have typically been applied to specific scenarios and are not directly applicable for calculating the external HRR in *CodeRed*. This creates a notable research gap, particularly in situations where traditional measurement instrumentation is not feasible for large-outdoor fires. Moreover, they do not adequately represent the complexities of fires in high-rise buildings especially with a sustainable building material like timber, which is inherently flammable if left exposed and as a result can add to the fuel load in a compartment fire. The varying compartment ventilation and fluctuating ambient conditions further complicate fire dynamics and the calculation of external HRR.

## 6.3 Inverse modelling and optimisation

The objective of solving an inverse problem is to estimate a variable within a system that cannot be directly measured or observed. In the context of this study, to calculate the external heat release rate (HRR), where the problem is mathematically represented by Eqn 6.11.

$$\varphi = \dot{Q} \tag{6.11}$$

Eqn 6.11, is solved either directly or using an optimisation approach which involves defining a forward problem given in equation 6.12, containing all known and unknown quantities.

$$y_{pred}(\varphi, w) = \begin{bmatrix} H(\varphi, w) \\ L(\varphi, w) \\ A(\varphi, w) \end{bmatrix} \tag{6.12}$$

Although Eqn 6.12 provides a general expression for the forward model, in this study, the model varies depending on different equations derived from the literature. This calculates the unknown variable $\dot{Q}$ (HRR) based on measured observations of external flames such as flame height (H), length (L), and angle (A), which are correlated with wind speed (w). The known quantities are obtained through direct measurements using an AI diagnostics tool. The next step involves defining the cost function—also referred to as the error or objective function—given by Eqn 6.13 with Eqn 6.14 as the expanded form of the general expression.

$$J(\varphi) = \sum_{i=1}^{N} \left(y_i - \hat{y}_i(\varphi)\right)^T \left(y_i - \hat{y}_i(\varphi)\right) \tag{6.13}$$

$$J(\varphi) = \sum_{i=1}^{N} \left( \begin{bmatrix} H_{obs_i} \\ L_{obs_i} \\ A_{obs_i} \end{bmatrix} - \begin{bmatrix} H(\varphi, w_i) \\ L(\varphi, w_i) \\ A(\varphi, w_i) \end{bmatrix} \right)^T \left( \begin{bmatrix} H_{obs_i} \\ L_{obs_i} \\ A_{obs_i} \end{bmatrix} - \begin{bmatrix} H(\varphi, w_i) \\ L(\varphi, w_i) \\ A(\varphi, w_i) \end{bmatrix} \right) \tag{6.14}$$

Optimising involves minimising the cost function by providing an initial guess for the unknown variable $\dot{Q}$, which iteratively adjusts until the function converges to a local minimum, thus optimising the solution given as an expression in Eqn 6.15.

$$\varphi^* = \arg\min_{\varphi} J(\varphi) \tag{6.15}$$

## 6.4 CodeRed#03

Computer vision (CV) offers a computationally efficient and instantaneous alternative to measure the characteristics of a flame as outlined in Chapter 5. This study seeks to bridge this gap by utilising image data from *CodeRed#03*, applying the diagnostics tool to extract parameters such as flame height, and pool fire diameter to calculate the internal heat release rate (HRR) of the compartment fire.

Four *CodeRed* experiments were conducted to study various aspects of fire dynam-

ics in compartment fires. Three experiments focused on the effects of varying ventilation and cross-laminated timber (CLT) encapsulation [8, 18, 20]. The third experiment, *CodeRed#03*, specifically investigated the effectiveness of a standard water mist suppression system in preventing rapid fire growth in a compartment with an exposed CLT ceiling [19]. This study utilised an automatic suppression system, activated by sensors, to evaluate its efficiency in mitigating fire in the absence of other fire-resistant measures such as CLT encapsulation. Detailed information on this study is published in [19] and previously elaborated in Chapter 3, where Fig 6.2 shows the internal of the compartment fire and the crib setup.



**Figure 6.2** – *Codered#03* experiment, showing the fire inside the compartment with sprinkler activation, and the wood crib prior to ignition.

This section presents a proof of concept for calculating the internal HRR from a crib fire inside a compartment over the duration of the experiment. Since no calorimetry instrumentation was installed inside, direct measurement of the internal HRR was not possible. Instead, we used cameras to measure from video footage as explained in Chapter 5. These measurements were then applied to existing empirical correlations from the technical literature. The first correlation, provided by Gunnar Heskestad, is presented in Eqn 6.16, where $\dot{Q}$ (HRR) is expressed as a function of the measured variables, where L is flame height and D is pool fire diameter both measurements are given in Fig 6.3 (a) [89].

$$L = -1.02D + 0.32\dot{Q}^{\frac{2}{5}} \tag{6.16}$$

The second correlation, proposed by P.H. Thomas in 1963 [231], is presented in Eqn 6.17, where the equation is rearranged so the mass burning rate per unit pool area, $\dot{m}''$, is given as a function of $\rho_a$ , which is multiplied by the pool fire area, heat of combustion,

$\Delta H_c$, of the wood sticks measured in a calorimetry experiment at 19.05 $MJ/kg^{-1}$ to give the internal HRR given in Eqn 6.18 [19]. The results are shown in Fig 6.3 (b), with the peak calculated HRR is between 762 kW and 1205 kW, and the average as 375 kW and 601 kW as shown in Tab 6.1. The discrepancy between these HRR values arises from the different definitions of flame height in the two correlations. Thomas defines flame height as the visible flame height, whereas Heskestad defines it as the average flame height over the duration of the experiment. Additionally, both correlations were originally developed for pool fires rather than crib fires and steady state. Furthermore, a spreading fire such as in *CodeRed#03* with a transient HRR is generally a hard problem to solve.

$$\frac{L}{D} = 42 \left( \frac{\dot{m}''}{\rho_a \sqrt{gD}} \right)^{0.61} \tag{6.17}$$

$$\dot{Q} = \frac{\dot{m}'' \cdot \Delta H_c \cdot \pi \cdot D^2}{4} \tag{6.18}$$

| **Correlation** | $\dot{Q}_{Max}$**(kW)** | $\dot{Q}_{Avg}$**(kW)** |
|---|---|---|
| **Heskestad** | 1205 | 601 |
| **Thomas** | 762 | 375 |

**Table 6.1** – Results for Internal HRR measurements for *CodeRed#03*.

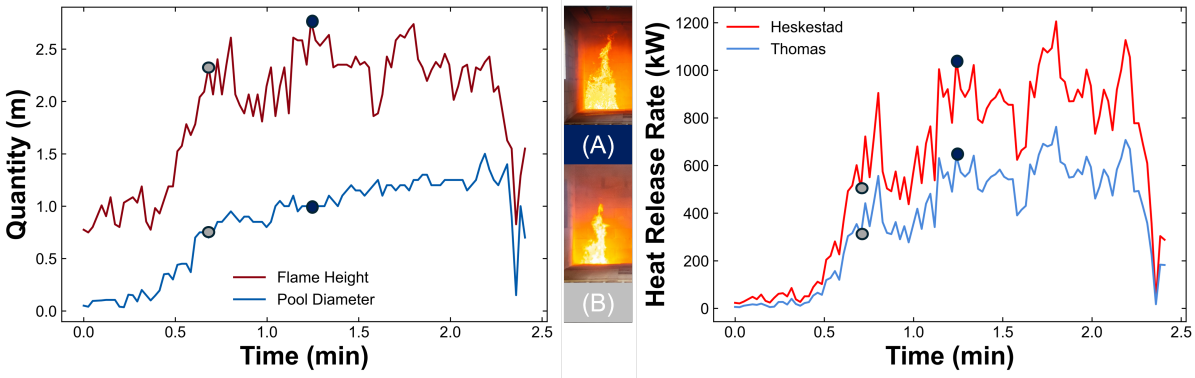



**Figure 6.3** – (a) shows the characteristic measurements of the pool fire diameter and flame height. (b) shows the calculation of the internal heat release rate of the compartment using Thomas and Heskestad correlations.

### 6.4.1 Validation of approach

Creating a proof-of-concept is important for developing a structured approach. We build on the work of previous researchers such as Jhan et al, Wang et al who used an

inverse problem to estimate heat release rate (HRR). However, none of those studies are for large scale compartment fire experiments where the previous work was on transient fires and small-scale lab experiments, presenting a notable research gap [95,100,328]. To validate our method, we used data from the NIST Fire Calorimetry Database, specifically from the Structure Separation Experiments Phase 1 tests, focusing on the heptane pan fire experiment. In this experiment, 300 mL of heptane served as the fuel, placed inside an aluminium pan with dimensions of 90 mm x 130 mm and 30 mm in height. A visual representation of the experiment setup is shown in Fig 6.4 (b).

The HRR during the experiment was originally measured using a cone calorimeter, providing direct measurements. In contrast, this study calculates the same measurement using two different correlations through a direct inverse solution. Following the methodology in the *CodeRed#03* [19], I employ a similar strategy. Flame height and pool fire diameter were measured and applied to Eqn(s) 16 and 18 to directly calculate the HRR, with the results presented in Fig 6.4 (a). Tab 6.2 provides the maximum and average HRR measurements from the three different methods. The percentage error as a function of time was calculated, whereby, the average of the two correlations was taken and the uncertainty was measured at each time step. This resulted in Fig 6.5, where by the uncertainty was 33% above and 25% below at each time step. This suggests that the validation method calculates the HRR as an ensemble of solutions, where the true HRR likely falls between the two correlations which is close to the measured values from the calorimetry as shown in Fig 6.4 (a).

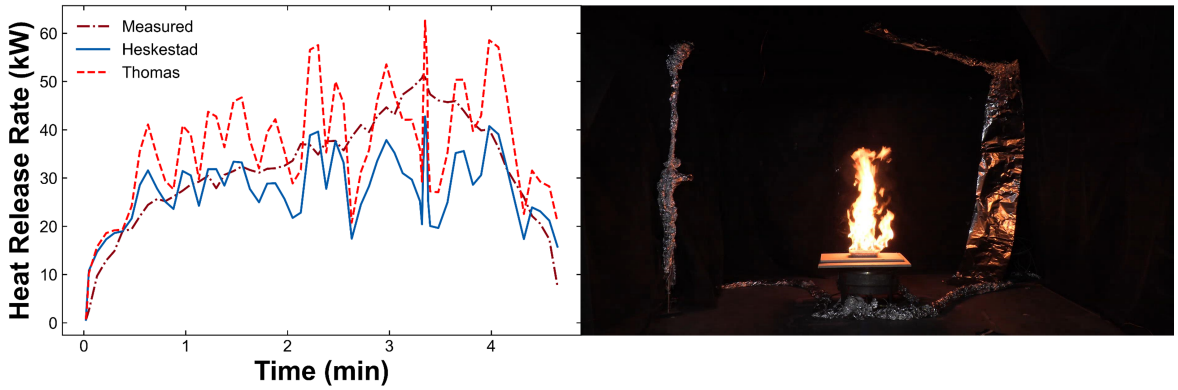



**Figure 6.4** – (a) Hestetad and Thomas present an ensemble of solutions where the calculated heat release rate (kW) lies between the two curves. (b) Heptane pan NIST experiment.

| Measurements | NIST (kW) | Heskestad (kW) | Thomas (kW) |
|---|---|---|---|
| **Maximum** | 51 | 50 | 73 |
| **Average** | 32 | 27 | 36 |

**Table 6.2** – Calculation for validation HRR with a comparison of maximum and average HRR.

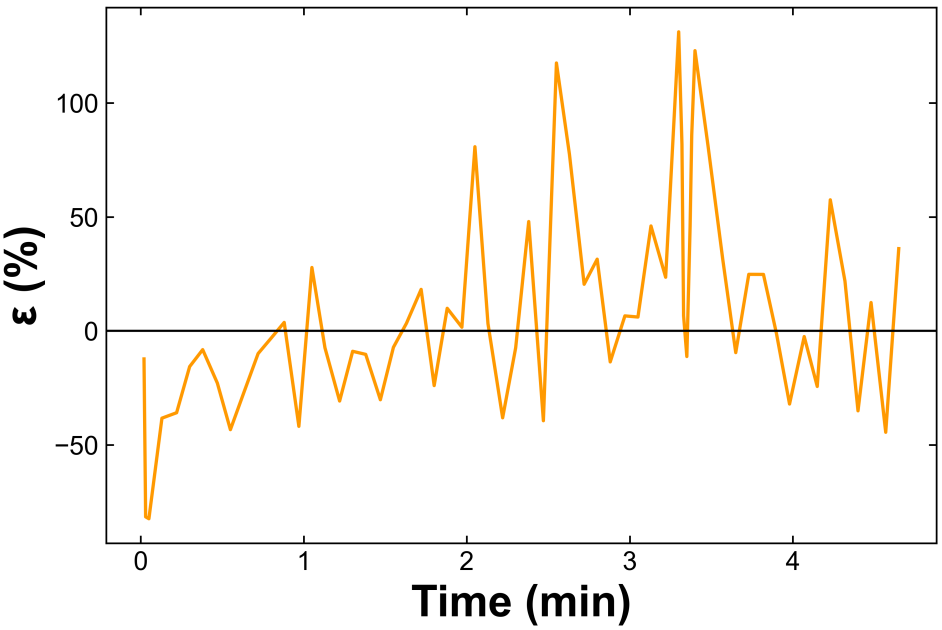



**Figure 6.5** – Illustrates the percentage error of the two correlations as a function of time, where by the positive was 33% and the negative was 25% on average.

## 6.5 External heat release rate: *CodeRed*

### 6.5.1 Quiescent Conditions

The external flaming for *CodeRed#01*, *CodeRed#02*, and *CodeRed#04* was calculated with correlations based on only flame height applicable for calculating the external heat release rate (HRR). The four correlations discussed earlier in this chapter [305, 322–324] all represent external HRR as a function of flame height. In the *CodeRed* experiments, there are two types of openings a window and a door, however, for consistency, here i analysed opening 7, a window, across all experiments (as other data was not available). The flame characteristics were obtained using the AI diagnostic tool detailed in Chapter 5. The resulting external HRR calculations shown in Fig(s) 6.6, 6.7 and 6.8. These results represent an ensemble of solutions, with the true external HRR expected to lie within this range. An ensemble, in this context, reflects the potential range of external HRR outcomes based on variations in direct measurement(s) and the system defined by

the correlation.

In *CodeRed#02*, the maximum external HRR reached 2.81 MW, with an average of 0.78 MW. By contrast, *CodeRed#01* and *CodeRed#04* showed significantly lower maximum HRR values of 0.70 MW and 0.75 MW, respectively. These variations are attributed to differences in compartment ventilation, with reduced oxygen levels inside the compartment causing pyrolysis gases to ignite outside, leading to taller external flames and higher HRR, whilst uncontrolled variables add to the uncertainty of measurements [309,310]. As flame height increases, the HRR also increases, if crosswinds remain minimal and do not introduce a cooling effect [270]. These HRR values correlate well with the instantaneous flame height measurements presented in Chapter 5.

In *CodeRed#01* and *CodeRed#04*, experimental conditions remained unchanged for *CodeRed#01*, while *CodeRed#04* featured 50% encapsulated cross-laminated timber (CLT), which inherently limited the flammable fuel load inside the compartment. This resulted in smaller external flames and, consequently, a lower external HRR. These findings are consistent with the correlations, as smaller flames are associated with lower HRR, a relationship supported by several studies [309, 310].

Specifically, external HRR measurements using Lee et al.'s proposed correlations over predict for both *CodeRed#01* and *CodeRed#04* [305]. This is likely due to their study not accounting for the neutral plane of the flame at the opening, with the characteristic measurement being dimensionless. In comparison, Tang et al.'s correlations consider the location at which the flame protrudes from the opening, with their measurements aligning more closely with the ensemble of results [322].

Lu et al.'s correlation, on the other hand, consistently under predicts external HRR. Their study indicates that variations in the elevation of openings in their compartment experiments led to decreases in flame height and, consequently, external HRR. However, in the *CodeRed* experiments, the elevation of the openings remains constant. Additionally, flame height tends to decrease when the opening is closer to the ceiling, which is another factor not fully addressed by Lu et al. Moreover, their correlation does not consider aspect ratio of the opening, which is considered by both Sun et al. and Lee et al [323, 324].

This discrepancy in flame behaviour is evident in the *CodeRed* experiments, where differences between the door and window openings are observed. These differences are primarily due to air entrainment into the opening due to the change in aspect ratio, which

affects the buoyancy of the external flames and, in turn, influences both flame height and HRRe. Sun et al.'s correlation, specifically developed for large flames, calculated the highest external HRR in *CodeRed#02*, as this experiment recorded the tallest external flames, supporting their correlation to the measurements.

I have applied a set of correlations covering a wide range of experimental scenarios, including variations in opening geometry and elevation. However, none of these correlations account for the effects of sideward, perpendicular crosswinds. Crosswinds can reduce flame height and cause lateral flame deflection towards adjacent openings, increasing flame length [270].

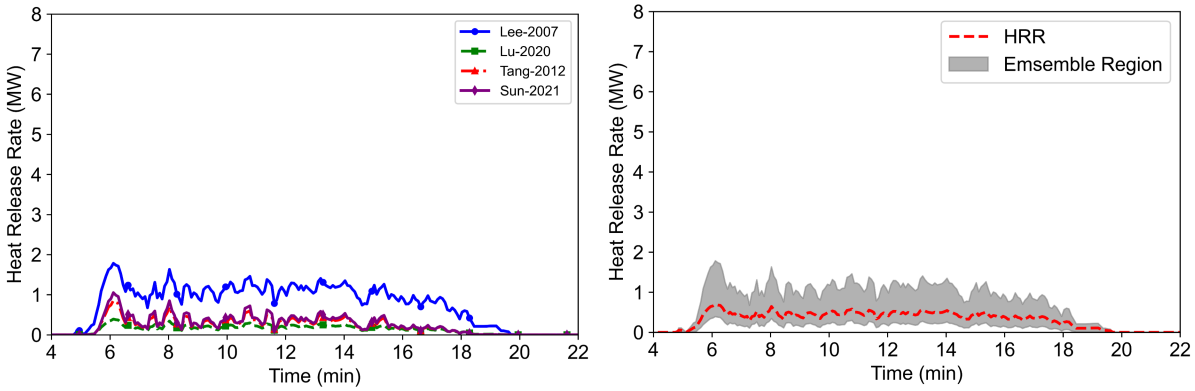



**Figure 6.6** – (a) The heat release rate calculations using existing correlations for *CodeRed#01*, opening , where Lee et al, has the highest prediction and Lu et al the lowest (b) shows the ensemble of solutions with the calculated heat release rate within the ensemble region. An average of 0.38 MW and maximum of 0.7 MW.

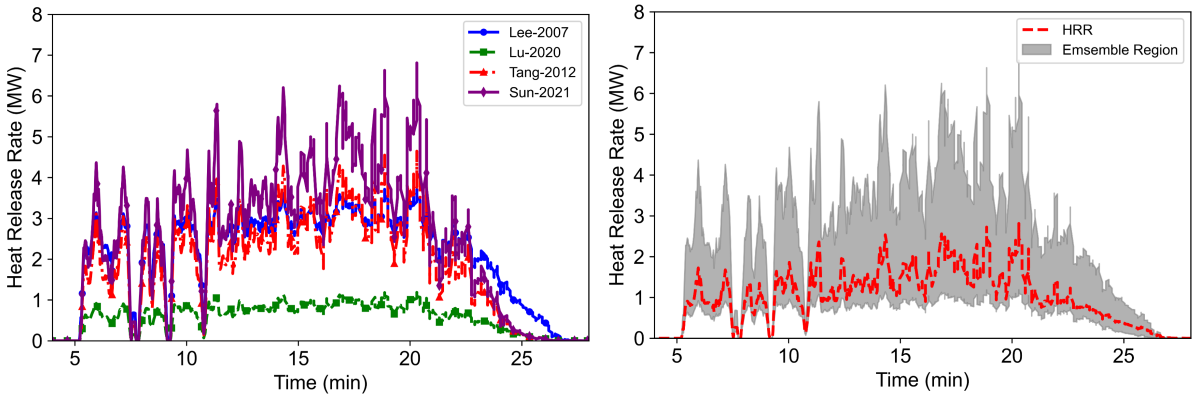



**Figure 6.7** – (a) The heat release rate calculations using existing correlations for *CodeRed#02*, opening , where Sun et al, has the highest prediction and Lu et al the lowest (b) shows the ensemble of solutions with the calculated heat release rate within the ensemble region. An average of 1.11 MW and maximum of 2.81 MW.

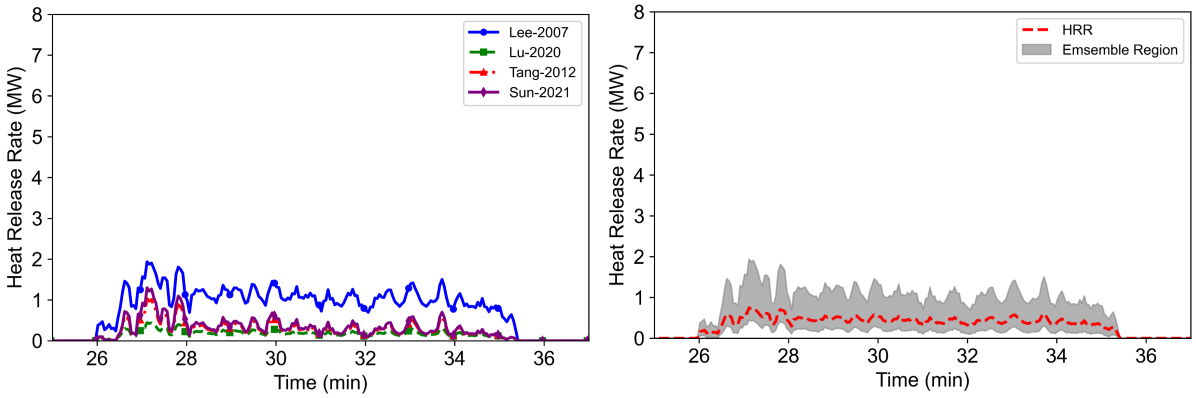



**Figure 6.8** – (a) The heat release rate calculations using existing correlations for *CodeRed#04*, opening , where Lee et al, has the highest prediction and Lu et al the lowest (b) shows the ensemble of solutions with the calculated heat release rate within the ensemble region. An average of 0.43 MW and maximum of 0.75 MW.

| External Heat Release Rate | Max (MW) | Average (MW) |
|---|---|---|
| CodeRed#01 | 0.70 | 0.38 |
| CodeRed#02 | 2.81 | 1.11 |
| CodeRed#04 | 0.75 | 0.43 |

**Table 6.3** – External heat release rates for opening 7 of the *CodeRed* experiment.

### 6.5.2 Perpendicular cross-winds

The *CodeRed* experiments as shown in Chapter 5, inclined flames were observed and measured, one of the causes being the presence of side-ward perpendicular crosswinds on the compartment even at times minimal. In *CodeRed#02*, opening 7 had an average flame inclination of 88°, where 90° indicates near-vertical flames. In contrast, *CodeRed#01* and *CodeRed#04* exhibited greater average inclinations of 69° and 78°, respectively, due to the influence of minimal side-ward perpendicular crosswinds.

Using Sugawa et al.'s correlation, *CodeRed#02* calculated a maximum external HRR of 5.1 MW and an average of 2.5 MW, while *CodeRed#01* reached a maximum of 0.97 MW and an average of 0.69 MW. *CodeRed#04* achieved a maximum HRR of 1.51 MW and an average of 0.81 MW given in Tab 6.4. These results align with correlations for quiescent conditions, indicating that the impact of crosswinds on flame inclination was small. The HRR calculations from Sugawa et al.'s correlation closely match the external HRR values derived from the ensemble in the previous sub-section, as shown in Fig(s) 6.9, 6.10, and 6.11.

In the presence of side-ward, perpendicular winds, external flame behaviour is affected.

Specifically, flame height tends to decrease, while flame length—defined as the horizontal extension of the flame—increases due to the air entrainment's influence on the plume [270]. Flame length represents the distance between the origin of the flame at the opening and its lateral extension parallel to the façade where they can potentially reach adjacent openings [300, 321].

This behaviour is critical to understand, as it poses a significant risk in fire safety design. In *CodeRed#01*, the proximity of the openings allowed flames to merge when tall enough, where there was a larger singular flame and resulting in a higher external HRR. Correlations support this observation, as taller flame heights are typically associated with higher HRR values [231, 300, 309–311].

Overall, ambient wind conditions play an important role in fire dynamics, particularly in outdoor fires and high-rise buildings, where wind almost always influences airflow into the compartment [270]. When wind speeds are low, airflow into the compartment is reduced, leading to incomplete combustion inside and the generation of external flames outside due to an imbalanced fuel-to-air ratio. This was observed in *CodeRed#02*, where minimal crosswinds contributed to taller external flames compared to *CodeRed#01* and *CodeRed#04*, further amplified by a 50% reduction in ventilation.

Currently, there is a lack of research on compartment fire studies under side-ward perpendicular crosswinds, which is essential for the fire-safe design of buildings, particularly in terms of the separation of openings and distance to adjacent structures.

| **External Heat Release Rate** | **Max (MW)** | **Average (MW)** |
|---|---|---|
| CodeRed#01 | 0.97 | 0.59 |
| CodeRed#02 | 5.05 | 2.51 |
| CodeRed#04 | 1.41 | 0.81 |

**Table 6.4** – External heat release rate calculation for conditions under side-ward perpendicular wind of opening 7 of all *CodeRed* experiments.

### 6.5.3 Total heat release rate - *CodeRed#01*

In compartment fire experiments, quantifying the contribution of external heat release rate (HRR) to the total HRR is critical. For the *CodeRed#01* experiment, the external HRR was calculated, as this was the only experiment where all data was available from one entire side of the compartment, as the other experiments had camera damage in-

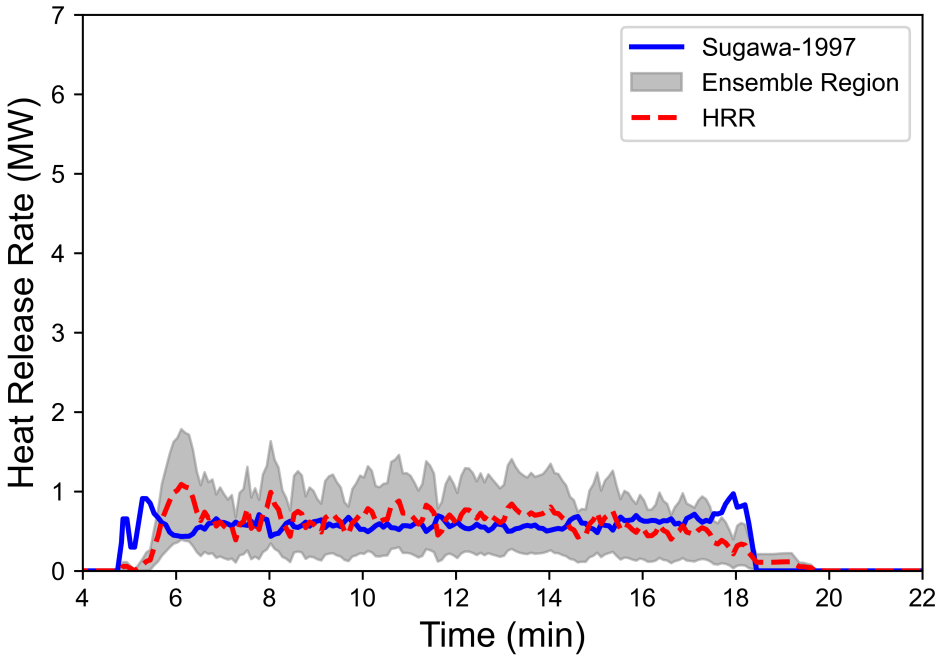



**Figure 6.9** – External heat release rate calculation correlating to wind velocity and resulting angle of inclination for *CodeRed#01*.

curring data loss. Fig 6.12 presents a contour plot where each block corresponds to an individual opening on the compartment wall similar to Fig 4.2 in Chapter 3. Furthermore, observations indicate that flames merged less frequently, as discussed in Chapter 5. Consequently, it was viable to treat each opening as a distinct source of external HRR. A data gap occurred around 12 minutes after ignition due to camera malfunction, resulting in the loss of flame measurements during that period. Each numbered opening in the contour plot represents the external HRR calculation, with values lying within the ensemble at each time step from ignition to flame extinction. The highest external HRR values were measured between the openings 2 and 10. This also aligns with observations that the cross-laminated timber (CLT) ceiling ignited in this region [8], resulting in taller external flames. These findings suggest that pyrolysis gases ignited outside the compartment openings due an imbalance of oxygen supply entering the compartment relative to the fuel consumption inside.

Based on these observations, the external HRR for the entire *CodeRed#01* compartment was calculated by assuming mirrored external flaming along the opposite compartment wall, which had symmetrical opening size and location as *CodeRed#01* had no change in ventilation conditions and CLT encapsulation.

Delichatsios et al. proposed a model for under-ventilated compartment fires, sug-

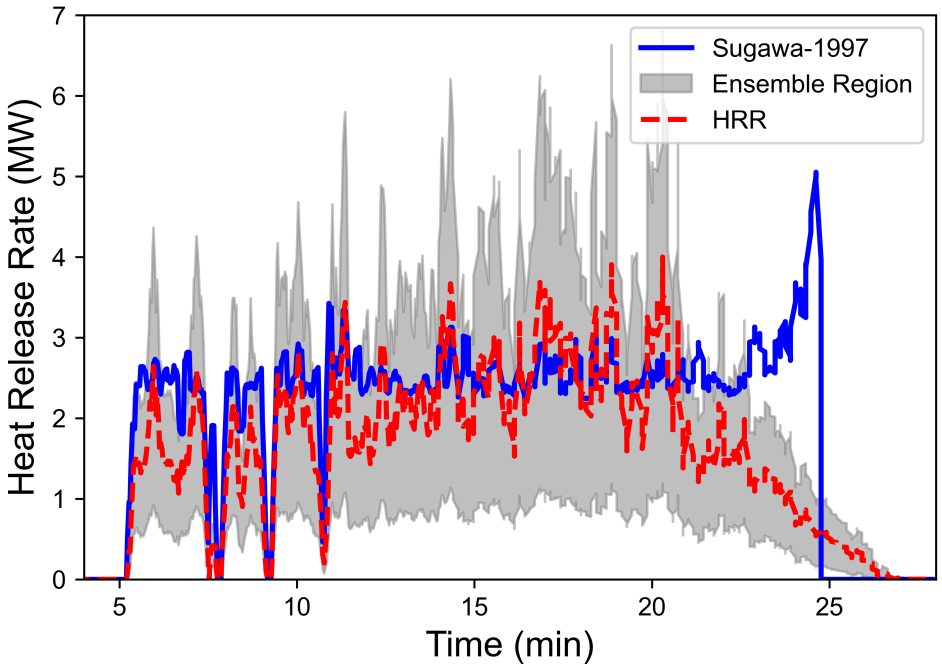



**Figure 6.10** – External heat release rate calculation correlating to wind velocity and resulting angle of inclination for *CodeRed#02*.

gesting that when the compartment reaches a transitional state between ventilated and under-ventilated conditions, all available fuel combusts outside the compartment [320]. As such, the external HRR of the compartment equals the total HRR, which is visually evident when the entire opening is filled with external flames. However, quantifying this in large compartment fires with multiple openings [301], such as in the *CodeRed* experiments, is considerably more challenging and can be looked into with future design fires and external flaming models.

The total HRR of the *CodeRed#01* compartment was calculated using similar methods employed in the x-ONE and x-Two experiments, where the fuel load, burning rate, and combustion efficiency were combined with the flame spread rate of the wood crib [8, 18, 20, 272, 273]. Fig 6.13 presents the total HRR from ignition to extinction, encompassing the external HRR contribution. The CLT ceiling alone contributed approximately 60 MW [8], demonstrating that exposed mass timber significantly adds to the fuel load of the fire and affects overall fire dynamics. This additional fuel load also influences external flaming, which is further impacted by ventilation, as observed in the *CodeRed#02* experiments.

This study plays a critical role in contributing to a research gap in quantifying the

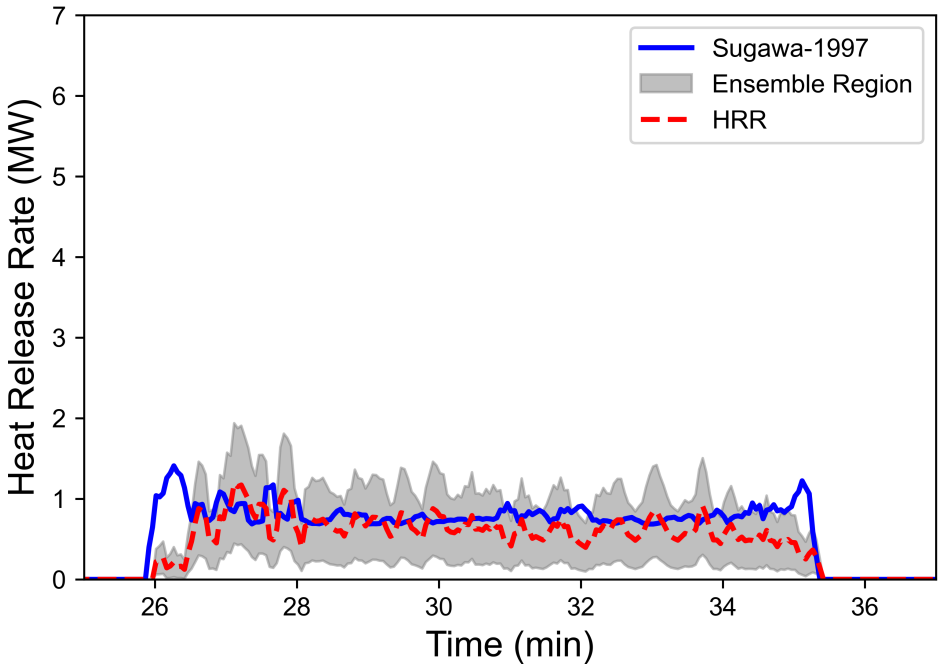



**Figure 6.11** – External heat release rate calculation correlating to wind velocity and resulting angle of inclination for *CodeRed#04*.

HRR of external flames from compartment openings and determining how much each individual opening contributes, as illustrated in Fig 6.12.

The external HRR of *CodeRed#01* reached a maximum of $43^{+14.2}_{-10.8}$ MW with an average of $10^{+3.3}_{-2.5}$ MW, including the propagating uncertainties from the validation case earlier in this chapter, where the total HRR of the *CodeRed#01*compartment fire was 120 MW and 99 MW, respectively. Approximately 36% of the total HRR was attributed to external flames outside the compartment, as shown in Fig 6.13. This understanding is critically important when designing buildings with exposed timber, as external flames can create the potential for ignition of adjacent openings, upper floors, or nearby buildings which can help and inform current fire safety guidance such as BR-187 [333]. As reiterated, quantifying this in large-scale experiments and outdoor fires is challenging due to the limitations of instrumentation, making this approach—using inverse modelling coupled with measurements from an AI-diagnostics tool—particularly valuable.

| **Measurements** | **Total HRR (MW)** | **Total External HRR (MW)** |
|---|---|---|
| Maximum | 120 | 43 |
| Average | 99 | 10 |

**Table 6.5** – Total and external heat release rates of *CodeRed#01*.

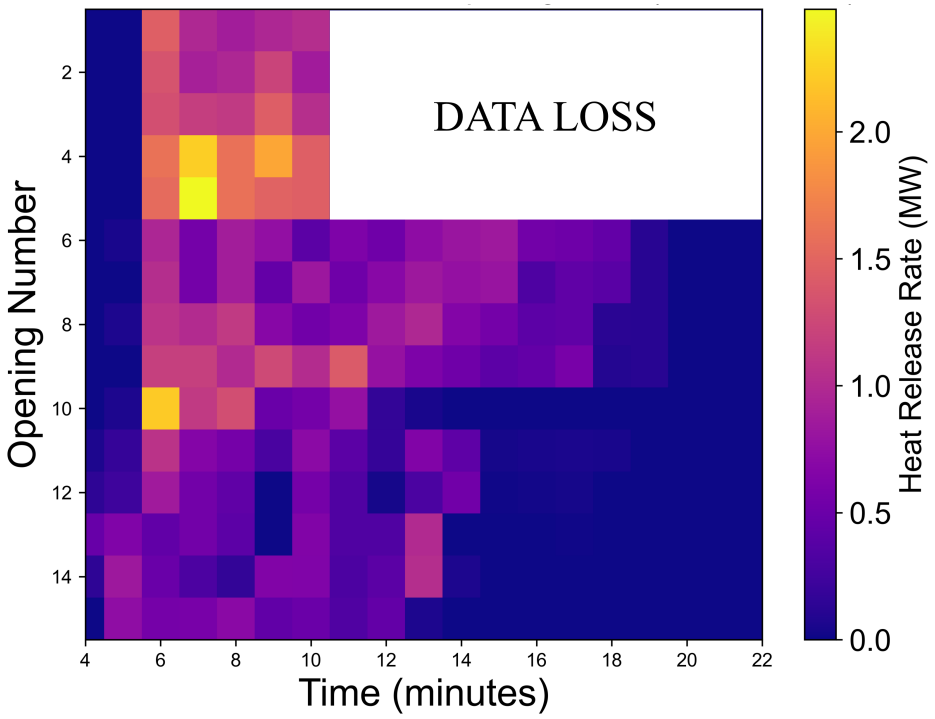



**Figure 6.12** – A contour plot for the external heat release rate from each individual opening of the *CodeRed#01* compartment where data loss incurred from openings 1-5 around 11-12 minutes after ignition.

## 6.6 Conclusions

Quantifying external heat release rate (HRR) is essential for understanding compartment fires and its external flaming behaviour. Most experimental studies in the literature are based on small-scale compartment experiments with varying opening geometries, at times subjected to sideward, perpendicular winds. These studies typically use oxygen calorimetry to measure HRR, a method that is not feasible for large-scale experiments like *CodeRed* and outdoor fires. Furthermore, many of the correlations presented in the literature rely on flame height as a proxy for HRR, resulting in limited variability and producing similar measurements. While there are correlations between wind velocity and inclination to infer the external HRR, there is a lack of research in compartment fire experiments subjected to side-ward, perpendicular crosswinds, which is important, especially since high-rise buildings are frequently exposed to wind. This study contributes to fire science and fire engineering by offering a method to calculate the external HRR in experiments where direct measurements from instrumentation are not feasible. It achieves this by utilising AI diagnostics coupled with inverse modelling. This approach allows for the calculation of the HRR for individual openings, enabling the measurement

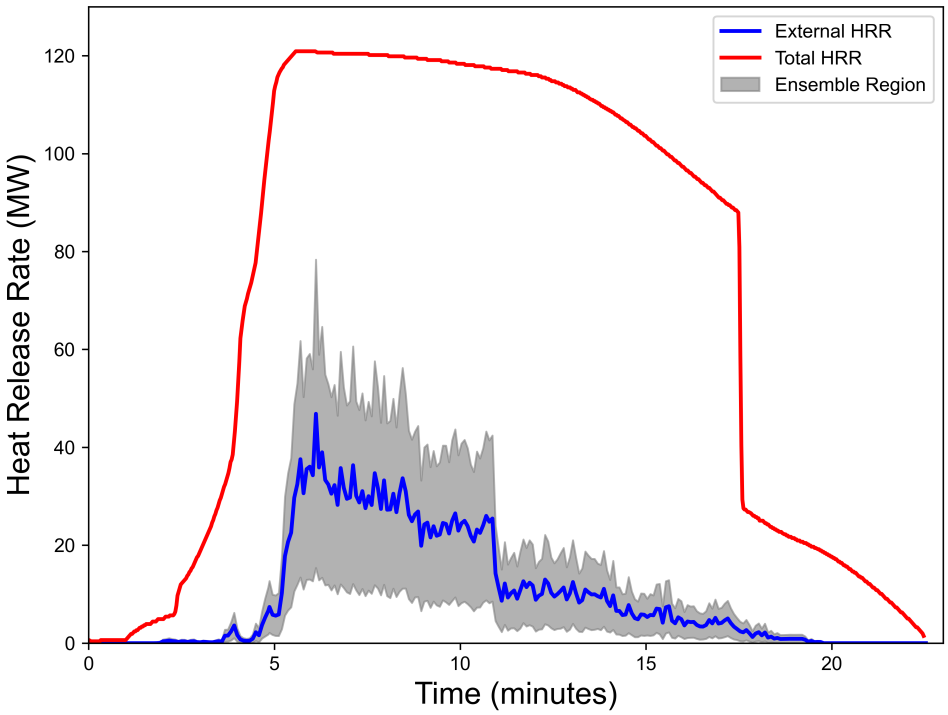



**Figure 6.13** – Total heat release rate of the *CodeRed#01* compartment where 36% of this was attributed to the external flames outside the compartment.

of the external HRR of a compartment fire—an aspect that has not been thoroughly explored in previous research. These are valuable for engineers when considering the fire behaviour of buildings with exposed timber and the potential for external flames to ignite areas such as the floor above or adjacent openings. From the *CodeRed* compartment series, *CodeRed#01* had a total HRR of 120 MW, where the calculated external heat release rate was a maximum of $43^{+14.2}_{-10.8}$ MW, which found that 36% of the total HRR was contributed by the external flames outside the compartment. For opening 7, across all experiments, *CodeRed#02* had the highest external HRR at $2.8^{+0.9}_{-0.7}$ MW, driven by reduced ventilation and the resultant ignition of pyrolysis gases outside the compartment. Conversely, *CodeRed#01* and *CodeRed#04* had lower external HRR of $0.7^{+0.23}_{-0.17}$ MW and $0.75^{+0.25}_{-0.19}$ MW respectively, where *CodeRed#04* due to the encapsulated CLT, which limited the contribution of mass timber as potential flammable fuel. The ability to calculate the external HRR of a compartment fire outside the lab and the quantity from each individual opening will provide engineers and designers with critical data for developing fire scenarios, improving external flame models in performance-based fire design and to real-time applications.

# Chapter 7

# Conclusions

This thesis explores the application of artificial intelligence (AI) in advancing the understanding and resolution of fire safety challenges, with a specific focus on hazards in high-rise timber buildings, including charring, external flaming, and external heat release rate. The contributions of this work pave the way for progress in the field by introducing an innovative technology that has been underutilised, while conventional approaches, such as numerical and computational solutions, continue to dominate. However, these traditional methods face limitations when applied to timber compartment fires due to the complex chemical reactions of timber and its kinetic parameters. AI offers a promising alternative to overcome these challenges and enhance fire safety analysis.

In Chapter 2, I examined the current applications of AI in fire science, building on the pioneering works in key areas such as the fundamentals of combustion, and fire dynamics in built and natural environments. As outlined in Chapter 1, timber has become a prominent material in construction, especially in high-rise buildings, as the growth of these structures is becoming more common, whether hybrid or stand-alone designs. This chapter also highlights the rapid growth of AI and the lack of research utilising it as a tool in building and structural engineering, particularly for advancing sustainable practices. Presently, research often leaps from simple methods to highly complex approaches, without covering intermediaries. AI serves as an effective tool by reducing the need for physical understanding compared to physical models, while offering computational simplicity. This chapter establishes the foundation for the rest of the thesis.

In Chapter 3, I created a novel dataset of mass timber charring experiments, VAQT, compiled into a large, centralised database—a resource that is currently lacking in fire

science, where accessible, consolidated data is rare. Charring of timber can be studied through experiments or physical models, but the complexity increases when flaming is involved. In this chapter, I develop a series of data-driven models to predict the charring rate, comparing them to the current industry standard, Eurocode-5 (EC5), which provides a single value for the average charring rate of mass timber across various wood types. EC5 had an error of 27%. The models ranged from supervised machine learning to complex deep learning architectures, with the best-performing model being the multi-layered neural network, achieving a 9% error rate. Notably, supervised machine learning models performed similarly well, with an 11% error, suggesting that complex AI techniques are not always necessary to outperform EC5. Additionally, I implemented Bayesian optimisation to prevent overfitting and reduce generalisation of predictions, conducting a sensitivity analysis to identify which parameters in the model had the greatest influence, compared to a physical understanding of the problem. This chapter marks the beginning of examining fire safety challenges at a small physical scale—charring of timber members, as illustrated in Fig 7.1. Future work should involve expanding the current database as more timber charring experiments are published or made publicly available. It is well established that data-driven models become more accurate and robust when trained on larger and variable datasets, so the addition of further experiments would significantly enhance the predictive power of these models.

In Chapter 4, I introduce *CodeRed*, the largest open-plan compartment fire experiment featuring a mass-timber ceiling, conducted in France during the COVID-19 pandemic, which i had the opportunity to work on. This chapter, along with chapter 6, increase the physical scale as illustrated in Fig 7.1. It highlights the potential hazards that arise in compartment fires involving exposed CLT, particularly under varying ventilation conditions and with different levels of CLT encapsulation. Additionally, I address the human challenges involved in conducting such an experiment during the pandemic, including the logistical efforts, instrumentation setup, and visual analysis methods required to quantify the size and shape of external flames and calculate the external heat release rate (HRR) of the experiment. The analysis employed computer vision and inverse modelling techniques. This chapter documents significant advancements in understanding large-scale compartment fires, particularly those relevant to open-plan office spaces and high-rise buildings and identifies the hazards studied in chapters 5 and 6.

In Chapter 5, I introduce an AI diagnostics tool built using computer vision to quantify the size and shape of external flames—marking the first time this hazard has been studied in large-scale compartment fires. This tool is versatile, with applications ranging from indoor laboratory experiments to outdoor fires, providing multi-scale analysis. It enables the simultaneous and instantaneous quantification of multiple flames, even under the influence of sideward, perpendicular crosswinds where traditional instrumentation such as thermocouples are not feasible. When applied to the *CodeRed* experiments, the tool demonstrated that reducing ventilation by 50% resulted in taller and longer-lasting external flames, whereas reducing the encapsulation of exposed timber by 50% significantly diminished the external flames, which also formed much later after ignition inside the compartment. Observations showed that external flaming ceased once the CLT flaming stopped. One limitation of this experiment is the lack of sideview cameras of the compartment, which could be used to measure flame thickness and, by extension, flame volume. This would enable the calculation of volumetric HRR from the projected surface area of the flame at each opening in the *CodeRed* compartment.

In Chapter 6, I measure the external heat release rate (HRR) of the *CodeRed* experiments using the AI diagnostics tool i built in Chapter 5, combined with direct inverse modelling. The current literature largely focuses on small-scale experiments, where HRR is measured using oxygen calorimetry. However, this approach is not feasible for large-scale experiments, outdoor fires, or situations where such instrumentation is unavailable. I propose a novel method of calculating external HRR using computer vision, addressing this research gap by analysing data from the *CodeRed* experiments in Chapter(s) 4 and 5. My findings show that 36% of the total heat release rate in the *CodeRed* experiment originates from outside the compartment. Similarly to the behaviour of external flames, the external HRR correlates with flame behaviour and varies depending on ventilation conditions and timber encapsulation.

For future work, it is crucial to conduct additional large-scale experiments, particularly to gather more experimental data on timber charring elements. This data can be integrated into the VAQT database, expanding and diversifying the dataset, as illustrated in Fig 7.1. Building on the findings of the *CodeRed* experiments, future studies should focus on external flames, leveraging side-view cameras to refine future design fires and develop external flaming models that could also potentially calculate the volumetric

HRR based on projected surface area There is also a significant gap in experimental data and correlations related to compartment fires induced by perpendicular winds as outlined in Chapter 6. An important area of study given that likeliness of high-rise buildings exposed to wind. Addressing this gap is critical for improving fire safety standards in urban environments, especially with timber buildings. Furthermore, AI modelling could be advanced by training a convolutional neural network (CNN), potentially in combination with reinforcement learning, to refine the thresholding of fire images from the *CodeRed* experiments, even if computationally expensive and time consuming. This approach could potentially enhance flame detection and reduce the uncertainties identified. Such developments would create a more sophisticated framework, evolving from simpler models to more complex ones, enabling more accurate quantification of external flame behaviour in large-scale compartment fires. These insights would be applicable also to lab-scale and outdoor fire scenarios.

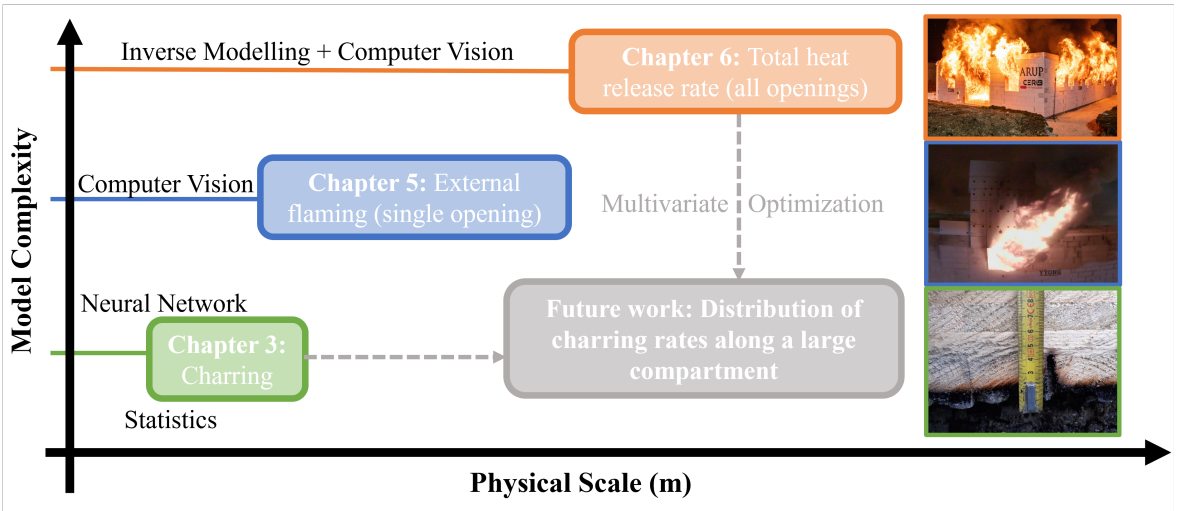



**Figure 7.1** – Chart to outline the physical scale of the hazards covered in the thesis and the modelling complexity required to solve them.

### 7.0.1 Summary

In summary, the hazards discussed throughout this thesis—charring, external flaming, and external heat release rate, as illustrated in Fig 7.1—represent significant challenges in fire safety. Charring, which occurs when timber burns, is crucial to understand and quantify as it directly affects the structural integrity of the material. This leads to external flaming, where pyrolysis gases from the charring of the CLT ceiling and burning of the

wood crib in *CodeRed* ignite outside the compartment when there is insufficient oxygen inside. The external HRR quantifies the heat transfer of the fire to the surroundings, both outside the openings and the compartment. All these hazards are interconnected and pose critical fire safety risks to buildings and their occupants. In this thesis, I leverage emerging technologies, specifically statistical modelling and AI algorithms, as a tool to better understand these hazards and the implications of exposed timber in large compartment fires. AI simplifies the modelling process by reducing computational complexity and minimising the need for detailed physical understanding. Traditional methods, particularly for modelling timber—a complex fuel—and large compartments, are challenging to apply. AI provides a solution to this difficult problem, offering a more efficient and scalable approach. The significance of this thesis lies in several key contributions: the creation of a centralised charring database that can be expanded, the development of an AI diagnostics tool for quantifying the size and shape of multi-scale fires, which enhances our understanding of timber's behaviour in buildings, and the formulation of external flaming models to promote a more sustainable built environment and improved fire safety.

# References


[1] M. H. Ramage, H. Burridge, M. Busse-Wicher, G. Fereday, T. Reynolds, D. U. Shah, G. Wu, L. Yu, P. Fleming, D. Densley-Tingley, J. Allwood, P. Dupree, P. F. Linden, and O. Scherman, "The wood from the trees: The use of timber in construction," 2 2017.

[2] Structural Timber Association, *Structural Timber Buildings Fire Safety in Use Guidance: Volume 6 - Mass Timber Structures; Compliance with Building Regulation B3(1)*. Alloa: Structural Timber Association, 2020.

[3] D. Safarik, J. Elbrecht, and W. Miranda, "State of tall timber 2022," *CTBUH Journal*, 2022.

[4] D. Barber, "Tall timber buildings: What's next in fire safety?," *Fire Technology*, vol. 51, no. 6, pp. 1279–1284, 2015.

[5] M. Spišáková and D. Mačková, "The use potential of traditional building materials for the realization of structures by modern methods of construction," *Selected Scientific Papers - Journal of Civil Engineering*, vol. 10, pp. 127–138, 11 2015.

[6] R. Abrahamsen, Sep 2024.

[7] google, Sep 2024.

[8] P. Kotsovinos, E. Rackauskaite, E. Christensen, A. Glew, E. O'Loughlin, H. Mitchell, R. Amin, F. Robert, M. Heidari, D. Barber, *et al.*, "Fire dynamics inside a large and open-plan compartment with exposed timber ceiling and columns: Codered# 01," *Fire and Materials*, 2022.

[9] C. Pettersson, "Fire safety in timber buildings-a review of existing knowledge," *Brandforsk*, vol. 10, 2020.

[10] M. Z. Naser, "Fire resistance evaluation through artificial intelligence - a case for timber structures," *Fire Safety Journal*, vol. 105, pp. 1–18, 4 2019.

[11] A. I. Bartlett, R. M. Hadden, and L. A. Bisby, "A review of factors affecting the burning behaviour of wood for application to tall timber construction," *Fire Technology*, vol. 55, pp. 1–49, 2019.

[12] J. Liu and E. C. Fischer, "Review of the charring rates of different timber species," *Fire and Materials*, vol. 48, pp. 3–15, 1 2024.

[13] H. Mitchell, P. Kotsovinos, F. Richter, D. Thomson, D. Barber, and G. Rein, "Review of fire experiments in mass timber compartments: Current understanding, limitations, and research gaps," *Fire and Materials*, vol. 47, no. 4, pp. 415–432, 2023.

[14] M. Bullen and P. Thomas, "Compartment fires with non-cellulosic fuels," in *Symposium (International) on Combustion*, vol. 17, pp. 1139–1148.

[15] A. Glew, R. Turnbull, F. M. Poulsen, E. Christensen, P. Kotsovinos, E. O'Loughlin, D. Barber, and J. Schulz, "A design approach to external fire spread from buildings with exposed mass timber," pp. 1701–1711, World Conference on Timber Engineering (WCTE 2023), 2023.

[16] P. Kotsovinos, H. Mitchell, E. Christensen, R. Amin, M. Heidari, G. Rein, D. Barber, and J. Schulz, "Flame spread characteristics in large compartments with an exposed timber ceiling," (Oslo, Norway), WCTE, 2023.

[17] H. Mitchell, *Flaming and smouldering hazards in large timber compartments*. Thesis, 2024.

[18] P. Kotsovinos, E. G. Christensen, E. Rackauskaite, A. Glew, E. O'Loughlin, H. Mitchell, R. Amin, F. Robert, M. Heidari, D. Barber, *et al.*, "Impact of ventilation on the fire dynamics of an open-plan compartment with exposed timber ceiling and columns: Codered# 02," *Fire and Materials*, 2022.

[19] P. Kotsovinos, E. Christensen, J. Gale, *et al.*, "The effectiveness of a water mist system in an openplan compartment with an exposed timber ceiling: Codered# 03," *SPFE Extra Magazine*, 2022.

[20] P. Kotsovinos, E. G. Christensen, A. Glew, E. O'Loughlin, H. Mitchell, R. Amin, F. Robert, M. Heidari, D. Barber, G. Rein, *et al.*, "Impact of partial encapsulation on the fire dynamics of an open-plan compartment with exposed timber ceiling and columns: Codered# 04," *Fire and Materials*, vol. 47, no. 4, pp. 597–626, 2023.

[21] I. Goodfellow, Y. Bengio, and A. Courville, *Deep Learning*. 2016.

[22] M. C. Valdez, C.-F. Chen, S. D. Chicas, and N. Mizoue, "Mapping the probability of wildland fire occurrence in central america, and identifying the key factors," *International Journal of Wildland Fire*, vol. 32, no. 12, pp. 1758–1772, 2023.

[23] M. J. Hurley, D. T. Gottuk, J. R. Hall Jr, K. Harada, E. D. Kuligowski, M. Puchovsky, J. M. Watts Jr, C. J. WIECZOREK, *et al.*, *SFPE handbook of fire protection engineering*. Springer, 2015.

[24] F. Rosenblatt, "The perceptron: A probabilistic model for information storage and organization in the brain," *Psychological Review*, vol. 65, no. 6, pp. 386–408, 1958.

[25] L. Brigato and L. Iocchi, "A close look at deep learning with small data," *2020 25th International Conference on Pattern Recognition (ICPR)*, pp. 2490–2497, 1 2021.

[26] A. Ali, A. N. Inglis, E. Prado, and B. Wundervald, "Bayesian linear regression," 2019.

[27] R. M. Neal, *Bayesian Learning for Neural Networks*, vol. 118. Springer New York, 1996.

[28] T. Hastie, R. Tibshirani, and J. Friedman, "Springer series in statistics the elements of statistical learning data mining, inference, and prediction," 2019.

[29] A. Géron, "Hands-on machine learning with scikit-learn and tensorflow: Concepts, tools, and techniques to build intelligent systems," 2017.

[30] J. T. Hancock and T. M. Khoshgoftaar, "Survey on categorical data for neural networks," *Journal of Big Data*, vol. 7, p. 28, 12 2020.

[31] Y. Yoo, "Hyperparameter optimization of deep neural network using univariate dynamic encoding algorithm for searches," *Knowledge-Based Systems*, vol. 178, pp. 74–83, 8 2019.

[32] A. Burkov, *THE HUNDRED-PAGE MACHINE LEARNING BOOK*. 2019.

[33] M. Jordan, J. Kleinberg, and B. Schölkopf, "Pattern recognition and machine learning," 2006.

[34] V. Wiley and T. Lucas, "Computer vision and image processing: A paper review," *International Journal of Artificial Intelligence Research*, vol. 2, p. 22, 2018.

[35] X. Huang, X. Wu, and A. Usmani, *Perspectives of Using Artificial Intelligence in Building Fire Safety*, pp. 139–159. Springer International Publishing, 2022.

[36] A. Gaur, A. Singh, A. Kumar, A. Kumar, and K. Kapoor, "Video flame and smoke based fire detection algorithms: A literature review," *Fire Technology*, vol. 56, no. 5, pp. 1943–1980, 2020.

[37] S. Geetha, C. S. Abhishek, and C. S. Akshayanat, "Machine vision based fire detection techniques: A survey," *Fire Technology*, vol. 57, no. 2, pp. 591–623, 2021.

[38] F. Abid, "A survey of machine learning algorithms based forest fires prediction and detection systems," *Fire Technology*, vol. 57, no. 2, pp. 559–590, 2021.

[39] M. Z. Naser, "Mechanistically informed machine learning and artificial intelligence in fire engineering and sciences," *Fire Technology*, vol. 57, pp. 2741–2784, 11 2021.

[40] H.-T. Thai, "Machine learning for structural engineering: A state-of-the-art review," *Structures*, vol. 38, pp. 448–491, 2022.

[41] I. Bakas and K. J. Kontoleon, "A review of the contributions of artificial intelligence in fire engineering, in a world rapidly realising the need for sustainable design," *IOP Conference Series: Earth and Environmental Science*, vol. 1196, no. 1, p. 012112, 2023.

[42] G. Philippe, P. Pierre, and T. Michel, "A tomographic study of measurements in a v-shaped h2air flame and a lagrangian interpretation of the turbulent flame brush evolution," *Combustion and Flame*, vol. 81, no. 3, pp. 229–241, 1990.

[43] G. J. Smallwood, L. Gülder, D. R. Snelling, B. M. Deschamps, and I. Gökalp, "Characterization of flame front surfaces in turbulent premixed methane/air combustion," *Combustion and Flame*, vol. 101, no. 4, pp. 461–470, 1995.

[44] O. Yoshiaki, "A primitive study of a fire detection method controlled by artificial neural net," *Fire Safety Journal*, vol. 17, no. 6, pp. 535–553, 1991.

[45] Turgay and D. Hasan, "Fire detection in video sequences using a generic color model," *Fire Safety Journal*, vol. 44, no. 2, pp. 147–158, 2009.

[46] M. Giuseppe, L. Markus, and B. Thomas, "An image processing technique for fire detection in video images," *Fire Safety Journal*, vol. 41, no. 4, pp. 285–289, 2006. 13th International Conference on Automatic Fire Detection, Duisburg, Germany.

[47] Y. Feiniu, "Video-based smoke detection with histogram sequence of lbp and lbpv pyramids," *Fire Safety Journal*, vol. 46, no. 3, pp. 132–139, 2011.

[48] S. McAllister, J.-Y. Chen, and A. C. Fernandez-Pello, *Non-premixed Flames (Diffusion Flames)*, pp. 139–154. New York, NY: Springer New York, 2011.

[49] L. Audouin, G. Kolb, J. L. Torero, and J. M. Most, "Average centreline temperatures of a buoyant pool fire obtained by image processing of video recordings," 1995.

[50] A. Kempf, F. Flemming, and J. Janicka, "Investigation of lengthscales, scalar dissipation, and flame orientation in a piloted diffusion flame by les," *Proceedings of the Combustion Institute*, vol. 30, no. 1, pp. 557–565, 2005.

[51] S. Baris Ali, R. H. Evatt, and M. Suresh, "Large eddy simulation of extinction and reignition with artificial neural networks based chemical kinetics," *Combustion and Flame*, vol. 157, no. 3, pp. 566–578, 2010.

[52] S. Baris Ali and M. Suresh, "Linear eddy mixing based tabulation and artificial neural networks for large eddy simulations of turbulent flames," *Combustion and Flame*, vol. 157, no. 1, pp. 62–74, 2010.

[53] L. C. F. Lucas, K. C. Athanasios, and R. Stelios, "Tabulation of combustion chemistry via artificial neural networks (anns): Methodology and application to les-pdf simulation of sydney flame l," *Combustion and Flame*, vol. 185, pp. 245–260, 2017.

[54] C. Cheng, X. Xiaopeng, and T. Dominique, "Efficient premixed turbulent combustion simulations using flamelet manifold neural networks: A priori and a posteriori assessment," *Combustion and Flame*, vol. 245, p. 112325, 2022.

[55] C. Cheng, J. Gábor, and T. Dominique, "On-the-fly artificial neural network for chemical kinetics in direct numerical simulations of premixed combustion," *Combustion and Flame*, vol. 226, pp. 467–477, 2021.

[56] R. Hernández and J. Ballester, "Flame imaging as a diagnostic tool for industrial combustion," *Combustion and Flame*, vol. 155, no. 3, pp. 509–528, 2008.

[57] J. Jie, W. Huaxian, G. Zihe, F. Yanyun, S. Jinhua, Z. Yongming, L. Kaiyuan, and H. Simo, "Experimental study on flame merging behaviors from two pool fires along the longitudinal centerline of model tunnel with natural ventilation," *Combustion and Flame*, vol. 173, pp. 307–318, 2016.

[58] S. Alankrit, B. V. Sandeep, and V. S. Ajay, "Experimental investigation of flame

morphology and instabilities in turbulent wind-driven flames," *Proceedings of the Combustion Institute*, vol. 40, no. 1, p. 105345, 2024.

[59] T. B. Maynard and J. W. Butta, "A physical model for flame height intermittency," *Fire Technology*, vol. 54, no. 1, pp. 135–161, 2018.

[60] Y. Weidong, L. Naian, Z. Hong, C. Haixiang, X. Xiaodong, and Z. Linhe, "Effect of cross-wind on firebrand flame: An experimental study and scaling analysis," *Proceedings of the Combustion Institute*, vol. 40, no. 1, p. 105621, 2024.

[61] H. Pengcheng, L. Jiao, L. Zhihui, L. Naian, and Z. Linhe, "Characterizing the flame geometries and radiation of axisymmetric turbulent buoyant diffusion flames based on 3d reconstruction," *Proceedings of the Combustion Institute*, vol. 40, no. 1, p. 105326, 2024.

[62] G. Mohsen, T. Paul, S. Olaf, G. Martin, and R. Andreas, "Flame lift-off detector based on deep learning neural networks," *Combustion and Flame*, vol. 260, p. 113215, 2024.

[63] H. Hua Wei, W. Qian, T. Hao Jie, Z. Min, and Z. Yang, "Characterisation of external acoustic excitation on diffusion flames using digital colour image processing," *Fuel*, vol. 94, pp. 102–109, 2012.

[64] P. Julio, O. G. Hugo, C. Juan, E. A. Luis, J. R. Alejandro, and F. Andrés, "Soot propensity by image magnification and artificial intelligence," *Fuel*, vol. 225, pp. 256–265, 2018.

[65] R.-G. Guilllermo, C.-G. Lis, S. Jose Antonio, G. Arantzazu, and J. C.-G. Fernando, "Vision based algorithm for automated determination of smoke point of diesel blends," *Fuel*, vol. 235, pp. 595–602, 2019.

[66] G. Sedat, T. Muhammed Fatih, and O. Cem, "Artificial neural network regression model to predict flue gas temperature and emissions with the spectral norm of flame image," *Fuel*, vol. 255, p. 115827, 2019.

[67] W. Kaidi, B. Camille, V. Luc, and D. Pascale, "Machine learning for detailed chemistry reduction in dns of a syngas turbulent oxy-flame with side-wall effects," *Proceedings of the Combustion Institute*, vol. 38, no. 2, pp. 2825–2833, 2021.

[68] L. Florian, C. Liming, Bruno, and P. Heinz, "Exploring the fuel structure depend-

ence of laminar burning velocity: A machine learning based group contribution approach," *Combustion and Flame*, vol. 232, p. 111525, 2021.

[69] S. Yao, B. Wang, A. Kronenburg, and O. T. Stein, "Conditional scalar dissipation rate modeling for turbulent spray flames using artificial neural networks," *Proceedings of the Combustion Institute*, vol. 38, no. 2, pp. 3371–3378, 2021.

[70] P. Rene, M. Matthias, E. Sven, K. Hartmut, and H. Christoph, "Machine learning techniques to predict the flame state, temperature and species concentrations in counter-flow diffusion flames operated with ch4/co/h2-air mixtures," *Fuel*, vol. 326, p. 124915, 2022.

[71] W. Yu, Y. Yuefeng, Z. Xiaolei, and Z. Zhongxiao, "Pattern recognition for measuring the flame stability of gas-fired combustion based on the image processing technology," *Fuel*, vol. 270, p. 117486, 2020.

[72] N. Mahdi, T. Mohammad Zabetian, and P. Hadi, "Experimental study on the flame stability and color characterization of cylindrical premixed perforated burner of condensing boiler by image processing method," *Energy*, vol. 189, p. 116130, 2019.

[73] S. Wenkai, L. Li, H. Qiming, L. Guichuang, W. Jiwei, Z. Ning, W. Shaohua, Q. Penghua, and S. Shaowei, "Combustion characteristics of ignition processes for lean premixed swirling combustor under visual conditions," *Energy*, vol. 218, p. 119521, 2021.

[74] S. Zhao and Y. Fan, "Experimental and numerical study on fuel distribution and flame expansion of the enhanced flame holding devices," *Energy*, vol. 203, p. 117850, 2020.

[75] S. Zhao, Y. Fan, D. Tiantai, and C. Danny, "Influence of injection scheme on flame characteristics in partially premixed combustion," *Energy*, vol. 205, p. 118058, 2020.

[76] Y. Mengfan, Z. Wenkun, W. Zhuozhi, G. Yuting, L. Gaoyang, C. Yongxin, P. Jiangbo, and S. Rui, "Diagnostic investigation of devolatilization, ignition, and flame fluctuation during laminar oxy-coal combustion," *Energy*, vol. 289, p. 130000, 2024.

[77] Soroush, T. Sadegh, G. Amirreza, and Sina, "A novel swiss-roll counterflow microcombustor: Experimental investigation of flame dynamic characteristics by spectroscopy and rgb image processing methods," *Energy*, vol. 299, p. 131495, 2024.

[78] I. Fikret, T. Gokmen, R. M. Tyler, and M. S. Selim, "Experimental and artificial neural network modeling study on soot formation in premixed hydrocarbon flames," *Fuel*, vol. 82, no. 12, pp. 1477–1490, 2003.

[79] L. Shiyu, W. Haiou, S. Zhiwei, F. Kae Ken, J. N. Graham, D. Xue, J. E. Michael, B. D. Bassam, L. Kun, and F. Jianren, "Reconstructing soot fields in acoustically forced laminar sooting flames using physics-informed machine learning models," *Proceedings of the Combustion Institute*, vol. 40, no. 1, p. 105314, 2024.

[80] I. Matthias, S. Christoph, and P. Heinz, "Optimal artificial neural networks and tabulation methods for chemistry representation in les of a bluff-body swirl-stabilized flame," *Proceedings of the Combustion Institute*, vol. 32, no. 1, pp. 1527–1535, 2009.

[81] A. S. Baris and M. Suresh, "Turbulent premixed flame modeling using artificial neural networks based chemical kinetics," *Proceedings of the Combustion Institute*, vol. 32, no. 1, pp. 1605–1611, 2009.

[82] J. L. Corentin, M. Antony, C. Nicolas, V. Denis, and P. Thierry, "Training convolutional neural networks to estimate turbulent sub-grid scale reaction rates," *Combustion and Flame*, vol. 203, pp. 255–264, 2019.

[83] S. Andrea, D. Pascale, V. Luc, and M. N. Zacharias, "Direct mapping from les resolved scales to filtered-flame generated manifolds using convolutional neural networks," *Combustion and Flame*, vol. 210, pp. 71–82, 2019.

[84] Y. Hans, P. J. Matthew, and M. Luca, "A data-driven kinematic model of a ducted premixed flame," *Proceedings of the Combustion Institute*, vol. 38, no. 4, pp. 6231–6239, 2021.

[85] D. Tianjie, R. Thomas, R. Stelios, and W. P. Jones, "Machine learning tabulation of thermochemistry in turbulent combustion: An approach based on hybrid flamelet/random data and multiple multilayer perceptrons," *Combustion and Flame*, vol. 231, p. 111493, 2021.

[86] Y. Vikas, C. Mario, and G. Abdulla, "Physics-informed recurrent neural networks for linear and nonlinear flame dynamics," *Proceedings of the Combustion Institute*, vol. 39, no. 2, pp. 1597–1606, 2023.

[87] D. Hao, Y. Xiaojun, K. Hailiang, and Z. Ke, "Prediction of combustion promotion

effect of high/low-frequency ac electric fields based on machine learning method," *Fuel*, vol. 346, p. 128348, 2023.

[88] A. Palacios and J. Casal, "Assessment of the shape of vertical jet fires," *Fuel*, vol. 90, no. 2, pp. 824–833, 2011.

[89] G. Heskestad, *Fire Plumes, Flame Height, and Air Entrainment*, pp. 396–428. New York, NY: Springer New York, 2016.

[90] M. Gómez-Mares, M. Muñoz, and J. Casal, "Axial temperature distribution in vertical jet fires," *Journal of Hazardous Materials*, vol. 172, no. 1, pp. 54–60, 2009.

[91] F. C. Christo, A. R. Masri, and E. M. Nebot, "Artificial neural network implementation of chemistry with pdf simulation of h2/co2 flames," *Combustion and Flame*, vol. 106, no. 4, pp. 406–427, 1996.

[92] K. Yingying, L. Yuxing, W. Sailei, D. Pengfei, Z. Jianlu, H. Hui, and H. Jinke, "Large-scale experimental study on jet flame length of hydrogen-blended natural gas and inverse methods for optimizing the weighted multi-point source model," *Fuel*, vol. 367, p. 131434, 2024.

[93] A. C. K. Jordan, C. Wai Tong, J. E. Michael, F. T. Zhao, R. M. Paul, and I. Matthias, "Predictions of instantaneous temperature fields in jet-in-hot-coflow flames using a multi-scale u-net model," *Proceedings of the Combustion Institute*, vol. 40, no. 1, p. 105330, 2024.

[94] R. M. Hadden, *Heat Release Rate*, pp. 603–610. Cham: Springer International Publishing, 2020.

[95] Z. Wang, Y. Ding, T. Zhang, and X. Huang, "Automatic real-time fire distance, size and power measurement driven by stereo camera and deep learning," *Fire Safety Journal*, vol. 140, p. 103891, 2023.

[96] K. Li, S. Mao, and R. Feng, "Estimation of heat release rate and fuel type of circular pool fires using inverse modelling based on image recognition technique," *Fire Technology*, vol. 55, no. 3, pp. 667–687, 2019.

[97] M. Bonner, W. Wegrzyński, and G. Rein, "Visual fire power: An algorithm for measuring heat release rate of visible flames in camera footage, with applications in facade fire experiments," *Fire Technology*, vol. 59, no. 1, pp. 191–215, 2023.

[98] C. Cheng, S. Srijith, and T. Dominique, "Data-driven discovery of heat release rate markers for premixed nh3/h2/air flames using physics-informed machine learning," *Fuel*, vol. 330, p. 125508, 2022.

[99] Z. Taotao, T. Peng, and Y. Taohong, "Machine learning based heat release rate indicator of premixed methane/air flame under wide range of equivalence ratio," *Energy*, vol. 263, p. 126103, 2023.

[100] Z. Wang, T. Zhang, and X. Huang, "Predicting real-time fire heat release rate by flame images and deep learning," *Proceedings of the Combustion Institute*, vol. 39, no. 3, pp. 4115–4123, 2023.

[101] R. Jose, Daniel, G. Michael, E. T. Claudio, and F.-P. Carlos, "A machine learning approach to predict the critical heat flux for ignition of solid fuels," *Fire Safety Journal*, vol. 141, p. 103968, 2023.

[102] A. S. Hansen and P. J. Hovde, "Prediction of time to flashover in the iso 9705 room corner test based on cone calorimeter test results," *Fire and Materials*, vol. 26, no. 2, pp. 77–86, 2002.

[103] A. Dexters, R. R. Leisted, R. V. Coile, S. Welch, and G. Jomaas, "Testing for knowledge: Application of machine learning techniques for prediction of flashover in a 1/5 scale iso 13784-1 enclosure," *Fire and Materials*, vol. 45, pp. 708–719, 10 2021.

[104] L. Yuchuan, K. Yoon, and L. Wonsook, "Rgb image-based hybrid model for automatic prediction of flashover in compartment fires," *Fire Safety Journal*, vol. 132, p. 103629, 2022.

[105] F. Linhao, T. Wai Cheong, T. Qi, F. Eugene Yujun, and L. Tianshui, "An explainable machine learning based flashover prediction model using dimension-wise class activation map," *Fire Safety Journal*, vol. 140, p. 103849, 2023.

[106] J. Wang, W. C. Tam, Y. Jia, R. Peacock, P. Reneke, E. Y. Fu, and T. Cleary, "P-flash – a machine learning-based model for flashover prediction using recovered temperature data," *Fire Safety Journal*, vol. 122, 2021.

[107] Z. Tianhang, W. Zilong, W. Ho Yin, T. Wai Cheong, H. Xinyan, and X. Fu, "Real-time forecast of compartment fire and flashover based on deep learning," *Fire Safety Journal*, vol. 130, p. 103579, 2022.

[108] W. C. Tam, E. Y. Fu, R. Peacock, P. Reneke, J. Wang, J. Li, and T. Cleary, "Generating synthetic sensor data to facilitate machine learning paradigm for prediction of building fire hazard," *Fire Technology*, vol. 59, no. 6, pp. 3027–3048, 2023.

[109] W. M. L. Eric, K. K. Y. Richard, S. M. Lo, K. C. Lam, and G. H. Yeoh, "A novel artificial neural network fire model for prediction of thermal interface location in single compartment fire," *Fire Safety Journal*, vol. 39, no. 1, pp. 67–87, 2004.

[110] K. K. Y. Richard, W. M. L. Eric, S. M. Lo, and G. H. Yeoh, "Prediction of temperature and velocity profiles in a single compartment fire by an improved neural network analysis," *Fire Safety Journal*, vol. 41, no. 6, pp. 478–485, 2006.

[111] J. L. Hodges, B. Y. Lattimer, and K. D. Luxbacher, "Compartment fire predictions using transpose convolutional neural networks," *Fire Safety Journal*, vol. 108, 9 2019.

[112] B. Y. Lattimer, J. L. Hodges, and A. M. Lattimer, "Using machine learning in physics-based simulation of fire," *Fire Safety Journal*, vol. 114, p. 102991, 2020.

[113] Z. Yang, T. Wang, L. Bu, and J. Ouyang, "Training with augmented data: Gan-based flame-burning image synthesis for fire segmentation in warehouse," *Fire Technology*, vol. 58, no. 1, pp. 183–215, 2022.

[114] B. Tyler, B. Serhat, and O. A. Ezekoye, "Brain-storm: A deep learning model for computationally fast transient high-rise fire simulations," *Fire Safety Journal*, vol. 125, p. 103443, 2021.

[115] J. Chen, L. Ding, J. Ji, and J. Zhu, "A combined method to build bayesian network for fire risk assessment of historical buildings," *Fire Technology*, vol. 59, no. 6, pp. 3525–3563, 2023.

[116] K. L. B. L. Xavier and V. K. Nanayakkara, "Development of an early fire detection technique using a passive infrared sensor and deep neural networks," *Fire Technology*, vol. 58, no. 6, pp. 3529–3552, 2022.

[117] D. Faouzi, "Performance improvement of fire detectors by means of gas sensors and neural networks," *Fire Safety Journal*, vol. 39, no. 5, pp. 383–398, 2004.

[118] B. Li, F. Xu, X. Li, C. Yu, and X. Zhang, "Early stage fire detection system based on shallow guide deep network," *Fire Technology*, vol. 60, no. 3, pp. 1803–1821, 2024.

[119] T. J. McAvoy, J. Milke, and T. A. Kunt, "Using multivariate statistical methods to detect fires," *Fire Technology*, vol. 32, no. 1, pp. 6–24, 1996.

[120] J. A. Milke, "Monitoring multiple aspects of fire signatures for discriminating fire detection," *Fire Technology*, vol. 35, no. 3, pp. 195–209, 1999.

[121] J. A. Milke, M. E. Hulcher, C. L. Worrell, D. T. Gottuk, and F. W. Williams, "Investigation of multi-sensor algorithms for fire detection," *Fire Technology*, vol. 39, no. 4, pp. 363–382, 2003.

[122] W. Mao, W. Wang, Z. Dou, and Y. Li, "Fire recognition based on multi-channel convolutional neural network," *Fire Technology*, vol. 54, no. 2, pp. 531–554, 2018.

[123] J. Martinsson, M. Runefors, H. Frantzich, D. Glebe, M. McNamee, and O. Mogren, "A novel method for smart fire detection using acoustic measurements and machine learning: Proof of concept," *Fire Technology*, vol. 58, no. 6, pp. 3385–3403, 2022.

[124] M. Jeon, H.-S. Choi, J. Lee, and M. Kang, "Multi-scale prediction for fire detection using convolutional neural network," *Fire Technology*, vol. 57, no. 5, pp. 2533–2551, 2021.

[125] L. Pu, Y. Yi, Z. Wangda, and Z. Miao, "Evaluation of image fire detection algorithms based on image complexity," *Fire Safety Journal*, vol. 121, p. 103306, 2021.

[126] Z. Zhang, T. Shen, and J. Zou, "An improved probabilistic approach for fire detection in videos," *Fire Technology*, vol. 50, no. 3, pp. 745–752, 2014.

[127] W. S. Qureshi, M. Ekpanyapong, M. N. Dailey, S. Rinsurongkawong, A. Malenichev, and O. Krasotkina, "Quickblaze: Early fire detection using a combined video processing approach," *Fire Technology*, vol. 52, no. 5, pp. 1293–1317, 2016.

[128] S. Thomas, K. Klaus, and K. Felix, "Image processing based deflagration detection using fuzzy logic classification," *Fire Safety Journal*, vol. 65, pp. 1–10, 2014.

[129] S. Anton, W. Tjark, and D. Klaus, "Comparison of intensity flickering features for video based flame detection algorithms," *Fire Safety Journal*, vol. 66, pp. 1–7, 2014.

[130] K. Byoung Chul, C. Kwang-Ho, and N. Jae-Yeal, "Fire detection based on vision sensor and support vector machines," *Fire Safety Journal*, vol. 44, no. 3, pp. 322–329, 2009.

[131] J. Baek, T. J. Alhindi, Y.-S. Jeong, M. K. Jeong, S. Seo, J. Kang, J. Choi, and H. Chung, "Real-time fire detection algorithm based on support vector machine with dynamic time warping kernel function," *Fire Technology*, vol. 57, no. 6, pp. 2929–2953, 2021.

[132] B. Jaeseung, J. A. Taha, J. Young-Seon, K. J. Myong, S. Seongho, K. Jongseok, S. We, and H. Yoseob, "Real-time fire detection system based on dynamic time warping of multichannel sensor networks," *Fire Safety Journal*, vol. 123, p. 103364, 2021.

[133] K. Byoung Chul, C. Kwang-Ho, and N. Jae-Yeal, "Early fire detection algorithm based on irregular patterns of flames and hierarchical bayesian networks," *Fire Safety Journal*, vol. 45, no. 4, pp. 262–270, 2010.

[134] G. K. Seong, J. Donglin, L. Shengzhe, and K. Hakil, "Fast fire flame detection in surveillance video using logistic regression and temporal smoothing," *Fire Safety Journal*, vol. 79, pp. 37–43, 2016.

[135] M. S. Mondal, V. Prasad, R. Kumar, N. Saha, S. Guha, R. Ghosh, A. Mukhopadhyay, and S. Sarkar, "Automating fire detection and suppression with computer vision: A multi-layered filtering approach to enhanced fire safety and rapid response," *Fire Technology*, vol. 59, no. 4, pp. 1555–1583, 2023.

[136] Z.-G. Liu, X.-Y. Li, and G. Jomaas, "Identifying community fire hazards from citizen communication by applying transfer learning and machine learning techniques," *Fire Technology*, vol. 57, no. 6, pp. 2809–2838, 2021.

[137] S. Jana and S. K. Shome, "Hybrid ensemble based machine learning for smart building fire detection using multi modal sensor data," *Fire Technology*, vol. 59, no. 2, pp. 473–496, 2023.

[138] Z. Wu, R. Xue, and H. Li, "Real-time video fire detection via modified yolov5 network model," *Fire Technology*, vol. 58, no. 4, pp. 2377–2403, 2022.

[139] A. Latif and H. Chung, "Fire detection and spatial localization approach for autonomous suppression systems based on artificial intelligence," *Fire Technology*, vol. 59, no. 5, pp. 2621–2644, 2023.

[140] Z. Dou, H. Zhou, Z. Liu, Y. Hu, P. Wang, J. Zhang, Q. Wang, L. Chen, X. Diao,

and J. Li, "An improved yolov5s fire detection model," *Fire Technology*, vol. 60, no. 1, pp. 135–166, 2024.

[141] T. Ono, H. Ishii, K. Kawamura, H. Miura, E. Momma, T. Fujisawa, and J. Hozumi, "Application of neural network to analyses of ccd colour tv-camera image for the detection of car fires in expressway tunnels," *Fire Safety Journal*, vol. 41, no. 4, pp. 279–284, 2006. 13th International Conference on Automatic Fire Detection, Duisburg, Germany.

[142] H. Dongil and L. Byoungmoo, "Flame and smoke detection method for early real-time detection of a tunnel fire," *Fire Safety Journal*, vol. 44, no. 7, pp. 951–961, 2009.

[143] X. Wu, Y. Park, A. Li, X. Huang, F. Xiao, and A. Usmani, "Smart detection of fire source in tunnel based on the numerical database and artificial intelligence," *Fire Technology*, vol. 57, no. 2, pp. 657–682, 2021.

[144] S. Bin, L. Xiaojiang, X. Zhao-Dong, and X. Dajun, "Bp neural network-based adaptive spatial-temporal data generation technology for predicting ceiling temperature in tunnel fire and full-scale experimental verification," *Fire Safety Journal*, vol. 130, p. 103577, 2022.

[145] B. Sun and Z.-D. Xu, "Automatic data generation method for precise ceiling temperature prediction of cables fire in the utility tunnel and full-scale experimental verification," *Fire Technology*, vol. 58, no. 5, pp. 2847–2869, 2022.

[146] H. Yao, K. Jianhong, and F. Ceji, "Rapid prediction of mine tunnel fire smoke movement with machine learning and supercomputing techniques," *Fire Safety Journal*, vol. 127, p. 103492, 2022.

[147] G. Xin, Y. Dong, J. Li, D. Tao, and L. Shan, "Full-field temperature prediction in tunnel fires using limited monitored ceiling flow temperature data with transformer-based deep learning models," *Fire Safety Journal*, vol. 148, p. 104232, 2024.

[148] Z. Xiaoning, C. Xinghao, D. Yifei, Z. Yuxin, W. Zilong, S. Jihao, J. Nils, and H. Xinyan, "Smart real-time evaluation of tunnel fire risk and evacuation safety via computer vision," *Safety Science*, vol. 177, p. 106563, 2024.

[149] S. M. Lo, M. Liu, P. H. Zhang, and R. K. K. Yuen, "An artificial neural-network

based predictive model for pre-evacuation human response in domestic building fire," *Fire Technology*, vol. 45, no. 4, pp. 431–449, 2009.

[150] W. Ke, S. Xiupeng, G. Algena Pei Xuan, and Q. Shunzhi, "A machine learning based study on pedestrian movement dynamics under emergency evacuation," *Fire Safety Journal*, vol. 106, pp. 163–176, 2019.

[151] G, A. Ridder, U. Barth, and M. Fontana, "A systematical bayesian approach for outcome-oriented fire service data collection," *Fire Safety Journal*, vol. 78, pp. 219–228, 2015.

[152] B. Adriana, C. Arturo, G.-V. Javier, O. Gemma, and A. Daniel, "Logistic regression vs machine learning to predict evacuation decisions in fire alarm situations," *Safety Science*, vol. 174, p. 106485, 2024.

[153] Y. Chunyu, F. Jun, W. Jinjun, and Z. Yongming, "Video fire smoke detection using motion and color features," *Fire Technology*, vol. 46, no. 3, pp. 651–663, 2010.

[154] Y. Wei, Z. Jianhui, W. Song, W. Yong, Z. Dengyi, and Y. Zhiyong, "Dynamic texture based smoke detection using surfacelet transform and hmt model," *Fire Safety Journal*, vol. 73, pp. 91–101, 2015.

[155] K. Jong-Hwan and Y. L. Brian, "Real-time probabilistic classification of fire and smoke using thermal imagery for intelligent firefighting robot," *Fire Safety Journal*, vol. 72, pp. 40–49, 2015.

[156] A. Nyma, N. Kien, C. Vinod, and B. Wageeh, "Combining multi-channel color space with local binary co-occurrence feature descriptors for accurate smoke detection from surveillance videos," *Fire Safety Journal*, vol. 102, pp. 1–10, 2018.

[157] L. Chenghua, Y. Bin, D. Hao, S. Hongling, J. Xiaoping, and S. Jing, "Real-time video-based smoke detection with high accuracy and efficiency," *Fire Safety Journal*, vol. 117, p. 103184, 2020.

[158] Y. Huang, X. Chen, L. Xu, and K. Li, "Single image desmoking via attentive generative adversarial network for smoke detection process," *Fire Technology*, vol. 57, no. 6, pp. 3021–3040, 2021.

[159] H. Yinuo, Z. Qixing, Z. Yongming, Z. Jiping, and W. Jinjun, "3dvsd: An end-to-end 3d convolutional object detection network for video smoke detection," *Fire Safety Journal*, vol. 134, p. 103690, 2022.

[160] G. Cheng, Y. Zhou, S. Gao, Y. Li, and H. Yu, "Convolution-enhanced vision transformer network for smoke recognition," *Fire Technology*, vol. 59, no. 2, pp. 925–948, 2023.

[161] M. A.-K. Abdullateef, J. T. Mohammad, P. A. Alex, and W. Yong, "Prediction of fire resistance of concrete filled tubular steel columns using neural networks," *Fire Safety Journal*, vol. 37, no. 4, pp. 339–352, 2002. 11th International Conference on Automatic Fire Detection.

[162] A. Zeinab, K. Manouchehr, A. Shahin, F. Hakimeh, W. G. Ulf, S. H. Mikael, and S. Mohammad Ebrahim, "Prediction and optimization of fireproofing properties of intumescent flame retardant coatings using artificial intelligence techniques," *Fire Safety Journal*, vol. 61, pp. 193–199, 2013.

[163] R. Amin, M. Yaxin, F. Richter, C. Kurzer, N. Werther, and G. Rein, "Predicting the average charring rate of mass timber using data-driven methods for structural calculations," *Fire Technology*, 2024.

[164] D. Norsk, A. Sauca, and K. Livkiss, "Fire resistance evaluation of gypsum plasterboard walls using machine learning method," *Fire Safety Journal*, vol. 130, p. 103597, 2022.

[165] T. N. T. Ho, T.-P. Nguyen, and G. T. Truong, "Concrete spalling identification and fire resistance prediction for fired rc columns using machine learning-based approaches," *Fire Technology*, vol. 60, no. 3, pp. 1823–1866, 2024.

[166] Y. Panev, P. Kotsovinos, S. Deeny, and G. Flint, "The use of machine learning for the prediction of fire resistance of composite shallow floor systems," *Fire Technology*, vol. 57, pp. 3079–3100, 11 2021.

[167] X. Jixiang, Z. Jincheng, S. Zhenseng, and L. Minglu, "Prediction of ultimate bearing capacity of tubular t-joint under fire using artificial neural networks," *Safety Science*, vol. 50, no. 7, pp. 1495–1501, 2012.

[168] N. Xu, R. Lovreglio, E. D. Kuligowski, T. J. Cova, D. Nilsson, and X. Zhao, "Predicting and assessing wildfire evacuation decision-making using machine learning: Findings from the 2019 kincade fire," *Fire Technology*, vol. 59, no. 2, pp. 793–825, 2023.

[169] A. Husain, A. A.-S. Yousef, M. E. Hussein, and H. A. Tarek, "Ann models for

prediction of residual strength of hsc after exposure to elevated temperature," *Fire Safety Journal*, vol. 106, pp. 13–28, 2019.

[170] C. Carlos, T. Qi, and G. Thomas, "Predicting the capacity of thin-walled beams at elevated temperature with machine learning," *Fire Safety Journal*, vol. 130, p. 103596, 2022.

[171] K. Turk, C. Kina, H. Tanyildizi, E. Balalan, and M. L. Nehdi, "Machine learning prediction of residual mechanical strength of hybrid-fiber-reinforced self-consolidating concrete exposed to elevated temperature," *Fire Technology*, vol. 59, no. 5, pp. 2877–2923, 2023.

[172] N. Zhuojun, O. Mhd Anwar, H. Xinyan, J. Yaqiang, and U. Asif, "Structural-fire responses forecasting via modular ai," *Fire Safety Journal*, vol. 140, p. 103863, 2023.

[173] G. Karaki and M. Z. Naser, "An approach for developing probabilistic models for temperature-dependent properties of construction materials from fire tests and small data," *Fire and Materials*, vol. 47, no. 6, pp. 758–773, 2023.

[174] K. Sunjoong, P. Soyeon, S. Jinwon, C. In-Rak, and C. Sungmo, "Deep-learning-based data loss reconstruction for spatiotemporal temperature in piloti structures: Enhancing applicability with limited datasets," *Fire Safety Journal*, vol. 140, p. 103887, 2023.

[175] S. Wanfeng, G. Haibo, and L. Cheng, "High-performance real-time fire detection and forecasting framework for industrial cables," *Fire Safety Journal*, vol. 148, p. 104228, 2024.

[176] X. Jixiang, Z. Jincheng, W. Wanzhen, and L. Minglu, "Prediction of temperature of tubular truss under fire using artificial neural networks," *Fire Safety Journal*, vol. 56, pp. 74–80, 2013.

[177] J. R. Martínez-de Dios, J. C. André, J. C. Gonçalves, B. C. Arrue, A. Ollero, and D. X. Viegas, "Laboratory fire spread analysis using visual and infrared images," *International Journal of Wildland Fire*, vol. 15, no. 2, pp. 179–186, 2006.

[178] J. L. Hodges and B. Y. Lattimer, "Wildland fire spread modeling using convolutional neural networks," *Fire Technology*, vol. 55, no. 6, pp. 2115–2142, 2019.

[179] Z. Chunjie, Z. Siyu, C. Zhaolou, and W. Xinmeng, "Learning-based prediction of wildfire spread with real-time rate of spread measurement," *Combustion and Flame*, vol. 215, pp. 333–341, 2020.

[180] J. Burge, M. R. Bonanni, R. L. Hu, and M. Ihme, "Recurrent convolutional deep neural networks for modeling time-resolved wildfire spread behavior," *Fire Technology*, vol. 59, no. 6, pp. 3327–3354, 2023.

[181] X. Li, X. Wang, S. Sun, Y. Wang, S. Li, and D. Li, "Predicting the wildland fire spread using a mixed-input cnn model with both channel and spatial attention mechanisms," *Fire Technology*, vol. 59, no. 5, pp. 2683–2717, 2023.

[182] S. Khanmohammadi, M. Arashpour, E. M. Golafshani, M. G. Cruz, and A. Rajabifard, "An artificial intelligence framework for predicting fire spread sustainability in semiarid shrublands," *International Journal of Wildland Fire*, vol. 32, no. 4, pp. 636–649, 2023.

[183] F. X. Catry, F. C. Rego, F. L. Bação, and F. Moreira, "Modeling and mapping wildfire ignition risk in portugal," *International Journal of Wildland Fire*, vol. 18, no. 8, pp. 921–931, 2009.

[184] N. Faivre, Y. Jin, M. L. Goulden, and J. T. Randerson, "Controls on the spatial pattern of wildfire ignitions in southern california," *International Journal of Wildland Fire*, vol. 23, no. 6, pp. 799–811, 2014.

[185] P. P. de Bem, O. A. de Carvalho Júnior, E. A. T. Matricardi, R. F. Guimarães, and R. A. T. Gomes, "Predicting wildfire vulnerability using logistic regression and artificial neural networks: a case study in brazil's federal district," *International Journal of Wildland Fire*, vol. 28, no. 1, pp. 35–45, 2019.

[186] L. K. Sharma, R. Gupta, and N. Fatima, "Assessing the predictive efficacy of six machine learning algorithms for the susceptibility of indian forests to fire," *International Journal of Wildland Fire*, vol. 31, no. 8, pp. 735–758, 2022.

[187] S. Younes Oulad, M. Hajar, and Hassan, "Predictive modeling of wildfires: A new dataset and machine learning approach," *Fire Safety Journal*, vol. 104, pp. 130–146, 2019.

[188] L. B. Harris, S. A. Drury, C. A. Farris, and A. H. Taylor, "Prescribed fire and fire suppression operations influence wildfire severity under severe weather in lassen

volcanic national park, california, usa," *International Journal of Wildland Fire*, vol. 30, no. 7, pp. 536–551, 2021.

[189] M. Bisquert, E. Caselles, J. M. Sánchez, and V. Caselles, "Application of artificial neural networks and logistic regression to the prediction of forest fire danger in galicia using modis data," *International Journal of Wildland Fire*, vol. 21, no. 8, pp. 1025–1029, 2012.

[190] F. Verdú, J. Salas, and C. Vega-García, "A multivariate analysis of biophysical factors and forest fires in spain, 1991–2005," *International Journal of Wildland Fire*, vol. 21, no. 5, pp. 498–509, 2012.

[191] B. Botequim, P. M. Fernandes, J. G. Borges, E. González-Ferreiro, and J. Guerra-Hernández, "Improving silvicultural practices for mediterranean forests through fire behaviour modelling using lidar-derived canopy fuel characteristics," *International Journal of Wildland Fire*, vol. 28, no. 11, pp. 823–839, 2019.

[192] B. John Ray, P. Claudio, R. Karin, and S. Alfred, "Predicting wildfire burns from big geodata using deep learning," *Safety Science*, vol. 140, p. 105276, 2021.

[193] S. R. Coffield, C. A. Graff, Y. Chen, P. Smyth, E. Foufoula-Georgiou, and J. T. Randerson, "Machine learning to predict final fire size at the time of ignition," *International Journal of Wildland Fire*, vol. 28, no. 11, pp. 861–873, 2019.

[194] S. B. Capps, W. Zhuang, R. Liu, T. Rolinski, and X. Qu, "Modelling chamise fuel moisture content across california: a machine learning approach," *International Journal of Wildland Fire*, vol. 31, no. 2, pp. 136–148, 2022.

[195] M. R. Azim, M. Keskin, N. Do, and M. Gül, "Automated classification of fuel types using roadside images via deep learning," *International Journal of Wildland Fire*, vol. 31, no. 10, pp. 982–987, 2022.

[196] L. Miller, L. Zhu, M. Yebra, C. Rüdiger, and G. I. Webb, "Projecting live fuel moisture content via deep learning," *International Journal of Wildland Fire*, vol. 32, no. 5, pp. 709–727, 2023.

[197] N. Phelps and D. G. Woolford, "Comparing calibrated statistical and machine learning methods for wildland fire occurrence prediction: a case study of human-caused fires in lac la biche, alberta, canada," *International Journal of Wildland Fire*, vol. 30, no. 11, pp. 850–870, 2021.

[198] X. Quan, M. Jiao, Z. He, A. Jaafari, Q. Xie, and X. Lai, "Effects of different sampling strategies for unburned label selection in machine learning modelling of wildfire occurrence probability," *International Journal of Wildland Fire*, vol. 32, no. 4, pp. 561–575, 2023.

[199] X. Quan, Q. Xie, B. He, K. Luo, and X. Liu, "Integrating remotely sensed fuel variables into wildfire danger assessment for china," *International Journal of Wildland Fire*, vol. 30, no. 10, pp. 822–822, 2021.

[200] A. Trucchia, G. Meschi, P. Fiorucci, A. Provenzale, M. Tonini, and U. Pernice, "Wildfire hazard mapping in the eastern mediterranean landscape," *International Journal of Wildland Fire*, vol. 32, no. 3, pp. 417–434, 2023.

[201] Q. Wang, M. Ihme, R. R. Linn, Y.-F. Chen, V. Yang, F. Sha, C. Clements, J. S. McDanold, and J. Anderson, "A high-resolution large-eddy simulation framework for wildland fire predictions using tensorflow," *International Journal of Wildland Fire*, vol. 32, no. 12, pp. 1711–1725, 2023.

[202] A. C. Cullen, B. R. Goldgeier, E. Belval, and J. T. Abatzoglou, "Characterising ignition precursors associated with high levels of deployment of wildland fire personnel," *International Journal of Wildland Fire*, vol. 33, no. 8, pp. –, 2024.

[203] O. Günay, K. Taşdemir, B. Uğur Töreyin, and A. E. Çetin, "Fire detection in video using lms based active learning," *Fire Technology*, vol. 46, no. 3, pp. 551–577, 2010.

[204] J. Fernández-Berni, R. Carmona-Galán, J. F. Martínez-Carmona, and Rodríguez-Vázquez, "Early forest fire detection by vision-enabled wireless sensor networks," *International Journal of Wildland Fire*, vol. 21, no. 8, pp. 938–949, 2012.

[205] T. Tom, R. Lucile, C. Antoine, C. Turgay, and A. A. Moulay, "Computer vision for wildfire research: An evolving image dataset for processing and analysis," *Fire Safety Journal*, vol. 92, pp. 188–194, 2017.

[206] C. Emmy Prema, S. S. Vinsley, and S. Suresh, "Multi feature analysis of smoke in yuv color space for early forest fire detection," *Fire Technology*, vol. 52, no. 5, pp. 1319–1342, 2016.

[207] C. Emmy Prema, S. S. Vinsley, and S. Suresh, "Efficient flame detection based on static and dynamic texture analysis in forest fire detection," *Fire Technology*, vol. 54, no. 1, pp. 255–288, 2018.

[208] X. Qiu, T. Xi, D. Sun, E. Zhang, C. Li, Y. Peng, J. Wei, and G. Wang, "Fire detection algorithm combined with image processing and flame emission spectroscopy," *Fire Technology*, vol. 54, no. 5, pp. 1249–1263, 2018.

[209] A. Khalil, S. U. Rahman, F. Alam, I. Ahmad, and I. Khalil, "Fire detection using multi color space and background modeling," *Fire Technology*, vol. 57, no. 3, pp. 1221–1239, 2021.

[210] M. Zhou, S. Liu, and J. Li, "Multi-scale forest flame detection based on improved and optimized yolov5," *Fire Technology*, vol. 59, no. 6, pp. 3689–3708, 2023.

[211] J. Wang, C. Wang, W. Ding, and C. Li, "Yolov5s-ace: Forest fire object detection algorithm based on improved yolov5s," *Fire Technology*, 2024.

[212] J. Li, H. Tang, X. Li, H. Dou, and R. Li, "Lef-yolo: a lightweight method for intelligent detection of four extreme wildfires based on the yolo framework," *International Journal of Wildland Fire*, vol. 33, no. 1, pp. –, 2024.

[213] K. Konstantinos, I. V. Eleni, and W. Haizhong, "Evacuation behavior of affected individuals and households in response to the 2018 attica wildfires: From empirical data to models," *Safety Science*, vol. 153, p. 105799, 2022.

[214] G. Jayavardhana, M. Slaven, and P. Marimuthu, "Smoke detection in video using wavelets and support vector machines," *Fire Safety Journal*, vol. 44, no. 8, pp. 1110–1115, 2009.

[215] T. Truong Xuan and K. Jong-Myon, "An effective four-stage smoke-detection algorithm using video images for early fire-alarm systems," *Fire Safety Journal*, vol. 46, no. 5, pp. 276–282, 2011.

[216] A. S. Pundir and B. Raman, "Deep belief network for smoke detection," *Fire Technology*, vol. 53, no. 6, pp. 1943–1960, 2017.

[217] A. S. Pundir and B. Raman, "Dual deep learning model for image based smoke detection," *Fire Technology*, vol. 55, no. 6, pp. 2419–2442, 2019.

[218] Y. Gao and P. Cheng, "Forest fire smoke detection based on visual smoke root and diffusion model," *Fire Technology*, vol. 55, no. 5, pp. 1801–1826, 2019.

[219] G. Lin, Y. Zhang, G. Xu, and Q. Zhang, "Smoke detection on video sequences using 3d convolutional neural networks," *Fire Technology*, vol. 55, no. 5, pp. 1827–1847, 2019.

[220] X. Gao, Z. Yongming, Z. Qixing, L. Gaohua, W. Zhong, J. Yang, and W. Jinjun, "Video smoke detection based on deep saliency network," *Fire Safety Journal*, vol. 105, pp. 277–285, 2019.

[221] Y. Huo, Q. Zhang, Y. Jia, D. Liu, J. Guan, G. Lin, and Y. Zhang, "A deep separable convolutional neural network for multiscale image-based smoke detection," *Fire Technology*, vol. 58, no. 3, pp. 1445–1468, 2022.

[222] G. Cheng, X. Chen, and J. Gong, "Deep convolutional network with pixel-aware attention for smoke recognition," *Fire Technology*, vol. 58, no. 4, pp. 1839–1862, 2022.

[223] C. E. Prema, S. Suresh, M. N. Krishnan, and N. Leema, "A novel efficient video smoke detection algorithm using co-occurrence of local binary pattern variants," *Fire Technology*, vol. 58, no. 5, pp. 3139–3165, 2022.

[224] F. Richter and G. Rein, "Heterogeneous kinetics of timber charring at the microscale," *Journal of Analytical and Applied Pyrolysis*, vol. 138, pp. 1–9, 2019.

[225] K. L. Friquin, "Material properties and external factors influencing the charring rate of solid wood and glue-laminated timber," *Fire and Materials*, vol. 35, pp. 303–327, 8 2011.

[226] P. B. Cachim and J.-M. Franssen, "Comparison between the charring rate model and the conductive model of eurocode 5," *Fire and Materials*, vol. 33, pp. 129–143, 4 2009.

[227] F. Richter, P. Kotsovinos, E. Rackauskaite, and G. Rein, "Thermal response of timber slabs exposed to travelling fires and traditional design fires," *Fire Technology*, vol. 57, pp. 393–414, 2021.

[228] Eurocode, "En 1995-1-2: Eurocode 5: Design of timber structures - part 1-2: General - structural fire design," 1995.

[229] J. Martinka, P. Rantuch, and M. Liner, "Calculation of charring rate and char depth of spruce and pine wood from mass loss," *Journal of Thermal Analysis and Calorimetry*, vol. 132, pp. 1105–1113, 5 2018.

[230] P. B. Cachim and J. M. Franssen, "Assessment of eurocode 5 charring rate calculation methods," *Fire Technology*, vol. 46, pp. 169–181, 2010.

[231] D. Drysdale, *An Introduction to Fire Dynamics*. Chichester: Wiley and Sons, 3 ed., aug 2011.

[232] R. H. White and E. V. Nordheim, "Charring rate of wood for astm e 119 exposure," 1992.

[233] N. Werther, "External an internal factors influencing the charring of timber - an experimental study with respect to natural fires and moisture conditions," *Structures in fire - SIF'2016*, pp. 650 – 658, 2 2016.

[234] M. Naser, "Ai-based cognitive framework for evaluating response of concrete structures in extreme conditions," *Engineering Applications of Artificial Intelligence*, vol. 81, pp. 437–449, 5 2019.

[235] G. Wegener, "Abbrandverhalten verschiedener holzarten und holzwerkstoffe," 1986.

[236] M. Jinfang and H. J. X. Yan, "Experimental study on single-sided carbonization and temperature field of glued bamboo," *Journal of Safety and Environment*, pp. 168–172, 2016.

[237] J. H. V. Fornather, "Brandverhalten von holz unter besonderer berücksichtigung stiftförmiger verbindungsmittel : experimentelle und numerische untersuchungen," pp. VII, 173 Bl., Ill., graph. Darst., 2003. Wien, Univ. für Bodenkultur, Diss., 2003.

[238] J. M. Njankouo, J.-C. Dotreppe, and J.-M. Franssen, "Experimental study of the charring rate of tropical hardwoods," *Fire and Materials*, vol. 28, pp. 15–24, 1 2004.

[239] K. Michael, F. Andrea, and H. Erich, "Experimental analysis of the fire behavior of finger-jointed timber members," *Journal of Structural Engineering*, vol. 140, p. 04013063, 3 2014. doi: 10.1061/(ASCE)ST.1943-541X.0000851.

[240] A. Gilka-Bötzow, A. Heiduschke, and P. Haller, "Zur abbrandrate von holz in abhängigkeit der rohdichte," *European Journal of Wood and Wood Products*, vol. 69, pp. 159–162, 2 2011.

[241] M. Peter and T. Göckerl, "Bemessung von voll-und brettschichtholzbauteilen aus maschinell sortiertem schnittholz für den brandfall—teil 2: Brandversuche zur bestätigung der theoretischen ergebnisse," *Institut des Zimmerer-und Holzbaugewerbes eV, Berlin (in German)*, 2006.

[242] M. Lache, "Untersuchungen zur abbrandgeschwindigkeit von vollholz und zur feuerwiderstandsdauer biegebeanspruchter brettschichtholzträger," 1992.

[243] A. Frangi, M. Fontana, E. Hugi, and R. Jübstl, "Experimental analysis of cross-laminated timber panels in fire," *Fire Safety Journal*, vol. 44, pp. 1078–1087, 11 2009.

[244] X. Qingfeng, L. Xiangmin, Z. Jin, M. Baogang, and X. Q. Li, "Experimental study on the mechanical properties of wooden beams after fire on three sides," *Journal of Civil Engineering*, pp. 64–70, 2011.

[245] J. König, "One-dimensional charring of timber exposed to standard and parametric fires in initially unprotected and postprotection situations," *Rapport / Trätek.*, p. 45, 1999. 2020-12-01T22:45:24.544+01:00.

[246] A. Lingens, "Untersuchung des abbrandes und der brandgase ausgewählter holzarten in abhängigkeit vom chemischen und strukturellen holzaufbau," 2003.

[247] R. Fahrni, M. Klippel, A. Just, A. Ollino, and A. Frangi, "Fire tests on glued-laminated timber beams with specific local material properties," *Fire Safety Journal*, vol. 107, pp. 161–169, 2019.

[248] A. Frangi, "Brandverhalten von holz-beton-verbunddecken," *IBK Bericht*, vol. 269, 2001.

[249] P. Čermák, A. Dejmal, Z. Paschová, M. Kymäläinen, J. Dömény, M. Brabec, D. Hess, and L. Rautkari, "One-sided surface charring of beech wood," *Journal of Materials Science*, vol. 54, pp. 9497–9506, 2019.

[250] N. Werther and M. Margesin, "Versuche zum einfluss der holzfeuchte auf das abbrandverhalten von nadelholz," 2013.

[251] A. Frangi and M. Fontana, "Charring rates and temperature profiles of wood sections," *Fire and Materials*, vol. 27, pp. 91–102, 3 2003.

[252] J. ichi Suzuki, T. Mizukami, T. Naruse, and Y. Araki, "Fire resistance of timber panel structures under standard fire exposure," *Fire Technology*, vol. 52, pp. 1015–1034, 2016.

[253] D. Singh and B. Singh, "Investigating the impact of data normalization on classification performance," *Applied Soft Computing*, vol. 97, p. 105524, 12 2020.

[254] M. Kuhn and K. Johnson, *Applied Predictive Modeling*. Springer New York, 2013.

[255] S. Rogers and M. Girolami, *A First Course in Machine Learning*. Chapman and Hall/CRC, 10 2016.

[256] A. Koutsoukas, K. J. Monaghan, X. Li, and J. Huan, "Deep-learning: investigating deep neural networks hyper-parameters and comparison of performance to shallow methods for modeling bioactivity data," *Journal of Cheminformatics*, vol. 9, p. 42, 12 2017.

[257] A. E. Hoerl and R. W. Kennard, "Ridge regression: Biased estimation for nonorthogonal problems," *Technometrics*, vol. 12, no. 1, pp. 55–67, 1970.

[258] R. Tibshirani, "Regression shrinkage and selection via the lasso," *Journal of the Royal Statistical Society: Series B (Methodological)*, vol. 58, pp. 267–288, 1 1996.

[259] D. J. C. MacKay, "Bayesian interpolation," *Neural Computation*, vol. 4, pp. 415–447, 5 1992.

[260] B. E. Boser, I. M. Guyon, and V. N. Vapnik, "Training algorithm for optimal margin classifiers," *Proceedings of the Fifth Annual ACM Workshop on Computational Learning Theory*, pp. 144–152, 1992.

[261] Y. Panev, T. Parker, and P. Kotsovinos, *The Use of Machine Learning in Heat Transfer Analysis for Structural Fire Engineering Applications*, pp. 380–402. CRC Press, 9 2022.

[262] J. Heaton, "Ian goodfellow, yoshua bengio, and aaron courville: Deep learning," *Genetic Programming and Evolvable Machines*, vol. 19, pp. 305–307, 6 2018.

[263] F. Hohman, K. Wongsuphasawat, M. B. Kery, and K. Patel, "Understanding and visualizing data iteration in machine learning," *Proceedings of the 2020 CHI Conference on Human Factors in Computing Systems*, pp. 1–13, 4 2020.

[264] S. Walczak and N. Cerpa, "Heuristic principles for the design of artificial neural networks," *Information and Software Technology*, vol. 41, pp. 107–117, 1 1999.

[265] J. Bergstra and Y. Bengio, "Random search for hyper-parameter optimization," *J. Mach. Learn. Res.*, vol. 13, p. 281–305, feb 2012.

[266] F. Hutter, H. H. H, and K. Leyton-Brown, *Sequential Model-Based Optimization for General Algorithm Configuration*, vol. 6683. Springer Berlin Heidelberg, 2011.

[267] T. Lie, "A method for assessing the fire resistance of laminated timber beams and columns," *Canadian Journal of Civil Engineering*, vol. 4, pp. 161–169, 6 1977.

[268] Z. C. Lipton and J. Steinhardt, "Troubling trends in machine learning scholarship," *Queue*, vol. 17, pp. 45–77, 2 2019.

[269] L. Breiman, "Random forests," *Machine Learning*, vol. 45, pp. 5–32, 2001.

[270] S. Xiepeng, T. Fei, L. Kaihua, R. Fei, S. Congling, M. Bart, and H. Longhua, "Fundamentals of window-ejected fire plumes from under-ventilated compartment fires: Recent progresses and perspectives," *Progress in Energy and Combustion Science*, vol. 94, p. 101039, 2023.

[271] H. Mitchell, R. Amin, M. Heidari, P. Kotsovinos, and G. Rein, "Structural hazards of smouldering fires in timber buildings," *Fire Safety Journal*, vol. 140, p. 103861, 2023.

[272] E. Rackauskaite, M. Bonner, F. Restuccia, N. Fernandez Anez, E. G. Christensen, N. Roenner, W. Wegrzynski, P. Turkowski, P. Tofilo, M. Heidari, *et al.*, "Fire experiment inside a very large and open-plan compartment: x-one," *Fire Technology*, pp. 1–35, 2021.

[273] M. Heidari, E. Rackauskaite, M. Bonner, E. Christensen, S. Morat, H. Mitchell, P. Kotsovinos, P. Turkowski, W. Wegrzynski, P. Tofilo, *et al.*, "Fire experiments inside a very large and open-plan compartment: x-two," *11th International Conference on Structures in Fire (SiF2020)*, 2020.

[274] M. Law, *Fire safety of bare external structural steel / Margaret Law and Turlogh O'Brien*. Ascot: Steel Construction Institute, 1989.

[275] M. Law, "Notes on the external fire exposure measured at lehrte," 1981.

[276] N. Otsu, "A threshold selection method from gray-level histograms," *IEEE Transactions on Systems, Man, and Cybernetics*, vol. 9, no. 1, pp. 62–66, 1979.

[277] C. Gorska and P. Beng, "Fire dynamics in multi-scale timber compartments school of civil engineering," 2019.

[278] C. Gorska, J. P. Hidalgo, and J. L. Torero, "Fire dynamics in mass timber compartments," *Fire Safety Journal*, vol. 120, p. 103098, 2021.

[279] Y. Cui, X. Cheng, L. Gong, L. Li, H. Zhang, and Y. Zhao, "Effect of opening geometry on the heat transfer characteristics for external flames impinging on an exterior wall," *Experimental Heat Transfer*, vol. 27, no. 3, pp. 213–230, 2014. doi: 10.1080/08916152.2012.757672.

[280] J.-L. Consalvi, Y. Pizzo, B. Porterie, and J. Torero, "On the flame height definition for upward flame spread," *Fire Safety Journal*, vol. 42, pp. 384–392, 2007.

[281] R. McNamee, J. Zehfuss, A. I. Bartlett, M. Heidari, F. Robert, and L. A. Bisby, "Enclosure fire dynamics with a cross-laminated timber ceiling," *Fire and Materials*, vol. 45, no. 7, pp. 847–857, 2021.

[282] T. Engel, S. Brunkhorst, F. Steeger, D. Butscher, C. Kurzer, N. Werther, S. Winter, J. Zehfuß, B. Kampmeier, and M. Neske, "Schlussbericht zum verbundvorhaben timpuls-brandschutztechnische grundlagenuntersuchung zur fortschreibung bauaufsichtlicher regelungen im hinblick auf eine erweiterte anwendung des holzbaus," report, Lehrstuhl für Holzbau und Baukonstruktion, 2022.

[283] J. Su, P.-S. Lafrance, M. Hoehler, and M. Bundy, "Fire safety challenges of tall wood buildings-phase 2: task 3-cross laminated timber compartment fire tests," tech. rep., 2018.

[284] S. Frizzi, M. Bouchouicha, J.-M. Ginoux, E. Moreau, and M. Sayadi, "Convolutional neural network for smoke and fire semantic segmentation," *IET Image Processing*, vol. 15, no. 3, pp. 634–647, 2021.

[285] W. Cai, X. Li, and L. Ma, "Practical aspects of implementing three-dimensional tomography inversion for volumetric flame imaging," *Applied Optics*, vol. 52, no. 33, pp. 8106–8116, 2013.

[286] H. C. Bheemul, L. Gang, and Y. Yong, "Digital imaging-based three-dimensional characterization of flame front structures in a turbulent flame," *IEEE Transactions on Instrumentation and Measurement*, vol. 54, no. 3, pp. 1073–1078, 2005.

[287] L. Gang, Y. Yong, and M. Colechin, "A digital imaging based multifunctional flame monitoring system," *IEEE Transactions on Instrumentation and Measurement*, vol. 53, no. 4, pp. 1152–1158, 2004.

[288] L. Gang, Y. Yong, M. Colechin, and R. Hill, "Monitoring of oscillatory characteristics of pulverized coal flames through image processing and spectral analysis," *IEEE Transactions on Instrumentation and Measurement*, vol. 55, no. 1, pp. 226–231, 2006.

[289] H.-W. Huang and Y. Zhang, "Flame colour characterization in the visible and infrared spectrum using a digital camera and image processing," *Measurement Science and Technology*, vol. 19, no. 8, p. 085406, 2008.

[290] M. Gómez-Mares, M. Muñoz, and J. Casal, "Axial temperature distribution in vertical jet fires," *Journal of Hazardous Materials*, vol. 172, no. 1, pp. 54–60, 2009.

[291] G. Yadav, V. Gupta, V. Gaur, and M. Bhattacharya, "Optimized flame detection using image processing based techniques," *Indian Journal of Computer Science and Engineering*, vol. 3, 2012.

[292] T. Qiu, Y. Yan, and G. Lu, "An autoadaptive edge-detection algorithm for flame and fire image processing," *IEEE Transactions on Instrumentation and Measurement*, vol. 61, no. 5, pp. 1486–1493, 2012.

[293] G. Lu, G. Gilabert, and Y. Yan, "Vision based monitoring and characterisation of combustion flames," in *Journal of Physics: Conference Series*, vol. 15, p. 194.

[294] K. Souflas, E. Z. Psarakis, P. Koutmos, and F. N. Egolfopoulos, "Low cost image processing of bunsen flame photography for estimation of flame speeds," *Combustion Science and Technology*, vol. 191, no. 7, pp. 1123–1138, 2019. doi: 10.1080/00102202.2018.1512105.

[295] D. Sun, G. Lu, H. Zhou, Y. Yan, and S. Liu, "Quantitative assessment of flame stability through image processing and spectral analysis," *IEEE Transactions on Instrumentation and Measurement*, vol. 64, no. 12, pp. 3323–3333, 2015.

[296] H. Yingping, Y. Yong, L. Gang, and R. Alan, "On-line flicker measurement of gaseous flames by image processing and spectral analysis," *Measurement Science and Technology*, vol. 10, no. 8, p. 726, 1999.

[297] K. Lu, L. Hu, M. Delichatsios, F. Tang, Z. Qiu, and L. He, "Merging behavior of facade flames ejected from two windows of an under-ventilated compartment fire," *Proceedings of the Combustion Institute*, vol. 35, no. 3, pp. 2615–2622, 2015.

[298] F. Tang, L. Hu, X. Zhang, X. Zhang, and M. Dong, "Burning rate and flame tilt characteristics of radiation-controlled rectangular hydrocarbon pool fires with cross air flows in a reduced pressure," *Fuel*, vol. 139, pp. 18–25, 2015.

[299] X. Zhang, W. Xu, L. Hu, X. Liu, X. Zhang, and W. Xu, "A new mathematical method for quantifying trajectory of buoyant line-source gaseous fuel jet diffusion flames in cross air flows," *Fuel*, vol. 177, pp. 107–112, 2016.

[300] L. Hu, X. Sun, X. Zhang, and F. Ren, "Facade flame height and horizontal ex-

tending distance from opening of compartment fire with external sideward wind," *Proceedings of the Combustion Institute*, vol. 37, no. 3, pp. 3859–3867, 2019.

[301] F. Ren, L. Hu, X. Zhang, X. Sun, J. Zhang, and M. Delichatsios, "Experimental study of transitional behavior of fully developed under-ventilated compartment fire and associated facade flame height evolution," *Combustion and Flame*, vol. 208, pp. 235–245, 2019.

[302] A. S. Bøe, K. L. Friquin, D. Brandon, A. Steen-Hansen, and I. S. Ertesvåg, "Fire spread in a large compartment with exposed cross-laminated timber and open ventilation conditions:# fric-01–exposed ceiling," *Fire Safety Journal*, p. 103869, 2023.

[303] F. ROBERT, "Épernon fire tests programme synthesis report," 2020.

[304] T. Engel and N. Werther, "Impact of mass timber compartment fires on façade fire exposure," *Fire Technology*, vol. 59, no. 2, pp. 517–558, 2023.

[305] Y.-P. Lee, M. A. Delichatsios, and G. W. H. Silcock, "Heat fluxes and flame heights in façades from fires in enclosures of varying geometry," *Proceedings of the Combustion Institute*, vol. 31, no. 2, pp. 2521–2528, 2007.

[306] L. G. Zheng, M. G. Yu, S. J. Yu, and C. Lu, "Measurement of flame height by image processing method," *Advanced Materials Research*, vol. 301- 303, 2011.

[307] B. M. Cetegen, E. E. Zukoski, and T. Kubota, "Entrainment in the near and far field of fire plumes," *Combustion Science and Technology*, vol. 39, no. 1-6, pp. 305–331, 1984. doi: 10.1080/00102208408923794.

[308] W. M. Pitts, E. Braun, R. Peacock, H. E. Mitler, E. L. Johnsson, P. A. Reneke, and L. G. Blevins, "Temperature uncertainties for bare-bead and aspirated thermocouple measurements in fire environments," in *Engineering, Environmenal Science*, 2003.

[309] J. Ji, X. Yuan, K. Li, and J. Sun, "Influence of the external wind on flame shapes of n-heptane pool fires in long passage connected to a shaft," *Combustion and Flame*, vol. 162, no. 5, pp. 2098–2107, 2015.

[310] W. M. Pitts, "Wind effects on fires," *Progress in Energy and Combustion Science*, vol. 17, no. 2, pp. 83–134, 1991.

[311] D. R. Weise and G. S. Biging, "Effects of wind velocity and slope on flame properties," *Canadian Journal of Forest Research*, vol. 26, pp. 1849–1858, 1996.

[312] Y. Lu, X. Huang, L. Hu, and C. Fernandez-Pello, "The interaction between fuel inclination and horizontal wind: Experimental study using thin wire," *Proceedings of the Combustion Institute*, vol. 37, no. 3, pp. 3809–3816, 2019.

[313] B. Li, H. Wan, Z. Gao, and J. Ji, "Experimental study on the characteristics of flame merging and tilt angle from twin propane burners under cross wind," *Energy*, vol. 174, pp. 1200–1209, 2019.

[314] P. Jiang and S.-x. Lu, "Pool fire mass burning rate and flame tilt angle under crosswind in open space," *Procedia Engineering*, vol. 135, pp. 261–274, 2016.

[315] R. Baldwin, "Flame merging in multiple fires," *Combustion and Flame*, vol. 12, no. 4, pp. 318–324, 1968.

[316] F. Tang, L. Deng, Q. He, and J. Zhang, "Mass burning rate and merging behaviour of double liquid pool fires under cross winds," *Proceedings of the Combustion Institute*, vol. 39, no. 3, pp. 4041–4052, 2022. Funding Information: This work was supported by National Natural Science Foundation of China under Grant No. 52076066 , CAS Pioneer Hundred Talents Program to Dr. Fei Tang, A nhui Provincial Natural Science Foundation (No. 2208085J34 ), High-end Foreign Experts Introduction Plan Project and Leading Academic Talents Training Program of USTC to Dr. Fei Tang. Publisher Copyright: © 2022 The Combustion Institute. Published by Elsevier Inc. All rights reserved. 10.1016/j.proci.2022.09.032.

[317] Great Britain Communities Local Government, *Building Regulations 2000 Approved Document B: Fire Safety Volume 1 Dwellinghouses - Changes to Content*. London, UK: TSO, 2007.

[318] L. Orloff and J. De Ris, "Froude modeling of pool fires," *Symposium (International) on Combustion*, vol. 19, no. 1, pp. 885–895, 1982.

[319] S. Yokoi, "Study on the prevention of fire-spread caused by hot upward current," 1960.

[320] M. Delichatsios, "Enclosure and facade fires: Physics and applications," vol. 11, pp. 3–27, International Association for Fire Safety Science, 2014.

[321] O. Sugawa, D. Momita, and W. Takahashi, "Flow behavior of ejected fire flame/plume from an opening effected by external side wind," *Fire Safety Science*, 1997.

[322] F. Tang, L. Hu, M. Delichatsios, K. Lu, and W. Zhu, "Experimental study on flame height and temperature profile of buoyant window spill plume from an under-ventilated compartment fire," *International Journal of Heat and Mass Transfer*, vol. 55, no. 1, pp. 93–101, 2012.

[323] K. Lu, Z. Wang, Y. Ding, J. Wang, J. Zhang, M. A. Delichatsios, and L. Hu, "Flame behavior from an opening at different elevations on the facade wall of a fire compartment," *Proceedings of the Combustion Institute*, vol. 38, no. 3, pp. 4551–4559, 2021.

[324] X. Sun, L. Hu, X. Zhang, F. Ren, Y. Yang, and X. Fang, "Experimental study on flame pulsation behavior of external venting facade fire ejected from opening of a compartment," *Proceedings of the Combustion Institute*, vol. 38, no. 3, pp. 4485–4493, 2021.

[325] X. Zhang, Z. Zhang, Z. Zhang, W. Xu, Q. Luo, H. Tao, and X. Li, "Experimental investigation of compartment fires with circular opening: From the aspects of internal temperature and facade flame," *Combustion and Flame*, vol. 213, pp. 107–116, 2020.

[326] X. Zhang, Z. Zhang, G. Su, F. Tang, A. Liu, and H. Tao, "Experimental study on thermal hazard and facade flame characterization induced by incontrollable combustion of indoor energy usage," *Energy*, vol. 207, p. 118173, 2020.

[327] R. Richards, B. Munk, and O. Plumb, "Fire detection, location and heat release rate through inverse problem solution. part i: Theory," *Fire Safety Journal*, vol. 28, no. 4, pp. 323–350, 1997.

[328] W. Jahn, G. Rein, and J. Torero, "Forecasting fire growth using an inverse zone modelling approach," *Fire Safety Journal*, vol. 46, no. 3, pp. 81–88, 2011.

[329] K. J. Overholt and O. A. Ezekoye, "Characterizing heat release rates using an inverse fire modeling technique," *Fire Technology*, vol. 48, no. 4, pp. 893–909, 2012.

[330] M. Price, A. Marshall, and A. Trouvé, "A multi-observable approach to address the ill-posed nature of inverse fire modeling problems," *Fire Technology*, vol. 52, no. 6, pp. 1779–1797, 2016.

[331] Y. Y. Chu, V. K. R. Kodur, and D. Liang, "A probabilistic inferential algorithm to determine fire source location based on inversion of multidimensional fire parameters," *Fire Technology*, vol. 53, no. 3, pp. 1077–1100, 2017.

[332] A. Kurzawski, J.-M. Cabrera, and O. A. Ezekoye, "Model considerations for fire scene reconstruction using a bayesian framework," *Fire Technology*, vol. 56, no. 2, pp. 445–467, 2020.

[333] R. Chitty, *External fire spread*. Bracknell, England: IHS BRE Press, 2 ed., Aug. 2014.

# Appendix A

# Chapter 5 - Appendix

| HSV | *CodeRed#01* | *CodeRed#02* | *CodeRed#04* |
|---|---|---|---|
| **Hue** | (2.3, 189.5) | (22.5, 127.5) | (6.8, 149.5) |
| **Saturation** | (12.1, 116.3) | (0, 48.1) | (0, 87.5) |
| **Value** | (166, 255) | (214.5, 250) | (242.8, 255) |

**Table A.1** – HSV calibration values for CodeRed Experiments

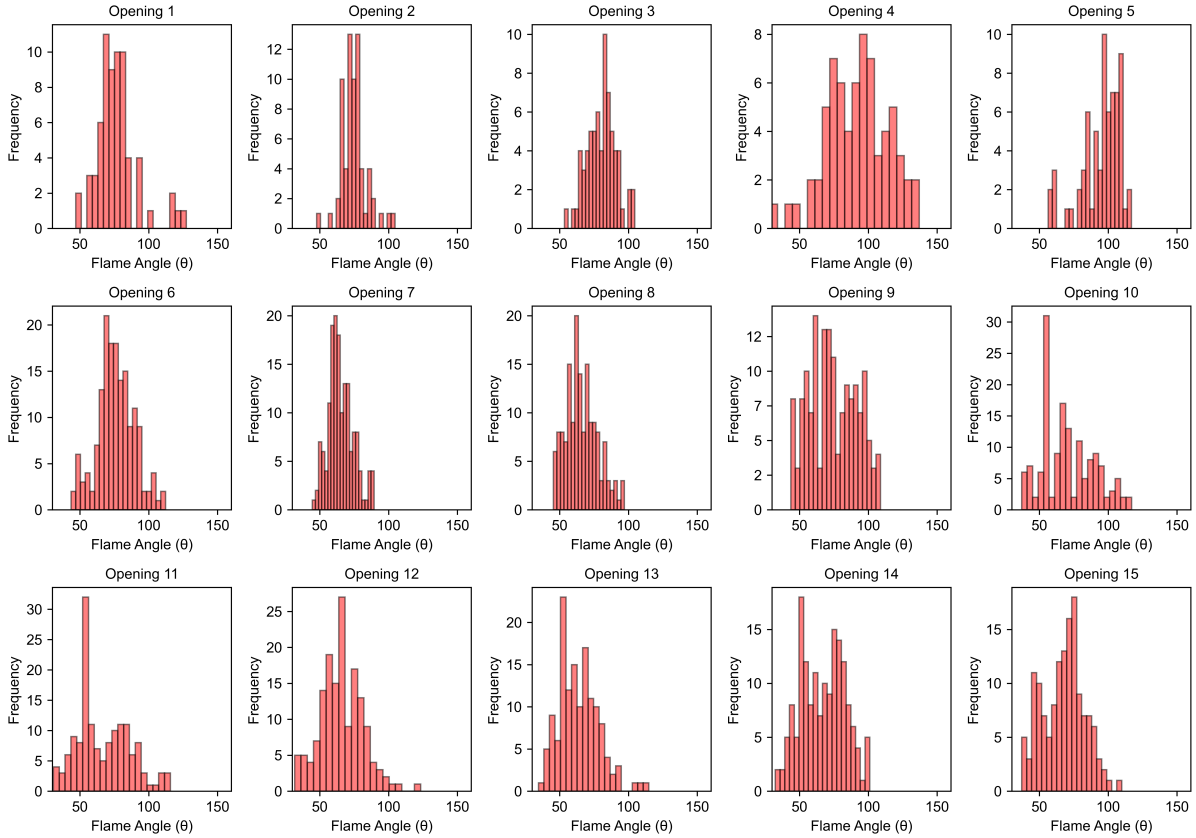



**Figure A.1** – Matrix of external flame angle from all openings in *CodeRed#01*

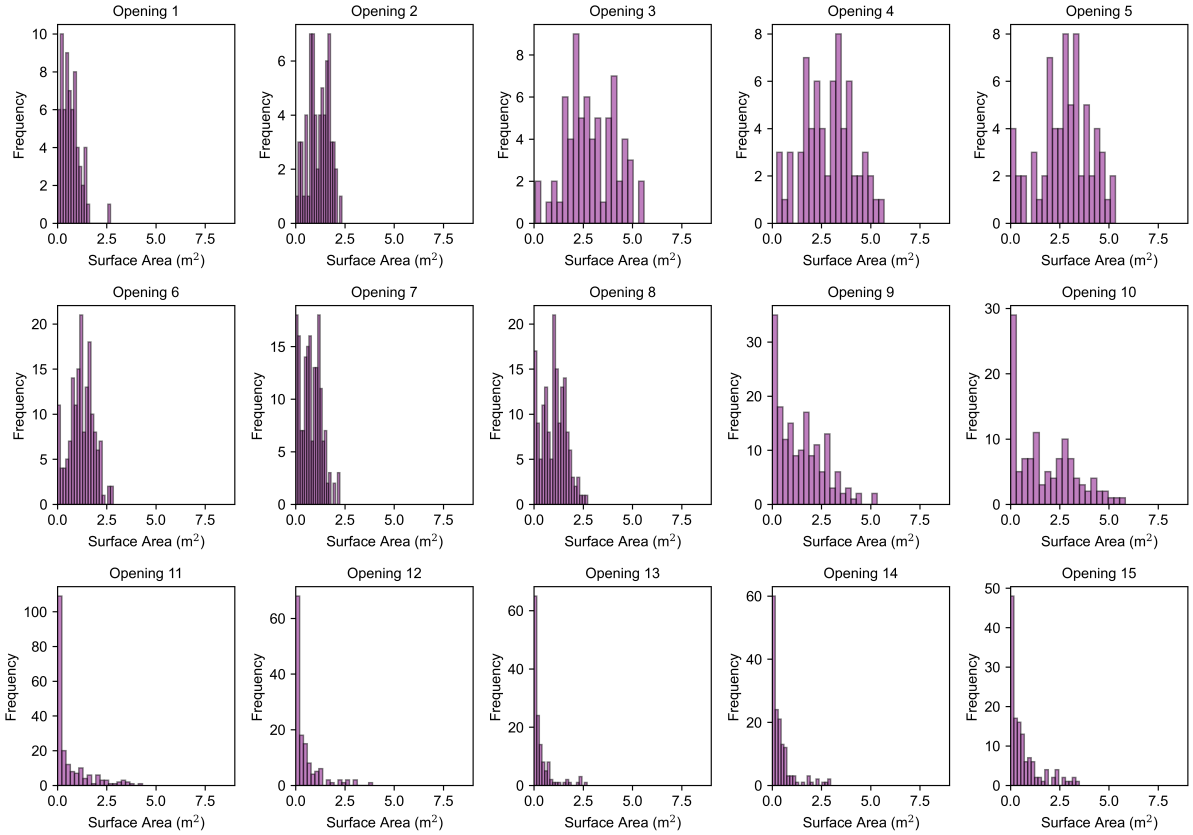



**Figure A.2** – Matrix of projected surface area of external flame from all openings in *CodeRed#01*

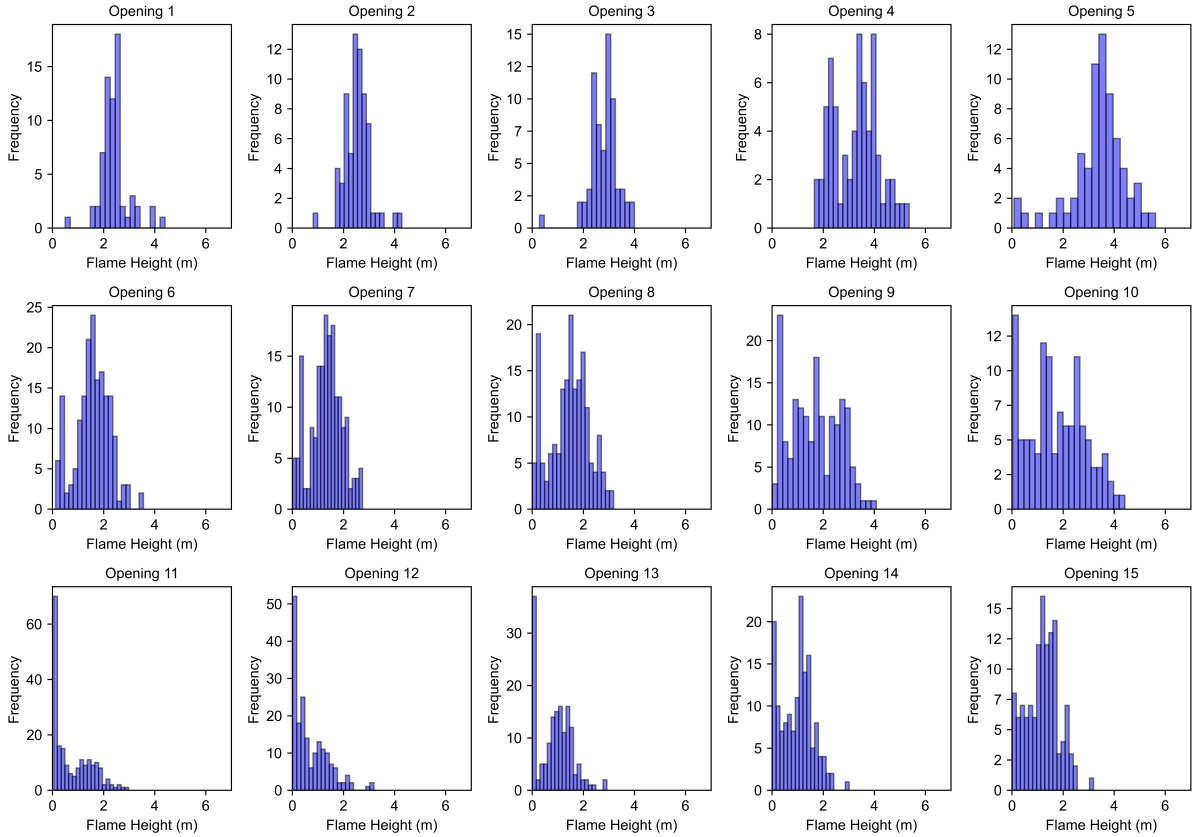



**Figure A.3** – Matrix of external flame height from all openings in *CodeRed#01*

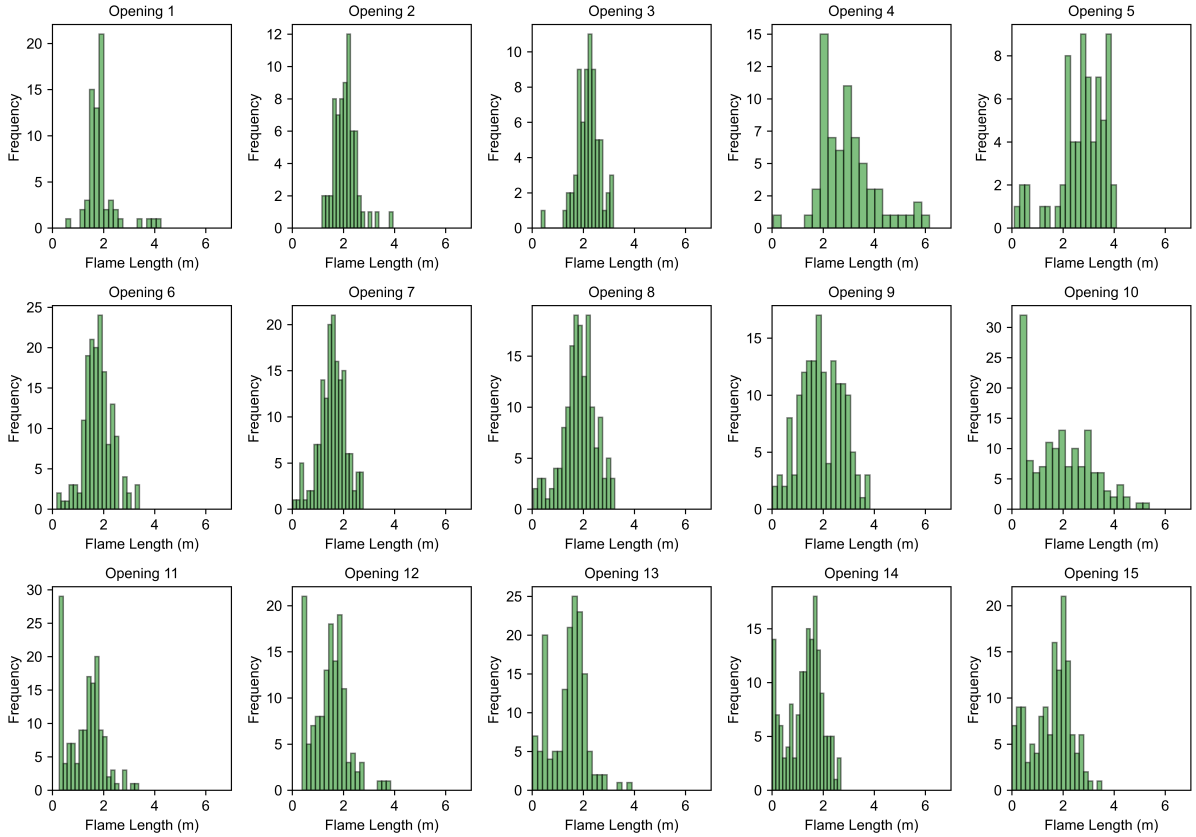



**Figure A.4** – Matrix of external flame length from all openings in *CodeRed#01*

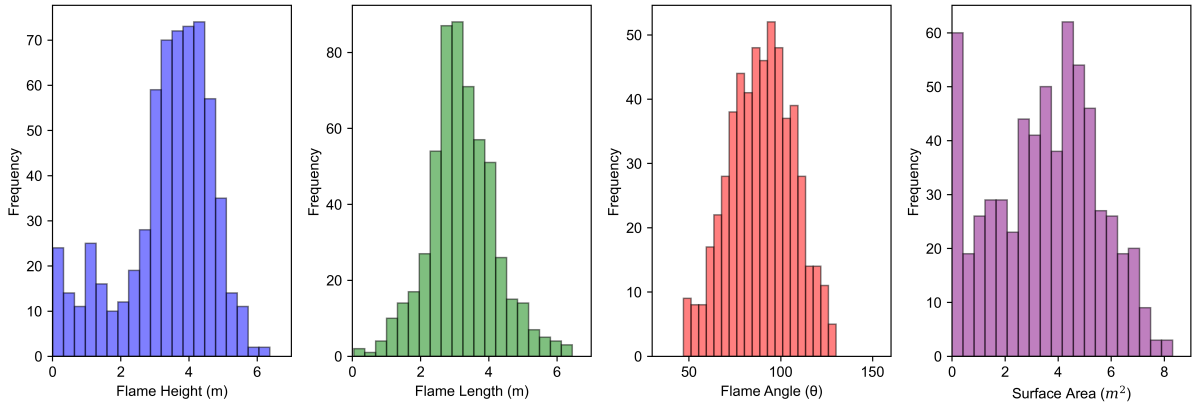



**Figure A.5** – Matrix of all external flame measurements from opening 7 in *CodeRed#02*

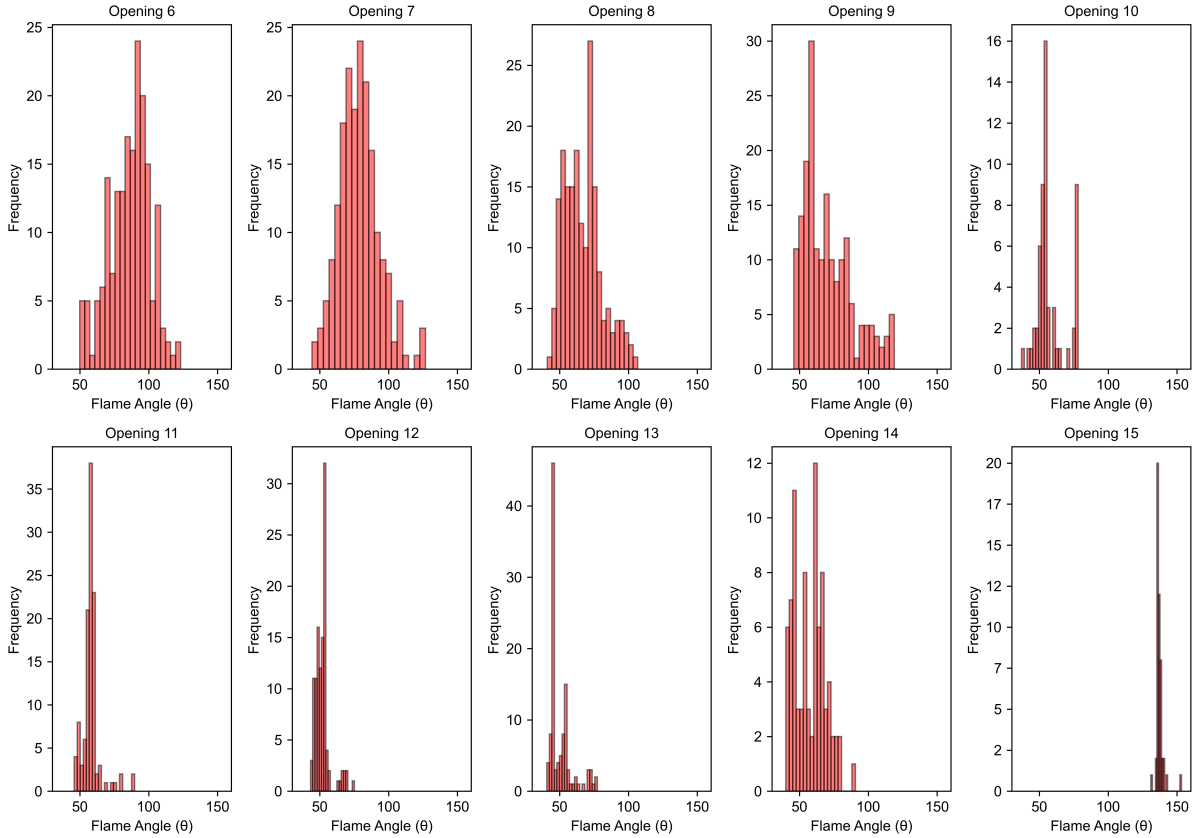



**Figure A.6** – Matrix of external flame angle from all openings in *CodeRed#04*

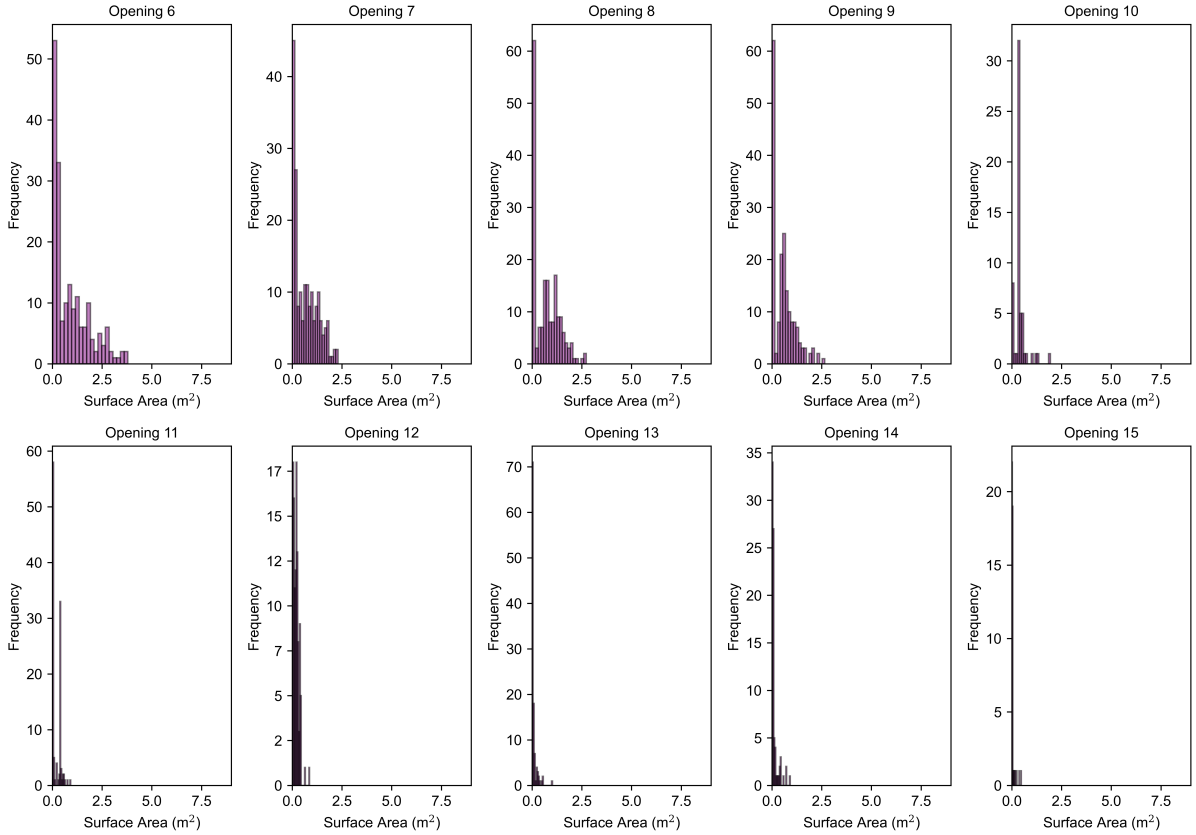



**Figure A.7** – Matrix of projected surface area of external flame from all openings in *CodeRed#04*

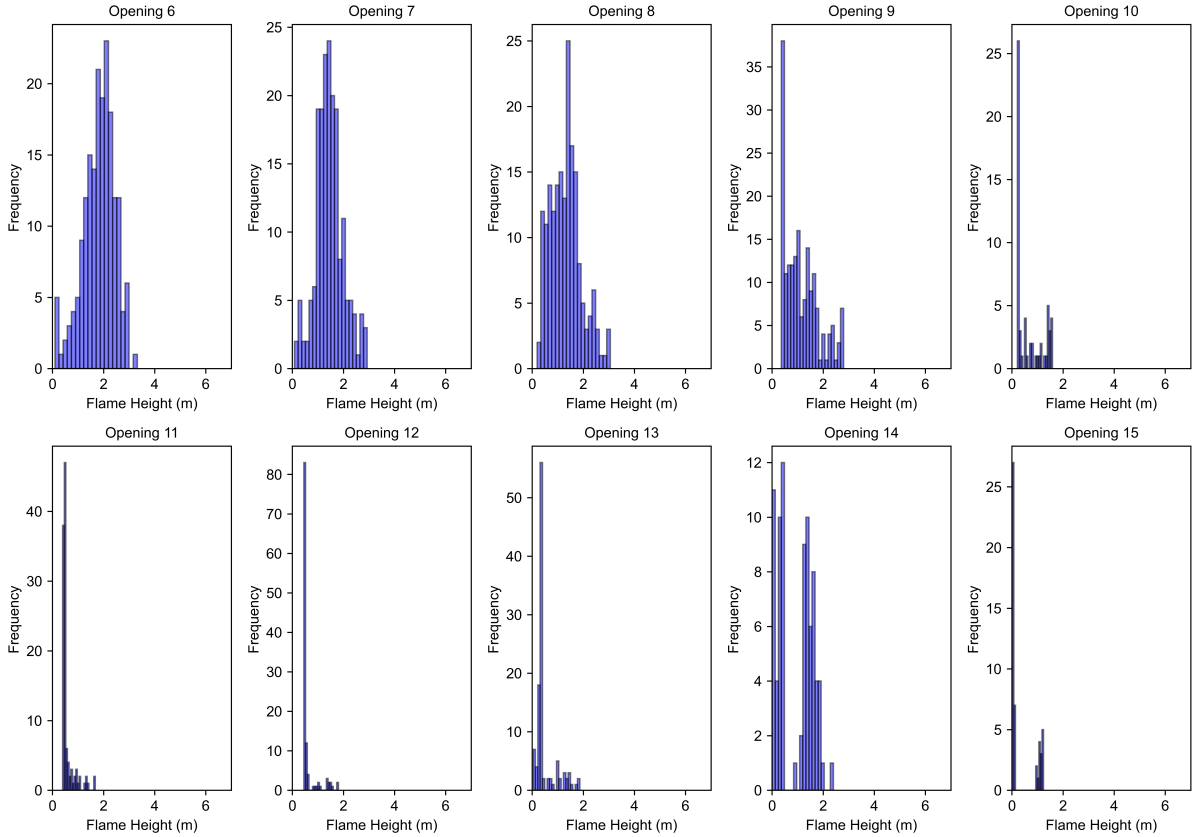



**Figure A.8** – Matrix of external flame height from all openings in *CodeRed#04*

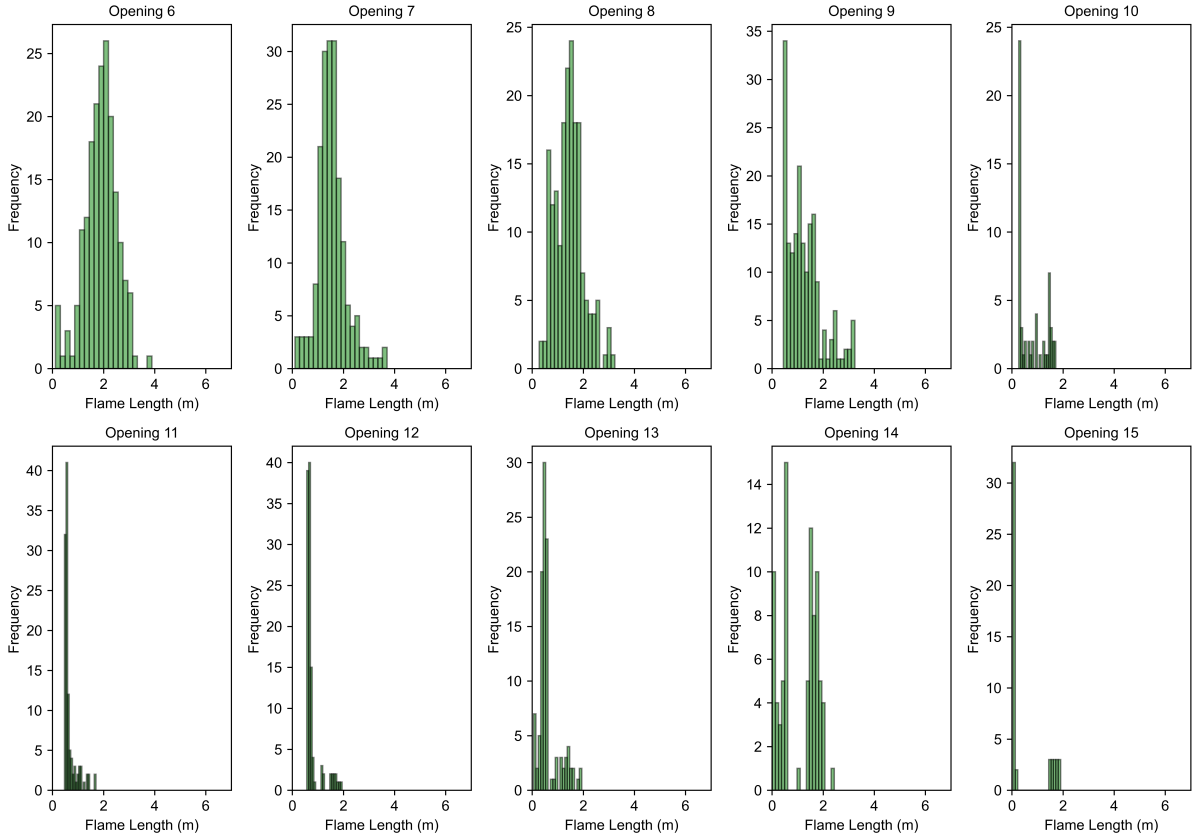



**Figure A.9** – Matrix of external flame length from all openings in *CodeRed#04*